A New Portable 3D Gyroscope System for the Evaluation of Upper Limb Function

Anita Man-Ar Chan

A thesis presented in partial fulfilment of the requirements for the degree of Doctor of Philosophy from the Department of Biomedical Engineering, University of Strathclyde, Glasgow, 2014

This thesis is the result of the author's original research. It has been composed by the author and has not been previously submitted for examination which has led to the award of a degree.

Signed:

Date:

Abstract

The shoulder joint plays a major role in positioning the hand for interaction with the environment. Individuals who are constrained at the shoulder often struggle to perform activities fundamental to daily life and experience a loss of independence and a reduction in quality of life. Current clinical methods of functional assessment are largely subjective and rely heavily on the clinician's experience. There is a great need for a quantitative and objective measure of function which can be readily applied within the clinical environment to aid decision making in treatment planning, evaluation of treatment interventions, and monitoring of rehabilitation.

A small and lightweight 3D gyroscope system comprising single-axis vibrating gyroscopes was developed to record the 3D kinematics of the upper limb. Motion data were collected from 20 subjects aged 20-30 years and 70+ years via a laptop computer during the performance of a range of planar motions, activities of daily living (ADL), and lifting tasks. Data were collected simultaneously with a "gold-standard" optoelectronic system for comparison.

Humerothoracic angle data from the two systems were highly correlated. 3D gyroscope system error in range of motion (ROM) was defined as $\pm 9.45^{o}$ for flexion-extension, $\pm 9.37^{o}$ for adduction-abduction, and $\pm 12.28^{o}$ for axial rotation based on upper and lower regression boundaries containing 90% of data values. Percentage error in ROM was 9.45%, 9.37%, and 12.28% respectively for a ROM of 100^{o}. Special attention should be paid to activities involving large axial rotation components which gave the largest 3D differences in angle values between the two systems.

Maximal planar motions indicated a loss of ROM with age. Age-related differences in movement performance were observed for the "hand to back of head" and "hand to same shoulder" activities where differences in mean maximal axial rotation between the young male and older female groups were 51^{o} and 59^{o} respectively compared with 26^{o} for all other ADL and lifting activities. The system provides a measure of 3D joint angles over the entire duration of the movement cycle and the inclusion of elbow and wrist angles would offer a powerful method of functional assessment. The system shows great promise as a tool to support and inform clinical decision making.

Acknowledgements

There are many people to whom I am greatly indebted for their contribution to this work.

Firstly, I would like to express my gratitude to Professor Sandy Nicol for his long-standing commitment to supervise this work through to completion and for the initial opportunity to come to Glasgow. I would like to thank Professor Bernie Conway for the opportunity to complete my studies within the Department of Biomedical Engineering. I would also like to thank Zimmer for providing the funding that enabled me to carry out this work.

This project would not have been possible without the students and staff of the department and the older participants who generously volunteered their time to act as test subjects and to whom I am very grateful.

Thanks to the technical staff: John MacLean for his painstaking efforts on the electronics hardware and for being available to respond to technical issues often at short notice; Robert Hay, Davy Robb and Stevie Murray for their work in the manufacture of the various hardware components; John Wilson for ferrying my elderly test subjects back and forth, even during his lunch break!

The writing of this thesis was conducted over many years and would never have been completed without the support and encouragement of friends and family. Thanks to Dad for believing that I was capable of undertaking such a huge challenge, to Susan for being tough with me, to Chris for listening to me, and to Mum for walking every step of this journey with me.

Table of Contents

List of Figures

List of Tables

In memory of Joseph Chan

Chapter 1: Introduction

The upper limb is essential to allow us to carry out activities of daily living (ADL) such as feeding, grooming, dressing, and toileting. The shoulder joint is a complex and important joint, working in coordination with the elbow and wrist to position the hand for interaction with the environment. Patients who are constrained at the shoulder joint often find it difficult to carry out activities fundamental to daily life, resulting in loss of independence and a decreased quality of life. Restoration of good function to the upper limb has therefore become an important clinical focus.

Current clinical methods of upper limb functional assessment involve physical examination to assess pain, muscle strength and neurological function, passive and active range of motion (ROM). Patient questionnaires such as the Oxford Shoulder questionnaire (Dawson et al., 1996, 2009) are commonly used to assess the level of pain and difficulty experienced during the performance of everyday functional activities via an analogue scale. This method has demonstrated usefulness as an outcome measure following shoulder surgery (Dawson et al., 1996, Olley and Carr, 2008) but does not permit comparisons to be drawn between patients since pain is subjective. Whilst these methods of assessment are valuable, they rely largely on the experience and judgement of the clinician and may not be truly representative of everyday upper limb function or the way in which a given clinical intervention affects the real life of patients (Bonato, 2005). The availability of quantitative motion data within the clinical environment would provide an objective measure of function to aid clinical decision making.

Motion analysis techniques are widely used in research environments for the quantitative assessment of 3D motion. They have also become a well established and powerful tool in the clinical environment for the detailed diagnosis and treatment planning of patients with gait and neurological disorders (Rau et al., 2000) as well as in the evaluation of treatment interventions and in the monitoring of rehabilitation. However, gait analysis techniques are not immediately transferable to record motion of the upper limb, which differs vastly in its characteristics. Compared with the cyclical, repeatable and largely planar nature of gait, the use of the upper extremities

is far more versatile, involving grasping, reaching and complex manipulation tasks, with large shoulder rotations possible in all three planes of motion. Hence, functional motions of the upper limb are not well defined. The definition of "normal" motion and the identification of deviation from this due to pathological change are complicated by the redundancy across upper limb joints which lead to larger variation in motion across both healthy and diseased individuals compared with gait. The complexity of the shoulder joint and large range of motion possible also poses challenges in the presentation of joint motion data in a way that is clinically meaningful. Subsequently, there is a lack of consensus for the development of standardised protocols for upper limb motion analysis which has hindered its application within the clinical environment. Furthermore, the operation of a full motion analysis system and interpretation of raw data requires specialist knowledge. At present gait analysis takes place in centres where a strong collaboration exists between clinicians and engineers and such techniques cannot be widely incorporated into standard clinical routine (Rau et al., 2000).

There is therefore a need for a method to quantify upper limb motion which is simple to use, can be readily applied within a clinical environment, and which is free from the complexities and cost of a full motion analysis system. Miniature kinematic sensors such as accelerometers, gyroscopes and magnetometers, provide a promising alternative to marker-tracker systems for use outside of the dedicated laboratory environment. As well as providing a quantitative measure of function, their use in clinical practice may facilitate the establishment of diagnostic patterns in injury or disease which would add objectivity to clinical judgement (Jordan 2001). Such sensors may also open up the possibility of monitoring individuals in their usual environment with minimal interference (Coley et al., 2007).

This thesis describes the development and testing of a novel 3D gyroscope system to record upper limb motion. Chapter 2 gives an overview of commonly used motion tracking systems in the research and clinical settings, followed by a review of kinematic sensors and their use in the quantification of human motion. Chapter 3 describes the development and configuration of the 3D gyroscope system and details the preliminary testing of the gyroscope sensors. Chapter 4 presents the theoretical

concepts used in this thesis for the description of 3D upper limb kinematics. Chapter 5 describes the measurement techniques used for the collection of kinematic data together with an overview of the data analysis steps taken to compute joint kinematics from the 3D gyroscope system. This is followed by a description of the statistical techniques used to compare the output from the 3D gyroscope and "gold-standard" Vicon systems. Findings of the experimental work are presented in Chapter 6 followed by a discussion of the main findings and recommendations for further work in Chapter 7.

Chapter 2: Motion measurement and assessment techniques

Throughout history, researchers have sought a better understanding of the relationship between muscle function and performance. Analysis of motion began in the late 1800s with the work of Muybridge who produced a series of stop-motion photographs of both human and animal motion. This technique was later used scientifically by Marrey who correlated ground reaction forces with movement as a precursor to modern motion analysis (Roetenberg, 2006).

Today, motion analysis has found widespread use in research and is a commonly used technique in clinical and sporting applications in both humans and animals. This thesis focuses on the use of motion analysis in the clinical environment, of which the major driving force is to provide a quantitative measure of function to inform clinical decision making, evaluate treatment interventions and to monitor rehabilitation.

Various methods have been employed for the recording and study of upper limb motion ranging from simple mechanical techniques such as a goniometer, to more complex motion tracking systems such as optical and electromagnetic systems, and most recently inertial sensors. These techniques are reviewed below.

2.1 Motion tracking systems

Remote measurement is based on the principle of tracking anatomical landmarks or surface markers attached in relation to these landmarks (Murray, 1999). Each segment is assumed to be a rigid body. The definition of a segment embedded frame enables the position and orientation of the segment to be described in relation to a global reference frame via a position vector and orientation matrix. The relative orientation of adjacent segments can also be analysed to give joint angular changes over time. These principles are described further in Chapter 4.

2.1.1 Video techniques

This technique uses multiple video cameras to film and record upper limb motion where anatomical landmarks are tracked with or without markers. External markers applied over anatomical landmarks are often two-dimensional and appear as circles in each camera view. For the collection of 3D data, markers should ideally be three-dimensional to represent the same size in each camera view (Murray, 1999). The locations of the relevant landmarks or markers are digitised frame-by-frame via manual or automatic digitising. Automatic digitisation employs pattern recognition techniques to quickly track corresponding markers in subsequent image frames and requires high contrast between the markers and the background (Murray, 1999). However, if landmarks are obscured or confused with neighbouring markers, the operator must intervene. Manual digitisation can be a time-consuming process, particularly when analysing 3D data. In addition, video techniques require intensive post-processing and motion information is therefore not available in real-time.

Video techniques have been used in upper limb studies. A four-camera video system was used with skin-mounted, spherical markers with a diameter of 25mm to record upper limb activities of everyday living (Murray and Johnson, 2004; Murray, 1999).

2.1.2 Optoelectronic techniques

Optoelectronic techniques were developed as an alternative to photogrammetry and have become widely used in commercial and academic fields. 3D markers affixed to the body segments can be active (e.g. light-emitting) or passive (e.g. reflective markers). Like automatic digitisation, the identification of individual markers is similarly achieved automatically through software pattern recognition techniques or via hardware (shape, colour, time, frequency multiplexing).

Active marker systems such as the Selspot, Selspot II and WATSMART systems use multiple active infra-red LEDs which are attached at relevant locations on each body segment. These pulsed-LEDs fire sequentially such that only one LED is activated in a given time interval of microseconds. A disadvantage of such systems is their sensitivity to marker light reflections on neighbouring surfaces which may lead to

marker identification problems and spurious data. LED markers must also be connected to a power supply which tethers the individual and may cause some restriction of movement. Wired landmarks are cumbersome but an advantage of their use is that they can be more readily identified.

Modern variations of the active LED approach such as the CODA System (Charnwood Dynamics) and the Optotrak system (Northern Digital Inc.) both overcome this tethering problem via battery-powered LEDs which are worn by the user (Welch and Foxlin, 2002). The infra-red signals emitted by the markers are measured by position sensors which contain three 1D charged coupled device sensors (CCD) mounted in a long bar. Measurements from each of the three devices give the X, Y and Z coordinates of each marker. Such systems are capable of producing real-time motion measurements. CODA has been used in a clinical setting to investigate 3D upper limb motion during a drinking activity in patients with tetraplegia (de los Reyes-Guzmán, 2010). The Optotrak system has been used to measure 3D scapula attitude (Herbert et al., 2000).

Reflective systems use passive 3D markers which reflect light rather than actively emitting light. The VICON system uses a ring of infrared (IR) LEDs mounted around the lens of the camera together with IR pass filters placed over the camera lens. The LEDs emit pulsed infra-red light and the cameras measure the reflection of this light from the segment mounted markers. Such systems are used with a custom user interface and comprehensive software package which facilitates full operation of the system. This includes calibration, collection and processing of raw image data, 3D landmark reconstruction and data smoothing. An advantage of such systems is the quick and easy application of markers which do not involve wires and thus do not interfere with or restrict movement. Care must be taken to avoid interference from other light sources such as sunlight or strong incandescent light, or reflections which may result in “ghost” markers (Roetenberg, 2006).

Commercial systems such as the Vicon or Optotrak systems have been extensively used in human movement analysis, are highly accurate, and are considered gold-standards in such applications (Roetenberg, 2006). However, they require time-consuming and intensive offline processing in the form of operator-supervised

sorting and reduction of data. A characteristic of optical systems is that they suffer from occlusion when a required light path is blocked. This may occur particularly in complex 3D upper limb motion where markers are obscured by other parts of the body. In such cases, individual identification of markers or extrapolation of marker trajectories can be carried out which further increases offline processing time.

Recently, new optical technologies intended for gaming applications, such as the Microsoft Kinect™ and Nintendo Wii systems, have been utilised for motion capture applications. These technologies exhibit potential for use in clinical motion analysis because of their low cost, portability and ease of use compared with the more complex optical systems described above. Sena et al. (2012) developed a passive IR marker tracking technique using the Kinect™ sensor as the optical measurement device. Depth and IR image data from the Kinect sensor were combined to track the 3D position of passive retroreflective markers placed on the lower limb of the subject. This was achieved through initial manual digitisation of passive markers and subsequently utilising human "pose" estimates from the Kinect system to automatically identify each marker. Bonnechére (2014) investigated the validity and reproducibility of the Kinect system to quantify upper and lower limb joint angles by comparison with simultaneously recorded data from a stereophotogrammetric system during planar ROM activities. While reproducibility was statistically similar between the two systems, measured ROMs were found to be different. This was likely due to a difference in joint centre estimation between the two systems. The Kinect and Nintendo Wii systems were developed for use as gesture recognition tools and their accuracy for quantitative motion applications has still to be fully validated. The use of multiple Kinect units may improve accuracy, reduce marker occlusion and facilitate the recording of 3D segment rotation data, but the validity of such a set-up has yet to be investigated.

2.1.3 Electromagnetic systems

Electromagnetic devices have been used in the measurement of lumbar spine kinematics (van Herp et al., 2000), cervical spine kinematics (Jordan et al., 2000) and kinematics of the shoulder (Borstad and Ludewig, 2002). Three orthogonal

electromagnetic fields are generated from a source transmitter and are used to determine the position and orientation, relative to the stationary system, of one or more remote sensors placed on the relevant parts of the body (Jordan 2001). Several systems exist such as the ISOTRAK and FASTRAK systems (from Polhemus, Colchester, Vermont, USA) and the Flock of Birds system (Ascension Technology, Burlington, Colchester, Vermont, USA), which vary in the number of receivers (2 to 4), operation range (5 to 10 feet) and latency i.e. the rate at which real-time position and orientation information is updated.

Utilising the 6DOF measurement ability of an electromagnetic system, Johnson et al. (1993) developed a scapula locator as a non-invasive method to reliably track the three dimensional motion of the scapula. An electromagnetic sensor is attached to the three-pointed scapula locator, which is an adjustable frame that is applied over three specified bony landmarks (the acromial angle, the inferior angle, and the root of the scapula spine). The scapula locator is readjusted over the bony landmarks as the arm is held still in several recording positions across a movement of interest. Tracking of the scapula is thus achieved via a quasi-static approach since dynamic tracking of the scapula is difficult (Veeger et al., 2006). The scapula locator has been used in several studies together with a sensor-mounted pointer to facilitate the digitisation of anatomical landmarks in the reference frames of the corresponding segment mounted sensors (Veeger et al., 2006; Vermeulen et al., 2002; Meskers et al, 1998). Thus, local bone coordinate systems can be constructed and joint and segment angles computed.

An advantage of electromagnetic systems is that they do not suffer from line of sight problems, and are capable of producing dynamic, real-time position and orientation information. Additionally, user-worn sensors are small. However, they are limited in range and are sensitive to magnetically permeable materials (Roetenberg, 2006; Anglin and Wyss, 2000) which could be potentially problematic in a clinical environment. Wired sensors may lead to tethering of the subject, although Polhemus and Ascension do offer wireless magnetic systems (Welch and Foxlin, 2002) at an increased cost.

2.1.4 Acoustic systems

Acoustic systems use the transmission and sensing of sound waves. Position is determined by timing the flight duration of a brief ultrasonic pulse from a sound source to a receiver (Welch and Foxlin, 2002). The transmitter can either be placed on the body segment or fixed in the measurement volume, referred to as an outside-in or inside-out configuration respectively (Roetenberg, 2006).

Ultrasonography has been used to record the kinematics of gait (Kiss et al., 2004), the cervical spine (Dvir and Prushansky, 2000), shoulder (Nyiri et al., 2010; Illyés and Kiss, 2007), and upper limb (Coley et al., 2007). Ultrasound-based motion measurement systems, such as the Zebris CMS-HS (Zebris, Medizintechnik GmbH, Germany), consist of a head of three fixed sonic emitters which send out bursts of ultrasound to body-mounted receivers which are usually attached in triplets on each segment. The spatial coordinates (x, y, z) of each receiver can be determined by computing its distance from all three transmitters. A pointer with two ultrasonic receivers may also be used to calibrate the position of anatomical landmarks relative to the corresponding receiver triplets. Thus, anatomical coordinate systems can be constructed, and 3D segment/joint rotation angles computed.

The accuracy, update rate and range of acoustic tracking systems are limited by the physics of sound. Accuracy can be affected by wind when measuring outdoors, and speed of sound can be affected by temperature, humidity, and air currents. As with optical systems, a clear line of sight must be maintained to minimise tracking disturbance by reflections of sound (Roetenberg, 2006). Room reverberation may affect update rate and it may be necessary to wait several milliseconds for echoes of the previous measurement to die out before initiating a new recording (Foxlin and Welch, 2002).

2.1.5 Limitations of motion tracking systems for clinical use

Whilst the motion tracking systems described above provide complete and high resolution 3D kinematic information, they are primarily laboratory based. Operation of the systems, mounting of markers, sensors or receivers, and interpretation of

kinematic data require bio-engineering expertise to obtain meaningful results (Zheng et al., 2005). For the evaluation of lower limb function, clinical gait analysis has become an important tool in the assessment of gait and neurological disorders, but is only conducted at centres where a strong collaboration between engineers and clinicians exists. Equipment is often fixed or bulky and too cumbersome to set up in a clinician's consulting room (Cutti et al., 2008). This, together with their high cost and complexity, mean that they can only be operated within a dedicated laboratory environment (Coley et al., 2007). In addition, the performance of movements and activities within a highly controlled environment may mean that the resulting measurements are not representative of usual performance e.g. activities of daily living. These constraints, together with the time and resources needed for data analysis, have hindered the application of such techniques in routine clinical practice (Coley et al., 2007, Aminian et al., 2002). Thus, clinical approaches to monitor body position and movement rely largely on clinician observation and patient recall (Zheng et al., 2005).

The availability of miniature body mounted sensors such as accelerometers, gyroscopes and magnetometers may be a useful and inexpensive alternative to full motion tracking systems which allow measurements to be made outside of the laboratory environment with minimal interference. They measure physical quantities such as velocity and acceleration of the objects to which they are attached. They are therefore sourceless and overcome problems associated with operation range and line of sight. Advances in technology mean that these sensors are extremely small (micro-machined) and so are particularly suited to the measurement of upper limb motion. Systems comprised of inertial and magnetic sensors cannot replace the professional experience of clinicians, such as in the evaluation of quality and ease of movement or the assessment of pain (Jordan et al., 2001). Rather, they have the potential to provide a quantitative and objective measurement of upper limb function to aid clinical decision making. Their use in clinical practice may facilitate the establishment of diagnostic patterns in injury or disease which would add objectivity to clinical judgement (Jordan et al., 2001). Such sensors also open up the possibility of monitoring individuals in their usual environment with minimal interference (Coley et al., 2007). These sensors are described further in section 2.2.

2.2 Mechanical, inertial and magnetic sensors

2.2.1 Goniometers

Goniometers are inexpensive devices which measure joint angles between two body segments. Several types of goniometer exist including the universal goniometer, fluid or pendulum goniometer, and electrogoniometer. The universal goniometer is a plastic or metal protractor-like device which comprises two arms of varying lengths which are aligned with the proximal and distal segments of the joint. The fluid or pendulum goniometer is an inclinometer with a fluid level or a weighted needle respectively which measures the orientation of the segment relative to the gravity vector. Both the universal and the fluid or pendulum goniometers have been used to measure joints of the upper extremity (Riddle et al., 1987; Armstrong et al., 1998; de Winter et al., 2004), lower extremity (Watkins et al., 1995; Brosseau et al., 2001), and cervical spine (Youdas et al., 1991; Haynes et al., 2002), and are the types most commonly used in clinical assessment to quantify joint range of motion. They measure the static maximum ROM of a joint or inclination of a segment in one plane at a time. As such, they cannot build composite pictures of movement such as combinations of planes of movement or velocity of movement (Jordan et al., 2000).

Electrogoniometers convert angular motion at the joint into an electrical signal. They are capable of measuring joint motion over the entire movement cycle in more than one plane simultaneously. Barker et al. (1996) applied several types of flexible electrogoniometer to measure upper limb joint angles during functional movements. Twin-axis electrogoniometers monitored angles of elbow and wrist flexion. A specially constructed uniaxial rotation electrogoniometer (Barker 1990) measured pronation/supination of the forearm, and a triaxial flexible electrogoniometer recorded 3D angles of the shoulder complex. Flexible electrogoniometers have been applied in other studies to measure kinematics of the wrist and forearm (Hansson et al., 2004; Johnson et al., 2002), and knee angle in the sagittal plane during activities of daily living (Myles et al., 2002; Rowe et al., 2000). Electrogoniometers are anthropometric dependent meaning a range of devices is needed for different sized limbs, and are primarily used only in research applications.

Goniometers have several practical limitations associated with their use as instruments to measure joint motion. They must be attached across a joint which poses several considerations. Firstly, goniometers must be aligned exactly with the joint rotation centres and axes of rotation. Secondly, flexible electrogoniometers are prone to cross talk as a large source of error i.e. a false abduction/adduction signal that appears during pure flexion as a function of rotation between the two end blocks of the instrument (Hansson et al., 2004; Hansson et al, 1996). Thirdly, goniometers may cause some restriction or interference of the natural movement pattern depending on the size, weight and location of the instrumentation. This is particularly true if several joints are to be measured simultaneously as carried out by Barker et al. (1996). Finally, goniometers may be vulnerable to breakage where they cross a joint (Zheng et al., 2005), or may move from their original placement (Veltink et al., 1996, Bachmann, 2000).

Thus a measurement technique for clinical application is sought which overcomes these practical limitations and which can provide 3D movement information over the duration of the movement cycle. Inertial sensors provide a promising method of recording human motion outside of the specialised laboratory environment due to their low cost, small size and sourceless characteristics. Suitable sensors for body-mounted measurement of human motion are accelerometers, magnetometers and gyroscopes. Each have their own advantages and disadvantages (Luinge et al., 2007) and are described further below.

2.2.2 Accelerometers

Micromachined accelerometers are small, relatively cheap and have low energy consumption (Luinge et al., 2007). The accelerometer output is a result of both linear acceleration and acceleration due to gravity. They can therefore be used as an inclinometer for movements where the linear acceleration is negligible in comparison to gravity (Luinge and Veltink 2004; Kemp et al., 1998; Veltink et al., 1996). Position and orientation information can also be estimated through double integration of the accelerometer signal (Giansanti et al., 2003).

Accelerometers have been used in applications of ambulatory motion analysis to monitor daily physical activity, posture and postural changes. Najafi et al. (2003) utilised two single axis accelerometers with one gyroscope for the detection of body postures including sitting, standing, lying, and also walking. Veltink et al. (1996) used combinations of two and three uniaxial accelerometers to classify both static postures and dynamic activities such as walking, ascending and descending stairs, and cycling. Bouten et al. (1997) utilised the output from three orthogonally mounted uni-axial accelerometers as an indicator of metabolic energy expenditure due to physical activity.

Accelerometers have also been used to measure kinematic transients during gait. Wu and Ladin (1996) combined a tri-axial accelerometer and a tri-axial gyroscope to identify heel strike and toe-off transitions from the kinematics of the foot, shank and thigh during walking and running. Each kinematic sensor unit was large and bulky with mass 100g, and the authors acknowledged their potential to alter the normal gait pattern. For full kinematic analysis of body movements using accelerometers, multiple sensors are required to be attached to a single segment (Veltink 1996, Wu and Ladin, 1996) which greatly increases bulk e.g. if angular acceleration is required, a pair of accelerometers fixed on a rigid object is necessary (Tong and Granat, 1999). Mayagoitia et al. (2002) used two pairs of uni-axial accelerometers mounted at each end of an aluminium strip to measure the linear and angular accelerations of lower limb segments. A similar configuration was previously utilised by Willemsen (1990) who computed lower extremity angles in the sagittal plane from pairs of uni-axial accelerometers without the need for integration. van den Bogert et al. (1996) used four triaxial accelerometers mounted on the upper body to record kinematic variables (linear and gravitational acceleration, angular velocity and angular acceleration) for inverse dynamics analysis at the hip during the single support phase.

In addition to the cumbersome nature of the above described sensor configurations, accelerometers have inherent limitations associated with their use. Firstly, inclination estimates are only reliable for static postures or slow movements (Veltink, 1996) since the linear acceleration must be sufficiently small in comparison to gravity (Luinge and Veltink, 2004). Additionally, accelerometers do not give

information about rotation around the vertical and therefore do not give a complete description of orientation (Luinge and Veltink, 2005). Secondly, the double integration of the accelerometer signal in the computation of position and orientation information is prone to large error over time due to integration drift (van den Bogert et al., 1996). Thus, the severe time restrictions over which integrated 3D accelerometer data is reliable render this method unfeasible for long term body segment position and orientation estimation (Giansanti et al., 2003). Thirdly, the output of the accelerometer is dependent upon its attachment site on the limb segment (Aminian et al., 2002). Some attenuation of the signal may result if placed too close to the centre of rotation (Godfrey et al., 2008).

Accelerometers have been used in combination with magnetometers and gyroscopes to overcome some of these limitations. Magnetometers and gyroscopes are described further below.

2.2.3 Magnetometers

Magnetometers measure the direction and intensity of the local earth magnetic field vector (Zheng 2005). Although not strictly sourceless like inertial sensors, the existence of the earth's magnetic field means the magnetic source is present almost everywhere (Sabatini, 2011). Magnetometers can therefore provide additional orientation information for rotations about the vertical axis. Kemp (1998) combined a triaxial magnetometer and a triaxial accelerometer to monitor body position in 3D. However, the implementation of such a system is limited. Firstly, as described above, the vertical orientation information provided from accelerometers is reliable only for static or slowly moving objects. Secondly, magnetometers are sensitive to the presence of ferromagnetic materials and by electronic equipment generating magnetic fields; both will disturb the local magnetic field and consequently distort the orientation estimation (Luinge et al., 2007; Welch and Foxlin, 2002). This problem becomes especially acute within man-made indoor environments (Sabatini, 2011) and impedes the use of these sensors for motion tracking.

Bachmann (2000) and Zhu and Zhou (2004) combined magnetometers with accelerometers and gyroscopes. Gyroscopes are described further in section 2.2.4. While gyroscopes help achieve accurate orientation estimates from accelerometers for highly dynamic motions (Sabatini, 2011), the problem of magnetic field disturbance still exists. Roetenberg et al. (2005) have shown that magnetic field disturbance can be eliminated by appropriate filtering algorithms and sensor fusion techniques under controlled conditions. For the recording of human motion, the practical implementation of such filtering techniques would require the location and distance from ferromagnetic materials in the vicinity of the sensor to be taken into account and filter parameters adjusted accordingly for each recording site. This is a complex process which could not readily be carried out by clinicians. In ambulatory environments with unknown materials and magnetic objects in the vicinity, inaccuracy in orientation estimation is very likely to occur (Roetenberg et al., 2006). Thus the technique is largely restricted to the controlled laboratory environment.

2.2.4 Gyroscopes

Gyroscopes measure angular velocity, and change in orientation can be estimated by integration of the gyroscope signal. Angular rate sensors used in inertial sensing systems are commonly one of three types; spinning rotor gyroscopes, laser gyroscopes, and vibrating mass gyroscopes (Zheng et al., 2005; Luinge, 2002). Spinning rotor and laser gyroscopes have been widely used in satellites, aircraft and other vehicles for attitude estimation and navigation purposes. Despite their proven success in these applications, they are not suitable for use in human motion analysis as they are bulky and expensive.

In contrast, the vibrating mass gyroscopes are small, inexpensive and have low power requirements, making them ideal for human motion measurement applications (Zheng et al., 2005; Luinge, 2002). Low power consumption means that they can be battery operated thus improving the portability of the system. Their small size and low mass render them unlikely to affect or restrict the natural production of an individual's movement when attached to the body. This is an important consideration particularly for clinical applications where pain may be an issue. The

principle of operation of the gyroscope is the measurement of the Coriolis acceleration of a vibrating device (Tong and Granat, 1999). This is further described in Chapter 3.

An advantage of the use of gyroscopes is that they are not sensitive to linear acceleration and are unaffected by the influence of earth's gravity. Therefore, the gyroscope's output will be the same no matter where it is placed along the length of the limb segment (Aminian et al., 2002) and can theoretically be used to calculate the segment inclination and the relative joint angle (Tong and Granat, 1999). Gyroscopes have been used in applications of ambulatory motion analysis to detect postural changes and monitor daily physical activity in the elderly (Najafi et al., 2003). They have also shown great promise for use in gait analysis to measure spatiotemporal parameters (Aminian et al., 2002) and kinematics of gait (Mayagoitia et al., 2002; Tong and Granat, 1999; Wu and Ladin, 1996). All but the latter of the above cited studies utilised the uni-axial Murata ENC series gyroscopes which have a length of less than 2cm, and a mass of under 1g.

Tong and Granat (1999) used two single gyroscopes attached to the thigh and shank respectively to derive segment inclination and knee angle during gait. Only single axis gyroscopes were used on account that gait occurs mainly in the sagittal plane. Drifting of the gyroscope signal was observed during turning. However, this was corrected by high pass filtering (frequency 0.3 Hz) and automatic reset of inclination angle during mid-stance. Gyroscopes were attached directly to the skin to reduce subject encumbrance.

Mayagoitia et al. (2002) used a combination of accelerometers and gyroscopes affixed to rigid aluminium strips which were mounted on the thigh and shank. This was an identical configuration to that used earlier by Nene et al. (1999). The system was used during gait to measure kinematic parameters in the sagittal plane as an alternative to optical motion capture. One uni-axial gyroscope mounted in the centre of each aluminium strip measured the sagittal plane angular velocity from which segment inclination was subsequently derived. Two pairs of accelerometers mounted at each end of the strip measured the linear and angular accelerations of each limb segment. However, the authors noted that this configuration was cumbersome.

Since change in orientation is derived by integrating the angular velocity signal, a small offset in the gyroscope output will introduce large integration errors over time. For current commercially available micromachined gyroscopes, the time of accurate measurement is restricted to less than 1 minute (Luinge and Veltink, 2005). Such sensors are therefore not suitable for long-term ambulatory monitoring of movement. As previously described, inclination information can be derived from the accelerometer signal when linear acceleration is negligible. Thus, accelerometers can potentially be used to correct for integration drift in the gyroscope orientation estimate (Zheng et al., 2005). Luinge (2002) described the principles of fusing gyroscope and accelerometer signals using a Kalman filter and the method was shown to be reliable for reducing drift in inclination estimation (Luinge and Veltink, 2005). Similarly, the magnetometer, which measures the local earth magnetic field vector, can be used to correct for integration drift in gyroscope orientation estimates around the vertical axis provided that there is no magnetic field disturbance.

Accelerometers, magnetometers and gyroscopes each have their own advantages and disadvantages as described in sections 2.2.2, 2.2.3 and 2.2.4 respectively. The fusion of signals from different sensors, as described by Luinge (2002) and Roetenberg et al. (2005) may be useful for long term ambulatory monitoring of human movement. However, this technique requires complex filtering algorithms and involves increased hardware and software costs. A Kalman filter is computationally intensive which is not acceptable for applications which require real-time output or are computationally constrained (Saxena et al., 2005). To maximise clinical applicability and uptake, a practical system should be simple, unobtrusive, and low cost whilst providing enough relevant information. Sensor fusion may be unnecessarily complex for the clinical application of functional assessment where a recording time of less than one minute is sufficient to record an upper limb motion or activity of interest. The limited recording time associated with the use of current commercially available micromachined gyroscopes is acceptable for the intended application. The gyroscope therefore provides a promising means of obtaining quantitative human motion data for clinical use outside of the dedicated laboratory environment.

2.3 Aims and objectives

This thesis focuses on the use of motion analysis in the clinical environment to provide a quantitative and objective measure of upper limb function to inform and support clinical decision making.

The first aim of this study is to develop a novel inertial sensor-based system for the measurement of 3D upper limb motion which can be readily applied within a clinical environment. The system is required to be simple, unobtrusive and cost effective to maximise ease of use and potential clinical uptake. The gyroscope was the sensor of choice for this study.

Secondly, the 3D gyroscope system will be used to collect upper limb motion data from unimpaired subjects during the performance of functional activities. It is anticipated that this data will contribute to a database of normative motion.

The third aim of this study is to determine the effectiveness of the 3D gyroscope system as a tool for clinical upper limb functional assessment by comparison of 3D angle data with simultaneously recorded values from the "gold standard" Vicon motion analysis system.

Chapter 3: Development of the 3D gyroscope system

This chapter describes the construction and calibration techniques used in the design and development of the 3D gyroscope system.

3.1 Single axis gyroscope

A coriolis force or vibrating mass gyroscope consists of a mass which is brought into vibration by a piezoelectric element (figure 3.1). The piezoelectric element drives the mass from one side to vibrate in one plane. When the gyroscope is rotated about its longitudinal axis, the mass experiences a coriolis force, which causes the mass to undergo additional vibration in the plane perpendicular to both the driven vibration and the angular velocity vector. The amplitude of the additional vibration is detected by a second piezoelectric transducer, and is proportional to the input angular rate, therefore indicating the speed of gyroscope rotation. The magnitude of the coriolis force F_C is given by:

$$\mathbf{F_C = 2m \cdot v \cdot \omega} \tag{3.1}$$

where m is the mass, *v* the momentary speed of the mass, and ω the angular velocity.

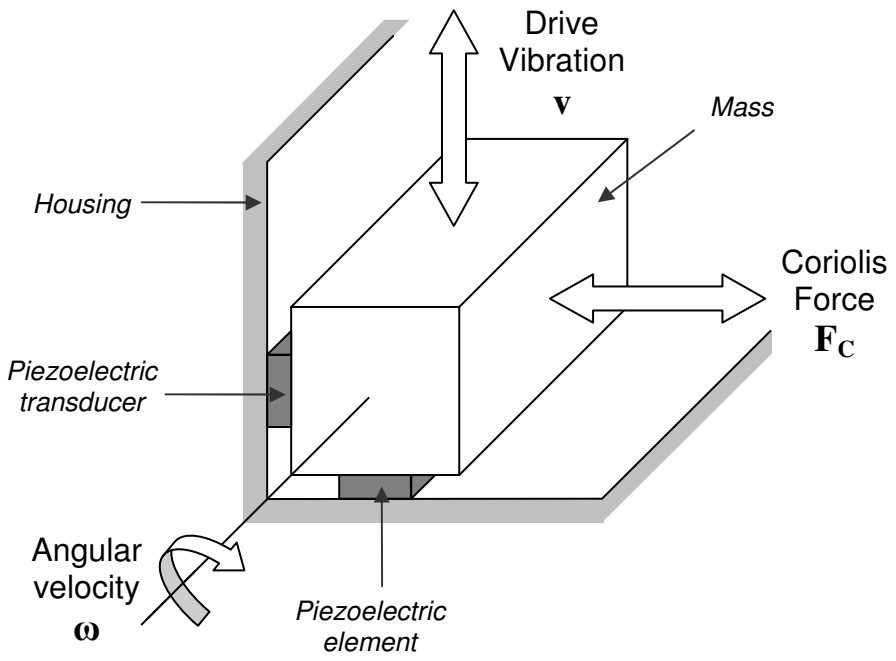

Figure 3.1 Diagram of coriolis vibrating mass gyroscope function.

A coriolis force single axis gyroscope (Murata ENC 03JA) was chosen to develop a clinically applicable motion analysis system. Its small dimensions (15.5x8.0x4.3mm) and light mass (1g) make it ideal for applications in human movement analysis. The gyroscope and its dimensions are shown in figures 3.2a and 3.2b respectively. Rotation about the sensitive (longitudinal) axis produces a voltage output which is proportional to the angular rate.

The relationship between the output voltage of the gyroscope and the angular velocity is as follows:

$$\omega = \frac{V - V_0}{S_v} \tag{3.2}$$

where ω is the angular velocity (deg/s), V is the output voltage (V), V_0 is the static output voltage (V), and S_v is the scaling factor (mV/deg/s) taken from the manufacturers specifications.

Angular displacement data is computed via a single stage of integration of gyroscope angular velocity data.

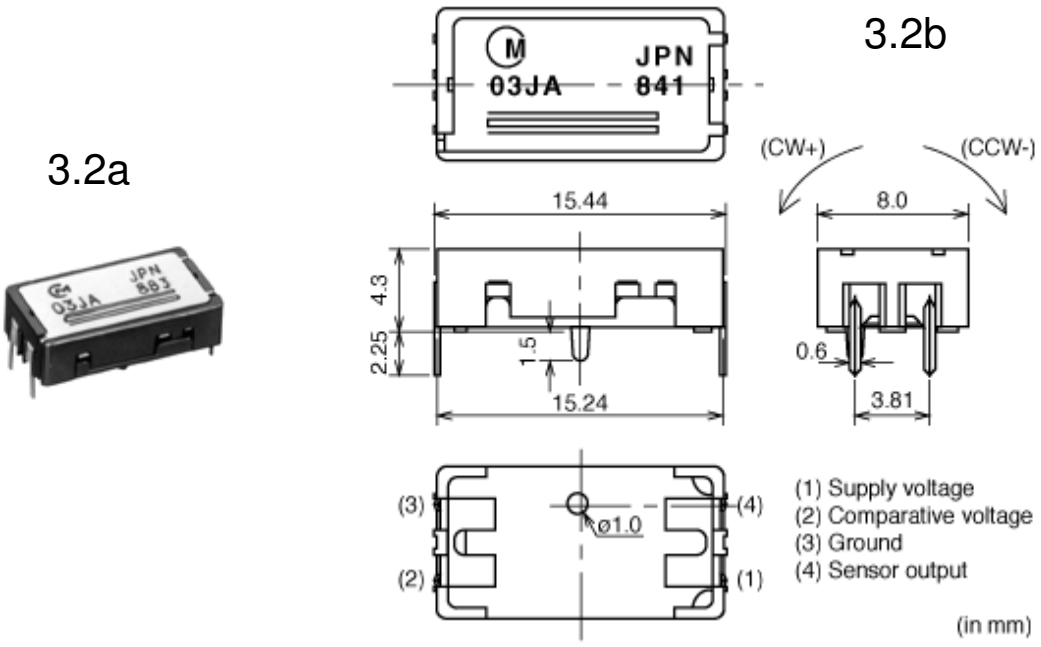

Figure 3.2a and 3.2b Single axis gyroscope (Murata ENC 03JA) and dimensions. Pictures from Murata Manufacturing Co. Ltd.

3.2 Validation of single axis gyroscope

Preliminary testing of the single axis gyroscope was carried out to determine the accuracy and repeatability of the angular displacement data calculated from planar movements of the gyroscope. For this purpose, a pendulum was designed and manufactured, to which the gyroscope could be attached, and with which gyroscope angular displacement data could be validated.

3.2.1 Design of pendulum

A pendulum (Figure 3.3a and 3.3b) was designed and manufactured with dimensions as shown in figure 3.4, to investigate the response of the single axis gyroscope.

The pendulum possessed a number of key features, namely:

(i) The pendulum arm was attached via low friction bearings to allow free swing of the pendulum arm.

(ii) A low friction potentiometer (Vishay Spectrol 157, figure 3.5a and 3.5b) was housed in a metal cylinder at the rear of the solid upright and was firmly secured in place via a plastic cap to prevent movement of the potentiometer body. The shaft of the potentiometer was secured to the pendulum arm in such a way to enable it to measure the angular displacement of the pendulum arm. The potentiometer was connected to a 5V power supply and 16-bit analog-to-digital convertor via cables which were directed down the reverse of the solid upright piece.

(iii) A visual measurement of angular displacement was provided via a 360^{o} protractor attached to the solid upright, and a pointer attached to the top of the pendulum arm. The zero position was measured with the pendulum arm at rest and the pointer vertically upwards. The maximum range of angles used was limited to +/- 90^{o} (see figure 3.4) due to an open section in the potentiometer resulting in a “dead section”. This was also the range within which the pendulum arm would freely swing.

(iv) The pendulum arm had gyroscope attachment sites at 50mm intervals along its length, to allow the gyroscope to be attached at a minimum and maximum distance of 100mm and 550mm respectively from the centre of rotation.

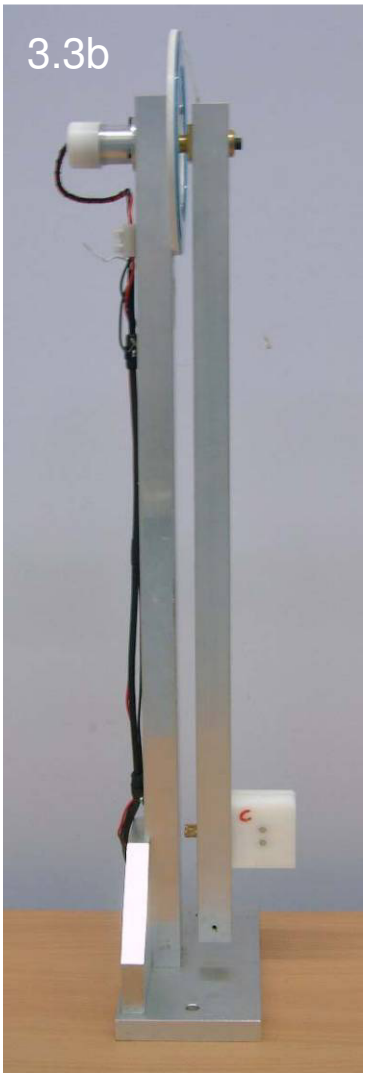

Figure 3.3a and 3.3b Front and side view of pendulum.

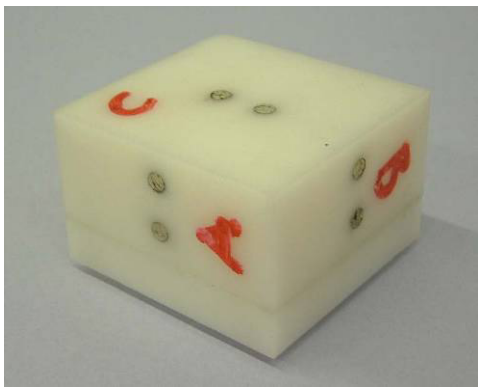

Figure 3.3c Acetal block.

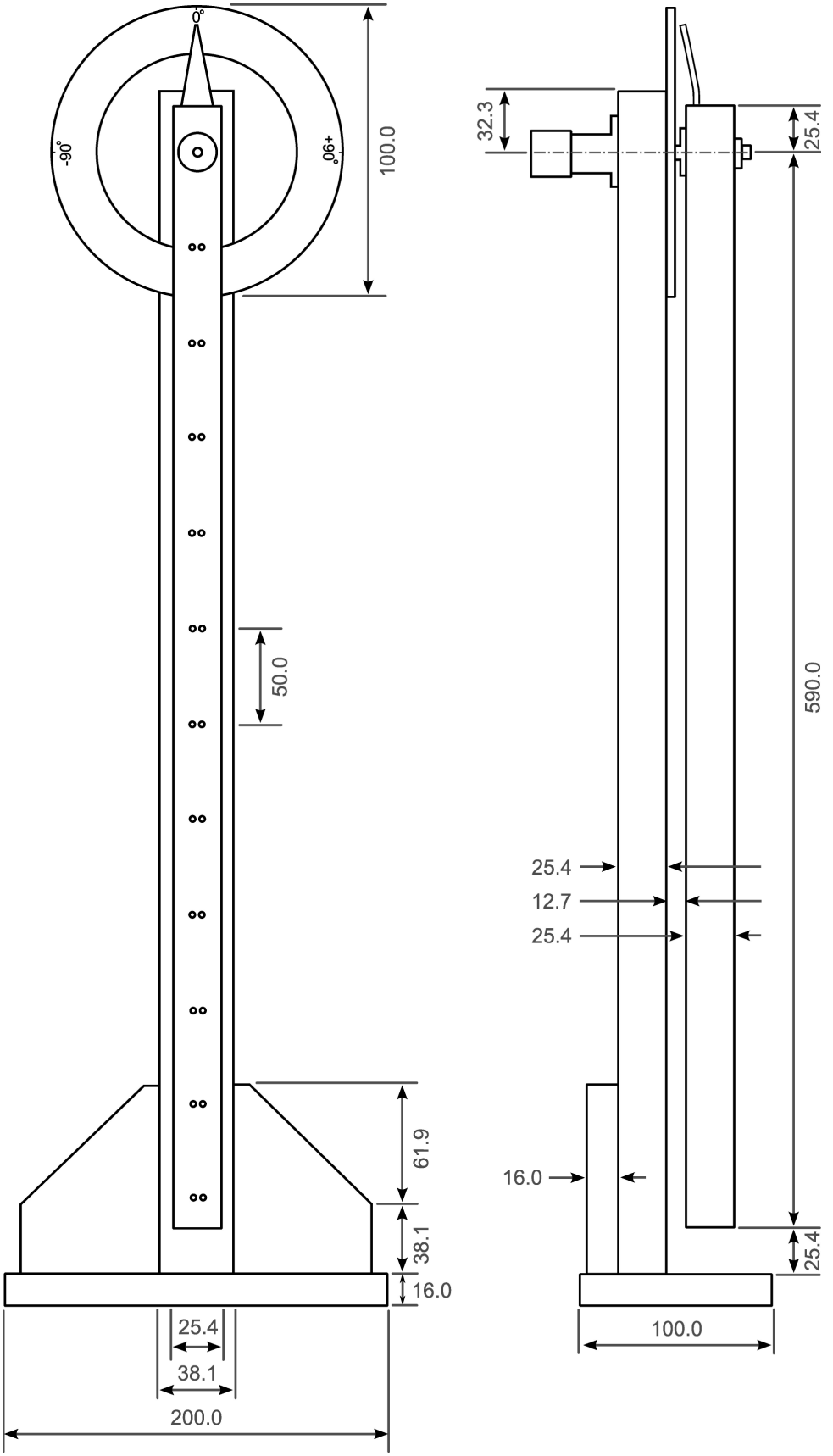

Figure 3.4 Pendulum dimensions in mm

In order to facilitate mounting of the gyroscope onto the pendulum arm, an acetal block (figure 3.3c) was used, in which the gyroscope was encased. The acetal block could be attached in three different orientations A, B and C in order to record data from the sensitive axis of the gyroscope (A) and the other two non-sensitive axes (B and C). The acetal block was securely attached to the pendulum arm via two long metal screws which ensured that there was no relative movement between the acetal block and the pendulum arm.

3.5a

3.5b

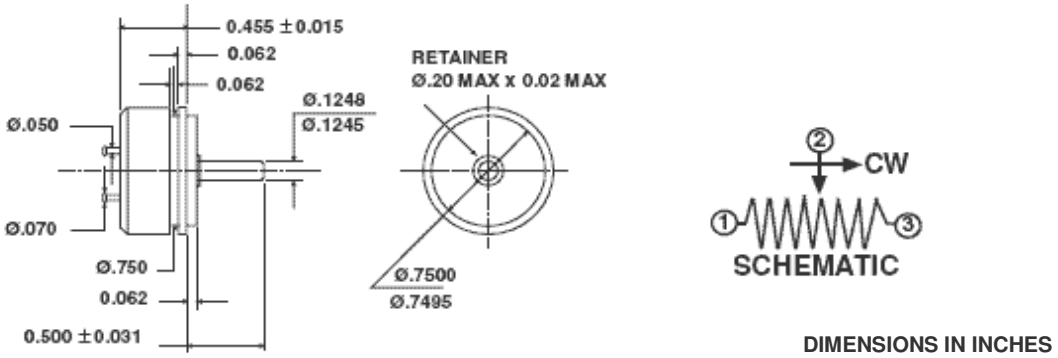

Figure 3.5a and 3.5b Vishay Spectrol 157 low friction potentiometer and dimensions. Pictures from of Vishay Spectrol.

3.2.2 Potentiometer calibration

It was necessary to determine the relationship between the angular displacement of the pendulum arm, and the corresponding potentiometer voltage output. The potentiometer was calibrated over a range of 180^{o} by varying the pendulum angular displacement from -90^{o} to $+90^{o}$ (measured relative to the zero position) in increments of 10^{o}, whilst recording the corresponding voltage output. Five trials were recorded.

A calibration graph of angular displacement versus voltage output is presented in figure 3.6. A straight line was fitted to each curve and a mean R-squared value of 0.99994 was calculated indicating a linear response for all five trials. The low standard deviation value (2.48×10^{-5}) indicated that the potentiometer measurements were highly repeatable with low variability, and that the potentiometer would therefore provide an accurate measure of angular displacement with which to validate gyroscope angular displacement data.

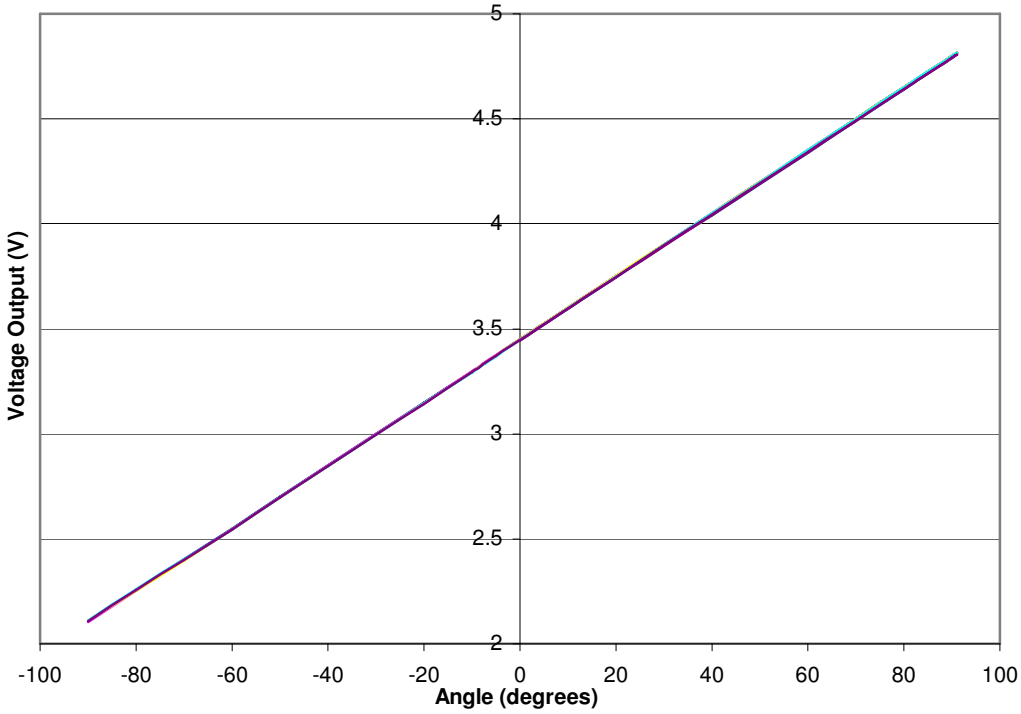

Figure 3.6 Calibration curve of low friction potentiometer showing five trials of varying pendulum arm angular displacement from -90^{o} to $+90^{o}$.

3.2.3 Validation of single axis gyroscope tests

Following potentiometer calibration, the pendulum was used as a validation tool to investigate the output characteristics of the gyroscope, namely the accuracy and repeatability of the gyroscope angular displacement data, sensitivity to linear velocity, and sensitivity to out-of-plane rotation. The pendulum arm was either allowed to swing freely until rest, or was moved in a random manner by the operator.

At the beginning of each trial, the pendulum arm was manually rotated from the zero position to the $+90^{o}$ position and then to the -90^{o} position before being released or randomly moved.

The gyroscope was attached to the pendulum in the following configurations:

1. The accuracy and repeatability of gyroscope angular displacement data

The gyroscope was attached to the pendulum arm in orientation A (sensitive axis) at a distance of 500mm from the pendulum arm rotation centre. The pendulum arm was allowed to swing freely until rest. This was repeated five times. With the same gyroscope configuration, the pendulum arm was then moved randomly by the operator. Again, this was repeated five times.

2. Sensitivity to linear velocity

The gyroscope was attached to the pendulum arm in orientation A (sensitive axis) at a distance of 100mm from the rotation centre and allowed to swing freely until rest. This data was compared with free swing data with the gyroscope attached at 500mm from the rotation centre in orientation A. This was repeated five times for each orientation.

3. Sensitivity to out-of-plane rotation

The gyroscope was attached to the pendulum arm at a distance of 500mm from the rotation centre in orientation A (sensitive axis), followed by B and C (non-sensitive axes) and allowed to freely swing until rest. Five trials were recorded for each orientation.

Following each trial, the pendulum arm was checked to confirm that it had returned to the zero position. Potentiometer and gyroscope data were sampled simultaneously at a frequency of 1080 Hz via a 16-bit analog-to-digital convertor using the Vicon 612 motion analysis system (Oxford Metrics Ltd.). Data were exported in ASCII format for further processing. Raw gyroscope data were filtered in Matlab (Mathworks Inc., MA) using a fourth order low pass Butterworth filter with a cut-off

frequency of 3Hz. Angular velocity was then calculated from the gyroscope data using the following equation:

$$\omega = (V - V_o) / \text{gain} / S_v \quad (3.3)$$

where ω is the angular velocity (deg/s), V is the output voltage (V), V_0 is the static output voltage (V), the gain is 2.78V, and S_v is the scaling factor of 0.67mV/deg/s taken from the manufacturers specifications. Gyroscope angular velocity data were then integrated to obtain angle data for validation with potentiometer data.

3.2.4 Results of single axis gyroscope validation

1. The accuracy and repeatability of gyroscope angular displacement data

Figure 3.7 shows graphs of angle (degrees) against time (s) for the integrated gyroscope output and potentiometer output with the gyroscope attached in orientation A at 500mm from the pendulum rotation centre during free swing movement (figure 3.7a), and random movement (figure 3.7b). These graphs show that for both free swing movement and random movement of the pendulum arm, the integrated gyroscope angular velocity data closely follows that recorded by the potentiometer. The integrated gyroscope data appears to be accurate in the time domain, with a slight underestimation of the potentiometer data in the amplitude domain. The potentiometer calibration indicated that the potentiometer data is accurate and repeatable, and therefore these graphs indicate that the gyroscope data is also accurate. Graphs of all trials can be found in Appendix A.

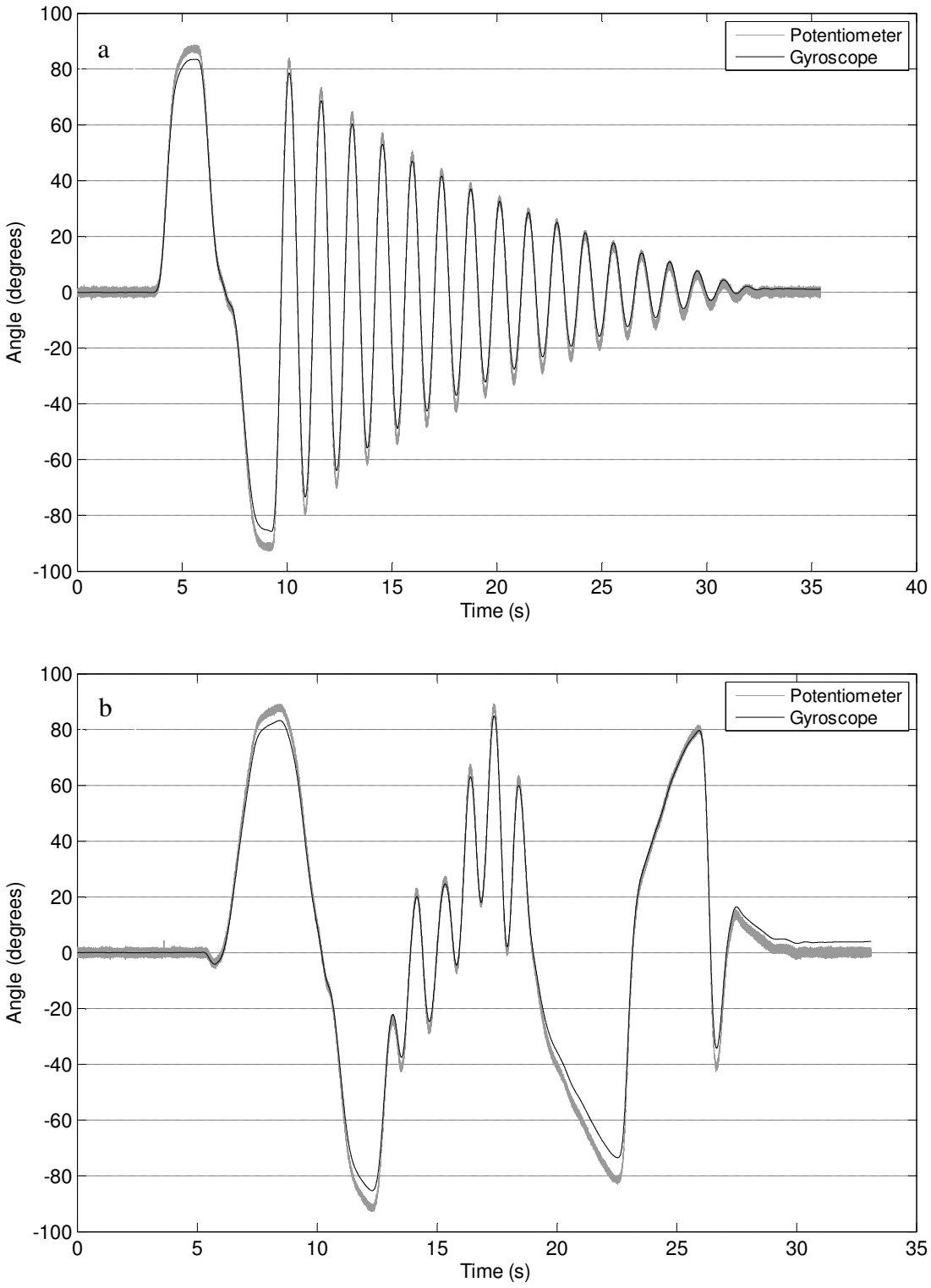

Figure 3.7 Potentiometer and integrated gyroscope data for a) free swing with gyroscope attached in position A and 500mm from pendulum rotation centre, and b) random movement with gyroscope attached in position A and 500mm from pendulum rotation centre.

Correlation values were calculated for potentiometer and integrated gyroscope data for each of the five trials of free swing and random movement of the pendulum. The results are presented below in table 3.1:

Trial	Free swing	Random
1	0.999458	0.999383
2	0.999072	0.999030
3	0.998224	0.999082
4	0.999031	0.999490
5	0.999601	0.999744
Average	0.999077	0.999350
SD	0.000536	0.000300

Table 3.1 Correlation values for integrated gyroscope and potentiometer data for free swing and random movement.

Table 3.1 shows that all of the correlation values approximate to a value of +1 for both free swing and random movement, indicating a strong linear relationship between integrated gyroscope and potentiometer data. The high mean correlation values (0.999077 and 0.99935) and low SD values (5.36×10^{-4} and 3.0×10^{-4}) indicate that the integrated gyroscope data is highly repeatable.

2. Sensitivity to linear velocity

Table 3.2 shows the correlation values for data recorded from the sensitive axis (A) with the gyroscope attached at a distance of 100mm and 500mm from the pendulum rotation centre.

Trial	100mm free swing	500mm free swing
1	0.999235	0.999458
2	0.999307	0.999072
3	0.998239	0.998224
4	0.998472	0.999031
5	0.999437	0.999601
Average	0.998940	0.999077
SD	0.000540	0.000536

Table 3.2 Correlation values for integrated gyroscope and potentiometer data for free swing at 100mm and 500mm from rotation centre.

Table 3.2 shows that all correlation values approximate to +1 for data recorded at 100mm and 500mm from the pendulum rotation centre indicating a strong linear association. The low standard deviation values ($5.4x10^{-4}$ and $5.36x10^{-4}$ for 100mm and 500mm free swing respectively) indicate that both sets of data are accurate and highly repeatable. In addition, the consistent correlation values for both 100mm and 500mm free swing (mean values 0.99894 and 0.999077 respectively) indicated that the distance of the gyroscope from the pendulum rotation centre had little affect on its output and the gyroscope is not affected by linear velocity.

3. Sensitivity to out-of-plane rotation

Table 3.3 shows the correlation values for data recorded from the sensitive axis (A) and the two non-sensitive axes (B and C).

Trial	Axis A	Axis B	Axis C
1	0.999458	-0.47085	-0.40729
2	0.999072	-0.07493	-0.07838
3	0.998224	-0.16615	-0.25240
4	0.999031	-0.32807	-0.37984
5	0.999601	-0.09883	-0.25466
Average	0.999077	-0.22780	-0.27450
SD	0.000536	0.16803	0.13046

Table 3.3 Correlation values for integrated gyroscope and potentiometer data for free swing movement recorded from Axis A (sensitive axis) and axes B and C (non-sensitive axes).

Table 3.3 shows that integrated gyroscope data for axis A is highly correlated with potentiometer data with values approximating +1 indicating a strong linear association. As expected, correlation values for axes B and C are much lower than those for axis A. Mean correlation values of -0.2278 and -0.2745 for axes B and C respectively indicate that integrated gyroscope data is not strongly associated with potentiometer data recorded from rotations about non-sensitive axes.

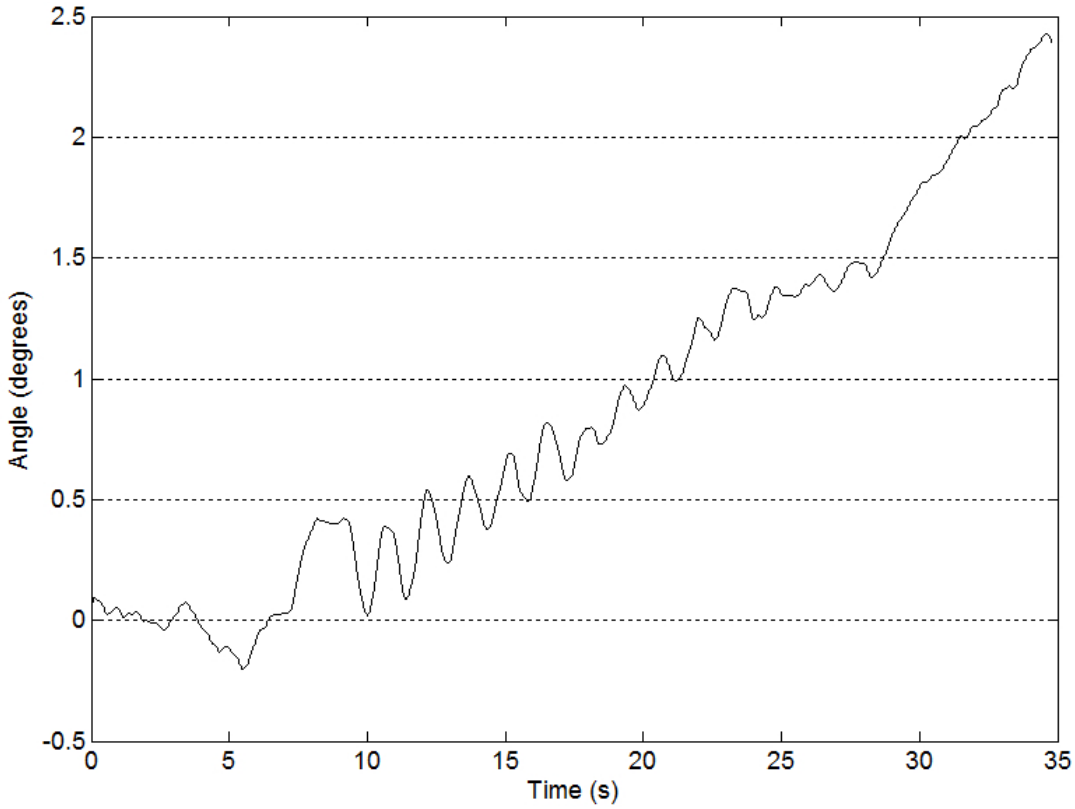

Figure 3.8 Integrated gyroscope output with gyroscope attached in position B (non-sensitive axis) 500mm from pendulum rotation centre. (Correlation value -0.1662)

Figure 3.8 shows a graph of angle (degrees) against time (s) for free swing movement of the gyroscope when attached in orientation B (non-sensitive axis). It can be seen that the gyroscope data shows an angular output which increases with time when recording from orientation B, and this was also seen when recording from orientation C. This increase in angular output may occur due to cumulative errors from the integration process. For the purposes of this study each upper limb activity tested with the 3D gyroscope system was therefore limited to a maximum of 20s in order to reduce the effect of cumulative integration error.

3.3 The 3D gyroscope system

This section describes the components of the 3D gyroscope system, developed following the validation of single axis gyroscope angular displacement data.

3.3.1 Plastic housing

A plastic housing (figure 3.9a and 3.9b) was designed and manufactured to hold three single axis gyroscopes (Murata ENC 03JA) in an orthogonal orientation to allow the recording of angular velocity in three dimensions. The plastic housing was manufactured from acetal to the dimensions shown in figure 3.10 and consisted of three components as follows:

1. An inner core to which the gyroscopes were mounted
2. A circular base
3. A conical shaped lid.

The plastic housing was designed to hold each of the three gyroscopes securely in their orthogonal orientations while at the same time being space efficient and aesthetically shaped. The three gyroscopes were mounted to the inner core within three channels machined to the same dimensions of the gyroscope for a close fit. The gyroscopes were attached using adhesive glue and the vertically orientated gyroscope was held in place via a horizontal plastic bar. Further security was provided by the circular base and conical shaped lid. The thin wires connected to each gyroscope were directed through small channels and met in the central cavity of the inner core to form one cable. This cable was routed out of the plastic housing via a channel in the inner core.

The 3D gyroscope unit is small (40mm diameter and 25mm high) and lightweight, weighing approximately 20g. The plastic housing was designed to be both space efficient by enclosing gyroscopes and wires within grooves that had been machined into the plastic core, and sturdy. Its circular shape and conical shaped lid minimised weight and bulk in order that the 3D gyroscope unit would be more readily acceptable to the subject.

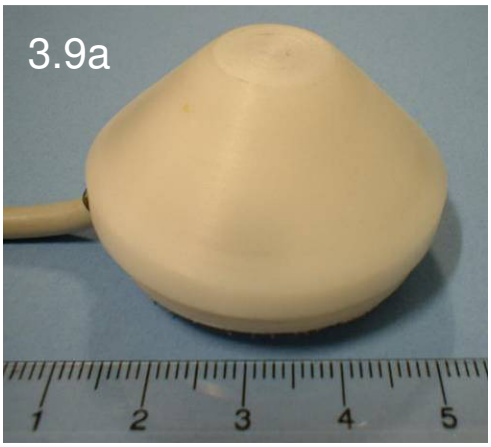

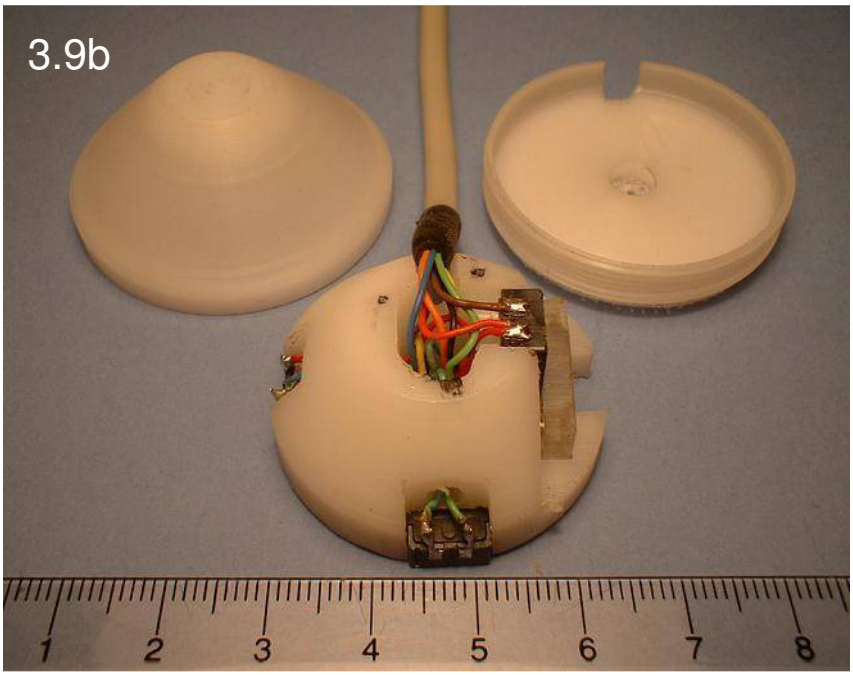

Figure 3.9a One 3D gyroscope unit and **Figure 3.9b** The three components of the plastic housing.

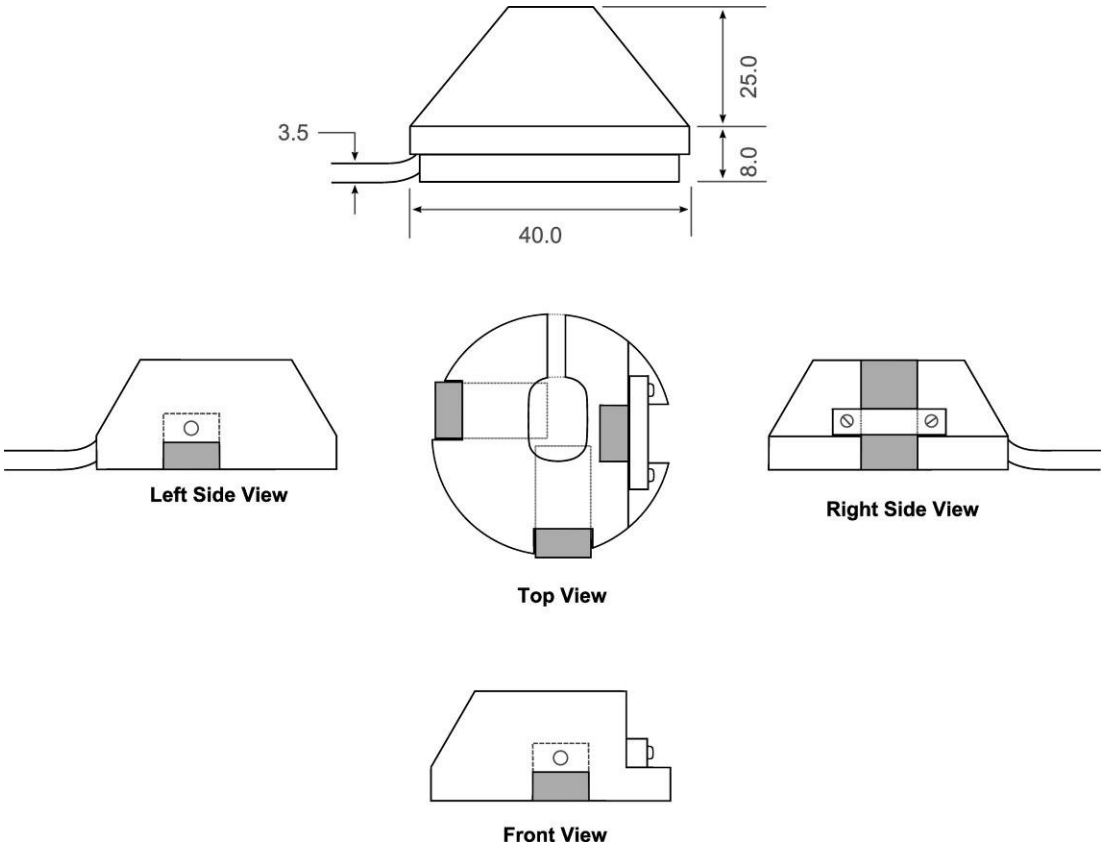

Figure 3.10 Outer dimensions and inner core of a 3D gyroscope unit

3.3.2 Components of the 3D gyroscope system

The 3D gyroscope system consisted of three identical units as described above, using a total of nine single axis gyroscopes. A nine channel amplifier circuit was built and enclosed in a plastic box alongside a +/-5V power supply. Each gyroscope unit was connected to this amplifier circuit via a 2.1m long cable which allowed a safe distance between the subject and the power supply. The long cable also enabled each gyroscope unit to be mounted onto the body independently of the other system components, thereby minimising the size and weight of the gyroscope unit so as not to affect the production of movement when attached to the upper limb of the subject. Gyroscope output data were sampled via an analog-to-digital convertor (National Instruments DAQCard – 6036E) in a laptop computer using a custom written LabVIEW programme.

3.4 Definition of 3D gyroscope coordinate system

When mounted onto the trunk, upper arm and forearm, the 3D gyroscope coordinate system was orientated as shown in figure 3.11. The trunk gyroscope unit was mounted on the subject's back as described in section 5.2.2. Each axis of the 3D gyroscope unit corresponded to the longitudinal sensitive axis of one planar gyroscope mounted within the plastic housing. The three rotations θ_x, θ_y and θ_z about the X_{gyro}, Y_{gyro} and Z_{gyro} axes of one gyroscope unit occur independently and positive rotations are defined as clockwise about the axis of rotation using a right-hand system.

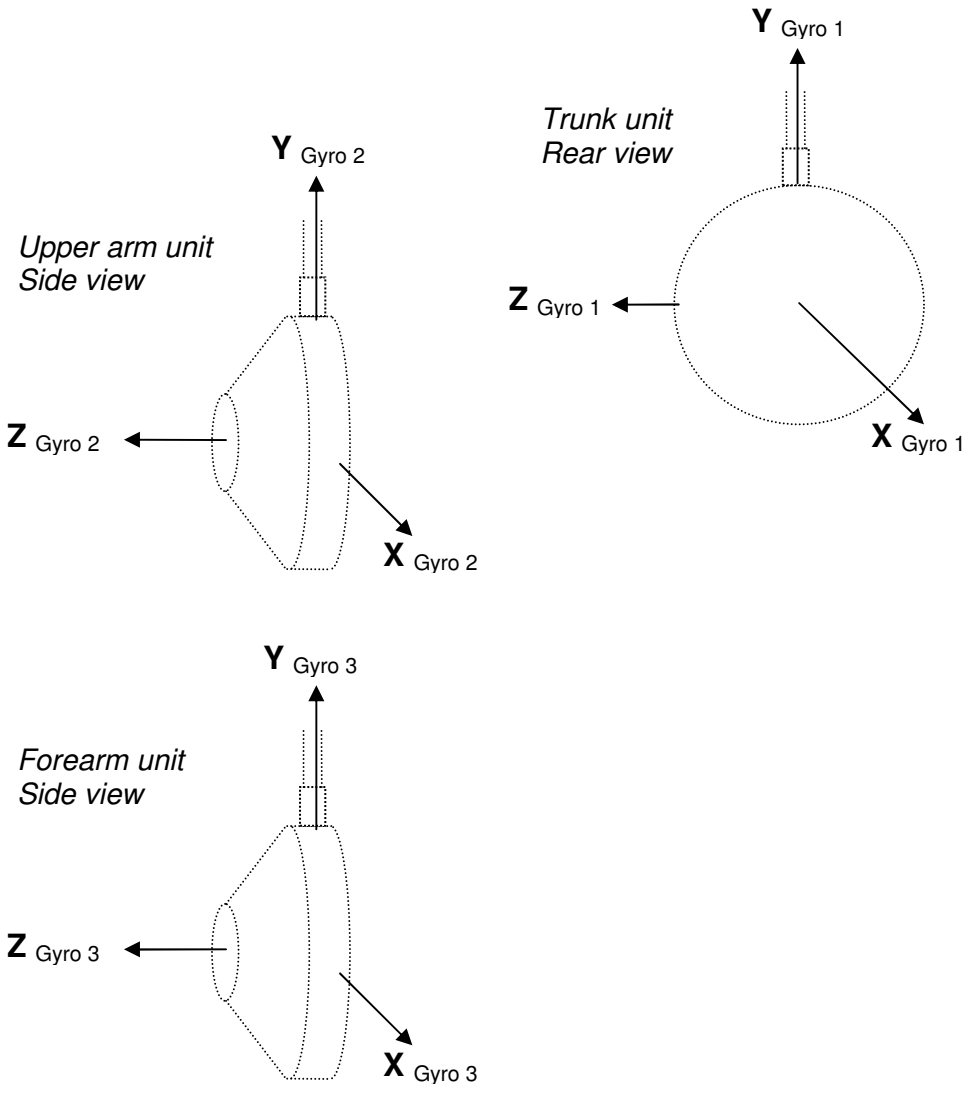

Figure 3.11 3D gyroscope coordinate system of the trunk, upper arm, and forearm 3D gyroscope units

3.5 Pendulum testing of the 3D gyroscope system

The output characteristics of each of the three 3D gyroscope units were investigated using the pendulum described in section 3.2.1. Each 3D gyroscope unit was mounted on to the pendulum arm at a distance of 500mm from the pendulum arm rotation centre via Velcro discs attached to both the acetal block and the underside of each 3D gyroscope unit. This allowed the 3D gyroscope unit to be mounted in three different orientations. Each orientation involved one axis of the gyroscope unit parallel with the rotation axis of the pendulum arm, and the other two axes perpendicular to the pendulum arm rotation axis. Data were sampled simultaneously from all three gyroscopes whilst the pendulum was allowed to swing freely until rest. As with validation of the single axis gyroscope, tests were carried out over a range of 180^{o} (from -90^{o} to $+90^{o}$ measured relative to the zero position) as this was the range within which the pendulum arm would freely swing. Gyroscope data were sampled via an A-D card (National Instruments DAQ Card-6036E) in a laptop computer, and potentiometer data were sampled simultaneously via a 16-bit analog-to-digital convertor. Data were sampled from three orientations from each gyroscope unit, and the correlation values for integrated gyroscope and potentiometer data for all nine gyroscopes are presented in table 3.4.

3D Gyroscope Unit 1			3D Gyroscope Unit 2			3D Gyroscope Unit 3		
X	Y	Z	X	Y	Z	X	Y	Z
0.0519	0.1998	**0.9872**	-0.0613	-0.0418	**0.9518**	-0.1714	0.1368	**0.9962**
-0.5810	**0.9777**	-0.0306	-0.2594	**0.9629**	-0.1389	0.1026	**0.9940**	-0.2271
-0.9972	-0.4896	0.1186	**-0.9943**	-0.4460	-0.0752	**-0.9670**	0.0391	-0.0067

Table 3.4 Correlation values of gyroscope and potentiometer data for all nine gyroscopes of the 3D gyroscope system. Numbers in bold indicate the gyroscope unit axis aligned with the pendulum arm rotation axis.

Table 3.4 shows that correlation values corresponding to the 3D gyroscope unit axis aligned with the pendulum arm rotation axis approximated a value of 1 indicating a strong linear relationship between the integrated gyroscope and potentiometer data

for free swing movement. It must be noted that positive and negative correlation values indicate the direction of rotation about the gyroscope axis (a positive correlation value is obtained from clockwise rotation about the 3D gyroscope unit axis, and a negative value is obtained from counter clockwise rotation). This is a direct result of the orientation of the 3D gyroscope unit when mounted onto the pendulum arm. Correlation values for the two non-sensitive axes of the gyroscope unit are much lower than those for the sensitive gyroscope unit axis, indicating that integrated gyroscope data is not strongly associated with potentiometer data during out-of-plane rotations. For three gyroscopes, correlation values of between 0.446 to -0.581 were recorded for out-of-plane rotations and indicate minor temporal association in angle data during pendulum swing.

3.6 Conclusion

This chapter has described the development and components of the 3D gyroscope system and the experimental techniques for validation of the single axis gyroscope. The integrated angular velocity data from the single axis gyroscope showed a strong linear association with potentiometer data and indicated that the gyroscope output was reliable and repeatable. While the integrated gyroscope data from out-of-plane rotation was not strongly associated with potentiometer data, the results indicated that errors in gyroscope angular displacement data may arise due to cumulative errors from the integration process. Therefore, the testing period for each upper limb activity investigated in this study was limited to a maximum of 20s in order to reduce the effect of cumulative integration error. The upper limb activities investigated are described in Chapter 5.

Chapter 4: 3D kinematics of the upper limb

This chapter gives a description of the techniques used in this thesis for the description of 3D upper limb kinematics. Details of the techniques used for the collection of kinematic data are given in Chapter 5 together with an overview of the data analysis steps taken for the calculation of joint kinematics from the 3D gyroscope system.

4.1 Kinematics

Kinematics is the study of body motion in space without reference to the forces which cause the motion. The study of kinematics provides a quantitative description of movement for the study of joint and muscle function, and clinically useful information for the treatment of patients with pathological movement disorders and for the planning and assessment of surgical interventions.

To fully describe the kinematics of the upper limb, the three dimensional position and orientation in space of the limb segments must be known at each instant in time. For kinematic analysis, limb segments are assumed to be rigid bodies. That is, they do not deform and the distance between any two points on a body does not change. This assumption enables the limb segment to be represented by an orthogonal bone-embedded coordinate system which moves rigidly with the bone, and whose position and orientation can be mathematically described in 3D space. Joint kinematics can then be described by the relative change in position and orientation between two bone-embedded coordinate systems.

4.2 Position and orientation

Any point in space can be described with respect to a global coordinate system as follows and shown in figure 4.1:

$$^{G}p = [p_i\, p_j\, p_k] \tag{4.1}$$

where ^{G}p is the position vector of point p in the global frame, G.

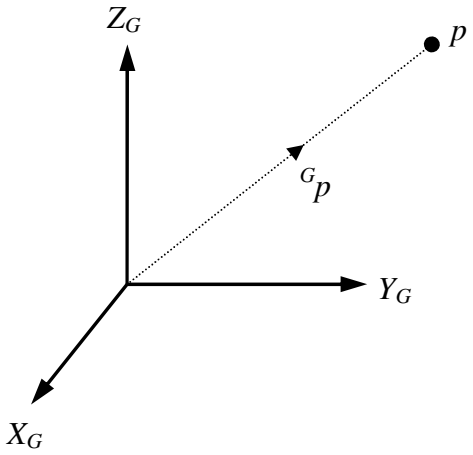

Figure 4.1 Position of point *p* in the global coordinate system.

The orientation of any bone-embedded coordinate system with respect to the global system, as shown in figure 4.2, can be described by a 3 by 3 rotation matrix as follows:

$$ {}^{G}_{A}R = \begin{bmatrix} r_{11} & r_{12} & r_{13} \\ r_{21} & r_{22} & r_{23} \\ r_{31} & r_{32} & r_{33} \end{bmatrix} = \begin{bmatrix} \mathbf{\imath} \cdot \mathbf{I} & \mathbf{\imath} \cdot \mathbf{J} & \mathbf{\imath} \cdot \mathbf{K} \\ \mathbf{j} \cdot \mathbf{I} & \mathbf{j} \cdot \mathbf{J} & \mathbf{j} \cdot \mathbf{K} \\ \mathbf{\kappa} \cdot \mathbf{I} & \mathbf{\kappa} \cdot \mathbf{J} & \mathbf{\kappa} \cdot \mathbf{K} \end{bmatrix} \tag{4.2} $$

where ${}^{G}_{A}R$ describes the orientation of frame A relative to the global frame, G, and i,j,k and I,J,K are the unit vectors of frame A and frame G respectively.

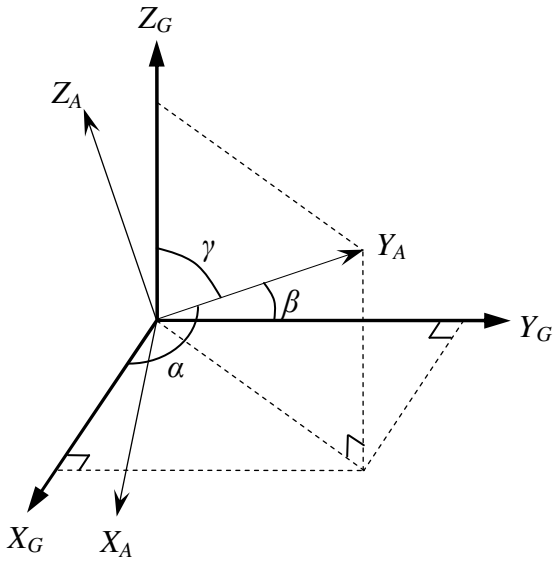

Figure 4.2 Orientation of frame A with respect to the global frame, G, showing the direction angles of Y_A with respect to the three coordinate axes of frame G.

The rotation matrix, ${}^{G}_{A}R$, is also termed the direction cosine matrix because each of its nine components are the cosines of the direction angles between the unit vector coordinate axes of the bone-embedded frame A, and those of the global frame, G. i.e. for the example illustrated in figure 4.2, the cosines of the angles α, β and γ give the three components of the second row of the rotation matrix, r_{21}, r_{22}, and r_{23}, where $r_{21} = \cos\alpha$, $r_{22} = \cos\beta$, $r_{23} = \cos\gamma$. The rotation matrix can also be used to describe a rotation from one orientation to another, as described in section 4.4 below.

4.3 Transformation

The rotation matrix described above allows the position of any point in system A, ${}^{A}p$, to be represented as a point in the global system, ${}^{G}p$, by the following transformation:

$$ {}^{G}p = {}^{G}_{A}R \cdot {}^{A}p + {}^{G}_{A}O \tag{4.3}$$

Where ${}^{G}_{A}O$ is the origin of the bone-embedded frame A expressed in the global system.

Conversely, any point in the global system, G, can be represented as a point in system A by the following:

$$ {}^{A}p = {}^{G}_{A}R^{-1} \cdot ({}^{G}p - {}^{G}_{A}O) \tag{4.4}$$

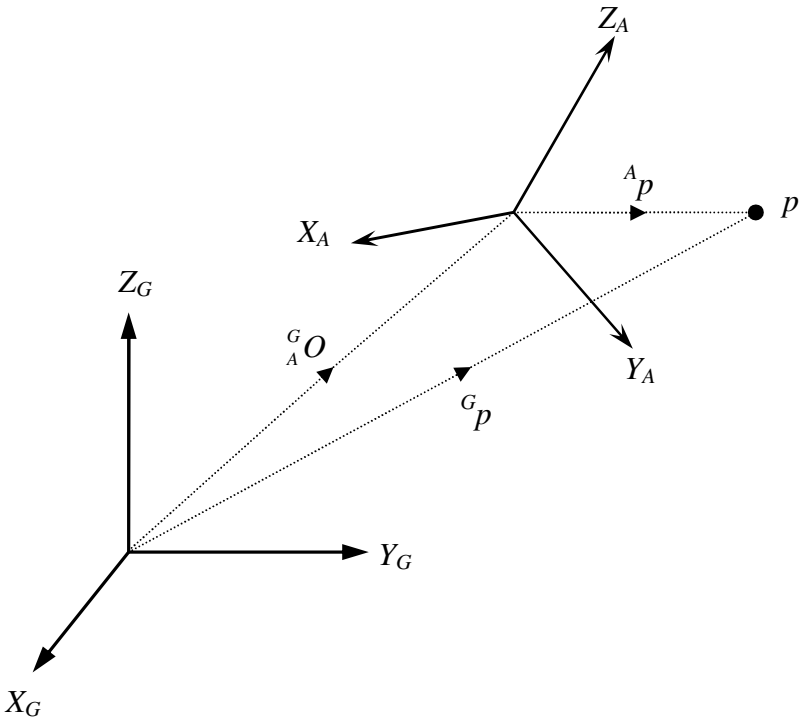

Figure 4.3 Transformation of point *p* between frame A and global frame G.

The rotation matrix also enables the description of the orientation of any local frame relative to another as shown in figure 4.4 and described below:

$$ {}^{A}_{B}R = {}^{G}_{B}R \cdot {}^{G}_{A}R^{-1} \tag{4.5} $$

where ${}^{A}_{B}R$ is the orientation of frame B relative to frame A.

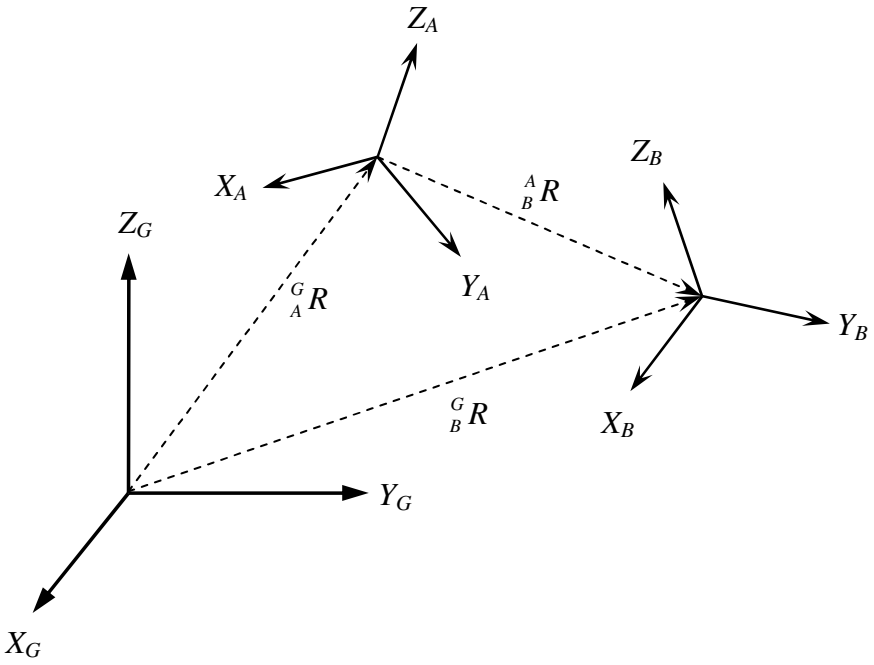

Figure 4.4 Orientation of frame B with respect to frame A.

4.4 Rotation

Rotation is a motion with three degrees of freedom, and the rotation matrix introduced in section 4.2 can be described in terms of a sequence of three rotations about defined axes. If α, β and γ represent angular rotation about the axes X, Y and Z respectively, three independent rotation matrices, Rα, Rβ and Rγ can be defined which completely describe the rotation of the bone-embedded coordinate system as follows:

For a rotation through angle α about the X axis:

$$R\alpha = \begin{bmatrix} 1 & 0 & 0 \\ 0 & \cos\alpha & \sin\alpha \\ 0 & -\sin\alpha & \cos\alpha \end{bmatrix} \tag{4.6}$$

For a rotation through angle β about the Y axis:

$$R\beta = \begin{bmatrix} \cos\beta & 0 & -\sin\beta \\ 0 & 1 & 0 \\ \sin\beta & 0 & \cos\beta \end{bmatrix} \tag{4.7}$$

For a rotation through angle γ about the Z axis:

$$R\gamma = \begin{bmatrix} \cos\gamma & \sin\gamma & 0 \\ -\sin\gamma & \cos\gamma & 0 \\ 0 & 0 & 1 \end{bmatrix} \tag{4.8}$$

Rotations can be global rotations, occurring about the three axes of the fixed global coordinate system, or body fixed rotations, occurring about the three axes of the moving bone-embedded frame. For a sequence of three rotations, the resulting transformation will differ according to the defined axes, and the order in which the rotations occur. Two commonly used techniques to describe joint rotations are the Euler and Cardan angle technique, and the floating axis technique, described in sections 4.4.1 and 4.4.2 below.

4.4.1 Euler and Cardan angles

The three independent rotation matrices Rα, Rβ, Rγ described above, can be combined as a sequence of three successive and ordered rotations to obtain a single rotation matrix which completely describes the rotation of a bone-embedded frame from one orientation to another. Combining the three rotation matrices changes the orientation of the bone-embedded frame from an XYZ system, to an X'''Y'''Z''' system through two intermediate frames (X'Y'Z' and X''Y''Z'') as shown in figure 4.5.

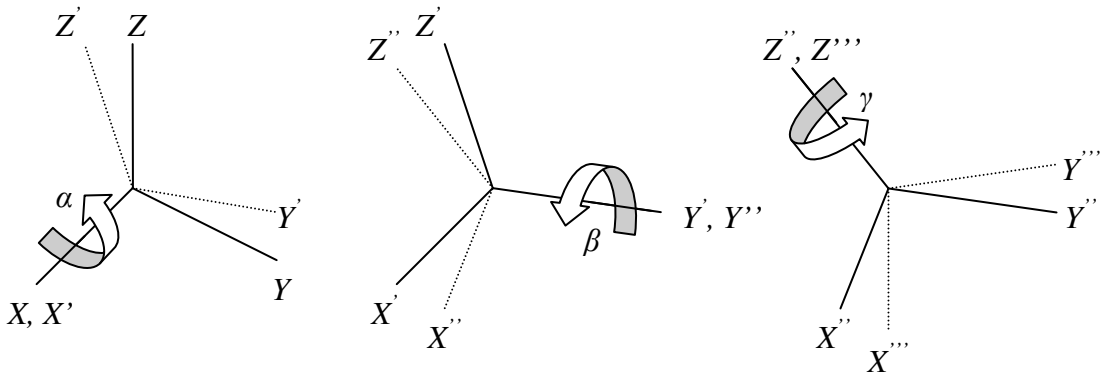

Figure 4.5 Three successive rotations about the bone-embedded frame axes to change the orientation from the ZXY system to the Z'''X'''Y''' system. The intermediate frames are denoted as X'Y'Z' and X''Y''Z'' respectively.

If a bone-embedded frame A is rotated through an α-β-γ sequence (where frame A is initially coincident with global frame G), a rotation matrix ${}^{G}_{A}R$ can be expressed as an ordered and sequential multiplication of the rotation matrices Rα, Rβ, and Rγ as follows:

$$ {}^{G}_{A}R = R\gamma R\beta R\alpha \tag{4.9} $$

$$ {}^{G}_{A}R = \begin{bmatrix} \cos\gamma & \sin\gamma & 0 \\ -\sin\gamma & \cos\gamma & 0 \\ 0 & 0 & 1 \end{bmatrix} \begin{bmatrix} \cos\beta & 0 & -\sin\beta \\ 0 & 1 & 0 \\ \sin\beta & 0 & \cos\beta \end{bmatrix} \begin{bmatrix} 1 & 0 & 0 \\ 0 & \cos\alpha & \sin\alpha \\ 0 & -\sin\alpha & \cos\alpha \end{bmatrix} \tag{4.10} $$

$$ {}^{G}_{A}R = \begin{bmatrix} \cos\beta\cos\gamma & \sin\alpha\sin\beta\cos\gamma + \cos\alpha\sin\gamma & -\cos\alpha\sin\beta\cos\gamma + \sin\alpha\sin\gamma \\ -\cos\beta\sin\gamma & -\sin\alpha\sin\beta\sin\gamma + \cos\alpha\cos\gamma & \cos\alpha\sin\beta\sin\gamma + \sin\alpha\cos\gamma \\ \sin\beta & -\sin\alpha\cos\beta & \cos\alpha\cos\beta \end{bmatrix} \tag{4.11} $$

The order of multiplication of the Rα, Rβ, and Rγ matrices is the opposite of the order of rotation of the angles α, β and γ. Since matrix multiplication is non-commutative, the resulting rotation matrix ${}^{G}_{A}R$ (equation 4.11) is therefore sequence dependent and a different form of ${}^{G}_{A}R$ will be obtained according to the angle

rotation sequence chosen. Rotation angles in which the first and the third rotations occur around the same axis (often called α-β-α-type rotations) are termed Euler angles. Cardan angles are a form of Euler angle but involve sequential rotations around all three coordinate axes in an α-β-γ-type sequence.

A disadvantage of using Euler/Cardan angles is the sequence dependency of the three rotations. Numerous rotation orders are possible (12 Eulerian sequences, 6 of which are Cardanian) and this, combined with the lack of standardised rotation orders in the literature, leads to difficulty in comparing kinematic results between studies. Furthermore, the Euler/Cardan angles do not directly correspond with the anatomical joint angles, which are actually the Euler/Cardan angles projected onto the clinical reference frame. This is due to the rotation around two intermediate frames which are not coincident with the clinical planes of motion. Therefore it is difficult to assign clinical meaning to the angles. Gimbal lock is an inherent problem of this technique and occurs when the first and the third rotation axes become aligned in the second rotation, when $\beta = \pm 90^{o}$. Gimbal lock is difficult to avoid at the shoulder joint due to the large range of motion possible, however its effects can be minimised by an appropriate choice of local coordinate system and rotation order (de Groot, 1997).

4.4.2 Floating axis technique

The floating axis technique is a joint coordinate system proposed by Grood and Suntay (1983) who applied the method to describe knee joint kinematics. The relative orientation between two adjacent segments is described in terms of three rotations, as for Euler and Cardan angles, around three unit vectors denoted as e_1, e_2, and e_3, however the joint axes used are not necessarily orthogonal. Two axes are body fixed axes; the first, e_1, is fixed in the proximal limb segment and represents flexion/extension; the second, e_3, is fixed in the distal limb segment and represents rotation about the segment's long axis. The third axis, e_2, is a floating axis which is mutually perpendicular to both e_1 and e_3, and represents abduction/adduction of the joint. The floating axis is so named because it is not fixed in either body segment and moves in relation to both. Joint kinematics derived from this method are

commonly defined by the rotation of the distal segment relative to the proximal segment. Cole et al. (1993) modified Grood and Suntay's proposed JCS in order that the method would be applicable in the general case. The floating axis system is illustrated in figure 4.6 and described below:

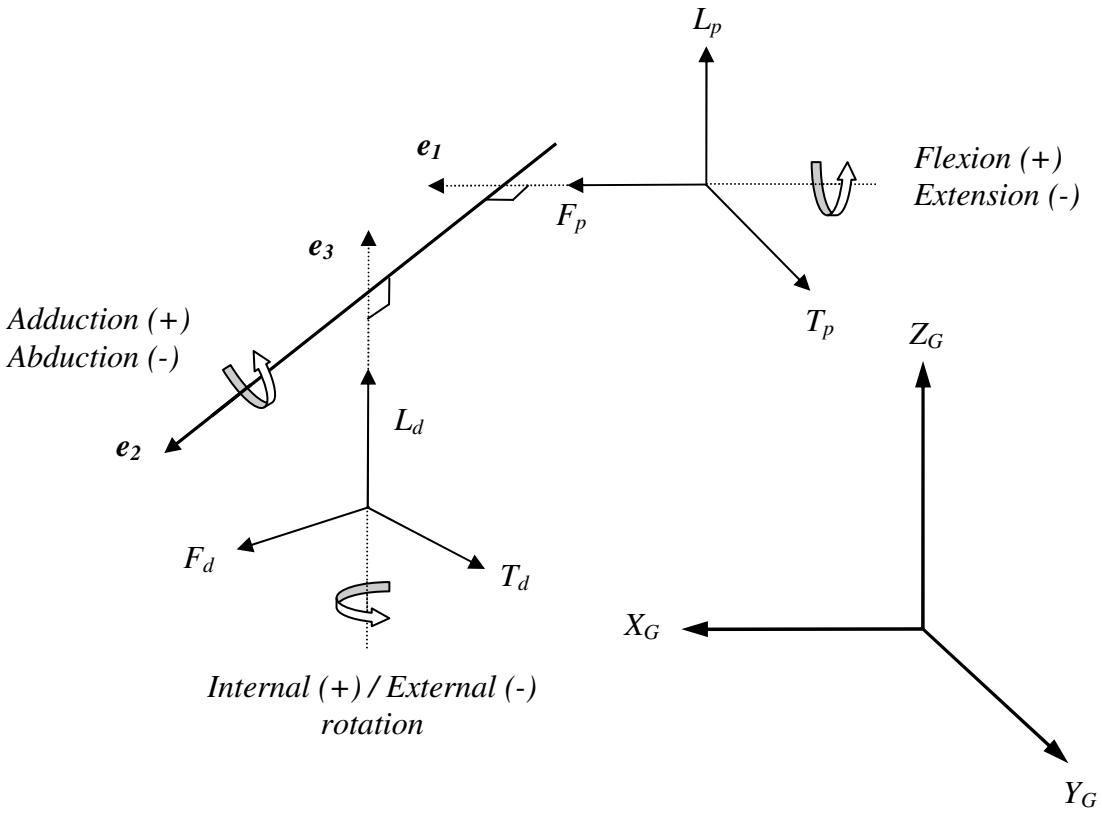

Figure 4.6 The floating axis system proposed by Grood and Suntay, (1983) and modified by Cole et al. (1993).

Cole et al. renamed segment axes with F (axis of flexion), L (longitudinal axis) and T (third axis as a cross product of the flexion and longitudinal axes). Thus, if the axes of the proximal segment are F_p, L_p, T_p, and the axes of the distal segment are F_d, L_d, T_d, then the joint coordinate system is given by e_1, e_2, and e_3 as follows:

$$e_1 = F_p \tag{4.12}$$

$$e_3 = L_d \tag{4.13}$$

$$e_2 = \frac{e_3 \wedge e_1}{\left| e_3 \wedge e_1 \right|} \cdot A \tag{4.14}$$

Where $A = -1$ if $(e_3 \wedge e_1) \cdot Y_d < 0$ and $((e_3 \wedge e_1) \wedge e_3) \cdot X_d > 0$

Otherwise $A = +1$ (4.15)

The three angles describing the joint rotation can then be calculated as follows:

$$\theta_1 = \cos^{-1}(e_2 \cdot T_p) \cdot \text{sign}(e_2 \cdot L_p) \tag{4.16}$$

$$\theta_2 = \cos^{-1}(r \cdot L_d) \cdot \text{sign}(F_p \cdot L_p) \text{ where } r = \frac{F_p \wedge e_2}{\left| F_p \wedge e_2 \right|} \tag{4.17}$$

$$\theta_3 = \cos^{-1}(e_2 \cdot T_d) \cdot \text{sign}(e_2 \cdot F_d) \tag{4.18}$$

The joint angles obtained using this technique are easy to visualise and clinically intuitive. It can be seen that the floating axis technique does indeed follow a Cardan angle sequence about specified axes (the second rotation is about the floating axis, and the first and third rotations are about the proximal and distal body fixed axes), and as such is susceptible to gimbal lock at $\pm 90^o$ abduction.

4.5 Bony anatomy

A Cartesian coordinate system must be specified for each limb segment in order to mathematically describe the relative rotations between them, as described in sections 4.1 to 4.4 above. For repeatability and to enable comparison between subjects, the definitions of the bone-embedded coordinate systems are based on the location of anatomical landmarks and are therefore termed anatomical coordinate systems. Before the coordinate systems for the thorax, upper arm, forearm, and hand can be defined, a brief description of the upper limb bony anatomy must be given.

The humerus

The humerus is the long bone which forms the upper arm, and extends from the scapula to the elbow. Proximally, the head of the humerus articulates with the glenoid fossa of the scapula. Below the head are the greater and lesser tubercles which lie on the antero-lateral and anterior surface respectively. These are rounded projections which form important sites for muscle attachment, separated by the intertubercular groove which accommodates a large tendon.

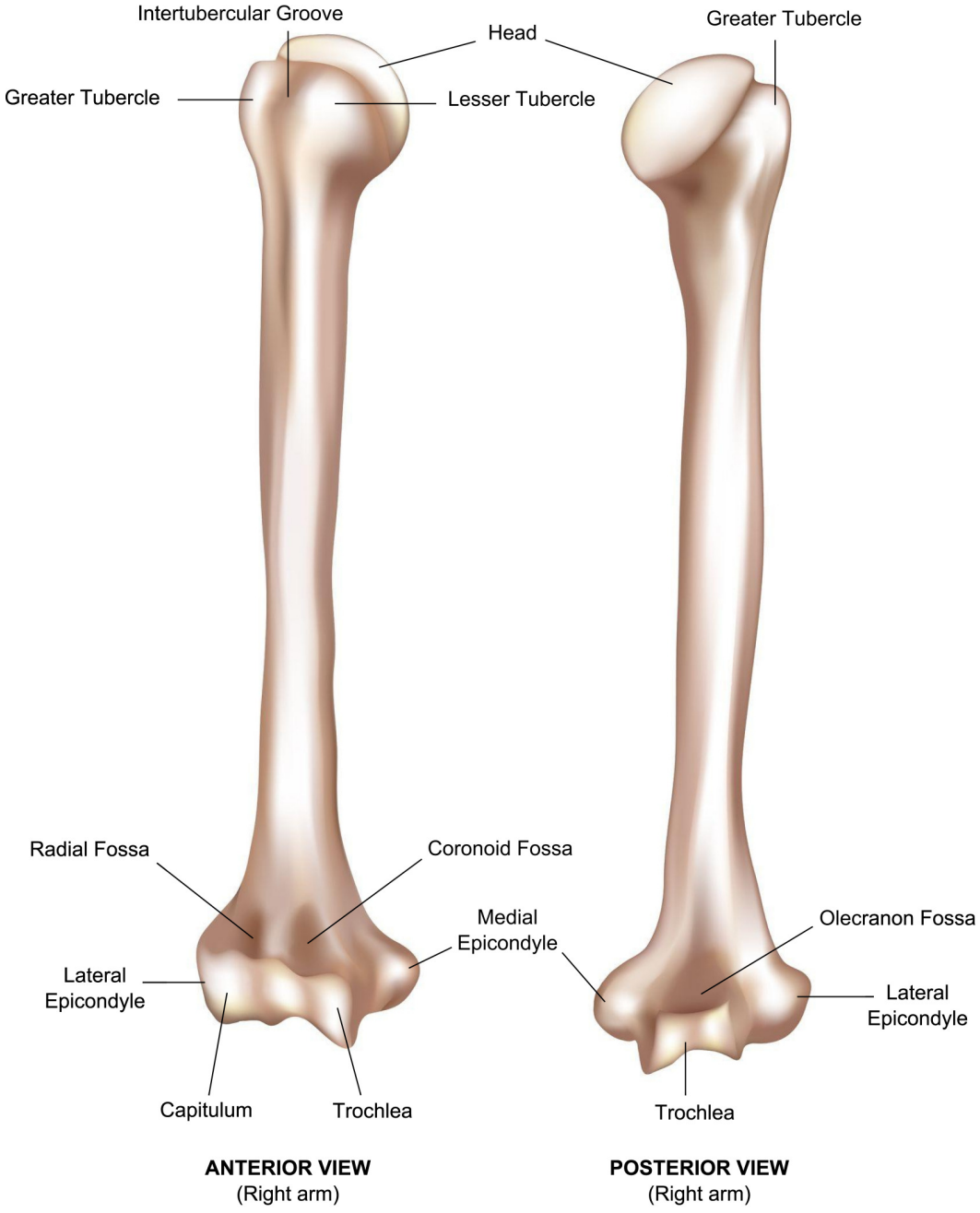

Figure 4.7 The humerus

At the distal end the shaft expands to either side to form the medial and lateral epicondyles. The humerus articulates with the bones of the forearm at the trochlea and capitulum, which together form the articular condyle of the humerus. The trochlea forms the medial surface of the condyle and articulates with the ulna. The capitulum lies lateral to the trochlea and articulates with the radius. Superior to the trochlea are the coronoid fossa on the anterior surface of the humerus, and the olecranon fossa on the posterior surface, which receive projections from the ulna during full flexion and extension of the elbow joint. Similarly, a shallow radial fossa located superior to the capitulum accepts a portion of the radial head during elbow flexion.

The ulna and radius

The ulna and radius are the bones of the forearm. The ulna lies medial to the radius in the anatomical position. At the proximal ulna, the trochlea notch articulates with the trochlea on the humerus to form the humeroulnar joint. The olecranon process is the point of the elbow, and together with the coronoid process forms the superior and inferior lip respectively of the trochlea notch. The coronoid and olecranon processes project into the coronoid fossa of the humerus in full elbow flexion, and the olecranon fossa of the humerus in full elbow extension. Lateral to the coronoid process is the radial notch, in which the head of the radius rotates at the proximal radioulnar joint during pronation and supination. At the distal end, the shaft of the ulna narrows before widening to form the head of the ulna, with the styloid process at its posterior, lateral surface of the distal extremity.

The radius is the lateral bone of the forearm. The disk-shaped radial head articulates with the capitulum of the humerus to form the humero-radial joint. Distal to the radial head, the bone narrows to form a shaft, which widens again at the distal portion of the radius. On the medial side of the distal radius is the ulnar notch which marks the articulation site with the head of the ulna, forming the distal radioulnar joint. The ulna notch rotates around the head of the ulna during pronation and supination. The styloid process on the lateral surface of the radius forms its most distal point.

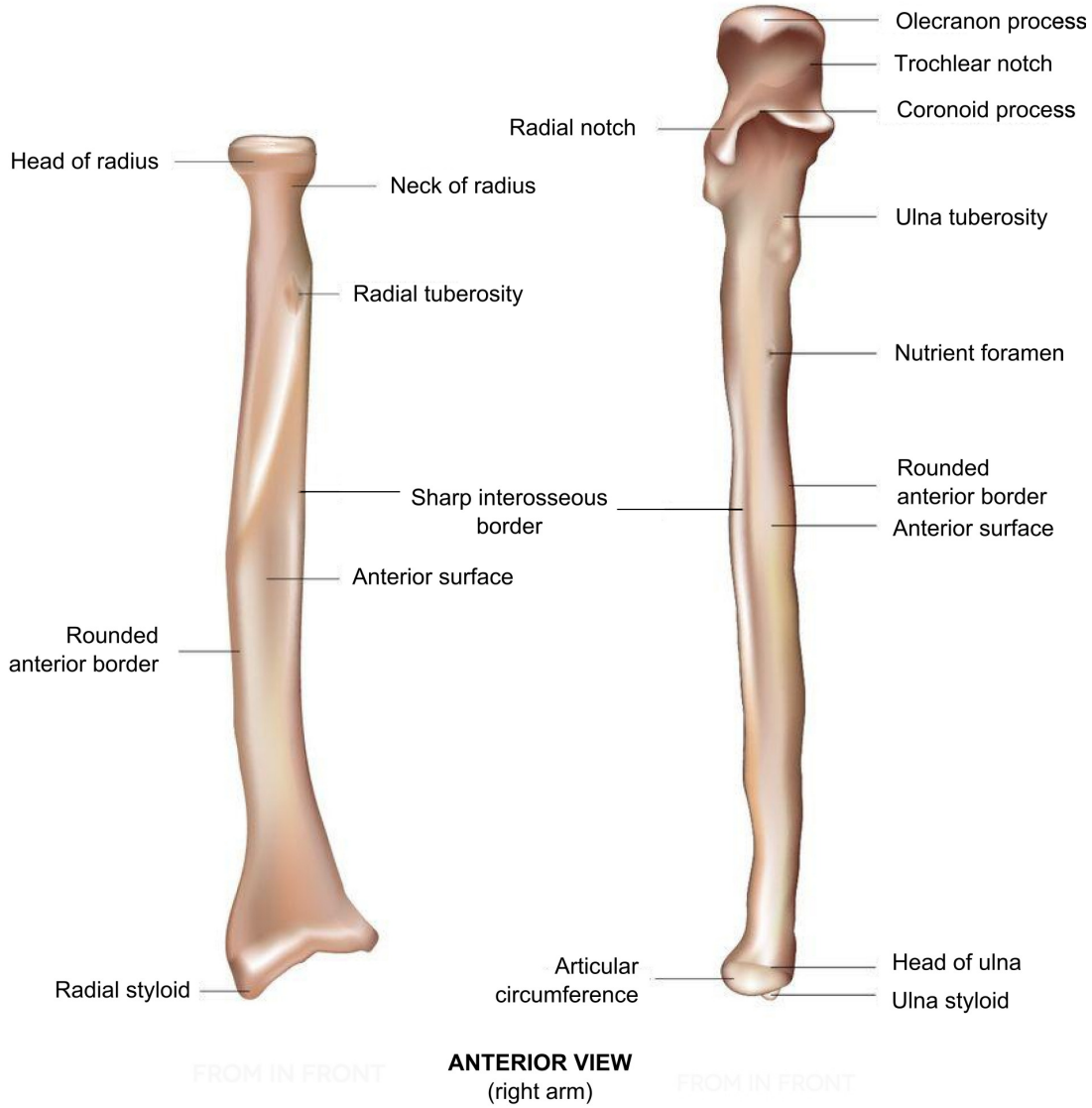

Figure 4.8 Radius and Ulna

The wrist and hand

The distal ulna and radius articulate with the proximal row of carpal bones in the wrist. There are eight carpal bones in total which are arranged in two rows: four proximal carpal bones and four distal carpal bones. The distal row of carpal bones articulates with five metacarpal bones which in turn articulate with the phalanges distally. There are 14 phalanges in total: each finger has three phalanges (proximal, middle and distal), and the thumb has two phalanges (proximal and distal).

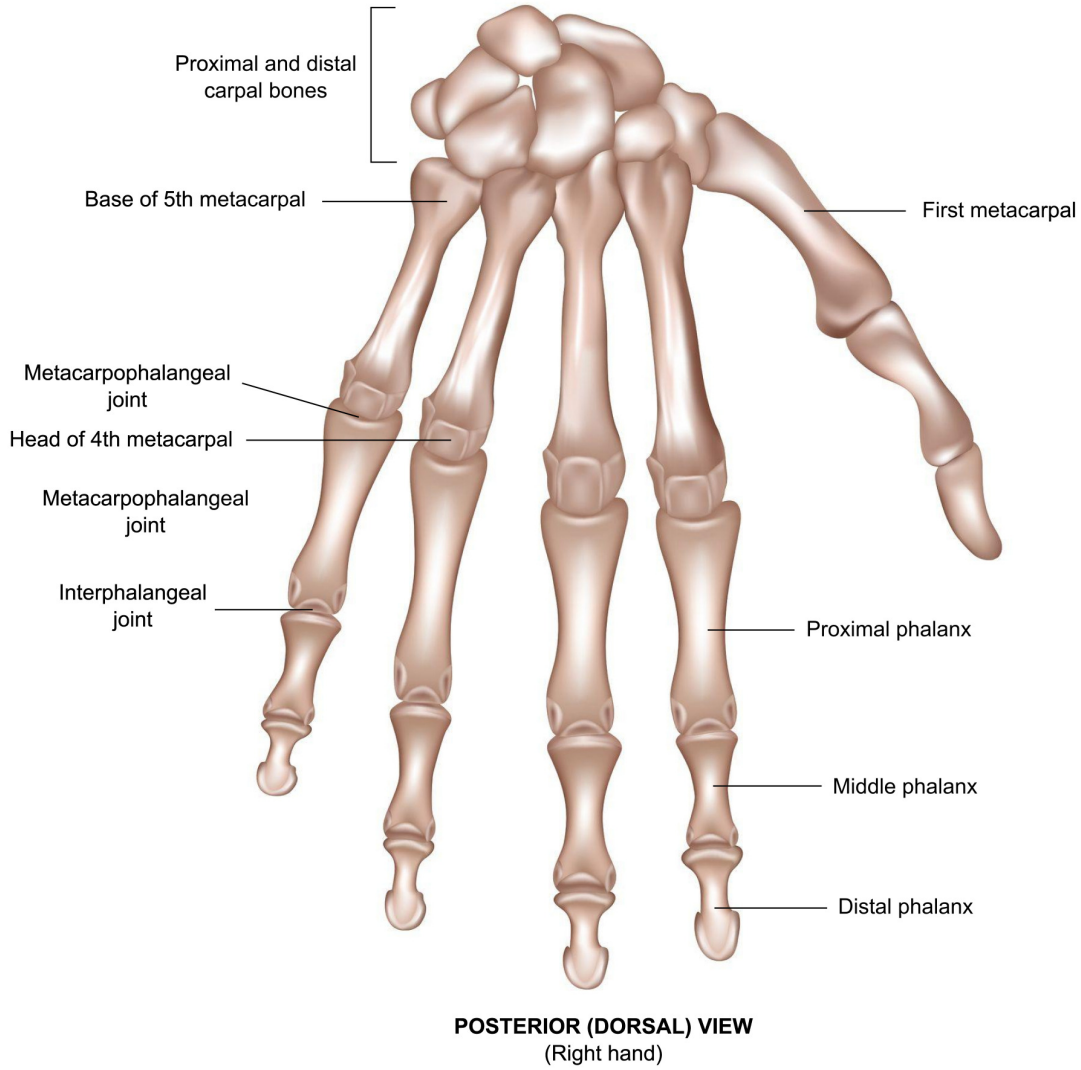

Figure 4.9 The wrist and hand

The pectoral girdle

The arm articulates with the trunk at the pectoral girdle, which consists of the scapula and the clavicle. These bones position the shoulder joint, and muscles originating from them help to move the upper extremity.

The scapula is a broad, flat, triangular shaped bone. It is supported and positioned by skeletal muscles, and has no direct joint articulations or ligamentous attachments with the thoracic cage. Skeletal muscles attach along the edges of the superior border, medial or vertebral border, and the lateral or axillary border. The superior, inferior and lateral angles form the three corners of the bony triangle, with the lateral angle broadening to form the shallow glenoid fossa. This is the site of scapula

articulation with the head of the humerus to form the shoulder joint, a ball and socket joint also known as the glenohumeral joint. The smooth, round articular head of the humerus is several times the diameter of the glenoid fossa. Projecting laterally superior to the humeral head are two prominent scapula processes called the acromion and coracoid process. The acromion articulates with the clavicle at the acromioclavicular joint. Medially, the clavicle articulates with the craniolateral border of the manubrium of the sternum at the sternoclavicular joint, and this forms the only direct articulation between the pectoral girdle and the axial skeleton.

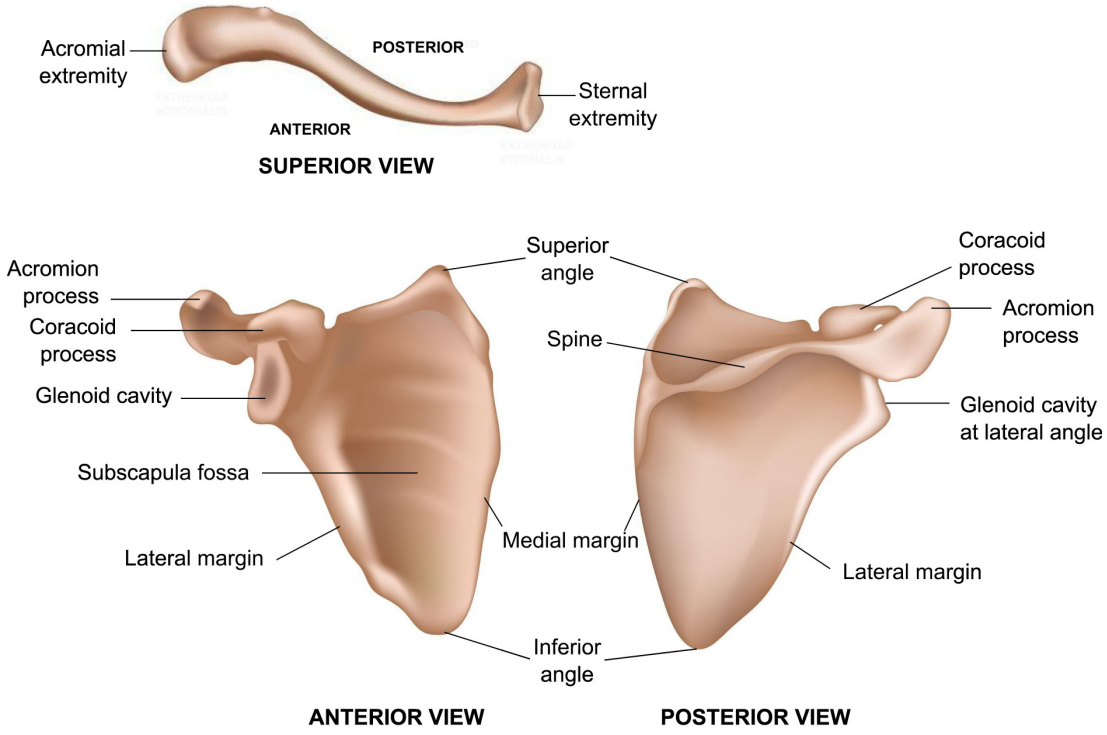

Figure 4.10 The clavicle and scapula

The thoracic cage and vertebral column

The anatomical landmarks used to define the trunk anatomical coordinate system are located on the thorax and vertebral column, and a brief description only of the relevant anatomy is given here.

The thoracic cage consists of the thoracic vertebrae, the ribs, and the sternum, and serves as an attachment point for muscles which bring about movement of the pectoral girdle and upper limb. The sternum forms the anterior midline of the thoracic wall, and has three components: the manubrium, the body, and the xiphoid

process. The manubrium is the widest and most superior portion of the sternum. Between the articulations with the clavicles is a shallow indentation on the superior surface of the manubrium called the jugular notch. The xiphoid process is the smallest and most inferior portion of the sternum and is attached to the inferior surface of the body of the sternum.

The twelve thoracic vertebrae form the superior portion of the back and articulate with the twelve pairs of ribs, the first seven pairs also articulating with the sternum via the costal cartilages. Superiorly to the thoracic vertebrae are seven cervical vertebrae which constitute the neck. Inferiorly to the thoracic vertebrae are five lumbar vertebrae which form the inferior portion of the back. The fifth lumbar vertebra articulates with the sacrum inferiorly, which in turn articulates with the coccyx. The two landmarks of the vertebral column used for the definition of the trunk anatomical coordinate system are the spinous processes of the eighth thoracic and seventh cervical vertebrae.

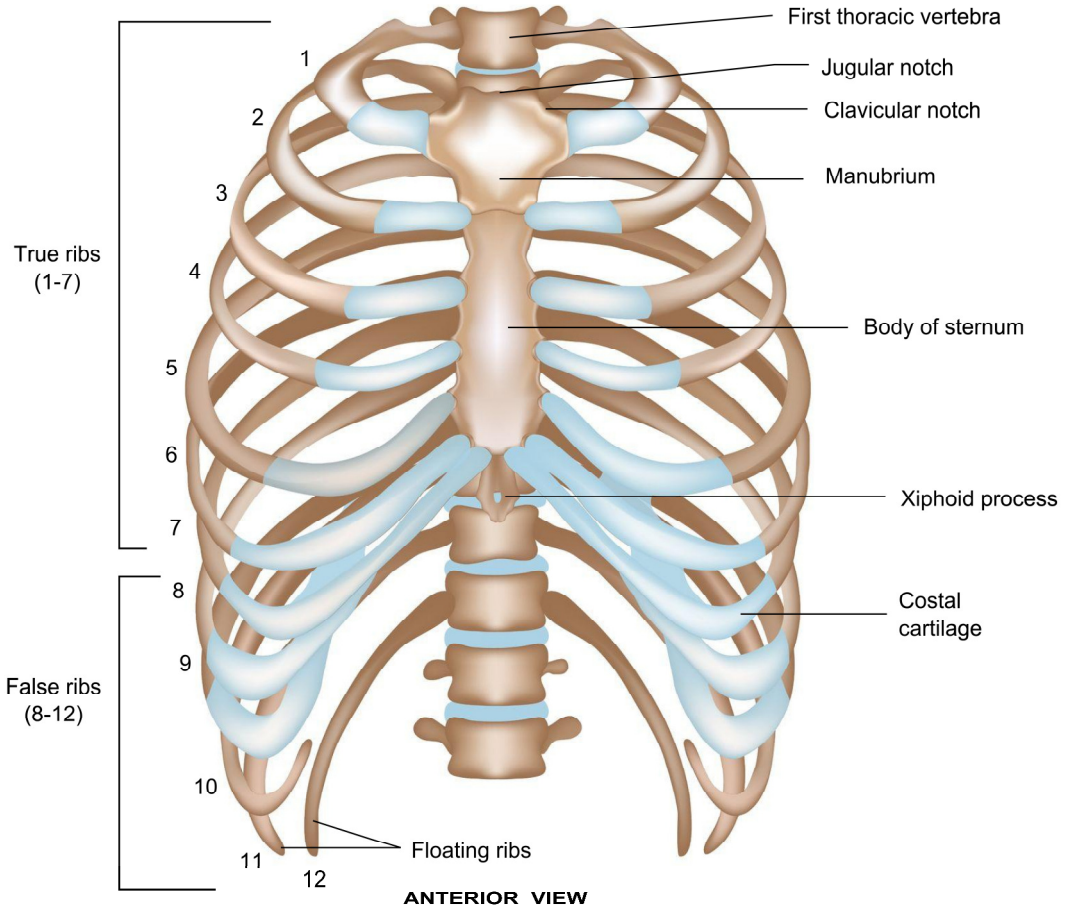

Figure 4.11 The thoracic cage

4.6 Anatomical coordinate systems

An anatomical coordinate system was defined for each upper limb segment using bony landmarks in accordance with the International Society of Biomechanics (ISB) recommended standardisations (Wu et al., 2005) as shown in figure 4.12. The following definitions are described for right limb segments only. Where left-handed subjects were tested, the raw position data were mirrored with respect to the sagittal plane (i.e. z = -z).

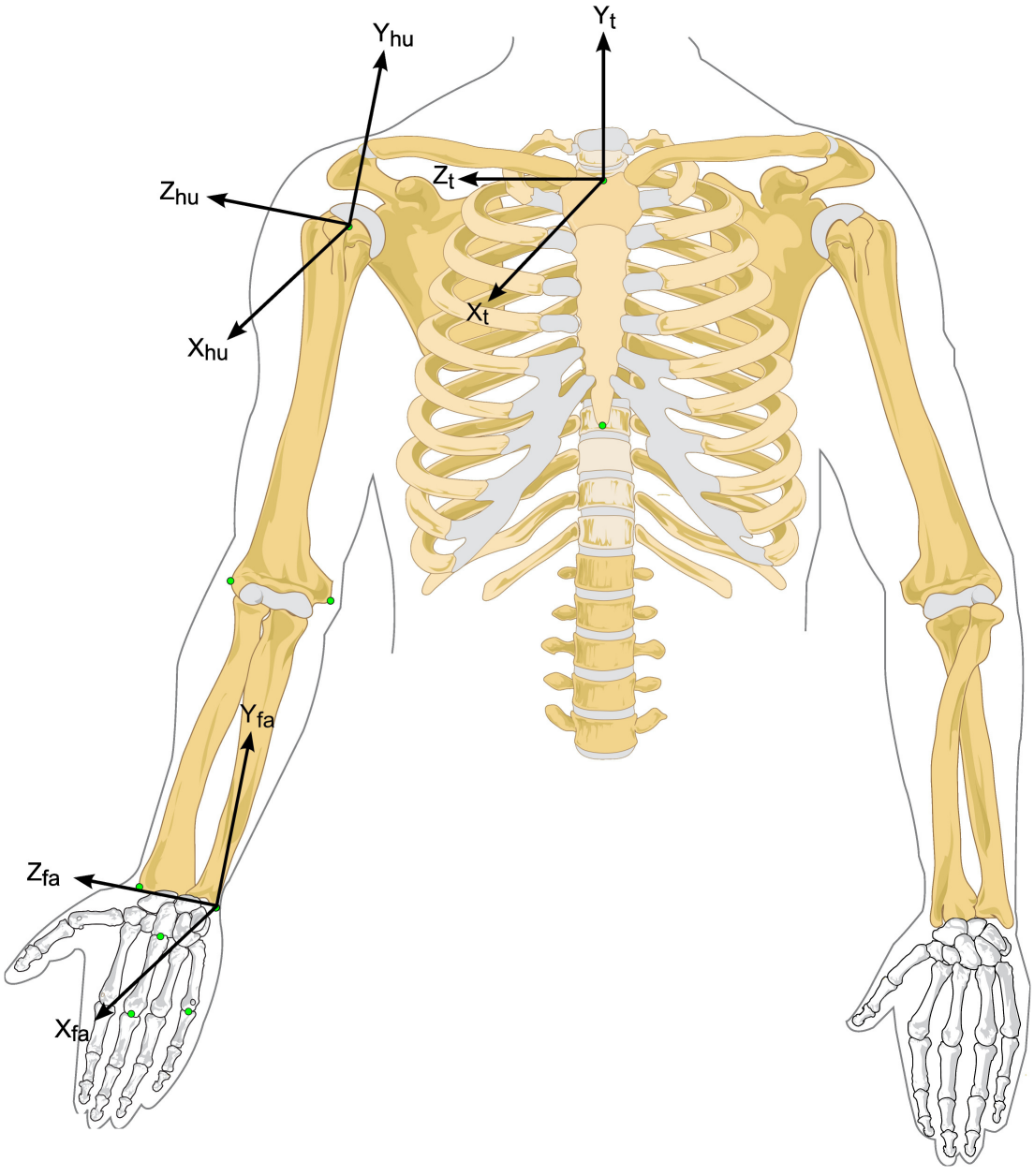

Figure 4.12 Anatomical coordinate systems for the thorax, humerus and forearm.

Thorax anatomical coordinate system

The anatomical landmarks required to define the thorax anatomical coordinate system are the deepest point of the Incisura Jugularis (IJ), most caudal point of the Processus Xiphoideus (PX), spinous process of the 7th cervical vertebra (C7) and spinous process of the 8th thoracic vertebra (T8). The coordinate system is described below:

O_t: The origin coincident with IJ.

Y_t: The line connecting the midpoint between PX and T8 and the midpoint between IJ and C7, pointing upward.

Z_t: The line perpendicular to the plane formed by IJ, C7, and the midpoint between PX and T8, pointing to the right.

X_t: The common line perpendicular to the Z_t and Y_t axes, pointing forwards.

Humerus anatomical coordinate system

The anatomical landmarks required to define the humerus anatomical coordinate system are the most caudal point on the medial and lateral epicondyles of the humerus (MEH and LEH), and the glenohumeral joint centre (GH) estimated by regression. The GH is not a bony landmark but is used to define the long axis of the humerus. In this study the GH was estimated by regression according to Wang (1996) and was located 37mm inferior, 14mm lateral, and 8mm anterior to the acromioclavicular (AC) joint, with the upper arm in the resting position. For clinical use in patients, it is suggested that estimation of GH by the instantaneous helical axis method (Stokdijk et al., 2000; Veeger et al., 1996, 2000), would be most appropriate, as recommended by the ISB. The following definition is in accordance with the first option of the ISB standardisations (Wu et al., 2005) for the humerus coordinate system:

O_{hu}: The origin coincident with GH.

Y_{hu}: The line connecting GH to the midpoint between MEH and LEH, pointing towards GH.

X_{hu}: The line perpendicular to the plane formed by MEH, LEH and GH, pointing forward.

Z_{hu}: The common line perpendicular to the Y_{hu} and X_{hu} axes, pointing to the right.

Forearm anatomical coordinate system

In this study, the ulna and the radius have been considered as one segment. The anatomical landmarks required to define the forearm anatomical coordinate system are the most caudal point on the medial and lateral epicondyles of the humerus (MEH and LEH), and the radial styloid (RS) and ulnar styloid (US). The coordinate system is described below.

O_{fa}: The origin coincident with US.

Y_{fa}: The line connecting US and the midpoint between MEH and LEH, pointing proximally.

X_{fa}: The line perpendicular to the plane formed by US, RS and the midpoint between MEH and LEH, pointing forward.

Z_{fa}: The common line perpendicular to the X_{fa} and Y_{fa} axes, pointing to the right.

Hand anatomical coordinate system

The anatomical landmarks required to define the hand anatomical coordinate system are the base of the third metacarpal bone (MC3p), head of the third metacarpal bone (MC3d), and the head of the fifth metacarpal bone (MC5d). Wu et al, (2005) recommends the definition of global wrist joint motion as the motion of the second and/or third metacarpal bone with respect to the radius. In this study, the radius was not tracked as an independent segment, however, the third metacarpal bone will be used in the definition of the hand anatomical coordinate system as shown in figure 4.13 and described below:

O_{ha}: The origin coincident with MC3d.

Y_{ha}: The line connecting MC3d and MC3p, pointing proximally.

X_{ha}: The line perpendicular to the plane formed by MC3d, MC3p and MC5d, pointing forwards

Z_{ha}: The common line perpendicular to the Y_{ha} and X_{ha} axes, pointing to the right.

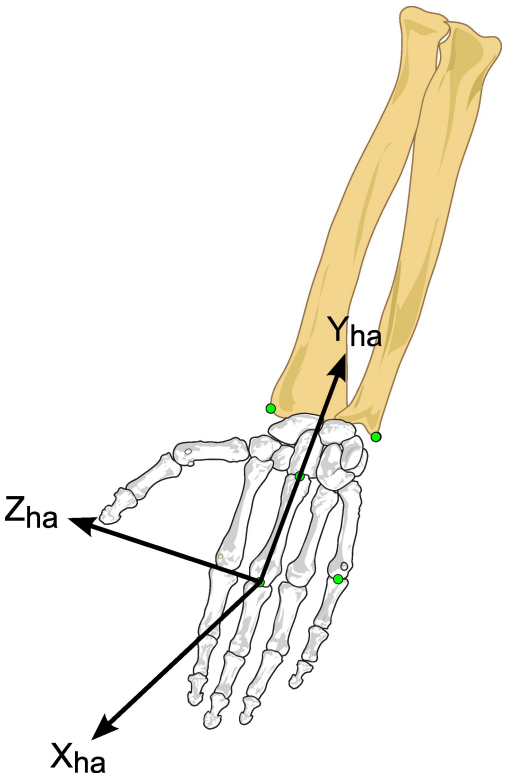

Figure 4.13 Hand anatomical coordinate system

Chapter 5: Materials and methods

This chapter gives a description of the techniques used for the collection of kinematic data from the upper limb during the performance of a variety of upper limb functional activities. An overview of the data analysis steps taken to generate joint angle data from the 3D gyroscope system raw data is given with reference to the detailed techniques presented in Chapter 4. Finally, a description of the statistical techniques used to compare the joint rotation data calculated from the Vicon and 3D gyroscope systems is given.

5.1 Kinematic measurement techniques

5.1.1 The Vicon System

Kinematic data were collected using a Vicon 612 motion analysis system (Oxford Metrics Ltd.) consisting of 8 cameras positioned evenly around a measurement volume. The camera configuration used is shown in figure 5.1. Each camera emits pulsed infrared light at a frequency of 120Hz and detects reflection of this light from any marker placed on a subject within its field of view. The markers used are spheres covered in retro-reflective tape which reflects the infra-red light directly back to the camera from which it originated. Any one camera produces a two dimensional image, therefore a marker must be viewed by at least two cameras in order to reconstruct the three-dimensional coordinates of the marker centre within the measurement volume.

During a calibration process, Vicon defines the absolute position of the origin of a global (laboratory) coordinate system, and the direction of its three orthogonal axes, and calculates the position and orientation of each camera relative to one another. This information is subsequently used in the reconstruction of the 3D marker trajectories from the 2D camera images. Vicon uses a two stage calibration technique called DYNACAL.

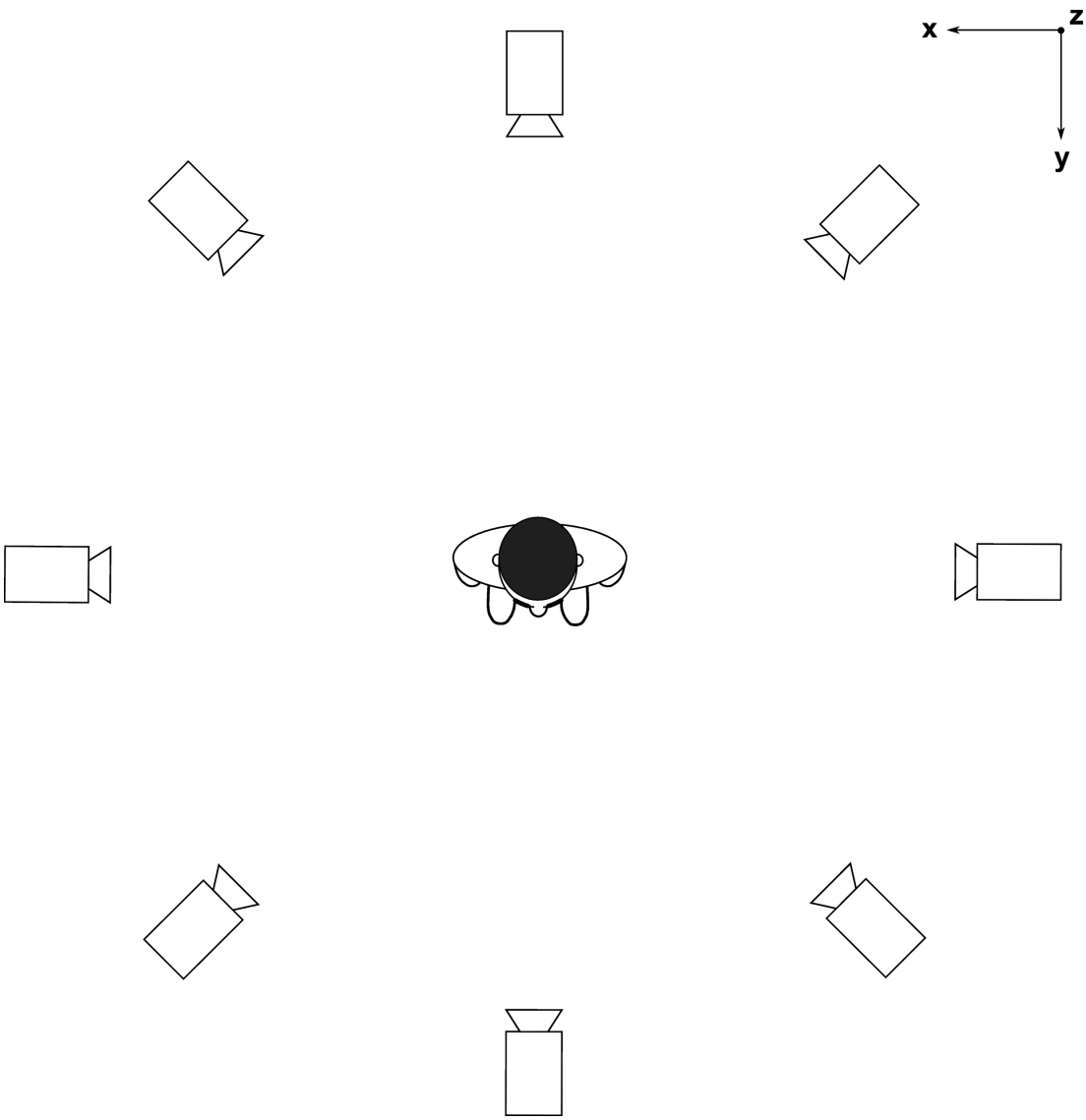

Figure 5.1 Vicon camera configuration.

The first stage involved placing an L-shaped calibration frame on the floor in the centre of the measurement volume whilst a 20s capture was recorded. The L-frame had four 25mm markers attached. Three markers were located in a straight line along the longest flank of the frame, and the fourth marker was located on the shortest flank. The markers were arranged in a manner to allow calculation of the absolute position of the origin of the laboratory axis system and the direction of its axes. The second stage utilised a calibration wand which consisted of two 50mm markers mounted at a separation of 500mm. Data were captured for a period of approximately 20s whilst the wand was waved evenly throughout the measurement

volume, and this enabled the calculation of the camera locations and orientations relative to each other.

Following the second calibration stage, a calibration residual was calculated for each camera. An individual camera residual is a measure of the mean distance by which the camera's own 2D image of the wand markers deviates from the reconstructed 3D image, averaged across all frames in the trial. Therefore the calibration residuals give a measure of the calibration accuracy for each camera and consequently the accuracy of subsequent measurements. Consistent values for all cameras as well as the absolute value are required. In this study, all calibration residuals were below 1mm for all trials. When the calibration residuals were above 1mm, the system was recalibrated until the required accuracy was obtained. A calibration residual of 2.0mm is the maximum allowed calibration error of the cameras. A calibration residual above this value can produce inaccurate data coordinates.

5.1.2 Marker System

The markers used in this study were spheres of 25mm and 14mm in diameter covered in retro-reflective tape. To fully describe the 3D kinematics of a rigid body in space, a minimum of three non-collinear markers must be tracked on each limb segment. In this study, rigid marker clusters were used on the trunk, upper arm and forearm segments. The clusters consisted of markers of 25mm in diameter, mounted onto rigid plastic mounts which had been heat moulded to follow the anatomical contours. The use of rigid clusters as opposed to skin mounted markers was considered appropriate in this study to reduce deformation of inter-marker distances which could give rise to inaccurate reconstruction of rigid body motion, especially on the upper arm and forearm segments where skin movement may be excessive. Furthermore, attachment of the clusters using elasticated strapping facilitates quick and easy mounting onto the subject and can also help to reduce soft tissue movements.

Four markers were used on the trunk cluster, and three makers each were used on the upper arm and forearm clusters. The trunk cluster was attached to the back directly

to the skin using double-sided hypoallergenic adhesive tape. Its position was chosen in order to reduce marker occlusion during upper limb cross-body activities. The upper arm and forearm units were attached using both hypoallergenic adhesive tape and elasticated Velcro strapping, and were attached on areas of least muscle mass in order to reduce soft tissue movement. In addition, three markers of 14mm in diameter were placed on the hand and attached to the skin directly over the base of the third metacarpal, and the distal heads of the third and fifth metacarpals using hypoallergenic tape. A fourth hand marker was attached midway between the base and the head of the second metacarpal bone, and served as a redundant marker in case of marker occlusion.

Fourteen tracking markers were used in total which remained on the subject throughout the testing procedure. Further description of the marker locations and their corresponding labels can be found in Table 5.1.

Marker number	Marker label	Marker description
1	THO1	Top thorax cluster marker
2	THO2	Right thorax cluster marker
3	THO3	Bottom thorax cluster marker
4	THO4	Left thorax cluster marker
5	UA1	Upper arm anterior cluster marker
6	UA2	Upper arm distal cluster marker
7	UA3	Upper arm posterior cluster marker
8	FA1	Forearm anterior cluster marker
9	FA2	Forearm distal cluster marker
10	FA3	Forearm posterior cluster marker
11	MC3p	Base of the third metacarpal bone
12	MC3d	Head of the third metacarpal bone
13	MC5d	Head of the fifth metacarpal bone
14	Hand 4	Fourth hand marker

Table 5.1 Description of the tracking markers used together with corresponding marker labels.

5.1.3 Technical coordinate systems

The technical coordinate system is a right-handed, orthogonal coordinate system which is considered to be a bone embedded frame. It is defined from the coordinates of three non-collinear tracking markers attached to each limb segment as shown in Figure 5.2 and described below.

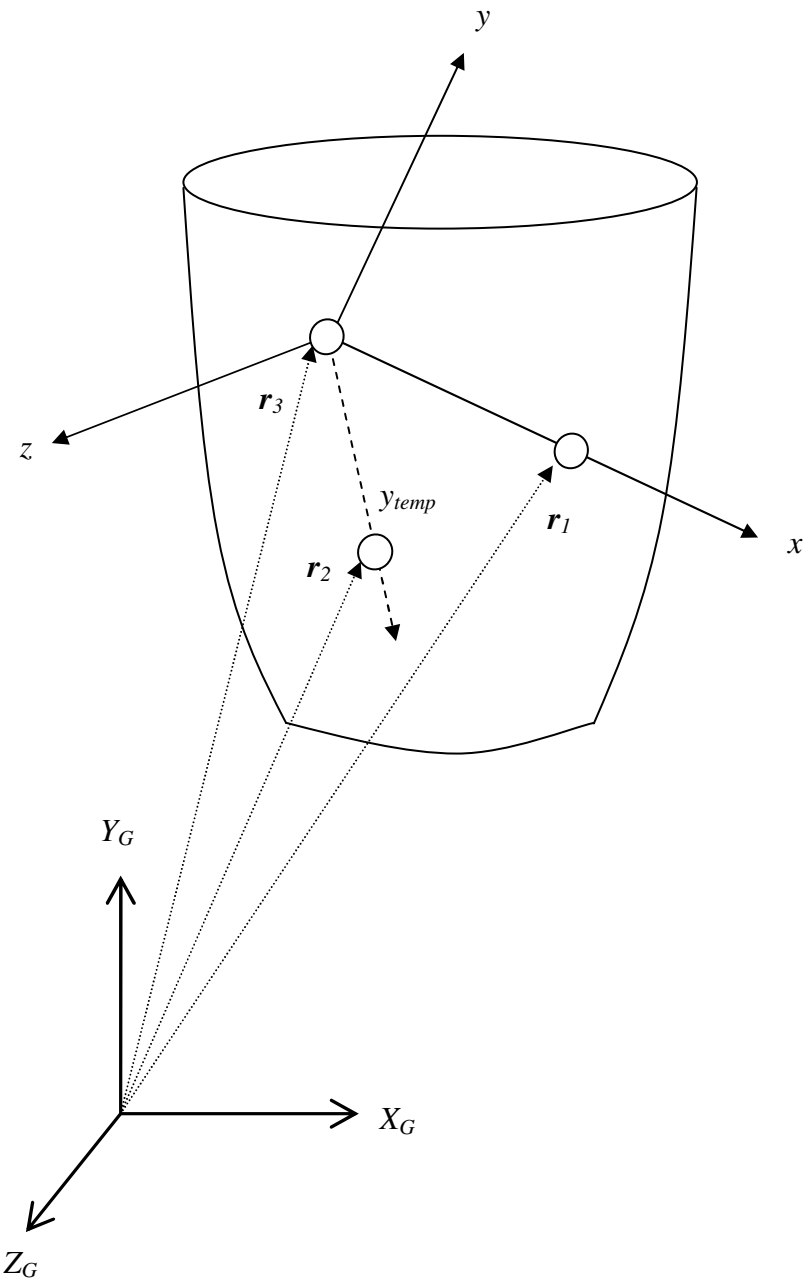

Figure 5.2 Technical coordinate system defined from three non-collinear markers.

Let $\mathbf{r}_1$, $\mathbf{r}_2$ and $\mathbf{r}_3$ be the three dimensional position vectors of the three markers in the laboratory or global system. The technical coordinate system can then be defined by three unit vectors as follows, where $\mathbf{r}_3$ is taken as the origin:

$$\mathbf{x} = (\mathbf{r}_1 - \mathbf{r}_3) / \left| \mathbf{r}_1 - \mathbf{r}_3 \right| \tag{5.1}$$

$$\text{Temporary } \mathbf{y} = (\mathbf{r}_2 - \mathbf{r}_3) / \left| \mathbf{r}_2 - \mathbf{r}_3 \right| \tag{5.2}$$

The **z** axis is perpendicular to the plane defined by the **x** and temporary **y** axes ($\mathbf{y}_{temp}$):

$$\mathbf{z} = (\mathbf{y}_{temp} \cdot \mathbf{x}) / \left| \mathbf{y}_{temp} \cdot \mathbf{x} \right| \tag{5.3}$$

The true **y** axis is then defined as perpendicular to the **xz** plane and is therefore the cross product between the x and z axes:

$$\mathbf{y} = (\mathbf{x} \cdot \mathbf{z}) / \left| \mathbf{x} \cdot \mathbf{z} \right| \tag{5.4}$$

The position and orientation of the technical coordinate system with respect to the global system can be described as a translation and a three dimensional rotation as described in sections 4.2 and 4.3.

5.1.4 Anatomical landmark calibration

The technical coordinate system is a bone embedded frame, however it may not coincide with an anatomical frame and its position and orientation relative to the bony anatomy may be arbitrary and non-repeatable (Cappozzo et al., 1995). In this study, marker cluster attachment sites were selected not according to the anatomy of the limb segment, but with the aim to minimise marker movement relative to the underlying bone and to maximise marker visibility to as many cameras as possible. To define an anatomical coordinate system from the tracking markers, the position of the bony landmarks with respect to the relevant technical coordinate system can be recorded following marker cluster attachment using an anatomical pointer calibration technique. Anatomical landmarks were chosen in accordance with the International

Society of Biomechanics (ISB) standardised recommendations (Wu et al., 2005), and were located by palpation.

The anatomical pointer calibration technique involves the use of a pointer of a known length with two 25mm diameter markers fixed at a known separation. The pointer tip is held against the anatomical landmark whilst data are captured for a few frames. The position vector of the pointer tip, $\mathbf{p}_{tip}$ in the global system can be determined using the following equation and is shown in Figure 5.3:

$$p_{tip} = \frac{(m_1 - m_2)}{|m_1 - m_2|} \cdot d + m_1 \tag{5.5}$$

where d is the distance between the marker $\mathbf{m}_1$ and the pointer tip.

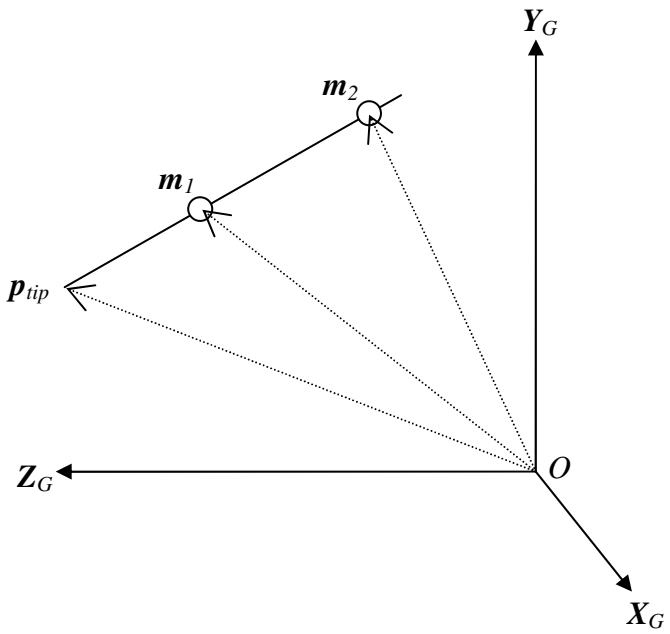

Figure 5.3 Pointer calibration technique.

The location of the pointer tip, and hence the anatomical landmark, in the technical coordinate system can be determined using equation 4.4 from section 4.3 as follows:

$${}^{T}p_{tip} = {}^{G}_{T}R^{-1} \cdot ({}^{G}p_{tip} - {}^{G}_{T}O) \tag{5.6}$$

During a dynamic trial, the position of the anatomical landmark can be tracked in the technical frame, and its position in 3D space at each instant in time can be reconstructed in the global coordinate system using equation 4.3 from section 4.3 as follows:

$$^{G}p = {}^{G}_{T}R \cdot {}^{T}p + {}^{G}_{T}O \tag{5.7}$$

Table 5.2 describes the anatomical landmarks and their corresponding technical coordinate systems.

Landmark	Landmark description	Technical coordinate system
C7	Processus Spinosus of the 7th cervical vertebra	Thorax
T8	Processus Spinosus of the 8th thoracic vertebra	Thorax
IJ	Deepest point of Incisura Jugularis	Thorax
PX	Processus Xiphoideus, most caudal point on sternum	Thorax
MEH	Most caudal point on medial epicondyle of humerus	Upper arm
LEH	Most caudal point on lateral epicondyle of humerus	Upper arm
US	Most caudal-medial point on radial styloid	Forearm
RS	Most caudal-lateral point on ulnar styloid	Forearm
AC	Most dorsal point on the acromioclavicular joint	Thorax

Table 5.2 Anatomical landmarks chosen in accordance with ISB recommendations (Wu et al., 2005), and the corresponding technical coordinate system to which they are calibrated for anatomical frame definition.

The use of a thorax cluster was preferred in the study, to which IJ, PX, C7, and T8 were calibrated. This was because the activities investigated involved upper limb cross-body movements, which gave rise to marker occlusion in the absence of the thorax cluster.

5.2 Data collection

Ethics and Safety approval from the Department of Biomedical Engineering Ethics and Safety Committees respectively was obtained for the experimental work.

5.2.1 Subject selection

Volunteers were organised into two age groups as follows:

Subjects aged 20-30 years: Ten healthy volunteers composed of 5 males and 5 females with no known shoulder and upper limb problems were recruited from the postgraduate students of the Department of Biomedical Engineering.

Sex	Age	Height (cm)	Mass (kg)
F	29	160.5	53
F	28	169.5	71.2
F	21	158	46.5
F	28	167.5	55.6
F	24	176.5	62.1
M	25	194	80
M	25	179	93
M	25	185.5	82
M	22	174.5	59.8
M	29	184	84

Table 5.3 Subject data for subjects aged 20-30 years of age

Subjects aged 70+ years: Ten healthy volunteers composed of 5 males and 5 females with no known shoulder and upper limb problems were recruited.

Sex	Age	Height (cm)	Mass (kg)
F	72	166	53
F	74	160	65.6
F	77	163.5	67.6
F	76	161.6	83
F	74	142	50.5
M	76	180	86.5
M	79	169.5	68
M	73	182	108
M	83	177.5	94.7
M	73	167.5	84

Table 5.4 Subject data for subjects aged 70+ years of age

All subjects were asked to complete an Oxford Shoulder Score (OSS) which is routinely used as part of clinical upper limb functional assessment, both pre- and post-operatively (Dawson et al., 1996, 2009). The questionnaire assesses the impact of shoulder pathology on the impairment of eight activities of daily living (ADL) with a further four questions related to pain. A score of 0-4 is assigned for each question where a score of 4 represents no pain or impairment and a score of 0 represents unbearable pain and inability to perform the task. When the 12 items are summed, the resulting overall score ranges from 0-48, with 48 representing the best outcome. The OSS data from volunteers used in this study are presented as mean scores for each subject group in table 5.5 below:

Age	Mean male scores	Mean female scores
20-30	48	48
70+	48	47.4 (range 45-48)

Table 5.5 Mean Oxford Shoulder Questionnaire scores for each subject group.

The results of the questionnaire indicated that all subjects recruited in this study were healthy at the time of testing. Although a mean score of 47.4 for female subjects aged 70+ was obtained, it has been noted that scores tend to worsen with age. Therefore a "normal" score in elderly patients may be somewhat less than 48 (Dawson et al., 2009).

Informed written consent was obtained from all subjects prior to data collection and subjects were excluded from the research if they fell into any of the following groups:

1. Individuals with an allergy to sticking plasters or tape.
2. Individuals with a history of shoulder or upper limb pathology.
3. Individuals incapable of giving informed written consent.

These exclusion criteria were rechecked prior to testing.

5.2.2 Method of attachment of the 3D gyroscope system

A total of three 3D gyroscope units were used and were attached to the trunk, upper arm and forearm segments as shown in figures 5.4a and 5.4b. The trunk 3D gyroscope unit was attached to the trunk marker cluster and the upper arm and forearm gyroscope units were attached to the elasticated Velcro straps surrounding the upper arm and forearm marker clusters. Each marker cluster had a flat level surface to aid the mounting of the gyroscope units. A series of markings on each marker cluster and 3D gyroscope unit pair facilitated placement of the gyroscope unit such that its coordinate system (defined in section 3.4) was coincident with the corresponding technical coordinate system defined from the markers of each marker cluster (section 5.1.3). The cables associated with each gyroscope unit were directed up the arm and secured with additional elasticated Velcro straps. The attachment of each 3D gyroscope unit to a corresponding marker cluster was solely for the purposes of comparison of 3D gyroscope data with motion analysis data. When used in a clinical setting in the absence of a motion analysis system and retroreflective markers, it is intended that the trunk unit is attached directly to the skin using doubled-sided hypoallergenic adhesive tape, and the upper arm and forearm units are attached using elasticated Velcro straps secured around each segment at an area of least muscle mass.

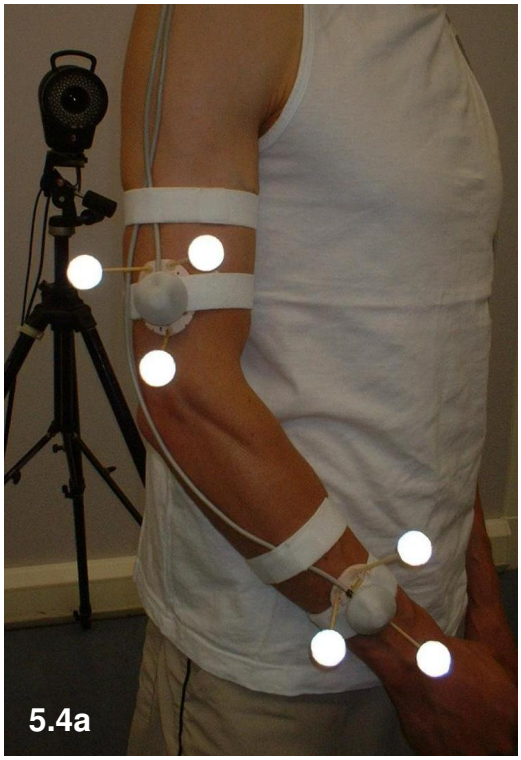

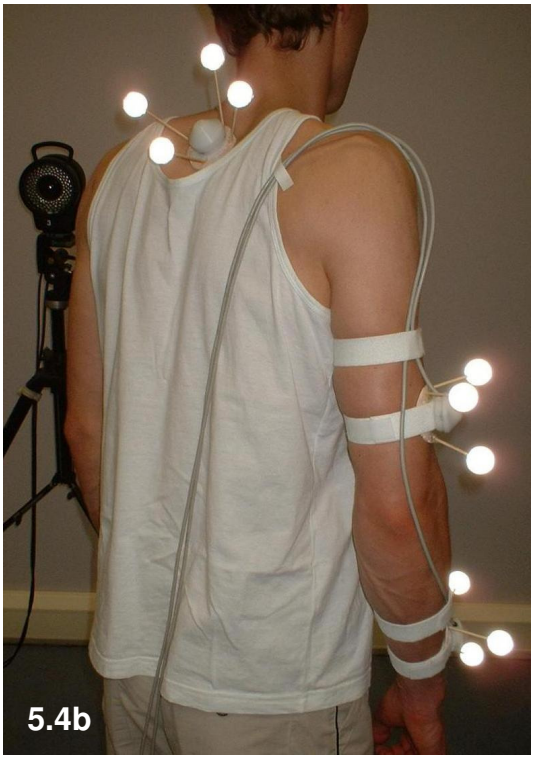

Figure 5.4a and 5.4b Front and rear view of 3D gyroscope system and retroreflective markers mounted onto healthy subject.

5.2.3 Description of test activities

When compared with gait which is cyclic and repeatable with the major components of movement occurring in the sagittal plane, upper limb movement shows much greater complexity and variability due to the large range of motion and complex structure of the shoulder joint. The variability and intricacy of the tasks which can be performed by the upper limb has meant that no standardised test protocols for upper limb motion analysis have yet been defined and widely applied. It was therefore necessary to select several movements which were most representative of both upper limb movement range and versatility, and those activities most commonly performed in everyday life. The movements selected were placed into three activity groups as follows:

Group 1: Planar movements used in clinical examination

The following movements are those commonly investigated in clinical assessment of upper limb function, and relate to the movement of the shoulder joint:

1a Maximal flexion

1b Maximal extension

1c Maximal abduction

1d Maximal external rotation

1e Maximal internal rotation

Group 2: Movements involved in activities of daily living (ADL)

These movements were chosen as they represent the most basic functions that are essential for survival and independent living without additional assistance.

2a Movement of the hand from the resting position at the side of the trunk to touch the mouth. This simulates a feeding activity.

2b Movement of the hand from the resting position to touch the back of the head. This simulates a grooming activity.

2c Movement of the hand from the resting position to touch the ipsilateral shoulder.

2d Movement of the hand from the resting position to touch the contralateral shoulder.

Movements 2c and 2d were chosen to mimic dressing movements.

Group 3: Lifting

The ability to perform lifting movements is important to ensure quality of life. The following movements were chosen to mimic lifting of an object to and from a shelf.

3a Lifting a can from a table up to shoulder height.

3b Lifting a can from a table up to head height.

The can used for the lifting activities had dimensions of 75mm in diameter and 110mm height, and a mass of 0.476kg. The can was chosen as it is a standard object commonly found in the home and could be comfortably grasped by all subjects. A pole with adjustable markers was used to give the subject a visual target height to lift

the can. The subject was asked to lift the can from a table 0.7m high from the ground, to either shoulder height (figure 5.5a) or head height (figure 5.5b), before returning the can to the table.

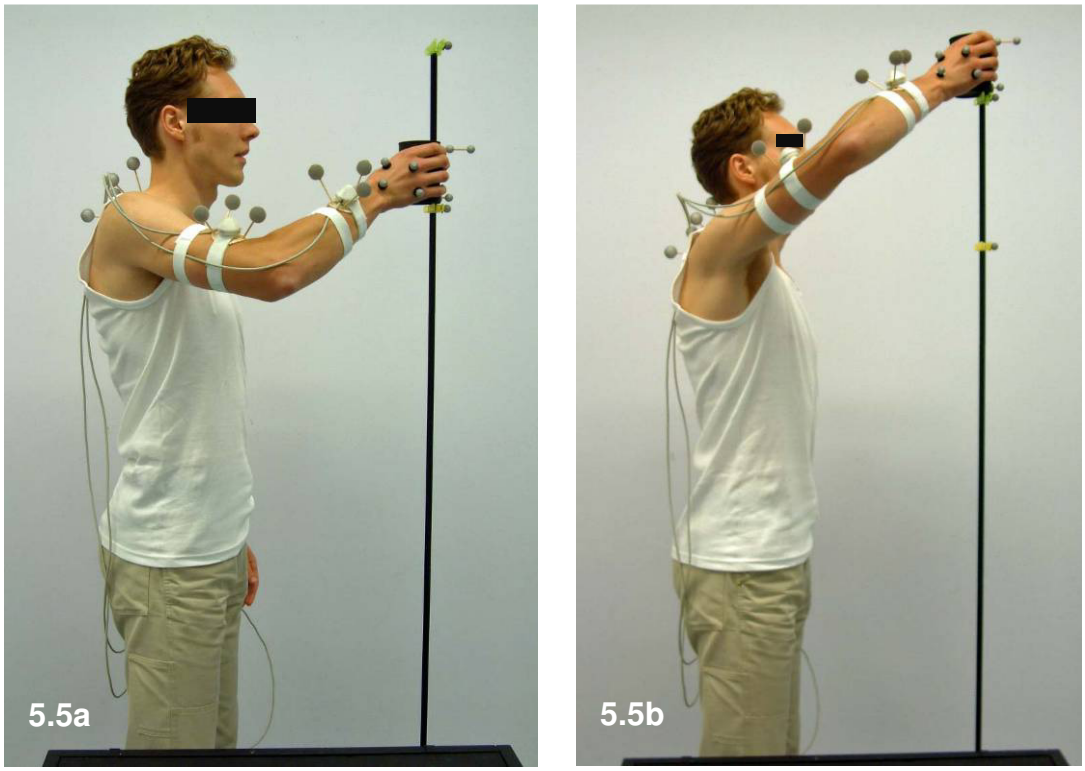

Figure 5.5 Lifting a can from a table to a) shoulder height, and b) head height.

The subject's height was measured prior to testing, and shoulder height was normalized to the subject using average segment lengths described by Drillis and Contini (1966). In addition, the horizontal distance between the subject and the pole was normalized for each subject and was calculated as the total length of the upper arm segment plus forearm segment. This distance was measured on the ground as the distance between the pole and the back of the subject's foot. The average segment lengths used for the above calculations are shown in figure 5.6.

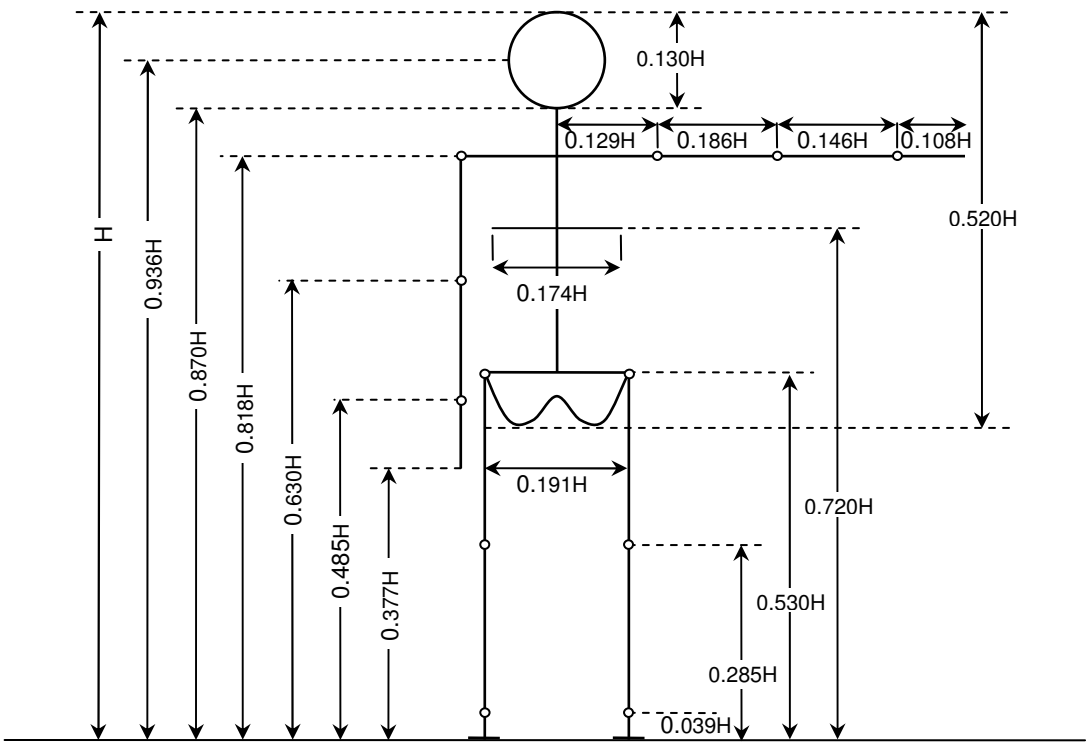

Figure 5.6 Body segment lengths expressed as fractions of body height H, Drillis and Contini 1966.

5.2.4 Experimental protocol for validation of 3D gyroscope system

The following testing procedures were observed in order to maintain consistency of the data collection process between trials and between subjects.

The subject was asked to start and finish each movement in the resting position. The resting position involved maintaining an upright posture whether seated or standing, with the upper arm, forearm and hand placed comfortably at the side of the trunk as shown in figure 5.7.

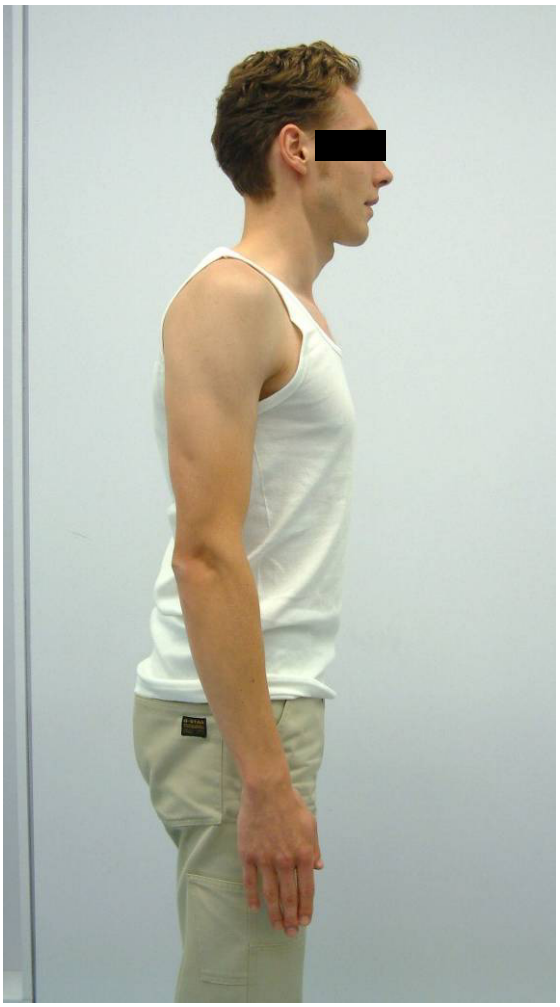

Figure 5.7 Upper limb neutral resting position.

With the arm beginning in the resting position, movement of the arm then commenced after a verbal signal from the test operator. No instructions were given to control the speed or duration of the movement. The only instruction given was to perform each movement at a comfortable speed. In addition, for group 1 activities the subject was asked to perform the maximal movement possible for each activity. Following each movement, the arm was then returned to the resting position. Each activity was repeated a total of three times and only the dominant arm was tested.

Group 2 activities were performed with the subject seated. This is because the older adult group consisted of elderly subjects aged 70 years and over, some of whom may have found it difficult to maintain a standing position for any length of time. However, subjects were required to stand for group 1 and group 3 activities to enable the movement to be performed.

Each test lasted no longer than 20s. This was in order to reduce the affects of cumulative integration error as described in section 3.2.4.

5.2.5 Data acquisition and pre-processing

3D gyroscope data were captured at a frequency of 600Hz using a National Instruments DAQ card (NI DAQCard – 6036E) in a laptop computer using a custom written LabVIEW program (National Instruments, v7.1). In order to validate the data collected from the 3D gyroscope system, motion data were captured simultaneously using an 8 camera Vicon 612 motion analysis system (Oxford Metrics Ltd.) at a frequency of 120Hz.

Following data collection, reconstruction and labelling of marker trajectories was carried out in Vicon workstation (v4.4). Data were smoothed and small gaps interpolated using a Woltring filter with a mean square error value of 20. Data were then processed using Bodybuilder for biomechanics (v3.55), which is a software package that enables the manipulation of kinematic and kinetic data collected using the Vicon system. Custom written Bodybuilder code was used. Following data acquisition, gyroscope and Vicon data were exported in ASCII format for further data processing in Matlab (Mathworks Inc., MA). A description of the data processing steps taken is given in section 5.3.

5.3 Data analysis

A detailed account of the techniques for the description of 3D kinematics used in this study was given in Chapter 4. This section gives a brief description of the specific steps taken to compute clinically relevant joint angle data from the 3D gyroscope system. "Joint" angles computed in this thesis were humerothoracic angles. The statistical techniques used for the comparison of the Vicon and 3D gyroscope systems are subsequently described. All data processing was carried out in Matlab (Mathworks Inc., MA) using custom written scripts.

5.3.1 Computation of joint angle data

Joint angle data were calculated from the Vicon coordinate data using Grood and Suntay's floating axis technique as described in section 4.4.2. The specific steps used to compute joint angle data from the raw output of the 3D gyroscope system are given below and summarised in Figure 5.8.

5.3.1.1 Calculation of gyroscope angular displacement

Raw voltage data were filtered using a low pass double recursive fourth order Butterworth filter with a cut-off frequency of 2Hz. Angular velocity was calculated from the voltage output of each of the nine gyroscopes using the following equation:

$$\boldsymbol{\omega = (V - V_o) / gain / S_v} \tag{5.8}$$

where ω is the angular velocity (deg/s), V is the output voltage (V), V_0 is the static output voltage (V), the gain is 2.78V, and S_v is the scaling factor of 0.67mV/deg/s taken from the manufacturer's specifications.

For each gyroscope unit, angular velocity data ω_x, ω_y and ω_z, corresponding to rotations about the X_{gyro}, Y_{gyro} and Z_{gyro} axes of the gyroscope unit (as defined in section 3.4), were integrated using the trapezoidal rule to give angular displacement data θ_x, θ_y and θ_z. Joint rotation angles were subsequently calculated as described below.

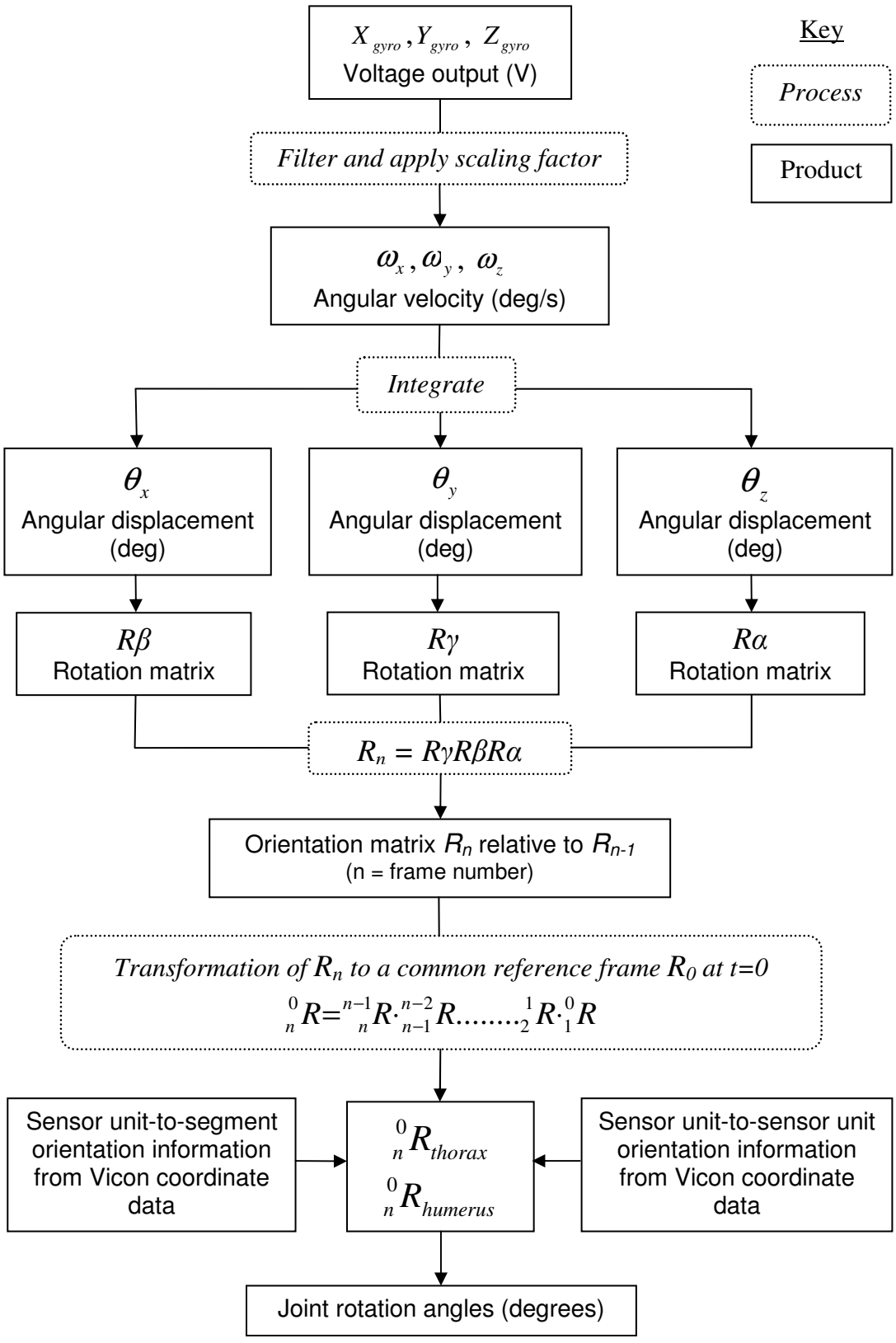

Figure 5.8 Calculation of joint rotation angle data from raw gyroscope data.

5.3.1.2 Calculation of gyroscope unit orientation matrix

Gyroscope angular displacement data were resampled at a frequency of 120Hz for calculation of joint rotation data and to facilitate comparison with Vicon data, which were also sampled at 120Hz.

An orientation matrix was defined from the 3-channel output of each gyroscope unit: three independent rotation matrices Rα, Rβ, and Rγ were defined from the angular displacement data θ_z, θ_x and θ_y respectively, where α represents rotation about the Z_{gyro} axis, β represents rotation about the X_{gyro} axis, and γ represents rotation about the Y_{gyro} axis in this study. The three rotation matrices were sequentially multiplied using an α-β-γ Cardan angle sequence to give a single orientation matrix, *R*, completely describing the rotation of the gyroscope unit from one orientation to another as follows and described in more detail in section 4.4:

$$R_n = R\gamma R\beta R\alpha \tag{5.9}$$

$$R_n = \begin{bmatrix} \cos\gamma & \sin\gamma & 0 \\ -\sin\gamma & \cos\gamma & 0 \\ 0 & 0 & 1 \end{bmatrix} \begin{bmatrix} \cos\beta & 0 & -\sin\beta \\ 0 & 1 & 0 \\ \sin\beta & 0 & \cos\beta \end{bmatrix} \begin{bmatrix} 1 & 0 & 0 \\ 0 & \cos\alpha & \sin\alpha \\ 0 & -\sin\alpha & \cos\alpha \end{bmatrix}$$

(5.10)

$$R_n = \begin{bmatrix} \cos\beta\cos\gamma & \sin\alpha\sin\beta\cos\gamma + \cos\alpha\sin\gamma & -\cos\alpha\sin\beta\cos\gamma + \sin\alpha\sin\gamma \\ -\cos\beta\sin\gamma & -\sin\alpha\sin\beta\sin\gamma + \cos\alpha\cos\gamma & \cos\alpha\sin\beta\sin\gamma + \sin\alpha\cos\gamma \\ \sin\beta & -\sin\alpha\cos\beta & \cos\alpha\cos\beta \end{bmatrix}$$

(5.11)

Where *n* = the time frame

The rotation matrices Rα, Rβ, and Rγ were derived from the frame-by-frame change in gyroscope angular displacement θ_z, θ_x and θ_y respectively. The resulting orientation matrix, R_n, therefore described the orientation of the gyroscope

coordinate system with respect to its orientation in the previous time frame, R_{n-1}, with the first orientation matrix, R_1, relative to the orientation of the gyroscope unit at the start of the movement cycle, R_0 at t=0, with the upper limb in the neutral resting position (section 5.2.4).

5.3.1.3 Calculation of relative orientation

Each frame-by-frame orientation matrix, R_n, was transformed to a common reference orientation for each gyroscope unit, which was taken to be R_0 at t=0. Transformation of each frame-by-frame rotation matrix to the common reference orientation was achieved through successive multiplication of the rotation matrices as described below:

From equation 4.5 in section 4.3, the description of the orientation of any local frame relative to another was given by the following equation:

$$ {}^{A}_{B}R = {}^{G}_{B}R \cdot {}^{G}_{A}R^{-1} = {}^{G}_{B}R \cdot {}^{A}_{G}R \qquad (5.12) $$

where ${}^{A}_{B}R$ is the orientation of frame B relative to frame A, and G is the global reference as shown in Figure 4.4.

Therefore, since ${}^{0}_{1}R$ and ${}^{1}_{2}R$ are known, ${}^{0}_{2}R$ was determined as:

$$ {}^{0}_{2}R = {}^{1}_{2}R \cdot {}^{0}_{1}R \qquad (5.13) $$

where ${}^{0}_{2}R$ is the orientation of R_2 at t=2 relative to the reference orientation, R_0 at t=0.

The orientation of R_3 at t=3, ${}^{0}_{3}R$, relative to the reference orientation, R_0, was then determined as:

$$ {}^{0}_{3}R = {}^{2}_{3}R \cdot {}^{0}_{2}R \qquad (5.14) $$

It follows that each frame-by-frame orientation matrix was transformed to a common reference orientation, R_0, through successive multiplication of the orientation matrices:

$$ {}^{0}_{n}R = {}^{n-1}_{n}R \cdot {}^{n-2}_{n-1}R \ldots\ldots\ldots {}^{1}_{2}R \cdot {}^{0}_{1}R \qquad (5.15) $$

where n = number of frames.

Following transformation, each frame-by-frame orientation matrix therefore gave the orientation of the gyroscope coordinate system relative to its orientation at the start of the movement cycle, R_0 at t=0.

In order to compute joint angles, i.e. the relative rotation between adjacent body segments, from the transformed gyroscope orientation matrices, the following essential information was required:

1. The relative orientation between adjacent gyroscope units for at least one frame during each recording.

2. The orientation of each gyroscope unit coordinate system relative to the corresponding anatomical coordinate system for each body segment (defined in section 4.6).

Since each transformed frame-by-frame orientation matrix gave the change in orientation relative to its starting orientation, R_0 at t=0, and not a measure of its absolute orientation in space, the relative orientation between gyroscope units was therefore unknown in the absence of additional data or recording procedures further to those previously described in sections 5.2.2 to 5.2.4. The orientation of each gyroscope unit coordinate system relative to the corresponding anatomical coordinate system was also unknown since each gyroscope unit was placed according to an area of least muscle mass and not according to the underlying bony anatomy of the limb segment. To obtain orientation information, a reference orientation must be measured at least once during each recording (Luinge and Veltink, 2005).

Additional calibration procedures were therefore required to obtain the necessary information for joint angle calculation.

A calibration method to determine the relative orientation between adjacent gyroscope units is proposed below. However, it was considered impractical and therefore not incorporated into the testing protocol. The recording of a reference orientation would firstly involve aligning each gyroscope unit with the thorax gyroscope unit, such that their orientations were coincidental. Each gyroscope unit would then be relocated to the appropriate position on the upper arm and forearm with the limb in the neutral resting position. Thus, a measure of the orientation of the upper and forearm gyroscope units expressed in the thorax gyroscope coordinate system would be obtained. However, since it is unlikely that the exact same resting position of the upper limb would be realised at the beginning of each movement cycle, it would be necessary to incorporate the measurement of a reference orientation into each recording. This calibration approach was therefore considered unsuitable on two counts: 1) the recording time of each trial would be considerably increased which could lead to large cumulative integration error; 2) the length of each test session would be increased which would not be appropriate in a clinical setting.

Several methods have been proposed in the literature to determine the sensor-to-segment orientation using inertial measurement units. These have included a functional approach whereby the direction of an anatomical axis can be defined using the direction of the angular velocity vector during rotation of the body segment about a joint's functional axis. A 3 x 3 orientation matrix can then be determined which expresses the orientation of the body segment in the sensor unit coordinate system (Luinge and Veltink, 2007; O'Donovan et al., 2007). The methods proposed in the literature to determine sensor-to-segment orientation and subsequently relative orientation between sensor units varied according to the combination of inertial and magnetic sensors used. These are discussed further in Chapter 7 together with proposals to acquire orientation information for independent functioning of the 3D gyroscope system.

The calculation of joint rotation angles was therefore carried out using additional orientation information obtained from Vicon coordinate data. Each 3D gyroscope coordinate system was coincidental with the technical coordinate system of the corresponding limb segment as described in section 5.2.2. The orientation of each 3D gyroscope unit relative to both the fixed laboratory coordinate system and the corresponding anatomical coordinate system was therefore known at each instant in time. Only one frame of Vicon coordinate data per trial was used to provide reference orientation information for the calculation of joint rotation angles from the 3D gyroscope system. R_0 was therefore taken as the absolute orientation of the technical coordinate system at t=0 with the arm in the neutral resting position. The relative orientations between adjacent gyroscope units and between gyroscope and anatomical coordinate systems were subsequently found using equation 5.12.

5.3.1.4 Calculation of joint rotation angles

Shoulder joint rotation angles were calculated using the floating axis technique as described in section 4.4.2. Axis e_1 represented flexion/extension of the shoulder joint and was coincident with the z-axis of the thorax coordinate system defined in section 4.6. Axis e_3 represented internal/external rotation and was coincident with the y-axis of the upper arm coordinate system. The floating axis, e_2, represented adduction/abduction and was calculated as the common axis perpendicular to e_1 and e_3. This joint coordinate system was also used to calculate joint angle data from Vicon coordinate data.

5.3.1.5 Joint angle data normalised to movement cycle

All joint rotation data were normalised to 100% of the movement cycle. The beginning and end of each movement cycle was defined when the resultant velocity of a specified marker approximated 0 m/s at the start and finish of each movement trial. The hand markers were chosen for this purpose since functional upper limb movements are carried out with the aim to position the hand for interaction with the environment to carry out a particular task.

5.3.2 Statistical methods

This section describes the statistical methods used to compare the joint rotation data calculated from the Vicon joint coordinate data and 3D gyroscope system output.

5.3.2.1 Correlation

The Pearson product moment correlation coefficient, r, is a measure of the strength of linear association between two measured variables, X and Y, and can take a value between -1 and +1. A value of 1 indicates a strong linear relationship between X and Y such that as X increases, Y increases. A value of -1 indicates a strong negative relationship between the two variables such that as X increases, Y decreases. A value of 0 indicates no linear relationship between the two variables.

Correlation analysis is usually performed prior to linear regression to establish that a linear relationship exists between the two variables before attempting to fit a function to the data.

5.3.2.2 Linear regression analysis

The goal of linear regression is to fit a line through the data which best predicts y from x. The linear model represents the dependent variable, y as a linear function of one independent variable, x as follows:

$$y = p_1 + p_2 x \tag{5.16}$$

The coefficients p1 (intercept) and p2 (gradient) are determined by fitting a line to the data which minimises the sum of the squared residuals (i.e. the vertical distances of the data points from the fitted line) using the least-squares method. The 95% confidence intervals for the fitted coefficients p1 and p2 show with 95% certainty that the true values of p1 and p2 lie within the 95% confidence bounds.

5.3.2.3 Goodness of fit statistics

To evaluate the goodness of fit of linear regression, the following statistics are calculated: sum of the squared residuals (SSR), root mean squared error (RMSE), R-squared (R^2) and adjusted R-squared ($\overline{R}^2$) values.

Sum of squared residuals (SSR) is also known as the sum of squares due to error (SSE). This statistic is a measure of the deviation of the response values, y_i, from the predicted response value, $\hat{y}_i$, and is given by the following equation:

$$SSR = \sum_{i=1}^{n} (y_i - \hat{y}_i)^2 \tag{5.17}$$

Since the goal of linear regression is to minimise SSR, a value closer to 0 indicates a better fit of the statistical model to the data.

Root mean square error (RMSE) also known as the standard error of the regression (SE) is given by the following equation:

$$RMSE = \sqrt{MSE} = \sqrt{\frac{SSR}{n-2}} \tag{5.18}$$

where MSE is the mean square error or the residual mean square, and $n - 2$ is the residual degrees of freedom defined as the number of response values, n, minus the number of fitted coefficients, (2 in the case of simple linear regression with an intercept term). An RMSE value closer to 0 indicates a better fit of the statistical model to the data.

R-squared (R^2) and adjusted R-squared ($\overline{R}^2$)

R^2, also known as the coefficient of determination, is the square of the correlation coefficient between the response values, y_i, and the predicted response values, $\hat{y}_i$, and is defined as follows:

$$R^2 = 1 - \frac{SSR}{SST} \tag{5.19}$$

where the total sum of squares (SST) is calculated as a measure of the deviation of the response values, y_i, from their mean value, $\bar{y}$:

$$SST = \sum_{i=1}^{n} (y_i - \bar{y})^2 \tag{5.20}$$

R^2 gives a measure of the proportion of variability in a data set that is accounted for by the statistical model and is called the coefficient of determination because it provides a measure of how well future outcomes will be predicted by the model. The R^2 statistic can take a value between 0 and 1. A value of 1 indicates that the regression line fits the data perfectly, that the data points lie exactly along a straight line, and that x can be used as a perfect predictor of y. An R^2 value of 0 indicates that there is no linear relationship between x and y, the regression line is a horizontal line ($p_1 = \bar{y}$, $p_2 = 0$), and x cannot be used as a predictor of y.

The adjusted R-squared statistic, $\overline{R}^2$, uses the R^2 statistic and adjusts it based on the residual degrees of freedom. $\overline{R}^2$ can take any value less than or equal to 1, again with a value closer to 1 indicating a better fit, and will always be less than or equal to R^2.

5.3.2.4 Difference between the two systems in 3D

The "error" between the Vicon and 3D gyroscope system data was examined by investigating two sets of derived variables:

1. The one-dimensional difference between the two systems for each movement plane.
2. The three-dimensional resultant vector of difference between the two systems.

A three dimensional vector was defined for each of the 11 upper limb activities using the range of motion (ROM) values derived from the joint rotation data from the three planes of motion i.e. flexion/extension (F), adduction/abduction (A), internal/external rotation (R). Vectors were defined from both the Vicon and gyroscope range of motion (ROM) data, and the magnitude of the resultant vector between the two was used as a measure of the three dimensional error between the two systems as shown in figure 5.9 and described below:

$$\text{Resultant vector (degrees)} = \sqrt{(F_V - F_G)^2 + (A_V - A_G)^2 + (R_V - R_G)^2} \tag{5.21}$$

where *F, A* and *R* are the three component rotations of the movement, and the subscripts $_V$ and $_G$ denote the Vicon and gyroscope data respectively.

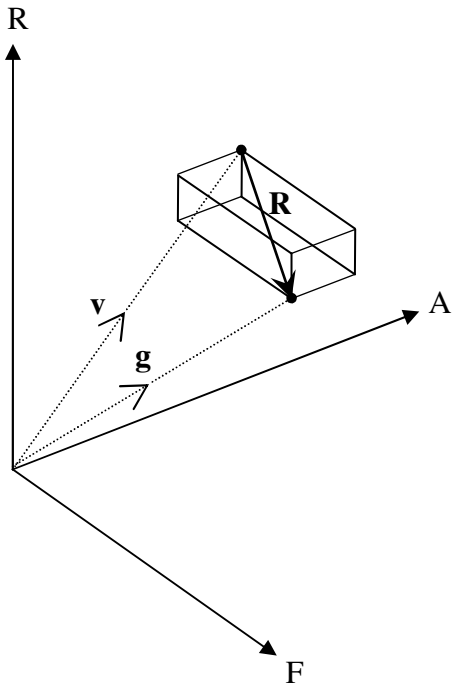

Figure 5.9 Resultant vector between Vicon and gyroscope systems, and "box".

The resultant vector formed a diagonal line between two opposite corners of a "box", the dimensions of which were the differences between the Vicon and gyroscope ROM values for each plane of motion. The dimensions and shape of the box gave an indication of the components of the error between the two systems, where the ideal box shape was a small cube. The ideal error was zero.

Chapter 6: Results

Following calculation of the shoulder joint rotation angles as described in chapter 5, further analysis of the joint rotation data was required in order to compare the outputs of the Vicon and 3D gyroscope systems. This chapter presents the joint rotation curves obtained, the calculations of joint rotation variables, and their subsequent statistical analysis for comparison of the two systems. All data analysis was carried out in Matlab (Mathworks Inc., MA).

6.1 Euler decomposition order

Shoulder joint rotation angles were calculated from the Vicon and 3D gyroscope system outputs using Grood and Suntay's floating axis method by means of a ZXY Cardan rotation order (FLEX/EX, ABD/ADD and INT/EXT respectively) as described in sections 4.4.2 and 5.3.1.4. Eleven upper limb activities were investigated in total, and categorised into three activity groups as described in section 5.2.3 (Group 1: pure movements used in clinical examination; Group 2: movements involved in activities of daily living; Group 3: lifting). An example of the joint rotation curves obtained from each activity group is presented in figures 6.1a-c for one subject. All joint rotation data were normalised to 100% of the movement cycle which began and ended with the arm in the rest position.

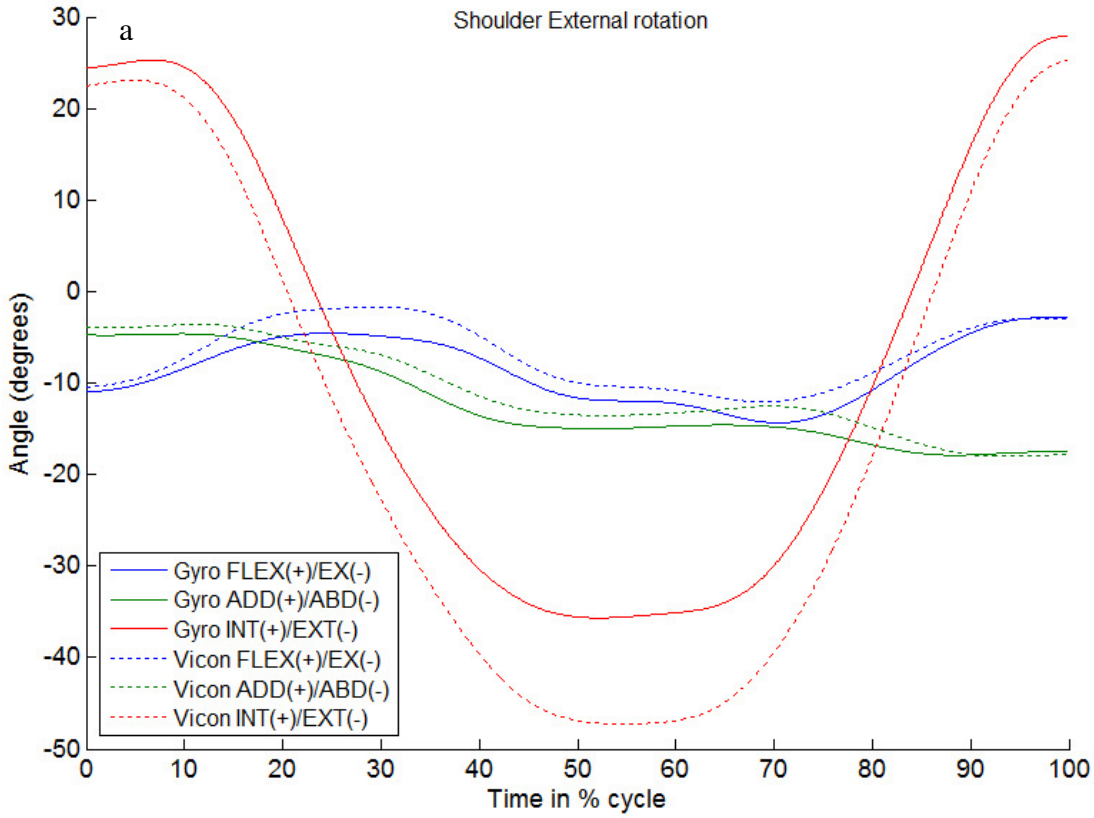
a
Shoulder External rotation
Angle (degrees)
Time in % cycle
Gyro FLEX(+)/EX(-)
Gyro ADD(+)/ABD(-)
Gyro INT(+)/EXT(-)
Vicon FLEX(+)/EX(-)
Vicon ADD(+)/ABD(-)
Vicon INT(+)/EXT(-)

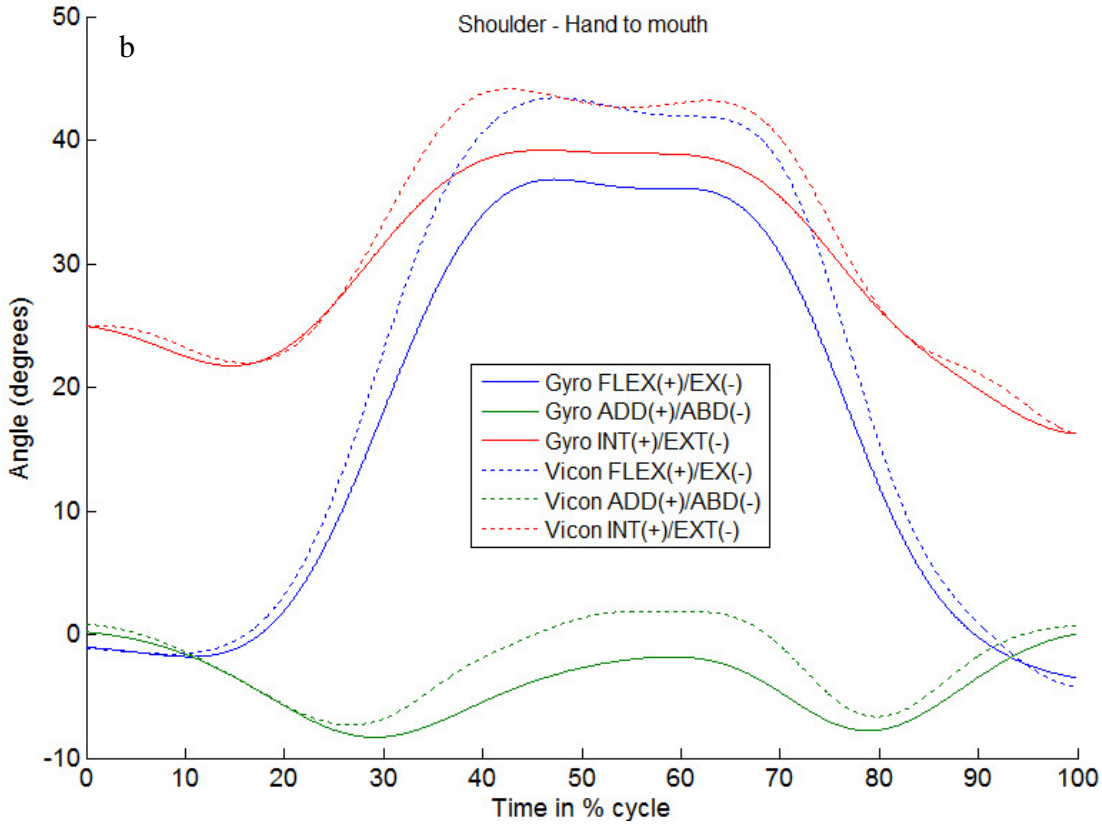
b
Shoulder - Hand to mouth
Angle (degrees)
Time in % cycle
Gyro FLEX(+)/EX(-)
Gyro ADD(+)/ABD(-)
Gyro INT(+)/EXT(-)
Vicon FLEX(+)/EX(-)
Vicon ADD(+)/ABD(-)
Vicon INT(+)/EXT(-)

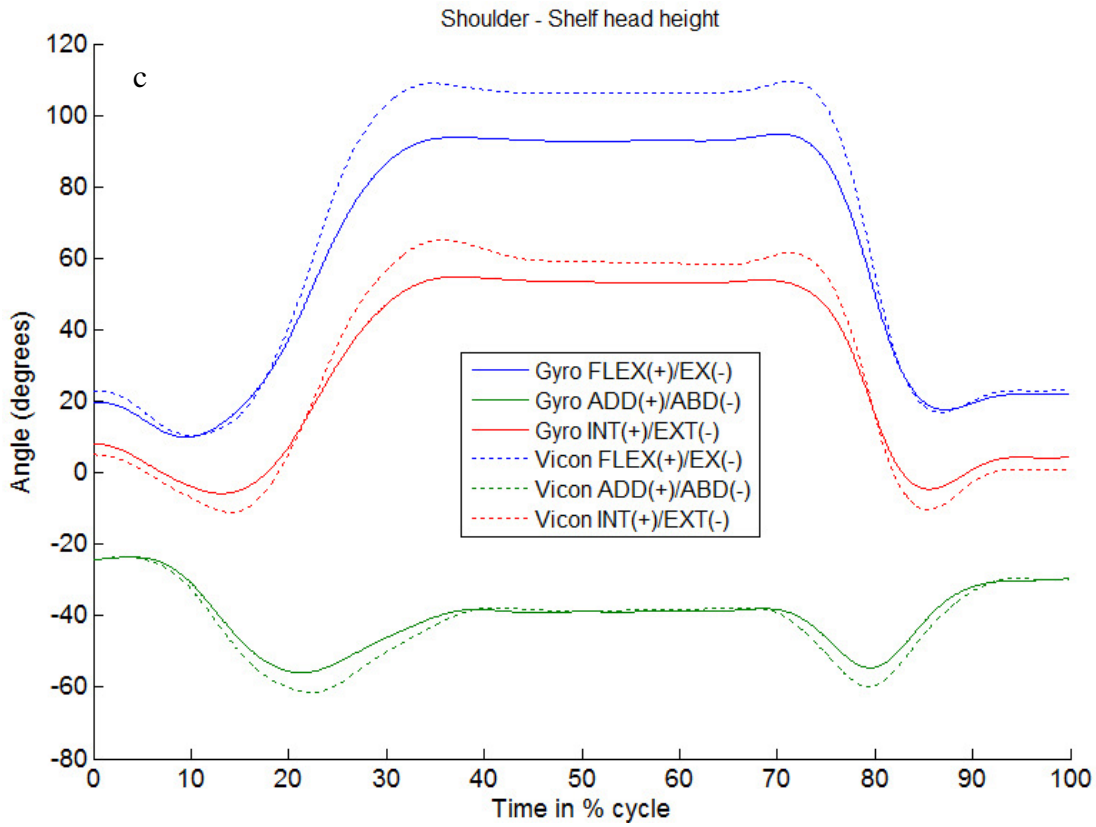

Figure 6.1 Example of humerothoracic "joint" rotation angles from the Vicon and 3D gyroscope systems during a) maximal external rotation (Group 1 activity – planar movements used in clinical examination), b) hand to mouth movement (Group 2 activity – movements involved in activities of daily living), c) lifting to head height (Group 3 activity – lifting movements). Joint rotation angles were recorded from a male subject aged 20-30 years.

The graphs show that the joint rotation data calculated from the 3D gyroscope system followed that calculated from the Vicon system in both the amplitude and the time domain in all three planes of motion. The joint rotation curves showed an "ascending" phase and a "descending" phase joined by a period of rest during which the target position of the hand was held.

Figures 6.1a-c were representative of the joint rotation curves obtained for the vast majority of upper limb movement activities investigated. However, a number of joint rotation curves calculated for the abduction activity displayed gimbal lock singularity. An example is presented in figure 6.2.

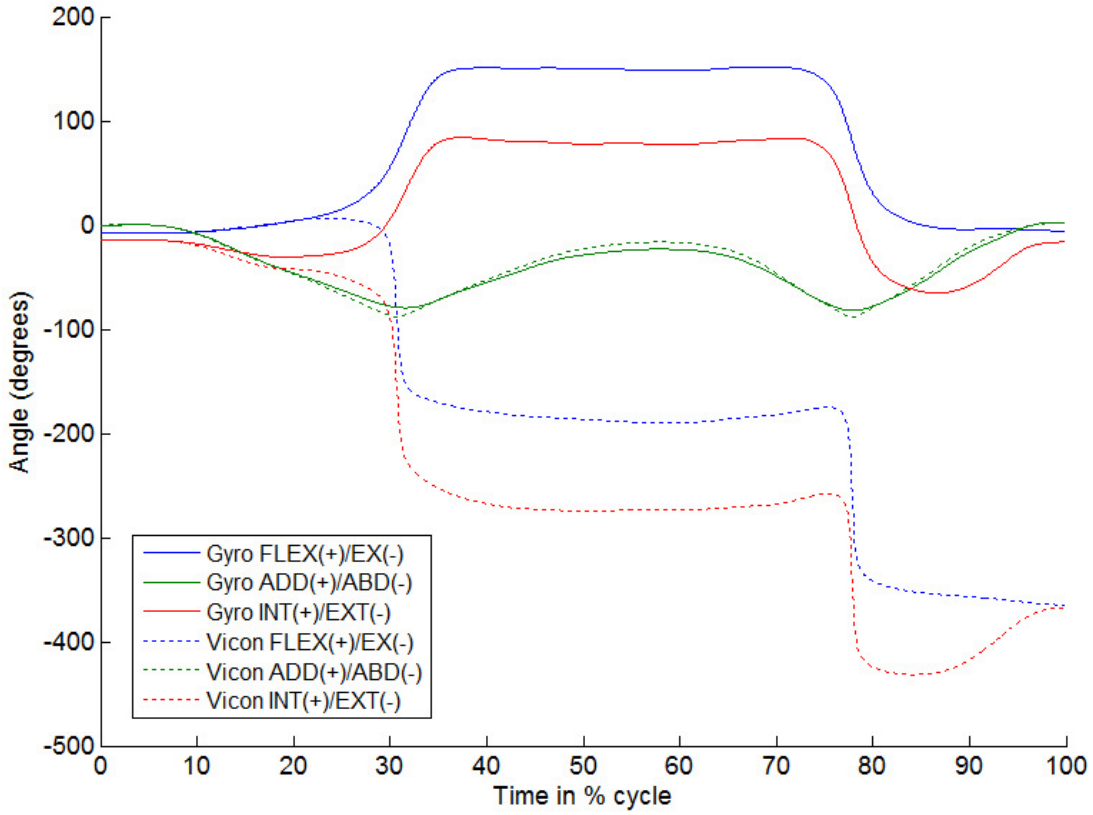

Figure 6.2 Example of gimbal lock singularity affecting Vicon humerothoracic joint angles calculated using the floating axis method during a shoulder abduction activity.

Figure 6.2 showed that gimbal lock occurred when the humerus approached 90° abduction and was seen to affect the FLEX/EX and INT/EXT Vicon joint angles at approximately 30% and 80% of the movement cycle. The gyroscope joint angles were unaffected in this example. For all Cardan decomposition sequences, gimbal lock occurs when the first and third axes of rotation become aligned in the second rotation when $\beta = \pm 90^{o}$ such that the joint angles are ill-defined. This results in the calculation of apparently extreme joint angle values which are not representative of the true movement of the limb segment. In this study, gimbal lock was only observed for the shoulder abduction activity since 90° humeral abduction/adduction was not reached during the Group 2 ADL or Group 3 lifting movements. Gimbal lock affected either the Vicon data, or the 3D gyroscope data, or both for four subjects only. Not every trial for each individual was affected (8 abduction trials out of a total of 60 were affected, that is 13%).

In order to eliminate the occurrence of gimbal lock, the use of an alternative decomposition order was considered. An Euler YXY decomposition order (plane of elevation, elevation angle, axial rotation) was applied in accordance with the ISB 2005 recommendations (Wu et al., 2005). However, gimbal lock was found to occur more frequently using this decomposition order. An example of the joint rotation curves obtained is presented in figure 6.3, which shows gimbal lock when the Vicon elevation angle approaches 0^{o} towards the end of the movement cycle.

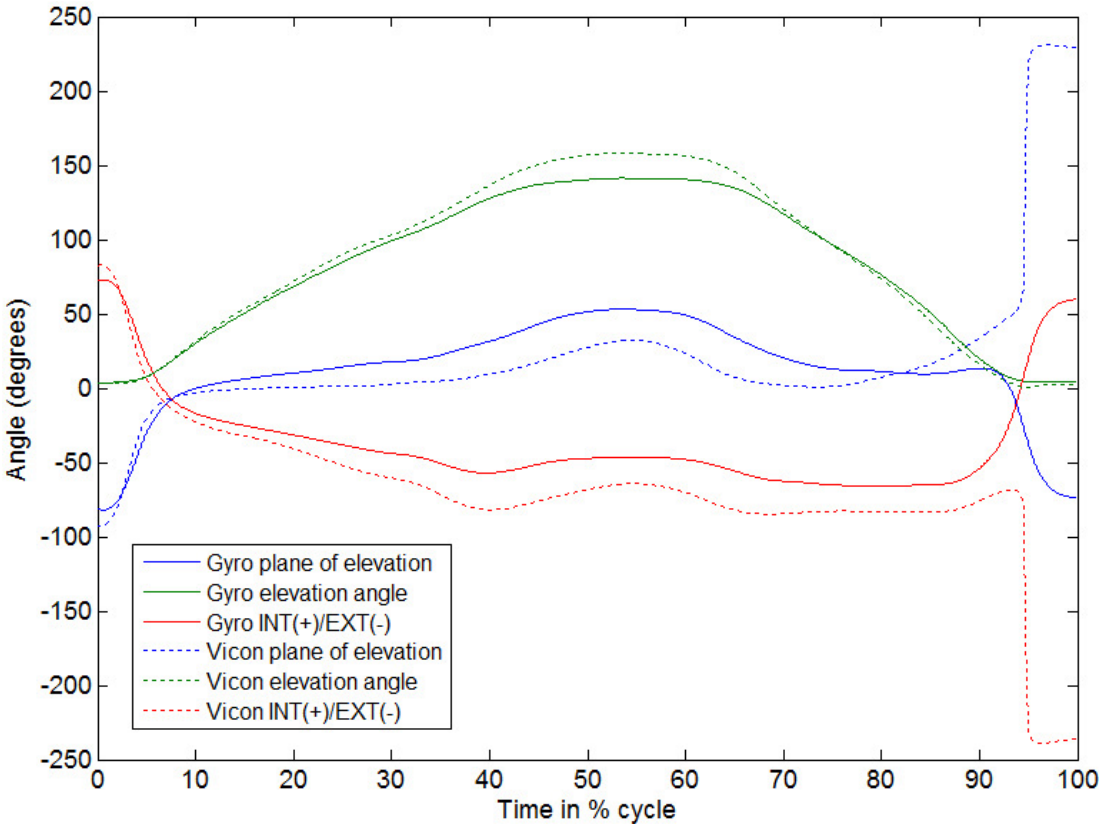

Figure 6.3 Example of gimbal lock singularity affecting Vicon humerothoracic joint angles calculated using an YXY Euler decomposition method during a shoulder abduction activity.

Figure 6.3 showed that when the upper limb approached the gimbal lock posture of 0^{o} elevation angle, even small changes in motion resulted in large changes in Vicon "plane of elevation" and axial rotation components. For all Euler decomposition orders, gimbal lock occurs when $\beta = 0^{o}$ and $\beta = 180^{o}$. Since all movements began and ended with the arm in a vertical starting position, gimbal lock occurred most frequently using this decomposition order and was observed for both planar Group 1

activities and Group 2 ADL activities. Gimbal lock was not observed for Group 3 lifting activities where the start and end of each movement cycle was defined when the hand was in contact with the can at the side of the trunk prior to and following lifting. The close proximity of the neutral upper limb reference position used to the singularity posture of 0^o humeral elevation therefore rendered this method unsuitable for this study.

In general, researchers recommend the use of the Euler YXY sequence for the description of both humerothoracic and glenohumeral motions. However, if motions around the gimbal lock postures (0^o and 180^o) are of importance, the use of more than one alternative rotation sequence has been suggested. Senk and Cheze (2006) found an Euler XZY decomposition to be the most suitable to describe elevation in the frontal plane according to gimbal lock incidence and amplitude coherence i.e. the computed angle amplitude of the primary component of motion is comparable to the maximal known angular range reported in literature. The use of both a ZXY sequence (FLEX/EX, ADD/ABD, INT/EXT) for approximately sagittal plane movements, and an XZY sequence (ADD/ABD, FLEX/EX, INT/EXT) for approximately frontal plane movements has been suggested and applied (Kontaxis et al., 2009; Cutti et al., 2008; Biomch-L, 2009).

Figures 6.4a and 6.4b show examples of abduction activity joint rotation curves computed using a ZXY and XZY Cardan decomposition order respectively.

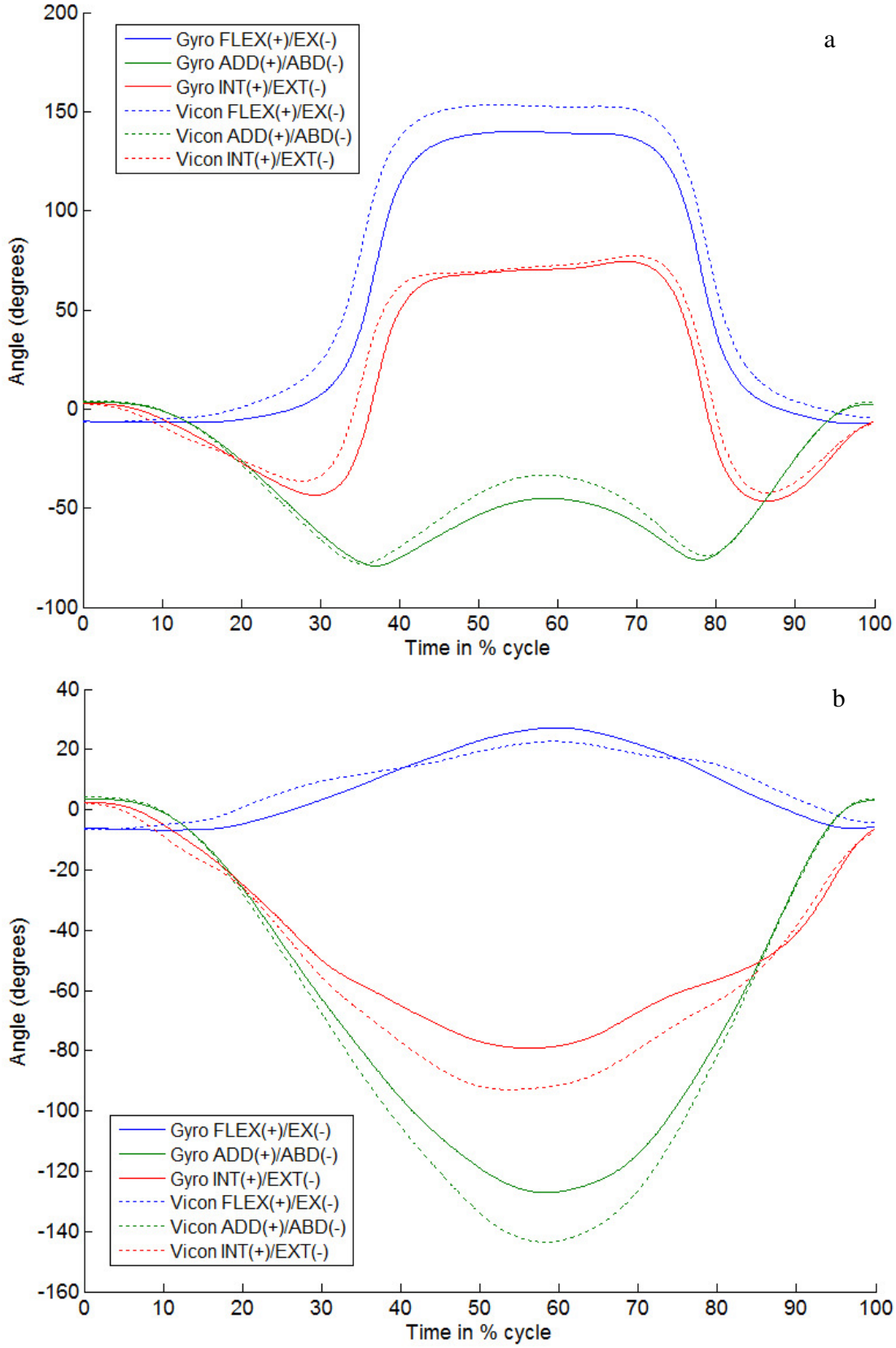

Figure 6.4 Example of humerothoracic joint angles calculated from an abduction activity using **a)** ZXY (non-gimbal lock trial) and **b)** XZY Cardan decomposition sequences.

It can be seen that changing the rotation sequence has a dramatic effect on the calculated joint angles. Use of the XZY sequence eliminated the occurrence of gimbal lock for all affected abduction trials. It is clear that the joint angles calculated using the ZXY sequence (figure 6.4a) appear less intuitive to interpret; large joint angles are calculated for all three movement dimensions and the ADD/ABD rotation is restricted to $\pm 90^{o}$. In contrast, the XZY curves (figure 6.4b) gave a large ADD/ABD rotation and a small FLEX/EX rotation which would be expected for a frontal plane motion. Use of the XZY sequence for largely frontal plane motions therefore not only eliminates gimbal lock but also gives joint angles which are more representative of the actual motion. The effect of decomposition order on joint angle output is discussed further in Chapter 7.

The assignment of the two Cardan decomposition orders as described above was straightforward for Group 1 planar movements. However, this was not the case for Group 2 ADL and Group 3 lifting activities where humeral movement tended to occur in between the sagittal and frontal planes. In a previous study where two Cardan decomposition orders were used, the plane of movement execution was also specified (Cutti et al., 2008). In this study, upper limb movements were performed freely, and the use of either decomposition order did not give rise to gimbal lock for Group 2 or 3 activities. Since it was not apparent which of the two sequences was most appropriate, all ADL and Lifting activities were decomposed using the ZXY (floating axis) sequence to facilitate comparison between activities. Examples of joint rotation curves from all movement activities can be found in Appendix B. The 11 upper limb activities and their corresponding Cardan angle decomposition sequences are presented in table 6.1 below.

Group	Movement activity	Cardan sequence
1: Planar movements used in clinical functional examination	Flexion	ZXY
	Extension	ZXY
	Abduction	XZY
	External rotation	ZXY
	Internal rotation	ZXY
2: Activities of daily living (ADL)	Hand to mouth	ZXY
	Opposite shoulder	ZXY
	Back of head	ZXY
	Same shoulder	ZXY
3: Lifting	Lift: shoulder	ZXY
	Lift: head	ZXY

Table 6.1 Cardan decomposition order used to calculate joint rotation angles for each upper limb activity.

6.2 Range of motion, maximum angle and target angle

Four sets of angle variables were calculated from the joint rotation data to facilitate comparison between subject groups and to investigate any differences between the Vicon and 3D gyroscope systems. These angle variables were:

1. Range of motion (ROM): The minimum angle subtracted from the maximum angle obtained during the movement activity.
2. Maximum angle: the largest humerothoracic angle obtained during the movement activity.
3. Minimum angle: the smallest humerothoracic angle obtained during the movement activity.
4. Target angle: The humerothoracic angle when the hand was in the target position. The target position was defined when the resultant linear velocity of a specified hand marker was 0 m/s in the middle of the movement cycle.

This section presents the joint angle variables computed from the 3D gyroscope system joint rotation curves for each subject group. Further statistical analysis to investigate differences between the Vicon and 3D gyroscope systems is described in sections 6.4 (Linear regression) and 6.5 (Difference between the two systems in 3D).

6.2.1 Group 1 activities

Figures 6.5a and 6.5b present the mean maximum and minimum angles, and mean target angles respectively of the Group 1 activities (Planar movements used in clinical functional examination), computed from the 3D gyroscope system joint rotation curves. Each bar represents a mean of 15 data points for one subject group (5 subjects, 3 trials each). Mean Group 1 ROM values for each subject group are presented in table 6.2a. Tables of mean maximum, minimum, target, and angle values at 0% movement cycle can be found in Appendix C.

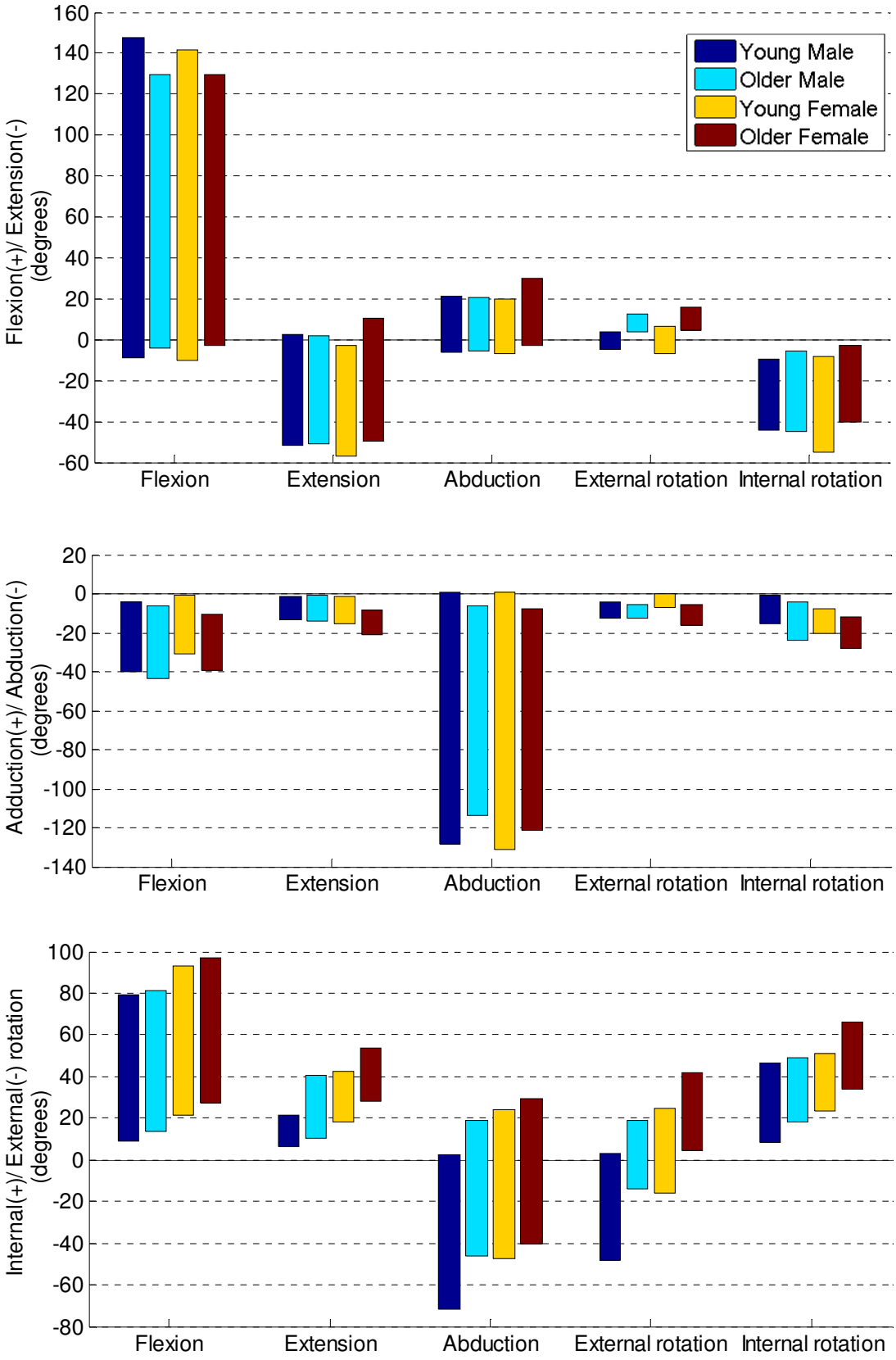

Figure 6.5a Mean 3D gyroscope system maximum and minimum angles (n=15) of Group 1 activities (Planar movements used in clinical functional examination).

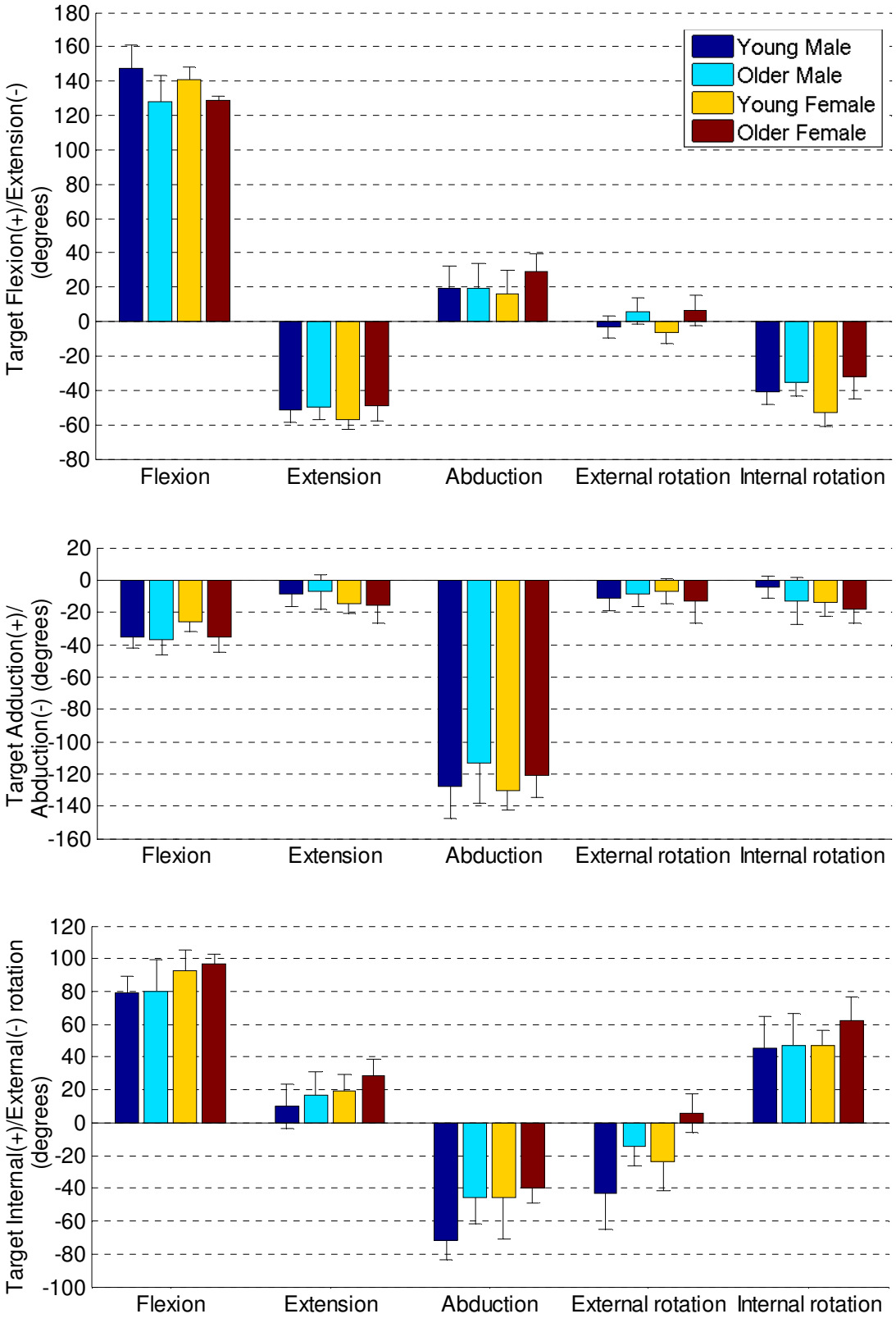

Figure 6.5b Mean 3D gyroscope system target angles (±1SD, n=15) of Group 1 activities (Planar movements used in clinical functional examination).

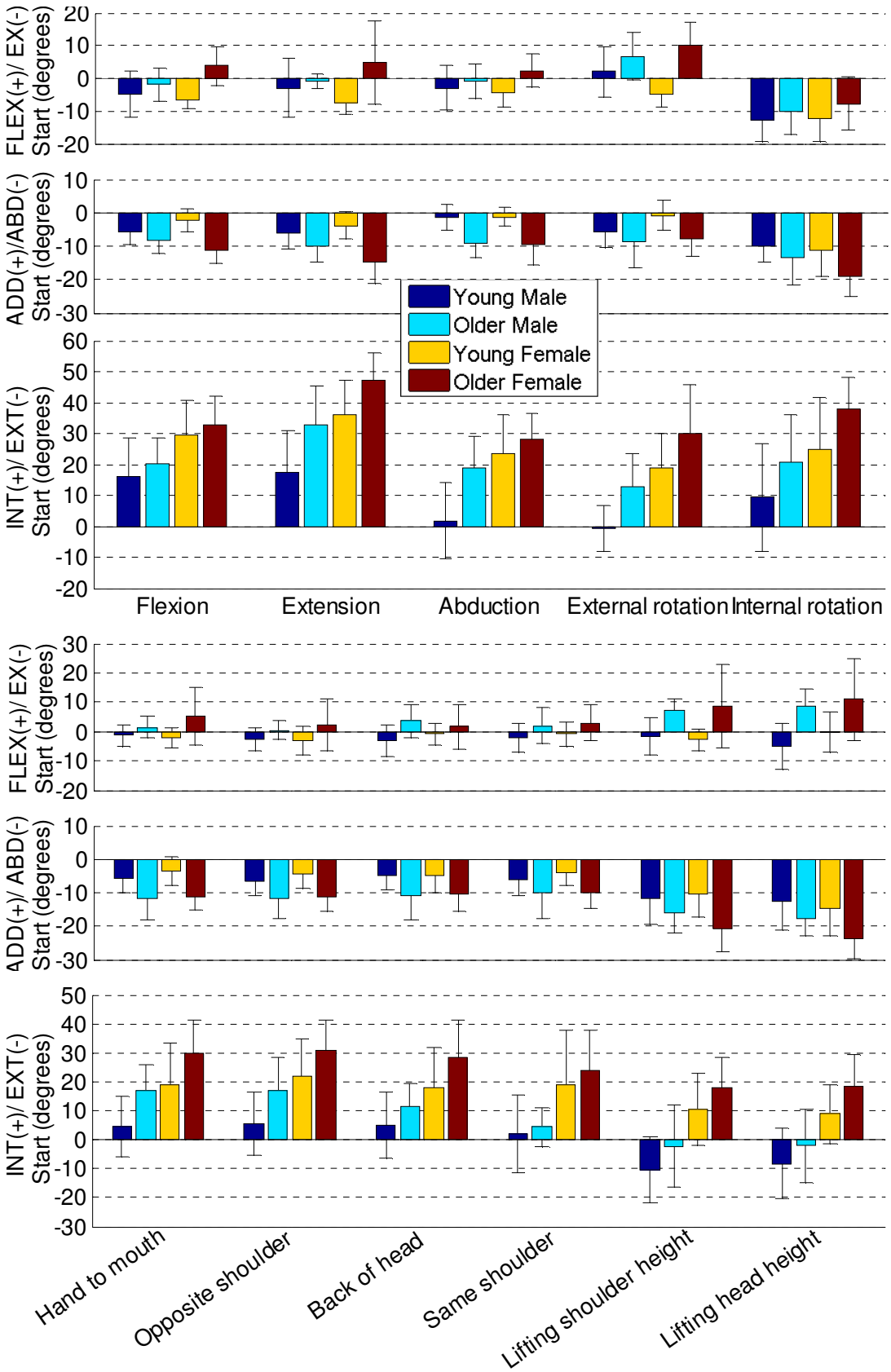

Figure 6.5c Mean 3D gyroscope system angles at 0% movement cycle (±1SD, n=15) for all 11 upper limb activities.

Activity	Group	Gyroscope ROM (degrees)					
		FLEX/EX		ADD/ABD		INT/EXT	
		Mean	*SD*	Mean	*SD*	Mean	*SD*
Flexion	YM	156.6	*13.1*	35.8	*6.0*	70.0	*19.8*
	OM	133.7	*11.9*	37.7	*10.7*	67.7	*18.9*
	YF	151.7	*8.3*	30.4	*9.3*	71.2	*11.0*
	OF	132.2	*6.5*	28.3	*6.8*	70.2	*11.1*
Extension	YM	54.0	*6.8*	12.2	*5.4*	15.3	*7.0*
	OM	52.9	*11.3*	13.1	*5.9*	30.2	*11.1*
	YF	54.6	*4.5*	13.8	*4.6*	24.0	*7.6*
	OF	60.7	*14.2*	13.0	*5.3*	26.0	*7.9*
Abduction	YM	27.2	*14.0*	129.3	*20.5*	74.7	*11.3*
	OM	26.3	*11.1*	107.6	*21.2*	64.6	*16.3*
	YF	27.0	*6.5*	132.0	*11.1*	71.4	*18.5*
	OF	32.7	*12.7*	113.7	*14.2*	69.6	*12.8*
External rotation	YM	8.8	*3.2*	8.2	*2.9*	51.5	*9.5*
	OM	6.8	*3.0*	5.6	*2.2*	34.3	*11.0*
	YF	8.2	*5.6*	7.9	*4.9*	46.8	*12.8*
	OF	11.0	*5.7*	11.1	*10.3*	37.5	*7.2*
Internal rotation	YM	34.9	*8.6*	14.5	*5.6*	38.1	*6.6*
	OM	39.7	*7.4*	19.8	*7.3*	30.9	*12.6*
	YF	46.9	*4.3*	12.6	*5.5*	27.5	*13.2*
	OF	37.4	*8.4*	16.3	*4.9*	31.7	*12.3*

Activity	Group	Gyroscope ROM (degrees)					
		FLEX/EX		ADD/ABD		INT/EXT	
		Mean	*SD*	Mean	*SD*	Mean	*SD*
Hand to mouth	YM	46.9	*10.6*	18.1	*3.5*	23.2	*9.6*
	OM	48.3	*5.2*	20.4	*4.8*	34.8	*7.7*
	YF	44.1	*4.7*	12.3	*5.4*	27.4	*3.7*
	OF	56.1	*12.0*	16.9	*8.4*	32.9	*8.7*
Opposite shoulder	YM	62.0	*9.6*	23.0	*9.1*	59.5	*9.4*
	OM	63.9	*5.4*	28.8	*6.4*	58.9	*8.2*
	YF	50.4	*7.6*	22.4	*5.1*	53.2	*4.3*
	OF	66.5	*12.9*	30.9	*6.1*	63.8	*10.3*
Back of head	YM	120.4	*23.9*	60.4	*17.6*	87.4	*42.2*
	OM	93.7	*13.6*	42.8	*7.5*	50.0	*17.3*
	YF	117.9	*12.3*	49.3	*16.2*	67.1	*28.8*
	OF	101.0	*10.3*	40.6	*11.0*	55.9	*13.4*
Same shoulder	YM	21.2	*17.0*	38.9	*18.7*	60.8	*23.8*
	OM	44.4	*21.8*	40.5	*8.5*	39.9	*8.6*
	YF	36.8	*11.0*	38.7	*16.4*	40.1	*15.5*
	OF	47.3	*19.5*	31.2	*16.2*	31.8	*11.7*
Shelf shoulder height	YM	58.7	*9.9*	28.1	*7.4*	32.9	*7.1*
	OM	47.5	*10.5*	24.0	*6.0*	32.2	*7.3*
	YF	50.9	*4.3*	18.9	*9.1*	25.4	*5.9*
	OF	60.5	*19.6*	25.1	*11.7*	45.5	*18.2*
Shelf head height	YM	108.7	*9.9*	50.7	*7.5*	68.6	*17.3*
	OM	85.3	*9.6*	38.9	*5.5*	59.0	*11.0*
	YF	95.2	*11.8*	35.5	*12.7*	52.6	*23.3*
	OF	80.3	*20.0*	29.7	*11.3*	52.4	*17.9*

Table 6.2a and 6.2b Mean 3D gyroscope ROM per subject group for all activities, showing major (white) and minor (grey) joint rotation components.

As described in section 6.1, joint angle data for all Group 1 movement activities were calculated using a ZXY decomposition order, except for the abduction activity where an XZY sequence was used. For all Group 1 activities, 0% movement cycle was defined with the arm in the neutral reference position except for the external rotation activity, where 0% movement cycle was defined with the elbow flexed to 90^{o} and the humerus vertically orientated at the side of the body. In the following descriptions, the term "maximum" may refer to the largest negative value where joint rotations are defined as negative e.g. external rotation.

A clear distinction can be seen between "major" and "minor" joint rotation components of the planar Group 1 activities (figure 6.5a and 6.5b). Major components formed the largest components of the overall joint motion and tended to form the main planes of clinical interest. Minor components tended to form the "out of plane" movements and in this study were defined as components with a mean ROM$<30^{o}$ for each subject group (highlighted in grey in table 6.2a). The categorization of minor components was largely found to be consistent across groups although variability did occur within subject groups, e.g. FLEX/EX component of the abduction activity for older females ($32.7^{o}\pm12.7$).

Since the aim of the clinically relevant Group 1 movements was to determine the maximal movement in a particular plane, this group was highly populated with minor joint rotation components which would not form the main clinical focus in upper limb functional examination. The extension and external rotation activities both displayed one major and two minor components with the principal axis of clinical interest as the major component. However, this was not the case for all Group 1 activities. Figures 6.5a-b and table 6.2a showed that both the flexion and abduction activities displayed large axial rotation components. Similarly, the internal rotation activity displayed more than one major component; figures 6.5a-b showed that the shoulder extension component was larger than the internal rotation component for three of the four subject groups, despite not being the component of primary clinical interest. This was due to the large amount of shoulder extension required to position the hand in the "reach up back" activity used to measure upper limb internal rotation.

This activity was therefore more characteristic of an ADL rather than a planar movement.

For the flexion, abduction and external rotation activities, mean ROM values were larger for young subjects compared with older subjects for the planes of primary clinical interest. This was also true for mean maximum and target angle values. Differences between young and older subjects were also observed for Group 2 activities as described in section 6.2.2.

For the INT/EXT component, a clear pattern in mean maximum, minimum and target values was evident for all Group 1 activities. Older females consistently displayed the largest internal rotation and smallest external rotation values of the four subject groups. The converse was observed for young males. Figure 6.5c showed that angle values at 0% movement cycle were largest for the INT/EXT plane and again followed the same inter-group pattern as for the other INT/EXT joint angle variables i.e. mean angle values at 0% movement cycle were consistently larger for females compared with males and consistently largest for older females and smallest for young males. The results suggest that the observed pattern in INT/EXT joint angle variables may be influenced by inter-group variability in the definition of 0^o axial rotation. This is discussed further in section 7.2.2.

The largest inter-group variability in INT/EXT maximum and target angle values was observed for the external rotation activity. A difference of 53^o was computed between young male and older female mean external rotation values compared with a difference of approximately 26^o for all other Group 1 activities. For the external rotation activity, older females were the only group to exhibit positive mean values (maximum: $4.5^o \pm 12.1^o$; target: $5.4^o \pm 11.8^o$) indicating internal rotation of the humerus with the hand in the target position. This was unintuitive for an external rotation activity. The large inter-group variability observed may be the result of differences in function between groups. This is discussed further in section 7.2.2.

For the internal rotation activity, the mean 3D gyroscope system angles at 0% movement cycle (figure 6.5c) show that the humerus was more extended and abducted in the starting position compared with the other Group 1 activities. To

prevent occlusion of the forearm markers during recording, the forearm marker cluster was relocated from the posterior to the anterior aspect of the forearm for this activity. The observed differences in FLEX/EX and ABD/ADD humerothoracic angles at 0% movement cycle compared with the other group 1 activities is therefore likely to be a reflection of this change in marker cluster position.

6.2.2 Group 2 and 3 activities

The joint angle variables of Group 2 (Activities of daily living) and Group 3 (Lifting) activities are presented in figures 6.6a and 6.6b. Each bar represents a mean of 15 data points for one subject group (5 subjects, 3 trials each). Mean Group 2 and 3 ROM values for each subject group are presented in table 6.2b. Tables of mean maximum, minimum, target, and angle values at 0% movement cycle can be found in Appendix C. As described in section 6.1, joint angle data for all Group 2 and Group 3 movement activities were calculated using a ZXY decomposition order. In the following descriptions, the term "maximum" may refer to the largest negative value where joint rotations are defined as negative e.g. external rotation.

In contrast to Group 1 activities, figures 6.6a and 6.6b showed that the distinction between major and minor joint rotation components was less pronounced for Group 2 and 3 activities. Movement in all three planes tended to form large components of the overall motion with fewer minor movement components (41% of joint rotation curves with ROM<30^{o} were Group 2 and 3 activities compared with 59% of Group 1 activities). This indicated that Group 2 and 3 activities were more complex in character compared with Group 1 activities and tended to occur outside of the clinically defined planes of motion. Figures 6.6a-b, and table 6.2b showed that minor movement components for Group 2 and 3 activities included the ADD/ABD components of the "hand to mouth", "opposite shoulder" and "lifting to shoulder height" activities. The ADD/ABD component tended to form the smallest component of all Group 2 and 3 activities. This was also true for Group 1 activities except for the shoulder abduction movement which was decomposed using an XZY sequence as described in section 6.1.

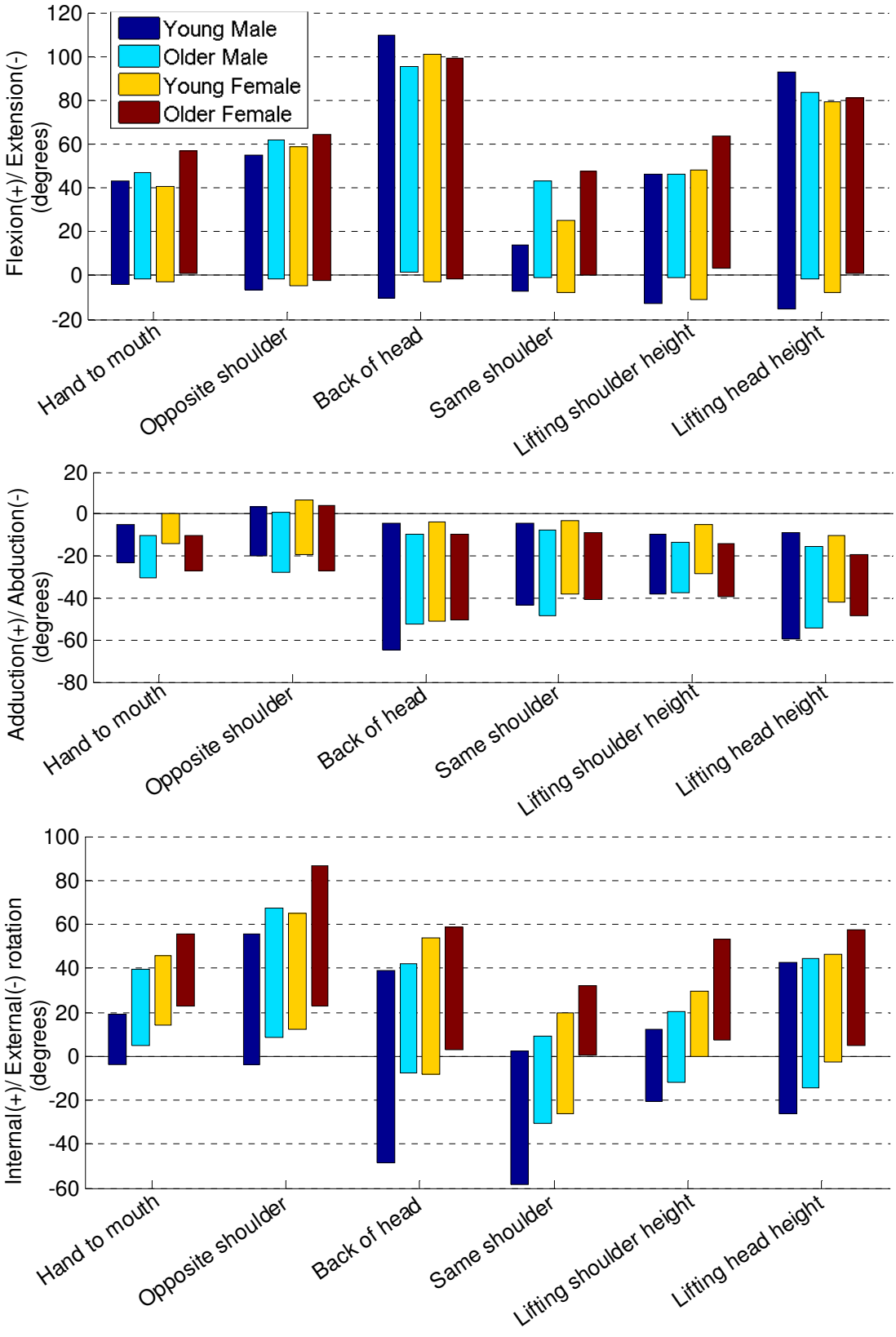

Figure 6.6a Mean 3D gyroscope system maximum and minimum angles (n=15) of Group 2 (Activities of daily living) and Group 3 (Lifting) activities.

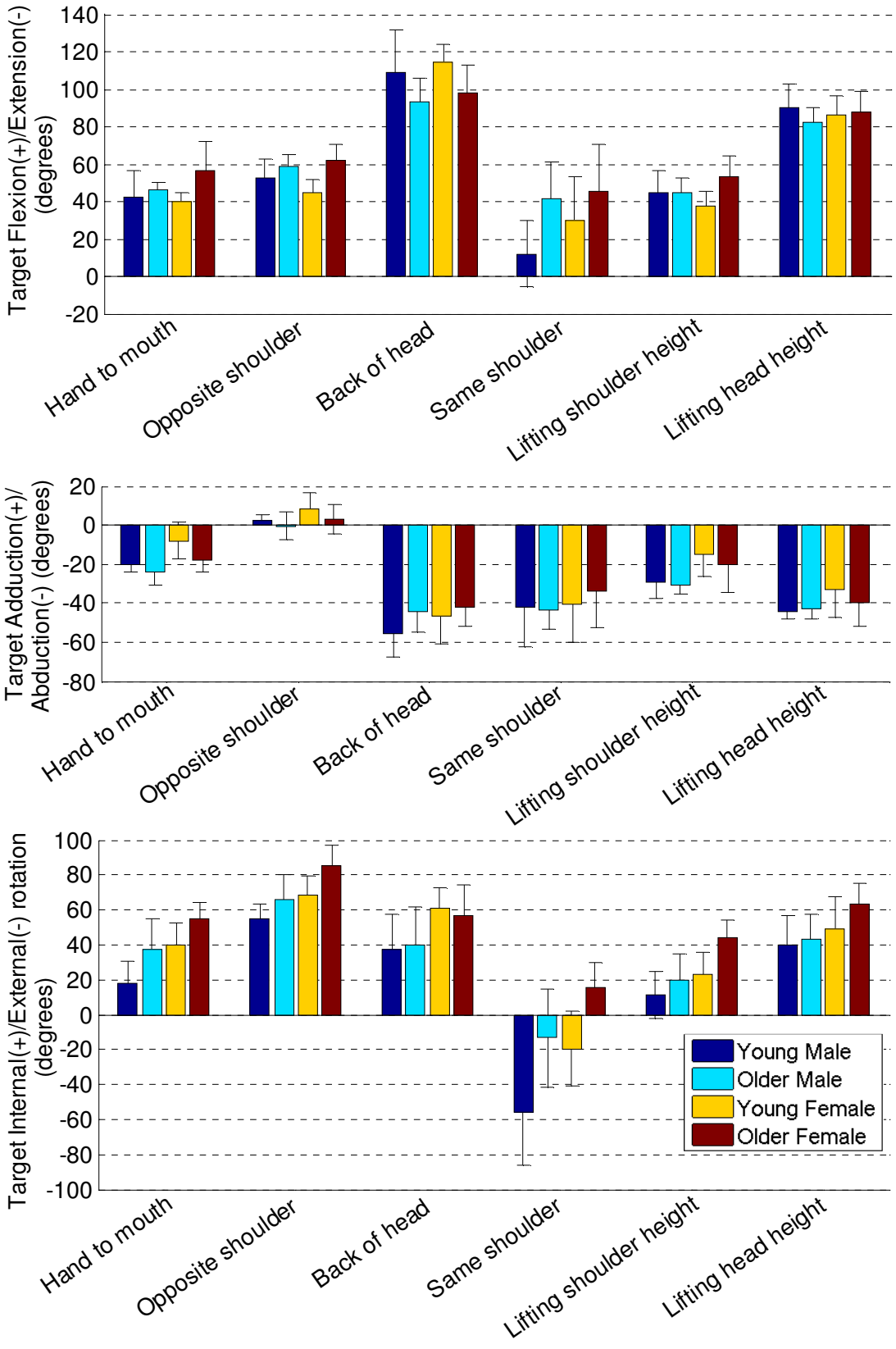

Figure 6.6b Mean 3D gyroscope system target angles (±1SD, n=15) of Group 2 (Activities of daily living) and Group 3 (Lifting) activities.

Figure 6.5c shows a clear difference in joint angle values at 0% movement cycle between Group 2 ADL and Group 3 lifting activities for all three planes. For Group 3 lifting activities, 0% movement cycle was defined when the hand grasped the can located at the side of the body prior to lifting. Figure 6.5c shows that the humerus was more abducted and less internally rotated/ more externally rotated in this position. This was in contrast to Group 2 ADL activities where 0% movement cycle was defined with the arm in the neutral reference position. For all activities, the start and end of the movement cycle was identified when the resultant velocity of a specified hand marker approximated 0 m/s towards the beginning and end of each movement trial.

A clear pattern in INT/EXT mean maximum, minimum and target angle values (figures 6.6a-b) and mean INT/EXT angles at 0% movement cycle (figure 6.5c) was again evident as described for Group 1 activities. The results suggest that the values of INT/EXT joint angle variables may be influenced by inter-group variability in the definition of 0^o axial rotation. This is further discussed in section 7.2.2. In addition to the observed pattern, large inter-group differences in external rotation components were evident for the "back of head" and "same shoulder" activities. A mean difference of approximately 50^o-60^o was computed between young male and older female axial rotation values for the "back of head" and "same shoulder" activities compared with a difference of approximately 26^o for all other Group 2 and 3 activities. These observations suggested differences in movement performance between groups for these activities which are described further below.

Intra- and inter-group variability in mean ROM values was most apparent for the components of the "hand to back of head" and "same shoulder" activities (table 6.2b and figures 6.6a-b) and indicated differences in movement performance between groups. The majority of subjects performed the "hand to back of head" activity in between the sagittal and frontal planes. However, it was observed that three young males and two young females performed this activity largely in the frontal plane. The resulting joint angle curves displayed an increase in ROM in all three dimensions compared to individuals with no planar preference as shown in figure 6.7. In addition, mean FLEX joint angle variables (ROM, maximum and target angle

values) were larger than mean ABD joint angle variables which was counter-intuitive. Joint angle curves for these five young individuals were comparable to those obtained from an abduction activity computed using a ZXY decomposition sequence (figure 6.4a). Although frontal plane motions decomposed using the ZXY sequence were prone to gimbal lock as described in section 6.1, this was not observed for the "back of head" joint angle curves, indicating that the humerus did not approach the singularity posture of 90^{o} abduction during this activity.

Differences in "hand to back of head" joint rotation curves due to movement preference were most apparent for the INT/EXT component. All subjects initially externally rotated the humerus at the beginning of the movement cycle before internally rotating to locate the hand in the target position. This external rotation component was much larger for subjects who exhibited a frontal plane preference compared to those with no planar preference, as shown in figure 6.7. This was particularly true for the young male group which displayed the largest EXT (negative) angle values and mean axial rotation ROM values of the four subject groups (figure 6.6a and table 6.2b). Thus, large inter-group variability in mean external rotation values was recorded which was in addition to the observed pattern in axial rotation described previously. For all groups, the humerus was internally rotated with the hand in the target position as indicated by the mean target angle values (figure 6.6b). Inter-group variation in mean internal rotation values was smaller compared with inter-group variation in external rotation components. The large axial rotation ROM recorded for young subjects were therefore the result of a larger external rotation component for these groups, particularly for young males.

The five individuals who demonstrated a frontal plane preference for the "hand to back of head" activity also exhibited differences in movement performance for the "same shoulder" activity. As for the "back of head" activity, large inter-group variability in mean external rotation joint angle variables (ROM, maximum and target angle values) was observed (figures 6.6a and 6.6b) which was in addition to the observed pattern in axial rotation described above. In contrast to the "back of head" activity, the humerus was externally rotated with the hand in the target position (figure 6.6b) with the exception of the older female group.

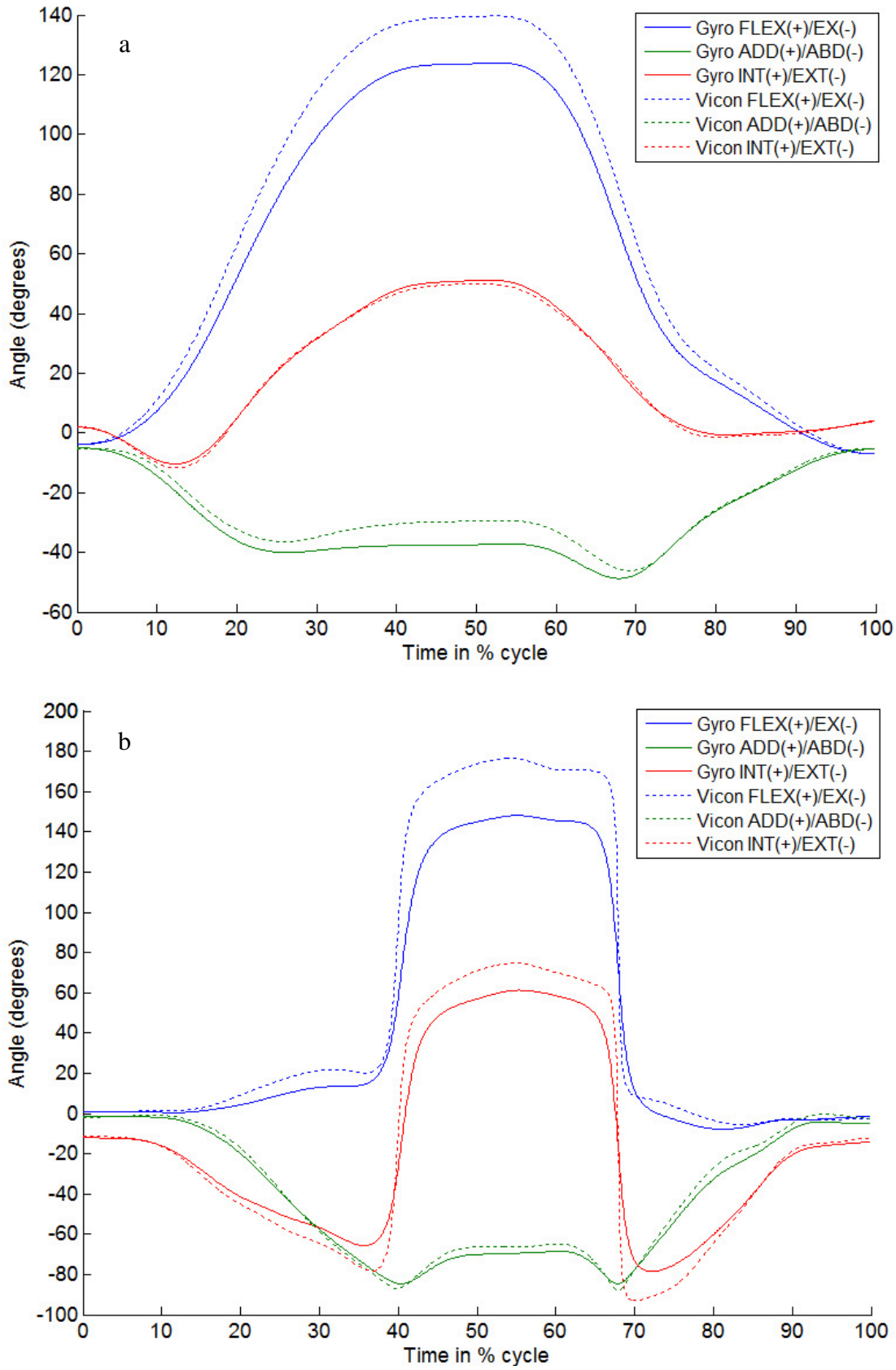

Figure 6.7 Joint rotation curves for a "hand to back of head" movement performed **a)** in between the frontal and sagittal planes, and **b)** largely in the frontal plane

For the five young individuals who exhibited differences in "hand to same shoulder" movement performance, external rotation formed the largest component of the activity and was accompanied by a very small shoulder flexion component to locate the hand in the target position. This was particularly apparent for the young male group, which displayed the largest external rotation and smallest flexion components of the four subject groups. In contrast for older subjects shoulder flexion formed the largest component of the overall motion and was accompanied by a smaller external rotation component. Mean ADD/ABD joint angle variables were relatively consistent across the four subject groups.

Mean target angles for the "same shoulder" activity (figure 6.6b) displayed large inter-group variability and were comparable to those recorded for the Group 1 external rotation activity (figure 6.5b). Common to both activities, the older female group was the only group to internally rotate the humerus with the hand in the target position. In addition, EXT target angles were larger for young subjects compared with older subjects, and this finding was also echoed in the mean ROM values (table 6.2b).

For Group 3 lifting activities, the mean target angle values indicated that the humerus was flexed, abducted, and internally rotated with the hand in the target position. As expected, mean ROM, maximum and target angle values for the "lifting to head height" activity were larger than for the "lifting to shoulder height" activity (table 6.2b and figures 6.6a-b). Mean joint angle variables recorded for the "lifting to head height" activity were similar in magnitude to those recorded for the "back of head" components.

6.3 Correlation

For each movement activity, the Pearson product moment correlation coefficient, r, between the Vicon and the 3D gyroscope system joint rotation curves were calculated. The mean correlation values and the mean gyroscope ROM values from 20 subjects are presented in Tables 6.3 and 6.4 respectively. The minor movement components (defined in section 6.2 as components with mean ROM<30^{o}) have been highlighted in grey and the major movement components in white.

Group	Movement activity	FLEX/EX	ADD/ABD	INT/EXT
1: Planar movements used in clinical functional examination	Flexion	0.999 ± 0.001	0.966 ± 0.030	0.996 ± 0.004
	Extension	0.999 ± 0.001	0.785 ± 0.246	0.911 ± 0.262
	Abduction	0.872 ± 0.273	0.999 ± 0.006	0.991 ± 0.011
	External rotation	0.822 ± 0.278	0.778 ± 0.277	0.995 ± 0.019
	Internal rotation	0.993 ± 0.009	0.749 ± 0.293	0.943 ± 0.183
2: Activities of daily living (ADL)	Hand to mouth	0.997 ± 0.015	0.929 ± 0.083	0.990 ± 0.021
	Opposite shoulder	0.998 ± 0.004	0.954 ± 0.059	0.998 ± 0.003
	Back of head	0.996 ± 0.009	0.979 ± 0.019	0.982 ± 0.026
	Same shoulder	0.920 ± 0.206	0.991 ± 0.012	0.987 ± 0.016
3: Lifting	Lift: shoulder	0.997 ± 0.004	0.933 ± 0.069	0.990 ± 0.008
	Lift: head	0.997 ± 0.002	0.895 ± 0.110	0.993 ± 0.005

Table 6.3 Mean correlation values for 20 subjects (n=20) showing major (white) and minor (grey) joint rotation components.

Group	Movement activity	FLEX/EX	ADD/ABD	INT/EXT
1: Planar movements used in clinical functional examination	Flexion	143.55 ± 14.79	33.04 ± 9.07	65.76 ± 15.43
	Extension	55.57 ± 10.14	13.03 ± 5.21	23.86 ± 9.98
	Abduction	28.27 ± 11.44	120.66 ± 19.78	70.08 ± 15.06
	External rotation	8.70 ± 4.68	8.19 ± 6.18	42.51 ± 12.25
	Internal rotation	39.73 ± 8.49	15.78 ± 6.31	32.07 ± 11.84
2: Activities of daily living (ADL)	Hand to mouth	48.88 ± 9.62	16.95 ± 6.42	29.58 ± 8.88
	Opposite shoulder	60.71 ± 10.97	26.25 ± 7.61	58.86 ± 9.00
	Back of head	108.24 ± 19.20	48.27 ± 15.54	65.09 ± 30.67
	Same shoulder	37.43 ± 20.11	37.32 ± 15.54	43.12 ± 18.94
3: Lifting	Lift: shoulder	54.41 ± 13.23	24.03 ± 9.21	34.01 ± 12.82
	Lift: head	92.36 ± 17.08	38.65 ± 12.23	58.16 ± 18.70

Table 6.4 Mean gyroscope ROM values (degrees) for all 20 subjects (n=60) showing major (white) and minor (grey) joint rotation components.

Table 6.3 shows that the mean correlation values were generally high, indicating a strong linear relationship between the calculated joint rotation data from the Vicon and 3D gyroscope systems. Low accompanying SD values indicated low intra and inter-subject variation of correlation values from the mean.

6.3.1 Group 1 activities

Whilst the majority of the mean correlation values were greater than 0.9, four of the five Group 1 activities displayed low mean correlation values of between 0.7 to 0.9. These were accompanied by high SD values greater than 0.2, indicating large variability of correlation values from the mean. These low mean correlation and high SD values tended to occur for the minor movement components, defined in section 6.2 as components with a mean ROM<30^{o} for each subject group. These components neither formed the main plane of clinical interest, nor a large component of the overall motion. Conversely, consistently high correlation values were recorded for major movement components, as indicated by high mean correlation values and low SD values. These major movement components tended to have mean ROM>30^{o} and formed either the largest components of the overall motion or the

main planes of interest. For example, the external rotation movement gave low mean correlation and high SD values greater than 0.2 for the FLEX/EX (0.822±0.278) and ADD/ABD (0.778±0.277) components which did not contribute largely to the overall motion. Conversely, high mean correlation and low SD values were obtained for the INT/EXT component (0.995±0.019) which formed the largest component of the overall motion.

The data showed a link between low correlation values and range of motion (ROM); 95% of correlation values of $r \leq 0.7$ were calculated from joint rotation curves with ROM<25^o, with 5% corresponding to a ROM between 25^o to 40^o. Low correlation values equal to or below 0.7 only formed 3.5% of the total number of correlation values (n=1980) obtained for all upper limb activities, subjects and trials. However, 26% of the total number of joint rotation curve pairs (n=1980) had ROM<25^o. This meant that whilst some low ROM components gave rise to low correlation values, the majority of correlation values calculated from joint rotation curve pairs with ROM<25^o were greater than 0.7 (83% greater than 0.7, 63% greater than 0.9). Low ROM components therefore gave rise to inconsistency in correlation values and displayed large intra- and inter-subject variability.

As described in section 6.2, the planar nature of Group 1 activities meant that this group was highly populated with minor movement components which would generally not form the main clinical focus in upper limb functional examination. More specifically, 66% of joint rotation curve pairs with ROM<25^o were Group 1 activity components. It follows that this movement group was more highly populated with low correlation values of $r \leq 0.7$ compared with groups 2 and 3. Indeed, 84% of the total number of correlations of $r \leq 0.7$ was obtained for Group 1 activity components. This therefore accounted for the high SD and low mean correlation values observed for this group compared with groups 2 and 3. Major movement components, in contrast, gave consistently high mean correlation values greater than 0.9 and low SD values. This indicated a consistently strong linear relationship between the Vicon and 3D gyroscope systems with low intra- and inter-subject variability of correlation values from the mean.

Flexion

Several further observations were made regarding Group 1 data from Tables 6.3 and 6.4 and the joint rotation curves (Appendix B). The shoulder flexion activity gave high mean correlation values greater than 0.9 for all three movement planes. SD values were also very low, being the only Group 1 activity which did not give SD values greater than 0.2 for any of its movement components. The joint rotation curves and ROM data presented in section 6.2 showed that both flexion and internal rotation formed major components of the overall motion. As the main plane of clinical interest, flexion formed the largest component of the overall motion with the highest mean correlation and lowest SD values (0.999±0.001) of the three components, followed by the internal rotation component (0.996±0.001). Movement in the abduction plane formed the smallest component of the overall movement. Despite a mean ROM of less than 40^o (GROM $33^o \pm 9^o$, n=60), no correlation values of $r \leq 0.7$ were obtained for any individual or trial. In relative terms, the abduction component gave the lowest mean correlation and highest SD values (0.966±0.030) of the three components, indicating relatively greater intra- and inter-subject variability of correlation values compared with the more consistent results obtained for the plane of interest.

Abduction

As described in section 6.2, axial rotation formed a major component of the abduction activity. As the main plane of clinical interest, abduction formed the largest component of the overall motion with the highest mean correlation and lowest SD values (0.999 ± 0.006) of the three components, followed by the external rotation component (0.991 ± 0.011). Flexion formed the minor movement component of the abduction activity which was reflected in the low mean correlation and high SD values (0.872 ± 0.273) indicating large variability of correlation values from the mean.

Internal rotation

As described in section 6.2, movement in both the FLEX/EX and INT/EXT planes formed the major components of the internal rotation activity due to the large amount

of shoulder extension required to position the hand in the "reach up back" activity. Despite forming the plane of interest, the mean ROM data (table 6.4) showed that movement in the INT/EXT plane was not the largest movement component, with a mean GROM of $32^{o}\pm12^{o}$. This was the only Group 1 activity to give correlation values of $r\leq0.7$ for a plane of interest. Movement in the FLEX/EX plane formed the largest component of the overall motion with a mean ROM of $40^{o}\pm9^{o}$ with no correlation values of $r\leq0.7$. The mean correlation and SD values indicated a consistently strong linear relationship between the two systems for the FLEX/EX plane (0.993±0.009) with more variable results for the INT/EXT plane (0.943±0.183). Movement in the ADD/ABD plane formed the minor component of this activity with mean ROM $16^{o}\pm6^{o}$. The minor movement component gave the lowest mean correlation and highest SD values (0.748±0.293) of the three components, indicating a large degree of intra- and inter-subject variability.

6.3.2 Group 2 and 3 activities

Mean correlation values for Group 2 and 3 activities (ADL and lifting) were generally consistently high ($r\geq0.9$) and SD values consistently low compared with Group 1 activities. As described in section 6.2, group 2 and 3 activities displayed fewer minor movement components compared with group 1 activities. Indeed, only 34% of joint rotation curve pairs with ROM$<25^{o}$ were obtained for Group 2 and 3 activities compared with 66% obtained for Group 1 activities. It follows that only a small proportion (16%) of the total number of correlation values of $r\leq0.7$ were obtained for Group 2 and 3 activities compared with 84% obtained for Group 1 activities as previously described. This therefore accounted for the high mean correlation and low SD values observed.

Two movement components gave elevated SD values. These were the FLEX/EX component of the "same shoulder" activity and the ADD/ABD component of the "lifting to head height" activity. The FLEX/EX component of the same shoulder activity had a relatively low mean correlation value and an SD value greater than 0.2 (0.920±0.206) indicating large spread of correlation values from the mean. The ADD/ABD and INT/EXT components, in contrast, had high mean correlation and

low SD values (0.991±0.012 and 0.987±0.016 respectively) indicating low intra- and inter-subject variability. As described in section 6.2, three young males and two young females displayed a strong preference to perform this activity in the frontal plane. This differed from the majority of subjects who performed this movement in between the frontal and sagittal planes. Inter-subject differences in movement execution gave rise to large variability in ROM values for all planes of motion (table 6.2b) which was reflected in the large SD values. In particular, subjects with a frontal plane preference displayed very low ROM FLEX/EX components compared to subjects with no planar preference. The FLEX/EX plane was the only component to give correlation values of $r \leq 0.7$ which accounted for the large variability in FLEX/EX correlation values observed in table 6.3. Nevertheless, the corresponding mean correlation value was greater than 0.9, indicating that only a small number of very low correlation values were computed. Although the ADD/ABD and INT/EXT components also displayed variability in ROM, no correlation values of $r \leq 0.7$ were calculated and mean correlation values were consistently high for both components. As described in section 6.2, a frontal plane preference was similarly observed for the "back of head" activity, giving rise to large inter and intra-group variability in ROM values as indicated by the high SD values (tables 6.2b and 6.4). ROM in each dimension was larger and no correlation values of $r \leq 0.7$ were computed.

The ADD/ABD component of the "lifting to head height" activity also gave a high SD and relatively low mean correlation value (0.892±0.108). The ADD/ABD component gave the lowest mean ROM for this activity ($37^o \pm 13^o$) and gave rise to correlation values of $r \leq 0.7$. The FLEX/EX and INT/EXT components displayed larger mean ROM values ($101^o \pm 21^o$ and $64^o \pm 20^o$ respectively) coupled with consistently high mean correlation values (0.997±0.003 and 0.993±0.005 respectively).

It can be seen from tables 6.3 and 6.4 that the ADD/ABD components tended to give both the lowest mean ROM values and the lowest mean correlation values of the three dimensions. This was true for group 1, 2 and 3 activities with the exception of the abduction and the "same shoulder" movements. In addition to the FLEX/EX component of the "same shoulder" activity, correlation values of $r \leq 0.7$ were also

obtained for the ADD/ABD components of the "hand to mouth", "lifting to shoulder height" and "lifting to head height" activities. These were the only Group 2 and 3 components to give correlation values of $r \leq 0.7$.

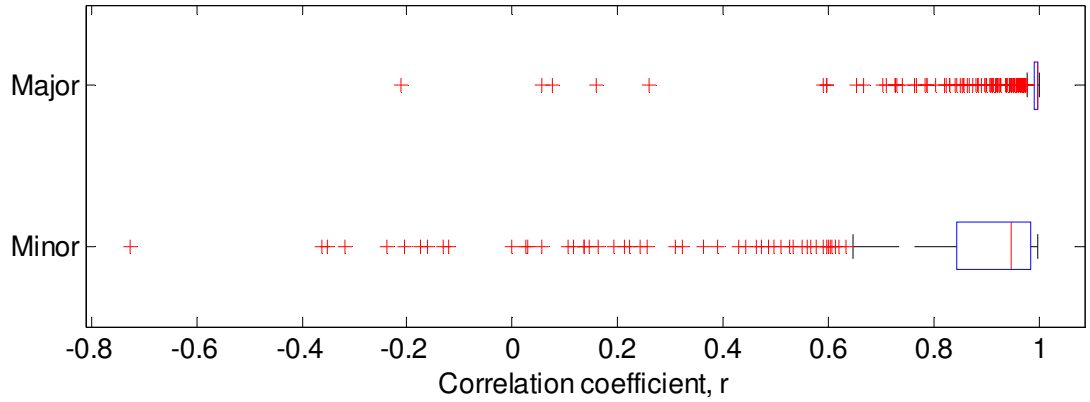

Figure 6.8 Box and whisker plots of correlation coefficient data (r) differentiated for major (1140 samples) and minor (540 samples) movement components.

Figure 6.8 shows a clear distinction between the distribution of correlation values for major and minor joint rotation components. Major movement components exhibited greater consistency in correlation values compared with minor components as shown by the narrow box and short whiskers, as well as fewer correlation values of less than 0.7. Major movement components which gave rise to correlation values of $r \leq 0.7$ were the INT/EXT component of the Group 1 internal rotation activity, the FLEX/EX component of the Group 2 "same shoulder" activity, and the ADD/ABD component of the Group 3 "lifting to head height" activity. As described in section 6.2.1, the internal rotation activity was more characteristic of an ADL movement and was the only Group 1 activity to give correlation values less than 0.7 for a major movement component. The "same shoulder" activity displayed very small FLEX/EX components due to subjects who preferred to perform this movement in the frontal plane, as described in section 6.2. The FLEX/EX component of the same shoulder activity was categorised as a major movement component, but formed a minor component for those subjects with a frontal plane preference.

6.4 Linear regression

Linear regression analysis was carried out using the ordinary least squares method by regressing the range of motion (ROM) variable, presented in section 6.2, calculated from the Vicon and the 3D gyroscope joint rotation curves. A description of linear regression analysis, regression coefficients and goodness of fit statistics can be found in sections 5.3.2.2 and 5.3.2.3. Three sets of regression analyses were carried out:

1. Regression per subject: regression for one subject at a time, looking at each plane of motion in turn (60 regressions in total).
2. Regression per movement component: regression for all 20 subjects at a time, looking at each of the 33 movement components in turn (33 regressions in total).
3. Regression per movement dimension: regression for each plane, involving 660 data pairs.

6.4.1 Regression per subject

The ROM variable calculated from the Vicon joint rotation curves was regressed against the ROM variable calculated from the gyroscope joint rotation curves for one subject at a time, looking at each of the three planes of motion in turn. 20 regression plots, one for each subject, were obtained for each of the three movement dimensions resulting in 60 sets of regression variables in total. Each regression plot consisted of 33 data points (three repeats for each of the 11 upper limb activities). Figures 6.9a-c and 6.10a-c present the regression plots for one young female and one older male respectively for the FLEX/EX, ADD/ABD, and INT/EXT rotation planes of motion. All 60 regression plots can be found in Appendix D.

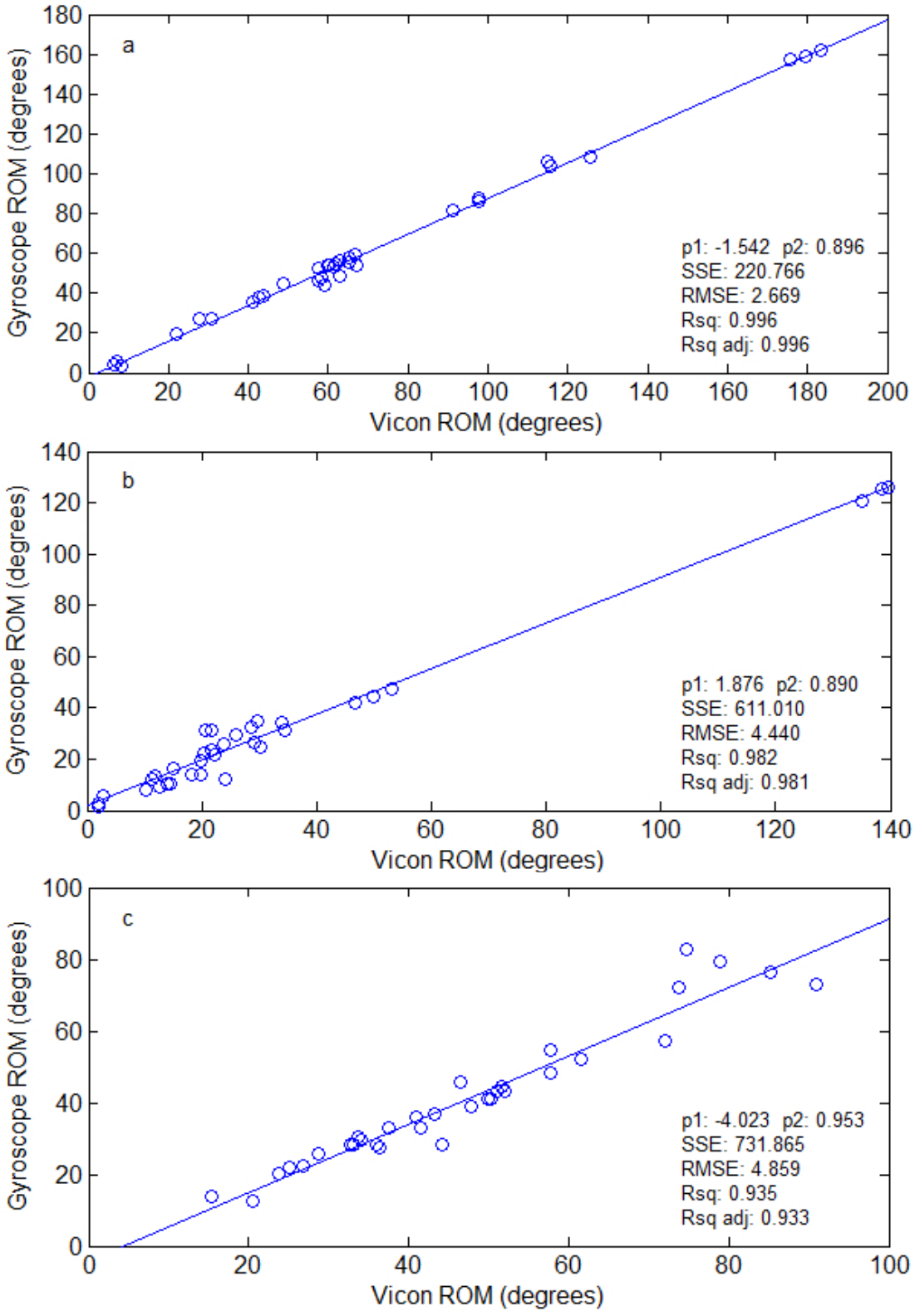

Figure 6.9 Regression plots for a young female subject for **a)** FLEX/EX, **b)** ADD/ABD, and **c)** INT/EXT ROM data.

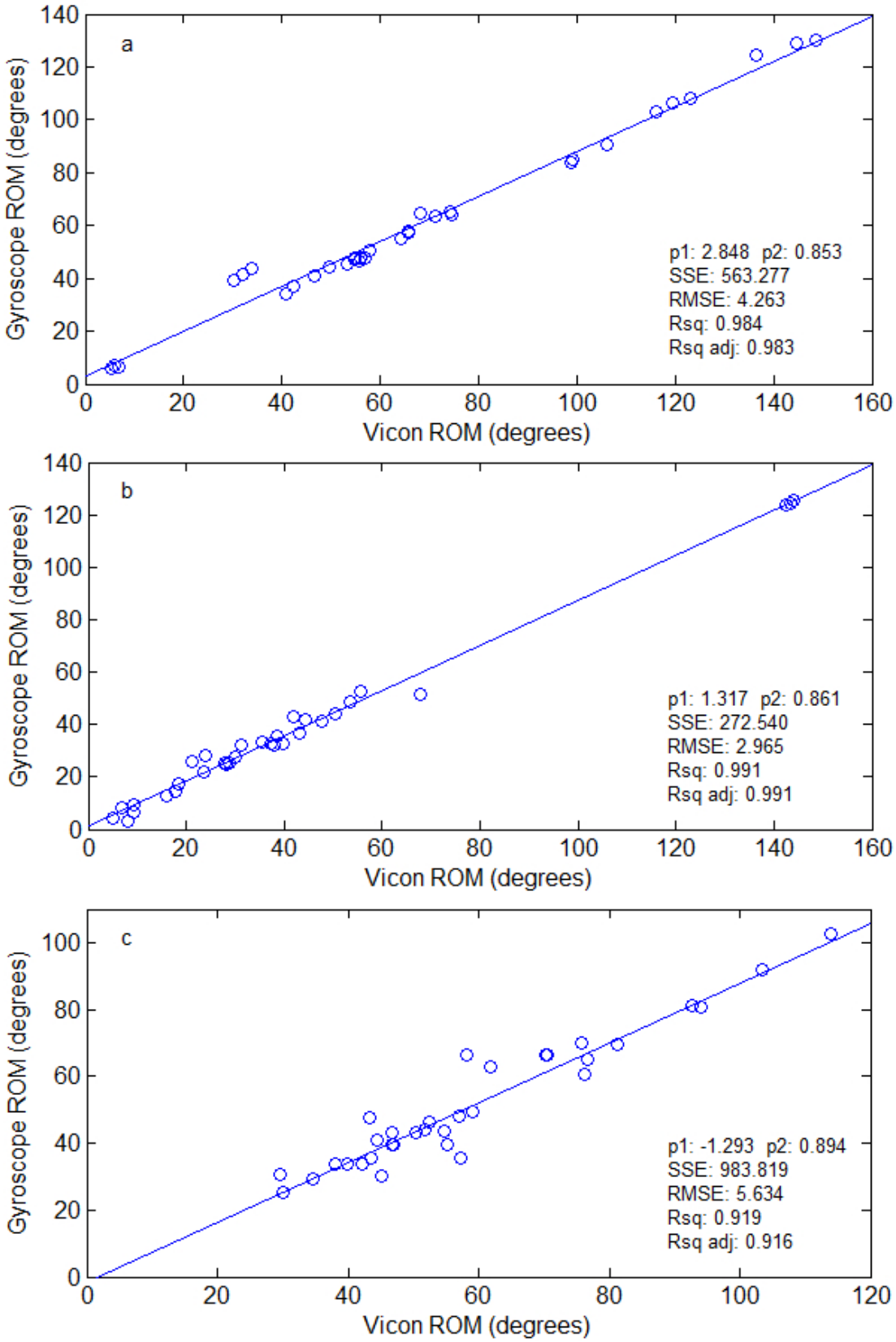

Figure 6.10 Regression plots for an older male subject for **a)** FLEX/EX, **b)** ADD/ABD, and **c)** INT/EXT ROM data.

Figure 6.9 shows the regression plots for one young female subject. It can be seen that the linear model fits the data well for each movement plane. Intercept (p1) values were low and gradient (p2) values were high, particularly for the INT/EXT component with a p2 value of 0.953. This indicated that for every 1^{o} change in Vicon ROM, there was a 0.953^{o} change in gyroscope system ROM. SSE and RMSE values were low for all movement dimensions but especially for the FLEX/EX plane, indicating low residual values i.e. the distance between the observed data values and the model's fitted values. In addition, R^2 and adjusted R^2 values were particularly high for the FLEX/EX plane with values of 0.996 and 0.996 respectively. This indicated that 99.6% of variation in the data sample was accounted for by the linear model. The highest SSE and RMSE values were observed for the INT/EXT plane (SSE: 731.865, RMSE: 4.859) with the lowest R^2 and adjusted R^2 values of the three dimensions (R^2: 0.935, R^2 adj: 0.933). The goodness of fit statistics obtained for the young female subject indicated a good fit of the linear model to the data for all movement dimensions.

Similar results were observed in figure 6.10a-c for an older male subject where intercept values were low and gradient values were high. SSE and RMSE values were particularly low for the ADD/ABD dimension (SSE: 272.540, RMSE: 2.965). The larger values of SSE and RMSE for the INT/EXT rotation dimension (SSE: 983.819, RMSE: 5.634) indicated slightly larger residual values than for the other two dimensions, as can be seen from figures 6.10a-c. Again, the goodness of fit statistics obtained for the older male subject indicated a good fit of the linear model to the data.

For both subjects, the largest data points on the ADD/ABD regression plot were calculated from the shoulder abduction movement. These data points were noticeably larger than the other values due to the use of the XZY sequence (described in section 6.1) where movement in the ADD/ABD plane formed the first and largest rotation in the sequence.

	FLEX/EX	ADD/ABD	INT/EXT
p1	-0.250 ± 3.042	1.970 ± 1.972	0.101 ± 3.289
p2	0.886 ± 0.034	0.883 ± 0.034	0.886 ± 0.080
SSE	795.016 ± 575.082	711.308 ± 411.764	1464.435 ± 1188.373
RMSE	4.798 ± 1.662	4.614 ± 1.321	6.426 ± 2.502
R^2	0.984 ± 0.012	0.975 ± 0.018	0.893 ± 0.099
R^2 adj	0.983 ± 0.013	0.974 ± 0.019	0.890 ± 0.103

Table 6.5 Mean regression coefficient and goodness of fit statistics of 20 subjects for regression of Vicon and gyroscope ROM data for each of the three planes of motion. p1 and p2 are fitted coefficients where y = p1 + p2x. Values obtained for all subjects can be found in Appendix D.

	FLEX/EX	ADD/ABD	INT/EXT
p1	-0.250 ± 3.042	1.970 ± 1.972	0.101 ± 3.289
CI lower	-3.501 ± 3.012	-0.471 ± 1.707	-5.974 ± 3.672
CI upper	3.001 ± 3.429	4.410 ± 2.432	6.175 ± 4.792
p2	0.886 ± 0.034	0.883 ± 0.034	0.886 ± 0.080
CI lower	0.846 ± 0.038	0.833 ± 0.042	0.781 ± 0.103
CI upper	0.925 ± 0.036	0.932 ± 0.034	0.992 ± 0.084

Table 6.6 Mean regression coefficient and 95% confidence interval bounds of 20 subjects for regression of Vicon and gyroscope ROM data for each of the three planes of motion. p1 and p2 are fitted coefficients where y = p1 + p2x. Values obtained for all subjects can be found in Appendix D.

Table 6.5 shows the mean regression coefficient and goodness of fit statistics of the 20 subjects. Regression data for individual subjects can be found in Appendix D. Mean gradient values (p2) were similar for all three movement planes with variability greatest for the INT/EXT plane (0.886±0.080). Mean intercept values (p1) were low for all planes of motion and close to zero, with little variability. Goodness of fit statistics indicated a good fit of the linear model to the data, particularly for the FLEX/EX and ADD/ABD planes where mean RMSE values were low with low variability (4.798 ± 1.662 and 4.614 ± 1.321 respectively) and mean R^2 and adjusted R^2 values were particularly high (greater than 0.97) with very low variability (SD<0.02) indicating consistency across all 20 subjects.

The mean regression coefficient and goodness of fit statistics for the INT/EXT plane showed the greatest inter-subject variability of the three movement dimensions. Mean RMSE value was the largest of the three dimensions (6.426 ± 2.502) with mean SSE value approximately twice as large as computed for the FLEX/EX and ADD/ABD dimensions (1464.435 ± 1188.373). Mean R^2 and R^2 adjusted values were the lowest of the three movement dimensions (less than 0.9) with the largest inter-subject variability. The INT/EXT dimension was the only plane for which p2 values greater than 1 were observed for individuals (p2 values 1.037 and 1.004 for two subjects) as well as p2 values less than 0.8 (p2 values 0.728, 0.798 and 0.799 for three subjects). These observations therefore accounted for the variability in mean values. It follows that the 95% confidence interval boundaries for the regression coefficient statistics (p1 and p2) were the widest for the INT/EXT plane as shown in table 6.6 (p1 CI: -5.974 ± 3.672 to 6.175 ± 4.792; p2 CI: 0.781 ± 0.103 to 0.992 ± 0.084). 95% confidence interval boundaries for p1 were most narrow for the ADD/ABD plane (-0.471 ± 1.707 to 4.410 ± 2.432), and for p2 were most narrow for the FLEX/EX plane (0.833 ± 0.042 to 0.932 ± 0.034).

6.4.2 Regression per movement component

The ROM variable calculated from the Vicon joint rotation curves was regressed against the ROM variable calculated from the gyroscope joint rotation curves for all 20 subjects at a time, for each of the 33 movement components in turn. 3 regression plots for each of the 11 upper limb movement activities were obtained, resulting in 33 sets of regression variables in total. Each regression plot consisted of 60 data points (20 subjects, three trials per subject). Regression plots for all 33 movement components can be found in Appendix D.

Figure 6.11 shows the regression plots for the "lifting to head height" activity for the three movement dimensions. Intercept (p1) values were low and gradient (p2) values were high for all three planes of motion. RMSE values were low for the FLEX/EX and ADD/ABD planes (4.018 and 5.450) and R^2 and adjusted R^2 values were high. The RMSE value was comparatively high for the INT/EXT rotation plane (8.696) with a large SSE value (4386.253) indicating large residual values compared with the

other two movement dimensions as evident from the regression plots. These observations were also reflected in the R^2 and adjusted R^2 values which were comparatively low (R^2: 0.787, R^2 adj: 0.784) indicating that 78.7% of variation in the data sample was accounted for by the linear model.

Table 6.7 shows the regression coefficient values and goodness of fit statistics for each movement component of the eleven upper limb activities. The 95% confidence bounds of the regression coefficients are displayed in table 6.8.

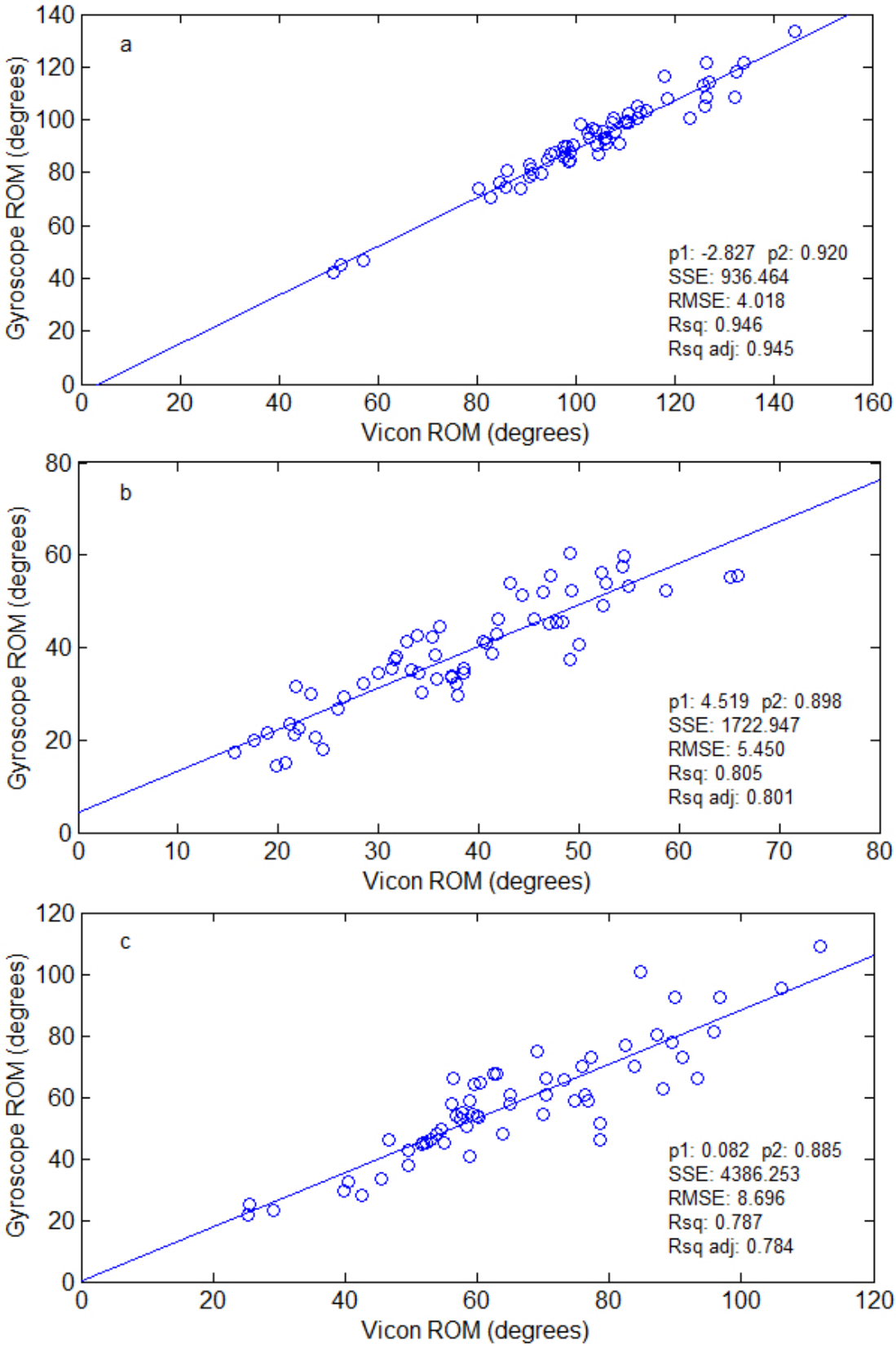

Figure 6.11 Regression plots of Vicon and gyroscope ROM data for the "lifting to head height" activity for all 20 subjects for a) FLEX/EX, b) ADD/ABD and c) INT/EXT components.

Movement activity	Plane	p1	p2	SSE	RMSE	R^2	R^2 adj
Flexion	FLEX/EX	3.126	0.883	717.447	3.517	0.944	0.943
	ADD/ABD	6.123	0.946	1585.283	5.228	0.673	0.667
	INT/EXT	16.869	0.805	5832.927	10.028	0.585	0.578
Extension	FLEX/EX	-0.189	0.881	217.267	1.936	0.964	0.964
	ADD/ABD	5.595	0.556	607.058	3.235	0.621	0.615
	INT/EXT	1.217	0.754	933.256	4.011	0.841	0.839
Abduction	FLEX/EX	7.718	0.797	4837.056	9.132	0.374	0.363
	ADD/ABD	1.942	0.879	1105.337	4.366	0.952	0.951
	INT/EXT	-7.229	0.929	3366.486	7.619	0.749	0.744
External rotation	FLEX/EX	-0.049	0.878	281.053	2.201	0.783	0.779
	ADD/ABD	0.359	0.811	311.364	2.317	0.862	0.860
	INT/EXT	-0.697	0.878	315.892	2.334	0.964	0.964
Internal rotation	FLEX/EX	0.149	0.844	408.159	2.653	0.904	0.902
	ADD/ABD	1.870	0.789	1426.290	4.959	0.394	0.383
	INT/EXT	4.344	0.794	993.290	4.138	0.880	0.878
Hand to mouth	FLEX/EX	0.893	0.846	317.998	2.342	0.942	0.941
	ADD/ABD	0.342	0.939	419.413	2.689	0.827	0.824
	INT/EXT	0.628	0.828	444.721	2.769	0.905	0.903
Opposite shoulder	FLEX/EX	-0.757	0.927	653.889	3.358	0.908	0.906
	ADD/ABD	0.513	0.785	634.900	3.309	0.814	0.811
	INT/EXT	-1.403	0.896	648.925	3.345	0.864	0.862
Back of head	FLEX/EX	-10.026	0.937	2170.740	6.118	0.900	0.899
	ADD/ABD	7.219	0.849	999.020	4.150	0.929	0.928
	INT/EXT	2.678	0.859	5801.633	10.001	0.895	0.894
Same shoulder	FLEX/EX	-0.595	0.794	1677.383	5.378	0.930	0.929
	ADD/ABD	-0.494	0.902	874.669	3.883	0.938	0.937
	INT/EXT	-0.137	0.887	950.552	4.048	0.955	0.954
Shelf shoulder height	FLEX/EX	-3.716	0.918	741.283	3.575	0.928	0.927
	ADD/ABD	0.761	0.937	1288.986	4.714	0.742	0.738
	INT/EXT	-4.052	0.974	1052.258	4.259	0.892	0.890
Shelf head height	FLEX/EX	-2.827	0.920	936.464	4.018	0.946	0.945
	ADD/ABD	4.519	0.898	1722.946	5.450	0.805	0.801
	INT/EXT	0.082	0.885	4386.253	8.696	0.787	0.784
Mean		1.054	0.861	1474.551	4.539	0.830	0.827
SD		4.645	0.078	1561.068	2.230	0.151	0.153

Table 6.7 Regression coefficients and goodness of fit statistics for regression of Vicon and gyroscope ROM data for each of the 33 movement components for all 20 subjects. p1 and p2 are fitted coefficients of the regression model where y = p1 + p2x.

Movement activity	Plane	p1	95% Confidence interval		p2	95% Confidence interval	
			Lower	Upper		Lower	Upper
Flexion	FLEX/EX	3.126	-5.875	12.127	0.883	0.827	0.940
	ADD/ABD	6.123	1.010	11.235	0.946	0.773	1.119
	INT/EXT	16.869	4.871	28.868	0.805	0.627	0.983
Extension	FLEX/EX	-0.189	-3.057	2.679	0.881	0.837	0.926
	ADD/ABD	5.595	3.855	7.334	0.556	0.442	0.669
	INT/EXT	1.217	-1.569	4.003	0.754	0.668	0.840
Abduction	FLEX/EX	7.718	0.339	15.098	0.797	0.526	1.068
	ADD/ABD	1.942	-5.145	9.030	0.879	0.827	0.931
	INT/EXT	-7.229	-19.169	4.712	0.929	0.788	1.071
External rotation	FLEX/EX	-0.049	-1.388	1.290	0.878	0.756	1.000
	ADD/ABD	0.359	-0.660	1.378	0.811	0.725	0.896
	INT/EXT	-0.697	-2.962	1.569	0.878	0.833	0.922
Internal rotation	FLEX/EX	0.149	-3.309	3.606	0.844	0.772	0.916
	ADD/ABD	1.870	-2.847	6.587	0.789	0.532	1.047
	INT/EXT	4.344	1.448	7.240	0.794	0.717	0.871
Hand to mouth	FLEX/EX	0.893	-2.303	4.088	0.846	0.790	0.901
	ADD/ABD	0.342	-1.769	2.453	0.939	0.826	1.051
	INT/EXT	0.628	-1.946	3.202	0.828	0.757	0.899
Opposite shoulder	FLEX/EX	-0.757	-5.972	4.459	0.927	0.849	1.004
	ADD/ABD	0.513	-2.833	3.859	0.785	0.686	0.883
	INT/EXT	-1.403	-7.738	4.932	0.896	0.803	0.989
Back of head	FLEX/EX	-10.026	-20.495	0.443	0.937	0.855	1.019
	ADD/ABD	7.219	4.050	10.388	0.849	0.787	0.911
	INT/EXT	2.678	-3.495	8.850	0.859	0.782	0.936
Same shoulder	FLEX/EX	-0.595	-3.674	2.484	0.794	0.736	0.851
	ADD/ABD	-0.494	-3.241	2.253	0.902	0.841	0.963
	INT/EXT	-0.137	-2.815	2.542	0.887	0.837	0.938
Shelf shoulder height	FLEX/EX	-3.716	-8.065	0.632	0.918	0.851	0.985
	ADD/ABD	0.761	-3.044	4.566	0.937	0.792	1.082
	INT/EXT	-4.052	-7.711	-0.394	0.974	0.884	1.063
Shelf head height	FLEX/EX	-2.827	-8.919	3.266	0.920	0.862	0.978
	ADD/ABD	4.519	-0.119	9.156	0.898	0.782	1.015
	INT/EXT	0.082	-8.165	8.328	0.885	0.764	1.006
Mean		1.054	-3.719	5.826	0.861	0.762	0.960
SD		4.645	5.398	5.566	0.078	0.103	0.088

Table 6.8 Regression coefficients p1 and p2 and their 95% confidence bounds for regression of Vicon and gyroscope ROM data for each of the 33 movement components for all 20 subjects. p1 and p2 are fitted coefficients of the regression model where $y = p1 + p2x$.

In general, the mean regression coefficient and goodness of fit values indicated a good fit of the linear model to the data. Table 6.7 indicated that the gradient of the regression line (p2) was always less than 1 for each of the 33 movement components (mean: 0.861±0.078) indicating that gyroscope ROM data tended to underestimate Vicon ROM data. Mean intercept (p1) value was low (1.054^{o}±4.645^{o}) with low variability. RMSE values were low for the majority of movement components (mean 4.539 ± 2.230) indicating a good fit of the linear model to the data. R^2 and adjusted R^2 values were generally high for the majority of movement components as indicated by the mean values (mean R^2: 0.830 ± 0.151, mean R^2 adj: 0.827 ± 0.153). Mean regression and goodness of fit statistics showed greater variability compared with mean values from "regression per subject" analysis. 95% confidence intervals displayed in table 6.8 for intercept and gradient coefficients were in general narrow for the majority of the 33 movement components (mean p1 CI: -3.719 ± 5.398 to 5.826 ± 5.566; mean p2 CI: (0.762 ± 0.103 to 0.960 ± 0.088). However, there were some components which made a marked contribution to the observed variation in mean values.

Some of the largest RMSE values of the 33 movement components were obtained for four of the INT/EXT components. These were the Group 1 flexion and abduction activities, and the Group 2 and 3 "back of head" and "lifting to head height" activities, where corresponding RMSE values ranged from 7.62 to 10.03. Wide 95% confidence intervals for p1 and p2 estimates, as shown in table 6.8, were also observed for these components. These regression statistics indicated a wide spread of data from the regression line. Large p1 values observed for the INT/EXT components of the flexion activity (p1: 16.869) and the abduction activity (p1: -7.229) were accompanied with the widest p1 95% confidence bounds of all 33 movement components as shown in table 6.8 (flexion p1 CI: 4.871 to 28.868; abduction p1 CI: -19.169 to 4.712) indicating poor precision of p1 estimation for these components. These observations were consistent with outlier values on the regression plot which may have had a large influence on the fit of the regression line due to the requirement to minimise the SSE value. As previously described in section 6.4.1, "regression per subject" analysis for the INT/EXT plane showed the

greatest variability in mean regression coefficient and goodness of fit statistics of the three planes of motion, and the widest p1 95% confidence bounds.

The FLEX/EX components of the abduction and "back of head" activities also displayed large SSE and RMSE values, large intercept values and wide 95% confidence intervals for the regression coefficients. The FLEX/EX component of the abduction activity in particular gave large RMSE (9.132), large positive intercept value (7.718), and the widest p2 95% confidence bounds of all 33 movement components (p2 CI: 0.526 to 1.068) indicating poor precision of gradient estimation. The accompanying R^2 values were the lowest observed for all movement components and indicated that only 37.4% of variation in the data was accounted for by the linear model. The regression plot showed outlier values which likely had a large influence on the fit of the regression line. The "back of head" activity gave a large negative p1 value (-10.026) with a wide 95% confidence interval (p1 CI: -20.495 to 0.443). Wide p1 95% confidence bounds were also computed for the FLEX/EX components of the Group 1 Flexion activity (p1 95% CI: -5.88 to 12.13) and Group 3 "lifting to head height" activity (p1 95% CI: -8.92 to 3.27).

Similar observations were made for the ADD/ABD component of the flexion activity. An RMSE value of 5.228 was accompanied by a positive intercept value (6.123) and relatively low R^2 value (0.673). The p2 95% confidence interval was large (0.773 to 1.119). Other ADD/ABD components of interest included the internal rotation activity which displayed a large p2 95% confidence interval (0.532 to 1.047) and very low R^2 and adjusted R^2 values (0.394 and 0.383) indicating that only 39.4% of variation in the data was accounted for by the linear model. The gradient value for the extension activity was relatively low (0.556) as were R^2 and adjusted R^2 values (0.621 and 0.615). The ADD/ABD of the "back of head activity" exhibited a large positive intercept value (7.22) however 95% confidence bounds for this regression estimate were relatively narrow.

It can be seen from table 6.7 that Group 1 activity components (planar movements used in upper limb clinical functional examination) gave some of the lowest gradient and R^2 and adjusted R^2 values of the 33 movement components. In contrast, values for group 2 and group 3 activities (ADL's and lifting) remained consistently high.

6.4.3 Regression per movement dimension

The ROM variable calculated from the Vicon joint rotation curves was regressed against the ROM variable calculated from the gyroscope joint rotation curves for each movement plane. Each regression plot consisted of 660 data points based on three trials of 11 upper limb activities recorded from 20 subjects, and are presented in figures 6.12a-c. One set of regression coefficient values and goodness of fit statistics was obtained for each movement dimension, as presented in tables 6.9 and 6.10.

Plane	p1	p2	SSE	RMSE	R^2	R^2 adj
FLEX/EX	-0.242	0.885	18589.204	5.315	0.982	0.982
ADD/ABD	1.881	0.886	17002.836	5.083	0.974	0.974
INT/EXT	-0.146	0.894	34751.976	7.267	0.898	0.898

Table 6.9 Regression coefficient and goodness of fit statistics of 20 subjects for regression of Vicon and gyroscope ROM data for each of the three planes of motion. P1 and p2 are fitted coefficients where y = p1 + p2x.

Plane	p1	95% Confidence interval		p2	95% Confidence interval	
		Lower	Upper		Lower	Upper
FLEX/EX	-0.242	-1.004	0.520	0.885	0.876	0.894
ADD/ABD	1.881	1.316	2.445	0.886	0.875	0.897
INT/EXT	-0.146	-1.505	0.212	0.894	0.871	0.917

Table 6.10 Regression coefficient and 95% confidence interval bounds of 20 subjects for regression of Vicon and gyroscope ROM data for each of the three planes of motion. P1 and p2 are fitted coefficients where y = p1 + p2x.

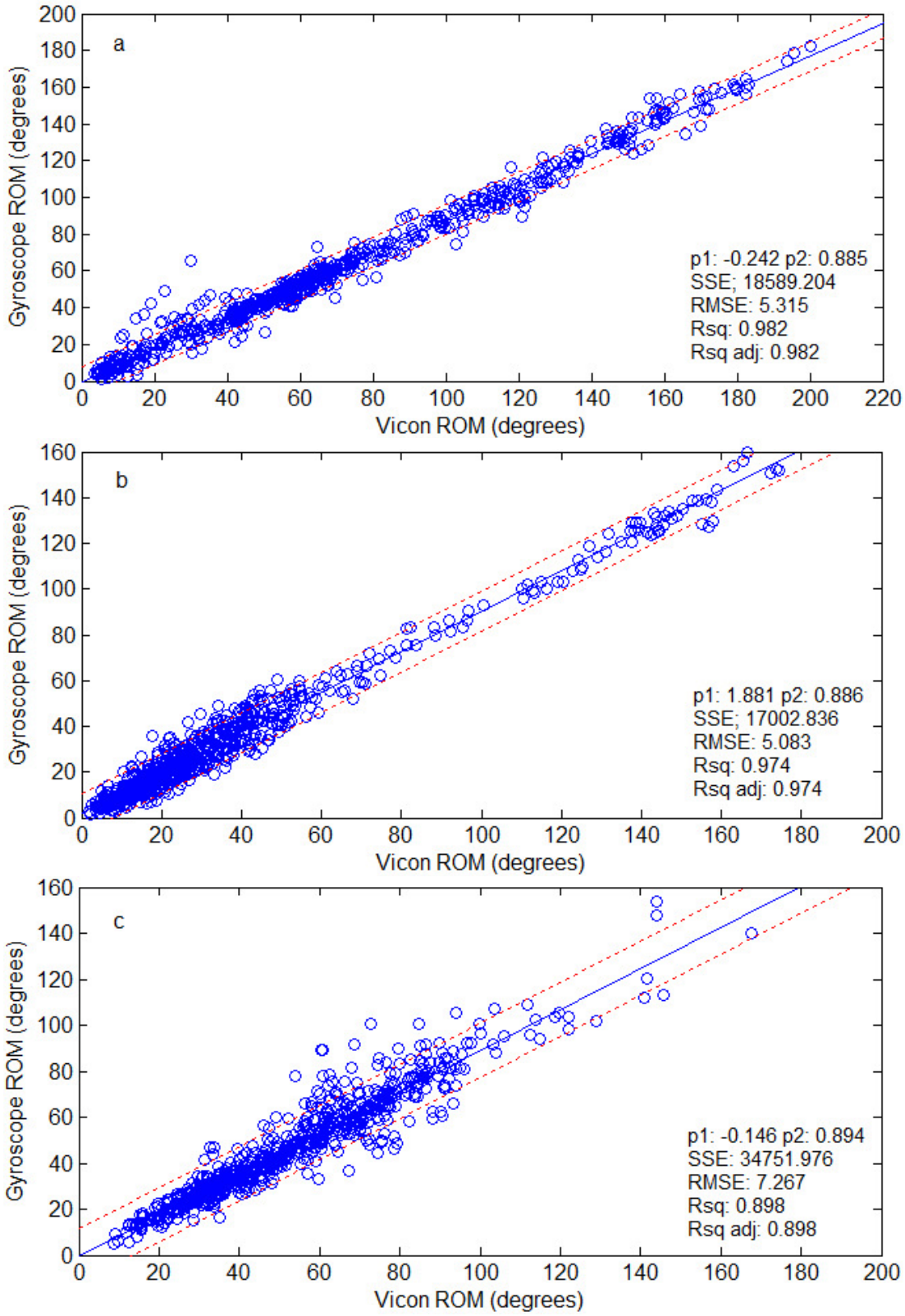

Figure 6.12 Regression plots of Vicon and gyroscope ROM data for a) FLEX/EX, b) ADD/ABD and c) INT/EXT planes, n = 660. Red dashed lines (--) indicated boundaries containing 90% of data points.

The data show a good fit of the linear regression line to FLEX/EX and ADD/ABD data with a relatively more variable fit for INT/EXT data. p2 values were comparable for all planes and p1 values were close to zero degrees. RMSE values were relatively low for the FLEX/EX and ADD/ABD planes (5.14 and 5.08 respectively) indicating low mean residual values, and R^2 and R^2 adjusted values were high indicating that a 98% and 97% respectively of variation in the data was accounted for by the linear model. RMSE value was slightly higher for the INT/EXT plane indicating wider spread of data from the regression line, which was clearly seen in figure 6.12c. This plane also exhibited marginally wider p2 95% confidence bounds. R^2 and adjusted R^2 values were slightly lower than for the other two planes but still indicated that a large proportion (89.8%) of variation in the data was accounted for by the linear model.

A number of large outlier values were evident on the regression plots, particularly for low FLEX/EX ROM values and INT/EXT Vicon ROM values between 50^o to 100^o. The red dashed lines on figures 6.12a-c represented the boundaries within which 90% of all data values fell. These boundaries were defined using the equation $y = (p_1 + p_2 x) \pm e$ where y was the estimated gyroscope ROM, x was the recorded Vicon ROM and values of e were computed as $\pm 8.20^o$ for the FLEX/EX plane, $\pm 8.60^o$ for the ADD/ABD plane, and $\pm 11.70^o$ for the INT/EXT plane. To characterise the error of the 3D gyroscope system, estimated error boundaries for a range of Vicon ROM values were computed as follows and presented in table 6.11.

$$\text{Absolute 3D gyroscope system error} = VROM - [(p_1 + p_2 \cdot VROM) \pm \text{e}] \quad (6.1)$$

Table 6.11 showed that, for all planes of motion, the estimated absolute error of the 3D gyroscope system increased with increasing Vicon ROM, and that overestimation errors were more likely to be computed from low ROM components e.g. for a Vicon ROM of 180^o in the FLEX/EX plane, 3D gyroscope system error was estimated at between 12.8^o and 29.2^o underestimation, and for a Vicon ROM of 30^o, 3D gyroscope system error was estimated at between -4.5^o (overestimation) and 11.9^o underestimation. Table 6.11 showed that estimated error boundaries were comparable between planes and were widest for measures of axial rotation.

Vicon Angle (degrees)	Absolute 3D gyroscope system estimation error boundaries (degrees)					
	FLEX/EX		ADD/ABD		INT/EXT	
	Lower	Upper	Lower	Upper	Lower	Upper
200	15.1	31.5	12.3	29.5	9.6	33.0
190	13.9	30.3	11.1	28.3	8.6	32.0
180	12.8	29.2	10.0	27.2	7.5	30.9
170	11.6	28.0	8.8	26.0	6.5	29.9
160	10.5	26.9	7.7	24.9	5.4	28.8
150	9.3	25.7	6.6	23.8	4.3	27.7
140	8.2	24.6	5.4	22.6	3.3	26.7
130	7.0	23.4	4.3	21.5	2.2	25.6
120	5.9	22.3	3.2	20.4	1.2	24.6
110	4.7	21.1	2.0	19.2	0.1	23.5
100	3.6	20.0	0.9	18.1	-1.0	22.4
90	2.4	18.8	-0.2	17.0	-2.0	21.4
80	1.2	17.6	-1.4	15.8	-3.1	20.3
70	0.1	16.5	-2.5	14.7	-4.1	19.3
60	-1.1	15.3	-3.7	13.5	-5.2	18.2
50	-2.2	14.2	-4.8	12.4	-6.3	17.1
40	-3.4	13.0	-5.9	11.3	-7.3	16.1
30	-4.5	11.9	-7.1	10.1	-8.4	15.0
20	-5.7	10.7	-8.2	9.0	-9.4	14.0
10	-6.8	9.6	-9.3	7.9	-10.5	12.9
5	-7.4	9.0	-9.9	7.3	-11.0	12.4

Table 6.11 3D gyroscope system error estimation boundaries (degrees). Positive values signify underestimation error and negative values signify overestimation error.

Correction of 3D gyroscope system ROM underestimation error

The well defined linear relationship between the 3D gyroscope and Vicon systems, as indicated by the narrow p_1 and p2 95% confidence bounds (table 6.10), suggested that the error of the 3D gyroscope system could be corrected for such that the estimated absolute error values were not dependent upon the ROM of the activity. Two correction factors were determined from the p1 and p2 estimates of the inverse regression analysis of Vicon ROM data (*y* axis) against 3D gyroscope ROM data (*x* axis). Regression coefficient values and goodness of fit statistics for the inverse regression are presented in table 6.12. p1 and p2 values presented in table 6.12 were then used to correct for 3D gyroscope ROM error using the equation $y = p_1 + p_2 x$ where *y* was the corrected 3D gyroscope ROM and *x* was the recorded 3D gyroscope ROM. Mean corrected 3D gyroscope ROM values across 20 subjects are presented in table 6.14.

Plane	p1	p2	SSE	RMSE	R^2	R^2 adj
FLEX/EX	1.540	1.110	23305.867	5.951	0.982	0.982
ADD/ABD	-1.112	1.099	21089.214	5.661	0.974	0.974
INT/EXT	5.629	1.005	39052.166	7.704	0.898	0.898

Table 6.12 Regression coefficient values and goodness of fit statistics for inverse regression analysis of Vicon ROM data (*y* axis) against 3D gyroscope ROM data (*x* axis)

Plane	p1	95% Confidence interval		p2	95% Confidence interval	
		Lower	Upper		Lower	Upper
FLEX/EX	1.540	0.695	2.386	1.110	1.098	1.121
ADD/ABD	-1.112	-1.755	-0.469	1.099	1.086	1.113
INT/EXT	5.629	4.255	7.003	1.005	0.979	1.031

Table 6.13 Regression coefficient values and 95% confidence bounds for inverse regression analysis of Vicon ROM data (*y* axis) against 3D gyroscope ROM data (*x* axis)

Group	Movement activity	FLEX/EX	ADD/ABD	INT/EXT
1: Planar movements used in clinical functional examination	Flexion	160.81 ± 16.41	35.21 ± 9.97	75.71 ± 15.50
	Extension	63.20 ± 11.25	13.21 ± 5.73	29.60 ± 10.03
	Abduction	32.91 ± 12.70	131.53 ± 21.75	76.04 ± 15.13
	External rotation	11.19 ± 5.19	7.89 ± 6.79	48.34 ± 12.31
	Internal rotation	45.62 ± 9.42	16.24 ± 6.94	37.84 ± 11.89
2: Activities of daily living (ADL)	Hand to mouth	55.77 ± 10.67	17.52 ± 7.06	35.34 ± 8.93
	Opposite shoulder	68.89 ± 12.18	27.75 ± 8.36	64.76 ± 9.05
	Back of head	121.63 ± 21.31	51.96 ± 16.98	71.02 ± 30.81
	Same shoulder	43.07 ± 22.32	39.92 ± 16.99	48.95 ± 19.03
3: Lifting	Lift: shoulder	59.01 ± 9.98	23.87 ± 8.25	37.12 ± 8.46
	Lift: head	106.91 ± 14.49	42.81 ± 12.80	66.73 ± 17.33

Table 6.14 Mean corrected 3D gyroscope ROM values across 20 subjects ±1 SD.

Subsequently, the regression of Vicon ROM data (*y* axis) against corrected 3D gyroscope ROM data (*x* axis) gave gradient and intercept values which approximated 1^{o} and 0^{o} respectively, as shown in the regression plots for each plane (figures 6.13a-c) and in table 6.15.

Plane	p1	p2	SSE	RMSE	R^2	R^2 adj
FLEX/EX	0.0001	1.000	23305.867	5.951	0.982	0.982
ADD/ABD	0.0000	1.000	21089.214	5.661	0.974	0.974
INT/EXT	0.0002	1.000	39052.166	7.704	0.898	0.898

Table 6.15 Regression coefficient values and goodness of fit statistics for regression analysis of Vicon ROM data (*y* axis) against corrected 3D gyroscope ROM data (*x* axis).

Plane	p1	95% Confidence interval		p2	95% Confidence interval	
		Lower	Upper		Lower	Upper
FLEX/EX	0.0001	-0.859	0.859	1.000	0.990	1.010
ADD/ABD	0.0000	-0.633	0.633	1.000	0.988	1.012
INT/EXT	0.0002	-1.506	1.507	1.000	0.974	1.026

Table 6.16 Regression coefficient values and 95% confidence bounds for regression analysis of Vicon ROM data (*y* axis) against corrected 3D gyroscope ROM data (*x* axis).

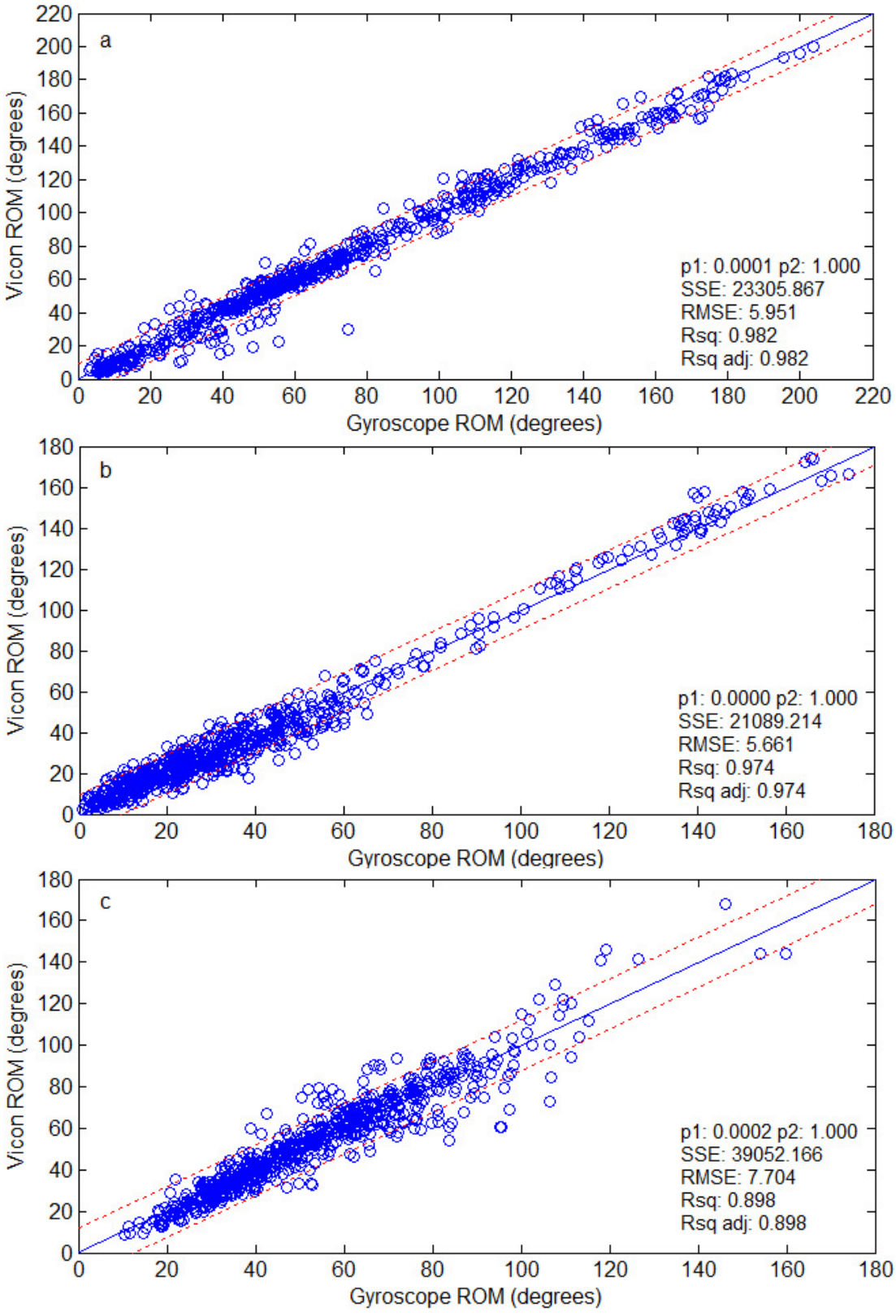

Figure 6.13 Regression plots of Vicon and gyroscope corrected ROM data for a) FLEX/EX, b) ADD/ABD and c) INT/EXT planes, n = 660. Red dashed lines (--) indicated boundaries containing 90% of data points.

Again, the red dashed lines on figures 6.13a-c indicated the boundaries within which 90% of data values fell and were computed as $y = (p_1 + p_2 x) \pm e$ where y was the estimated Vicon ROM, x was the corrected 3D gyroscope ROM, and values of e were computed as ±9.45° for the FLEX/EX plane, ±9.37° for the ADD/ABD plane, and ±12.28° for the INT/EXT plane. For error boundaries containing 95% of data values, the value of e was computed as ±11.90° for the FLEX/EX plane, ±11.32° for the ADD/ABD plane, and ±15.42° for the INT/EXT plane. Since gradient and intercept values approximated 1° and 0° respectively for all planes, the absolute error of the 3D gyroscope system was ±e, and was therefore independent of the ROM of the activity. The corrected 3D gyroscope ROM values were used for all subsequent analyses presented in this thesis.

Movement activity	Plane	p1	p2	SSE	RMSE	R^2	R^2 adj
Flexion	FLEX/EX	5.009	0.980	883.170	3.902	0.944	0.943
	ADD/ABD	5.619	1.040	1915.752	5.747	0.673	0.667
	INT/EXT	22.576	0.809	5886.713	10.075	0.585	0.578
Extension	FLEX/EX	1.331	0.978	267.453	2.147	0.964	0.964
	ADD/ABD	5.039	0.611	733.606	3.557	0.621	0.615
	INT/EXT	6.851	0.758	941.861	4.030	0.841	0.839
Abduction	FLEX/EX	10.104	0.884	5954.369	10.132	0.374	0.363
	ADD/ABD	1.024	0.966	1335.756	4.799	0.952	0.951
	INT/EXT	-1.633	0.934	3397.529	7.654	0.749	0.744
External rotation	FLEX/EX	1.486	0.974	345.973	2.442	0.783	0.779
	ADD/ABD	-0.717	0.891	376.271	2.547	0.862	0.860
	INT/EXT	4.929	0.882	318.804	2.345	0.964	0.964
Internal rotation	FLEX/EX	1.705	0.937	502.440	2.943	0.904	0.902
	ADD/ABD	0.944	0.868	1723.615	5.451	0.394	0.383
	INT/EXT	9.993	0.798	1002.449	4.157	0.880	0.878
Hand to mouth	FLEX/EX	2.531	0.938	391.452	2.598	0.942	0.941
	ADD/ABD	-0.735	1.032	506.844	2.956	0.827	0.824
	INT/EXT	6.260	0.832	448.822	2.782	0.905	0.903
Opposite shoulder	FLEX/EX	0.701	1.028	804.931	3.725	0.908	0.906
	ADD/ABD	-0.548	0.862	767.251	3.637	0.814	0.811
	INT/EXT	4.219	0.900	654.909	3.360	0.864	0.862
Back of head	FLEX/EX	-9.584	1.040	2672.160	6.788	0.900	0.899
	ADD/ABD	6.824	0.933	1207.276	4.562	0.929	0.928
	INT/EXT	8.319	0.863	5855.131	10.047	0.895	0.894
Same shoulder	FLEX/EX	0.880	0.880	2064.843	5.967	0.930	0.929
	ADD/ABD	-1.655	0.991	1057.003	4.269	0.938	0.937
	INT/EXT	5.492	0.891	959.317	4.067	0.955	0.954
Shelf shoulder height	FLEX/EX	-3.756	1.037	878.046	3.891	0.851	0.848
	ADD/ABD	2.806	0.887	1253.807	4.649	0.688	0.682
	INT/EXT	6.309	0.844	922.413	3.988	0.782	0.778
Shelf head height	FLEX/EX	1.455	0.992	1175.184	4.501	0.905	0.904
	ADD/ABD	4.212	0.987	2210.886	6.174	0.771	0.767
	INT/EXT	5.336	0.900	4577.292	8.884	0.742	0.737
Mean		3.434	0.913	1636.161	4.811	0.819	0.816
SD		5.315	0.092	1653.640	2.284	0.151	0.153

Table 6.17 Regression coefficients and goodness of fit statistics for regression of Vicon and corrected gyroscope ROM data for each of the 33 movement components for all 20 subjects.

Movement activity	Plane	p1	95% Confidence interval		p2	95% Confidence interval	
			Lower	Upper		Lower	Upper
Flexion	FLEX/EX	5.009	-4.978	14.995	0.980	0.918	1.042
	ADD/ABD	5.619	-0.001	11.240	1.040	0.849	1.230
	INT/EXT	22.576	10.522	34.629	0.809	0.630	0.988
Extension	FLEX/EX	1.331	-1.852	4.513	0.978	0.928	1.027
	ADD/ABD	5.039	3.127	6.951	0.611	0.485	0.736
	INT/EXT	6.851	4.052	9.650	0.758	0.671	0.844
Abduction	FLEX/EX	10.104	1.916	18.291	0.884	0.583	1.185
	ADD/ABD	1.024	-6.768	8.815	0.966	0.909	1.023
	INT/EXT	-1.633	-13.628	10.362	0.934	0.791	1.076
External rotation	FLEX/EX	1.486	0.001	2.971	0.974	0.839	1.109
	ADD/ABD	-0.717	-1.837	0.403	0.891	0.797	0.985
	INT/EXT	4.929	2.653	7.205	0.882	0.837	0.926
Internal rotation	FLEX/EX	1.705	-2.131	5.542	0.937	0.856	1.017
	ADD/ABD	0.944	-4.241	6.129	0.868	0.585	1.151
	INT/EXT	9.993	7.083	12.903	0.798	0.720	0.875
Hand to mouth	FLEX/EX	2.531	-1.014	6.075	0.938	0.877	1.000
	ADD/ABD	-0.735	-3.056	1.585	1.032	0.908	1.156
	INT/EXT	6.260	3.674	8.845	0.832	0.761	0.903
Opposite shoulder	FLEX/EX	0.701	-5.086	6.488	1.028	0.942	1.114
	ADD/ABD	-0.548	-4.226	3.130	0.862	0.754	0.971
	INT/EXT	4.219	-2.145	10.583	0.900	0.806	0.994
Back of head	FLEX/EX	-9.584	-21.199	2.031	1.040	0.949	1.131
	ADD/ABD	6.824	3.340	10.308	0.933	0.865	1.001
	INT/EXT	8.319	2.117	14.520	0.863	0.786	0.941
Same shoulder	FLEX/EX	0.880	-2.536	4.296	0.880	0.817	0.944
	ADD/ABD	-1.655	-4.675	1.365	0.991	0.924	1.058
	INT/EXT	5.492	2.801	8.182	0.891	0.840	0.942
Shelf shoulder height	FLEX/EX	-3.756	-10.742	3.230	1.037	0.923	1.151
	ADD/ABD	2.806	-1.114	6.726	0.887	0.730	1.044
	INT/EXT	6.309	1.908	10.711	0.844	0.726	0.961
Shelf head height	FLEX/EX	1.455	-7.591	10.502	0.992	0.907	1.076
	ADD/ABD	4.212	-1.538	9.963	0.987	0.846	1.129
	INT/EXT	5.336	-4.458	15.130	0.900	0.761	1.040
Mean		3.434	-1.867	8.735	0.913	0.804	1.023
SD		5.315	5.974	6.394	0.092	0.115	0.106

Table 6.18 Regression coefficients p1 and p2 and their 95% confidence bounds for regression of Vicon and corrected gyroscope ROM data for each of the 33 movement components for all 20 subjects.

6.5 Difference between the two systems in 3D

6.5.1 "Box" dimension data

The differences between the Vicon and corrected 3D gyroscope system ROM values (presented in section 6.4.3) were computed for each plane of motion for the 11 upper limb activities. Figure 6.14 shows the mean difference in ROM values in each plane of motion for each subject group, where each bar represents a mean of 165 data values (11 upper limb movements, 5 subjects, 3 trials each).

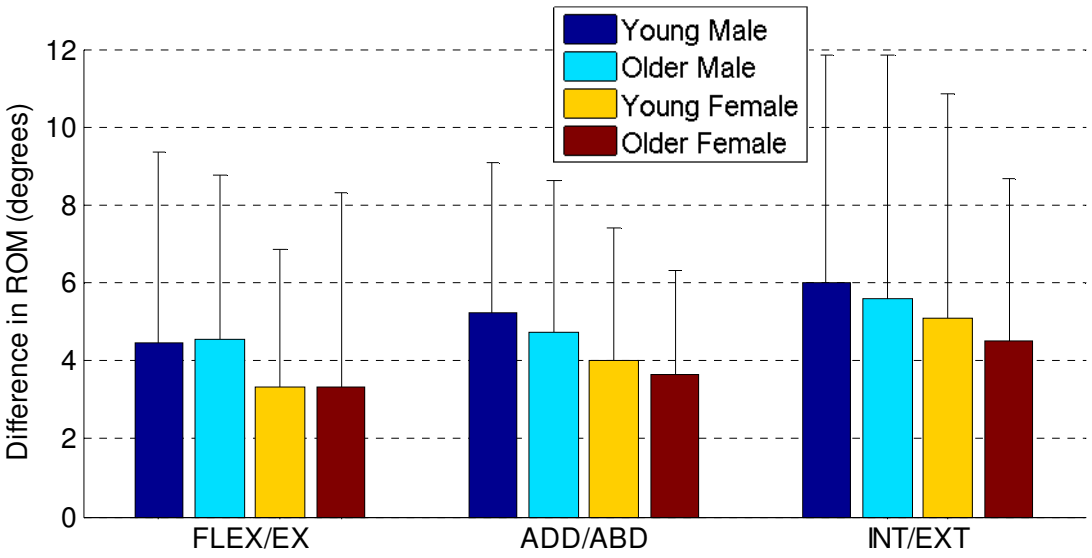

Figure 6.14 Mean difference in Vicon and corrected 3D gyroscope system ROM values (degrees) for each movement dimension. Each bar represents the mean of 165 values for one subject group and error bars represent 1 SD.

Plane	Young Male		Older Male		Young Female		Older Female	
	Mean	SD	Mean	SD	Mean	SD	Mean	SD
FLEX/EX	4.44	4.90	4.56	4.22	3.33	3.52	3.34	4.98
ADD/ABD	5.23	3.86	4.73	3.91	4.02	3.38	3.63	2.70
INT/EXT	5.98	5.88	5.58	6.27	5.09	5.76	4.51	4.15

Table 6.19 Mean absolute difference in Vicon and corrected 3D gyroscope system ROM values (degrees) ± 1 SD (n = 165).

ROM difference was computed by subtracting the corrected gyroscope ROM value from the corresponding Vicon ROM value. The resulting data therefore consisted of

positive and negative values indicating that gyroscope ROM was either smaller or larger than Vicon ROM. When computing the mean difference in ROM between the two systems, only absolute values were used in order to avoid under-representing differences due to a cancelling effect. The distribution of the positive and negative differences in ROM values between the two systems is shown in the form of histogram and box and whisker plots in section 6.5.2.

Figure 6.14 showed that the largest mean difference in ROM values was seen for the INT/EXT plane for all subject groups which was consistent with the values of $\pm e$ (defined in section 6.4.3) which was largest for INT/EXT plane. For all planes, males gave larger mean differences in ROM values compared with females, and the older female group gave the lowest mean differences in ROM. For all subject groups, the ADD/ABD dimension displayed the lowest variability of the three dimensions as shown in table 6.19.

The difference in ROM between the two systems was calculated as a percentage of the gold-standard Vicon ROM value. Figure 6.15 and table 6.20 showed that the mean percentage difference between the two systems was largest for the ADD/ABD plane for all groups, with mean values of between 16%-20%. Motion in the ADD/ABD plane tended to form the smallest components of the upper limb activities investigated as described in section 6.2 and shown in mean Vicon ROM values presented in figure 6.16 and table 6.21. Mean percentage difference for the FLEX/EX and INT/EXT planes were comparable for the older subjects and young female groups, with mean values of between 8%-12%. For young males, extremely large intra-group variability was observed for the FLEX/EX plane. This was due to the computation of a number of very large percentage differences values from very small FLEX/EX ROM components of the Abduction activity. This component exhibited low mean ROM (GROM $28.27^{o}\pm11.44^{o}$) and was identified in section 6.4.2 as a component with large residual data values from the fitted regression line. For all dimensions, males exhibited larger mean percentage differences compared to females, with the older female group showing the lowest values of all the groups. The lowest intra-group variability as indicated by the SD values was observed for the INT/EXT dimension.

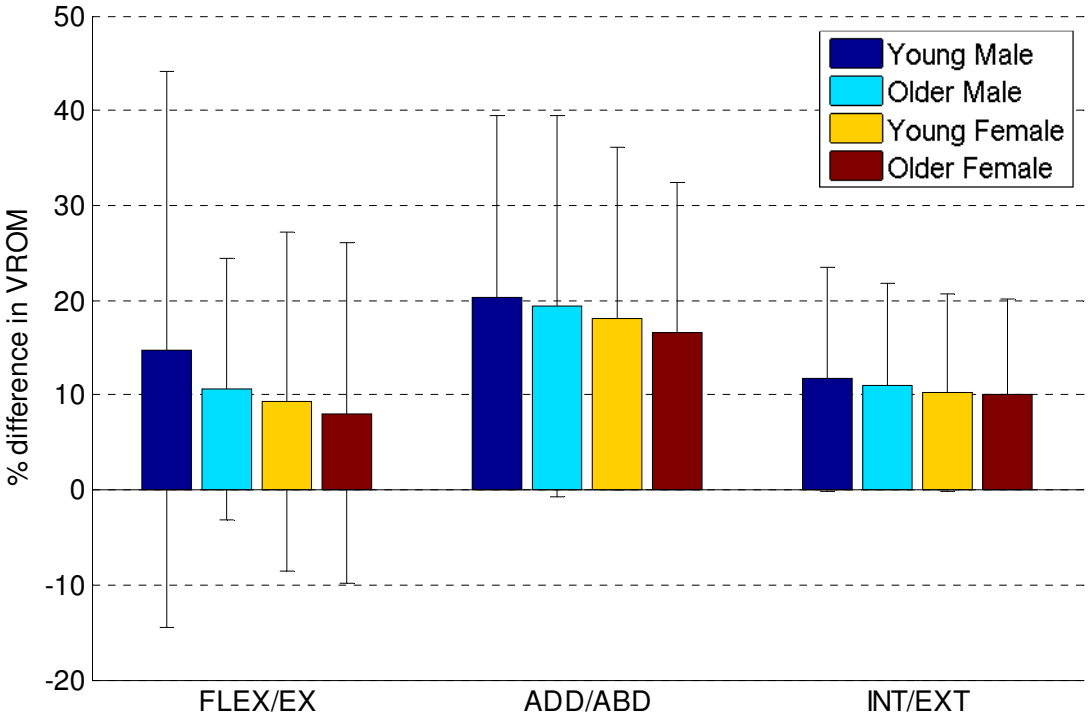

Figure 6.15 Mean percentage difference between Vicon and corrected 3D gyroscope system ROM data expressed as a percentage of VROM (%). Each bar represents a mean of 165 data points ± 1 SD.

Plane	Young Male		Older Male		Young Female		Older Female	
	Mean	SD	Mean	SD	Mean	SD	Mean	SD
FLEX/EX	14.81	29.31	10.61	13.79	9.35	17.89	8.11	17.96
ADD/ABD	20.28	19.28	19.41	20.14	18.04	18.03	16.50	15.82
INT/EXT	11.69	11.82	10.97	10.82	10.17	10.42	10.14	9.95

Table 6.20 Mean difference between the Vicon 3D gyroscope system ROM data expressed as a percentage of VROM.

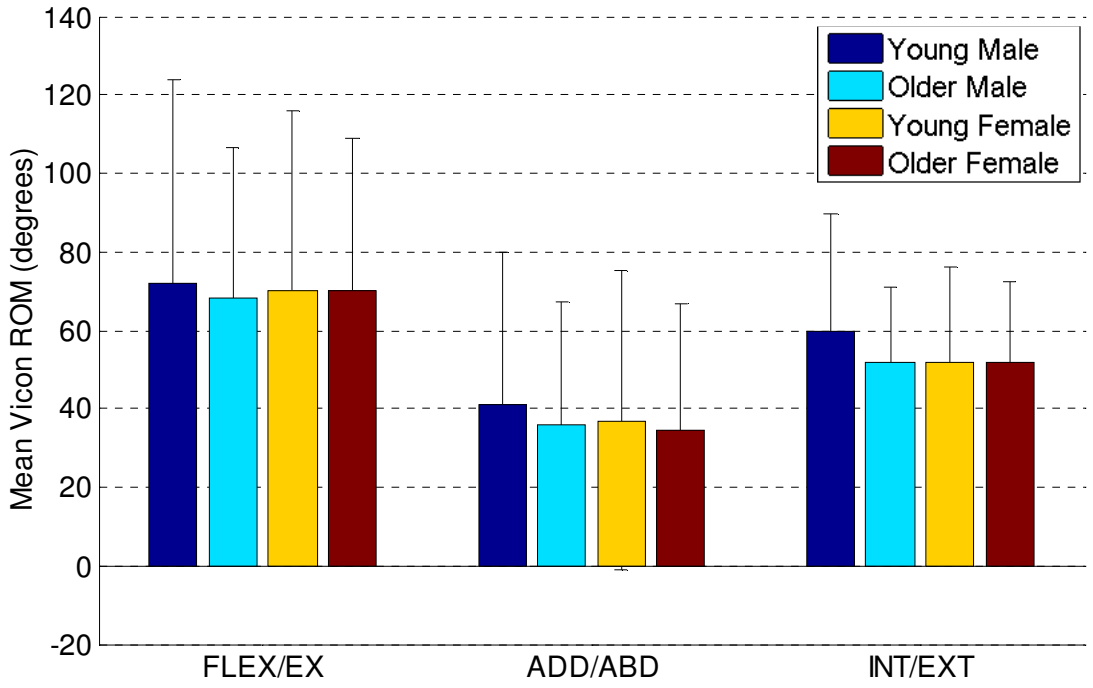

Figure 6.16 Bar chart showing mean VROM (degrees) of all 11 upper limb activities for each movement dimension. Each bar represents the mean of 165 values for one subject group and error bars represent 1 SD.

Plane	Young Male		Older Male		Young Female		Older Female	
	Mean	SD	Mean	SD	Mean	SD	Mean	SD
F	71.70	52.00	67.97	38.44	69.94	46.06	70.02	38.71
A	41.07	39.00	35.84	31.25	36.92	38.16	34.49	32.29
R	59.54	30.08	51.62	19.53	52.00	24.33	51.91	20.31

Table 6.21 Mean ± SD VROM values (degrees) of all 11 upper limb activities for each movement dimension for each subject group.

When analysed to minor and non-minor components (defined in section 6.2) as presented in table 6.22, minor ROM components exhibited larger percentage difference values. This was true for all groups with the exception of INT/EXT components for older males and young females which displayed comparable values for minor and non-minor components. Thus, a small absolute difference between the two systems was computed as a large relative difference for minor components. In particular, percentage difference values greater than 100% were computed for minor

components where the ROM difference between the two systems was larger than the Vicon ROM. Although this occurred infrequently, it was most often observed for planar Group 1 activities when out-of-plane ROM was small.

Movement component		Percentage difference (%)			
		Young Male	Older Male	Young Female	Older Female
FLEX/ EX	Minor (2)	48.10 ± 46.52	28.39 ± 20.15	31.46 ± 32.35	26.27 ± 36.49
	Major	7.41 ± 16.72	6.66 ± 7.64	4.44 ± 5.61	4.07 ± 4.03
ADD/ ABD	Minor (6)	25.16 ± 22.02	21.23 ± 19.90	23.01 ± 19.20	20.50 ± 18.99
	Major	14.40 ± 13.30	17.22 ± 20.35	12.09 ± 14.53	11.71 ± 8.86
INT/ EXT	Minor (1)	23.37 ± 18.60	10.77 ± 8.71	9.93 ± 10.42	15.96 ± 11.89
	Major	10.52 ± 10.30	10.99 ± 11.03	10.19 ± 10.45	9.55 ± 9.59

Table 6.22 Mean percentage difference values ± SD for minor and non-minor joint rotation components of the 11 upper limb activities. The number of minor movement components for each plane of motion is noted in brackets ().

The data therefore suggests that a measure of percentage to describe the difference between the two systems may give misleading results. Measures of absolute error were therefore considered a more appropriate and meaningful indicator of error between the two systems.

6.5.2 Distribution of box dimension data

Histograms presented in figure 6.17a-c show the distribution of difference in ROM values between the two systems for all 11 upper limb activities recorded. Three dimensional histograms were plotted to give a visual comparison of data between subject groups for each plane of motion. Bin widths were defined in 1^{o} increments. Distribution of error between the two systems was further summarised in a box and whisker plot in figure 6.18. Boxplot data showed the median values of the distribution with 1^{st} and 3^{rd} quartiles of the data represented by the boundaries of the box. Whiskers represented data values within 1.5 times the inter-quartile (IQ) range. Values extending beyond the whiskers were considered as potential outliers and plotted as red crosses (+). Measures of central tendency (mean, median and mode

values) of the histogram and boxplot data are presented in table 6.23. Mode values were computed as integers.

The histograms presented in figures 6.17a-c showed the distribution of positive and negative differences in ROM values between the two systems. As described in section 6.5.1, the sign of the data value indicated that gyroscope ROM was either smaller (positive value) or larger (negative value) than Vicon ROM. The highest frequency of ROM difference occurred near the centre of each distribution, and figures 6.17 and 6.18, and table 6.23 showed that measures of central tendency (mean, median and mode values) were close to 0^{o} for all three dimensions. The mean values of histogram data in table 6.23 were lower than mean absolute values presented in table 6.19, since they were computed from both positive and negative values. The histogram data showed that distribution of error values were comparable across subject groups for each movement dimension. Values of ROM difference for all trials can be found in Appendix C.

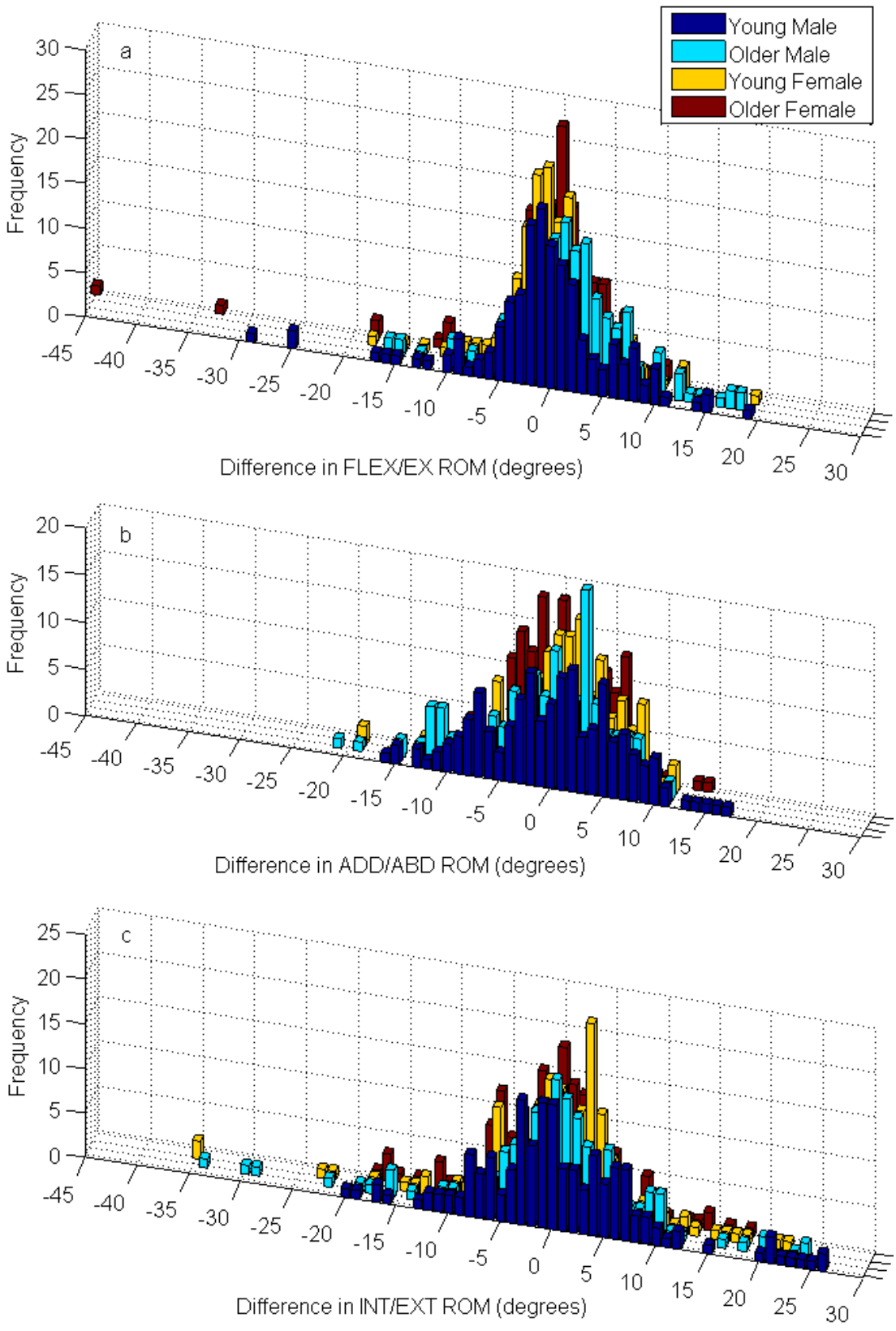

Figure 6.17 3D histograms of box dimension data for corrected 3D gyroscope ROM gradient for **a)** FLEX/EX, **b)** ADD/ABD, and **c)** INT/EXT rotation planes of motion.

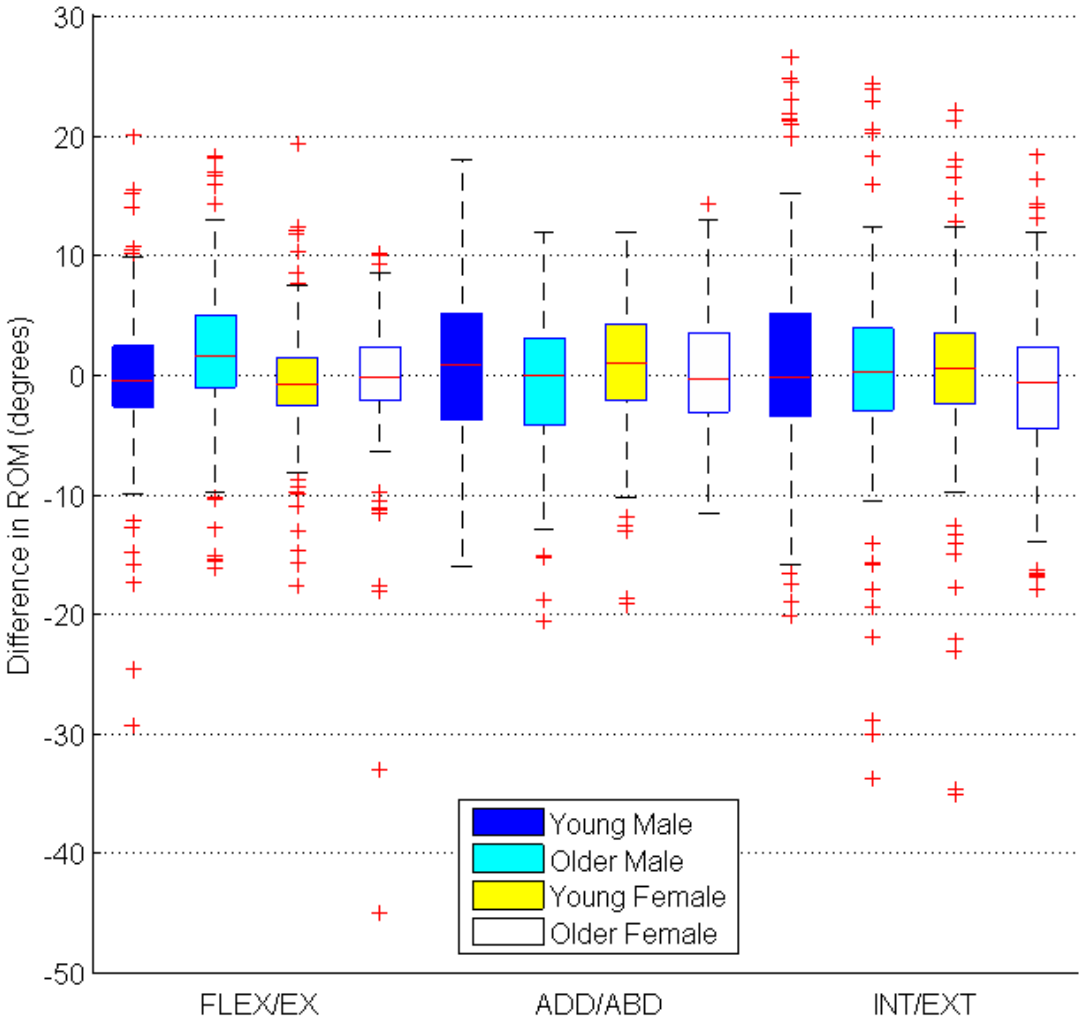

Figure 6.18 Box and whisker plot of difference in ROM between the Vicon and gyroscope systems. Whiskers represent values within 1.5 times the interquartile range. Red crosses (+) represent values greater than 1.5 times the interquartile range.

		YM	OM	YF	OF
FLEX/EX	Mean	-0.39 (6.61)	1.62 (6.00)	-0.56 (4.82)	-0.68 (5.97)
	Median	-0.53	1.58	-0.78	-0.25
	Mode	-1(20)	1(18)	-1(23)	0(27)
ADD/ABD	Mean	0.28 (6.51)	-0.93 (6.08)	0.69 (5.22)	-0.05 (4.53)
	Median	0.82	-0.08	1.02	-0.36
	Mode	2(13)	3(21)	2(17)	-2(18)
INT/EXT	Mean	0.75 (8.37)	0.09 (8.40)	0.11 (7.70)	-0.95 (6.06)
	Median	-0.23	0.15	0.56	-0.72
	Mode	-3(14)	0(16)	3(22)	0(18)

Table 6.23 Mean (±SD), median and mode of histogram data in degrees. Frequency of mode values are stated in brackets ().

Figure 6.17 showed that the largest errors between the two systems were represented in the tails of the histograms with the frequency of these values being very low at 1-2 occurrences. The INT/EXT plane showed the widest spread of data for all subject groups. The box and whisker plot data (figure 6.18) showed that many of the data values in the tails of the INT/EXT distribution were considered to be potential outliers. Large negative outlier values were computed from the Group 1 flexion activity and indicated large overestimation of Vicon ROM. Large positive outliers were computed from the Group 1 abduction activity (for older males, and young and older females), Group 2 "hand to back of head" activity (for young subjects only), and Group 3 "lifting to head height" activity (for young males only) and indicated large underestimation of Vicon ROM. The number of potential outliers for the INT/EXT dimension was larger than for the FLEX/EX and ADD/ABD planes.

For the FLEX/EX plane, large negative outlier values were particularly apparent for young males and older females. The majority of the negative values indicated on the box and whisker plot for the FLEX/EX dimension (figure 6.18) were computed from the Group 1 Abduction activity, where an XZY decomposition order was used as opposed to the ZXY decomposition used for all other upper limb activities. Large positive outlier values for the FLEX/EX plane were computed from the Group 2 "hand to back of head" and "same shoulder" activities.

The ADD/ABD plane gave the smallest spread of data of the three planes of motion. The box and whisker plot data showed that potential outlier values for the ADD/ABD component tended to be negative values and were computed from the Group 1 flexion activity. A number of negative values were also computed from the Group 2 "back of head" and Group 3 "lifting to head height" activities. The largest positive values observed for young males were computed from the Group 1 abduction activity which was decomposed using the XZY sequence as described in section 6.1. For older females, the largest positive values observed were computed from the Group 2 "opposite shoulder" activity.

6.5.3 Resultant vector of difference between the two systems

For each upper limb movement activity, a three dimensional vector was defined from the ROM values from the three planes of motion as described in section 5.3.2.4. Vectors were defined for both the Vicon and 3D gyroscope systems and the magnitude of the resultant vector between the two was taken as a measure of the three dimensional error between the two systems. A bar chart of mean resultant vector length for each upper limb activity is shown in figures 6.19a and 6.19b.

Figure 6.19 and table 6.24 showed that the largest mean resultant vector lengths were computed for the Group 1 flexion and abduction activities with mean resultant vector length values between 10^o and 20^o for all groups. In addition, the Group 2 "hand to back of head", "hand to same shoulder", and Group 3 "lifting to head height" activities gave mean resultant vector length values between 10^o and 20^o for one or both male groups. These activities exhibited the largest intra- and inter-group variability in resultant vector length. They involved one or more components previously identified in section 6.5.2 as components giving rise to error values in the tails of the histogram plots. They also involved components identified in section 6.4.2 as components displaying large residual data values for regression "per component" analysis, as indicated by the RMSE and p_1 and p_2 95% confidence intervals. Mean resultant vector lengths for all other activities were below 10^o, and were particularly low for the Group 1 external rotation and Group 2 "hand to mouth" activities.

Movement activity	Young Male		Older Male		Young Female		Older Female	
	Mean	SD	Mean	SD	Mean	SD	Mean	SD
Flexion	12.34	5.54	16.66	10.07	14.15	10.40	10.52	5.17
Extension	6.42	2.41	6.65	3.15	5.72	2.48	7.35	3.11
Abduction	12.50	7.93	15.50	8.26	12.84	5.64	14.07	11.98
External rotation	3.59	2.28	3.14	2.05	3.84	1.47	3.78	2.08
Internal rotation	8.24	2.10	8.97	2.20	8.88	2.44	8.52	1.53
Hand to mouth	4.69	2.01	4.95	2.70	2.41	0.95	3.84	1.95
Opposite shoulder	7.07	2.05	6.52	1.81	7.03	1.44	8.54	3.82
Back of head	18.18	9.15	9.46	4.37	9.48	7.10	9.84	3.88
Same shoulder	11.07	3.40	14.03	4.01	10.65	3.44	8.71	2.06
Lifting to shoulder	6.83	3.25	6.61	2.79	4.24	1.62	4.94	1.42
Lifting to head	12.96	7.92	9.45	4.05	9.12	5.93	6.23	2.85

Table 6.24 Mean resultant vector length (degrees) ± SD between Vicon and 3D gyroscope ROM data.

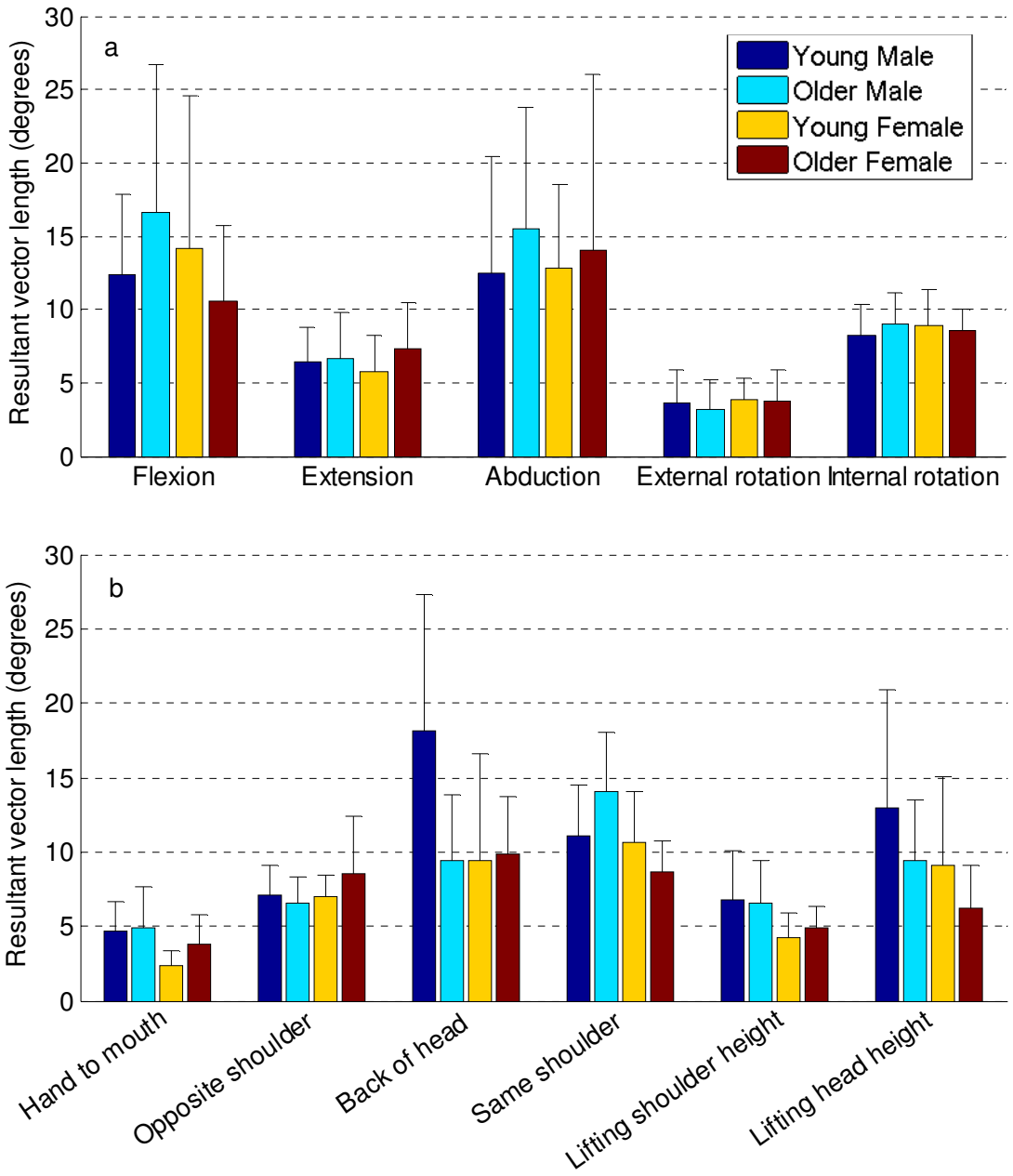

Figure 6.19 Mean resultant vector length (degrees) between Vicon and 3D gyroscope ROM data for **a)** Group 1 (Pure movements used in clinical functional examination) data and **b)** Group 2 (ADL) and Group 3 (Lifting) data.

Chapter 7: Discussion and recommendations for further work

7.1 Instrumentation

7.1.1 The 3D gyroscope system

Validation of single axis gyroscope angle data via pendulum testing (described in Chapter 3) showed that integrated gyroscope angular velocity data and potentiometer data were highly correlated for planar motions, with no detected sensitivity to linear velocity. Validation of the three 3D gyroscope units gave gyroscope angle data which were highly correlated with potentiometer data for rotation about the sensitive axes of all 9 gyroscopes, with $r>0.95$. For all trials, underestimation of the potentiometer angle magnitude was apparent predominantly at peak swing of the pendulum arm. Out-of-plane rotations were not highly correlated with potentiometer data. For three gyroscopes, minor temporal association in angle data was observed for out-of-plane rotations. Additionally, the results indicated that angle data from rotations around non-sensitive axes were prone to cumulative integration error. This was observed as an approximate integration error of 1^{o} in the first 20s of recording which increased exponentially over time (section 3.2.3). In order to eliminate cumulative integration error during the recording of upper limb motion, it was important to record a period of rest at the beginning or end of each trial to accurately determine and remove the voltage output offset. Furthermore, all testing trials were limited to 20s which was sufficient for the recording of upper limb functional tasks. No drift due to cumulative integration error was subsequently observed as discussed in section 7.1.3.

Thus, a simple 3D gyroscope system has been developed to record upper limb motion which can be easily and quickly attached to the thorax, upper arm and forearm via elasticated Velcro straps and hypoallergenic double-sided tape. Each gyroscope unit is small (40mm diameter and 25mm high) and lightweight with a mass of only 20g, is ideally attached at a site of least muscle mass, and does not require to be attached across a joint as is the case for goniometers and electrogoniometers. The system therefore promotes natural and unrestricted

movement. This is particularly important to minimise load and pain for patients as well as to facilitate the recording of true pathological movement, including primary deviations and secondary compensations. In this study, the thorax gyroscope unit was attached to the back as opposed to the sternum to prevent the occlusion of retro-reflective markers during cross-body activities. For use in the absence of retro-reflective markers, the thorax gyroscope unit would most ideally be placed over the body of the sternum.

The 3D gyroscope system does not involve a transmitter-receiver set-up such as for optoelectronic and electromagnetic systems. It can be operated from a laptop computer and is therefore portable, readily stored, and can be operated within a small space. This study has shown that such a system can be developed within a limited University budget and is therefore extremely cost effective.

Scapula motion was not measured in this study and the computed shoulder joint angles were therefore expressed in the form of humerothoracic rather than glenohumeral motion. Non-invasive scapula tracking is difficult due to the large amount of skin motion which occurs. The use of a scapula palpator has proven to be the most reliable method for the recording of non-invasive scapula motion, as described in section 2.1.3, but can only be achieved via a quasi-static approach. This technique cannot be applied using the 3D gyroscope system since it does not provide a measure of absolute orientation (discussed further in section 7.1.2). Indeed, clinical functional assessment is performed by evaluating the relative position of the humerus to the thorax and humerothoracic "joint" angle is thus considered a clinically relevant measure of shoulder function. Scapula motion has been tracked dynamically by attaching an electromagnetic sensor to the flattest part of the acromion (Karduna et al., 2001; Meskers et al., 2007) and has shown to be valid for humeral elevations up to 120^{o}. Similarly, a small cluster of retroreflective markers has been attached to the acromion (van Andel et al., 2009) and has shown to be valid for humeral elevations up to 100^{o}.

7.1.2 Independent functioning of the 3D gyroscope system and review of advances in inertial system development

Following the testing protocols defined in sections 5.2.2 and 5.2.4, the 3D gyroscope system does not provide sufficient information to independently determine the relative rotations between adjacent body segments, as described in section 5.3.1.3. This was because each gyroscope unit gave a measure of change in orientation relative to its own starting orientation rather than to a common reference orientation e.g. absolute orientation relative to a global reference frame. Additional calibration procedures are therefore required in order to provide sensor-to-sensor and sensor-to-segment orientation information which are both necessary for the computation of joint angles. In this study, this orientation information was obtained for each trial from one frame of Vicon coordinate data with the arm in the neutral reference position. Each gyroscope unit was attached to a marker cluster such that the gyroscope coordinate system was considered coincident with the technical coordinate system via an alignment procedure. Gyroscope joint angles were therefore expressed as rotations about anatomical rather than functional axes. This enabled the comparison of data from both systems and eliminated differences in joint angle output due to the use of different joint coordinate systems. Evaluation of the difference in computed angle between the two systems is discussed in section 7.1.3.

Since this project began, many advances have been made in the development of inertial systems for motion measurement, and a number of these are now available commercially. The most complex inertial systems include triaxial gyroscopes, triaxial accelerometers and triaxial magnetometers (e.g. XSens Technologies, Netherlands) and incorporate complex sensor fusion algorithms and Kalman filtering techniques (Roetenberg et al., 2005). These inertial and magnetic sensing (IMMS) systems are able to provide the absolute orientation of each sensor unit relative to an earth-based global reference system. This is achieved by utilising the gravity vector as a vertical reference axis, and the magnetic field vector as a second reference axis estimating the frontal plane (O'Donovan et al., 2007, de Vries et al., 2010). The inclusion of the magnetometer signal reduces heading errors which occur through use of inertial sensors (namely accelerometers) alone.

The use of multi-type sensors together with sensor fusion and Kalman filtering reduces integration drift of the raw gyroscope signal which occurs during long term motion recording. This enables IMMS systems to be applicable to a wide range of applications e.g. long term ambulatory monitoring (Spain et al., 2012; Bergmann et al., 2014) and sports applications (Roetenberg et al., 2013). For the purposes of upper limb functional assessment in a clinical setting, a 20s trial is sufficient to record a single functional movement and thus IMMS systems may be unnecessarily complex for this application. As discussed in section 7.1.1, all trials were limited to a recording length of 20s and no integration drift was subsequently observed. Thus, restricting the recording time eliminates the occurrence of integration drift and reduces the need for such complexity.

Although commercial IMMS are able to provide absolute orientation information, a disadvantage of using magnetometers is the susceptibility to magnetic field disturbance, particularly in the presence of ferromagnetic materials (de Vries et al., 2009). This could therefore lead to inaccurate orientation estimation. Although heading errors as a result of magnetic field disturbance can be eliminated by the incorporation of adequate sensor fusion (Luinge et al., 2007; Roetenberg et al., 2007), this may not be possible in all cases and may be highly dependent on the environment in which it is used. A more complex system also imposes an increase in the time and cost of operation due to longer offline processing and the requirement for more sophisticated hardware and software.

For less complex systems involving fewer sensors, various approaches to determine sensor-to-sensor orientation have been employed according to the combination of inertial and/or magnetic sensors used. Luinge et al, (2007) utilised anatomical constraints to determine the relative rotations between segments using only gyroscopes and accelerometers; the authors measured the orientation of the forearm with respect to the upper arm using the assumption that the elbow joint does not permit adduction-abduction, thereby eliminating the need for a second reference axis.

In order to determine the sensor-to-segment orientation, a functional approach has most frequently been used regardless of the complexity of the inertial system. During rotation of the body segment about a joint's functional axis, the direction of

the rotation axis can be estimated using the direction of the angular velocity vector. The change in orientation and hence the axis of rotation can be determined from integration of the gyroscope signal (O'Donovan et al., 2007). In the presence of accelerometers, a second axis can be defined during a resting posture using the gravity vector (Picerno et al., 2008). de Vries et al. (2010) proposed a set of planar functional movements for the thorax, humerus, forearm and hand to determine joint functional axes from the angular velocity vector. Planar motion of the humerus during forward flexion was ensured by asking the subject to hold a light bar at shoulder breadth with the thumbs pointing laterally. Similarly, planar humeral axial rotation was achieved by supporting the elbows at the olecranon. Two functional axes with the least variability are chosen to define the functional frame. A third axis can then be defined as their cross product. Thus, a 3 x 3 orientation matrix can be determined which expresses the orientation of the body segment in the sensor unit coordinate system (Luinge et al., 2007; O'Donovan et al., 2007).

Another less commonly used technique to determine sensor-to-segment orientation has involved an anatomical calibration approach. Picerno et al. (2008) developed a special frame or "palpator" with an inertial and magnetic sensing system (IMMS) unit attached. The frame allowed the simultaneous palpation of two bony landmarks of a limb segment such that the orientation of the line joining them could be determined with respect to a global reference system. By recording the orientation of two non-parallel lines, an anatomical axis system was determined for each limb segment and its orientation expressed in the sensor unit coordinate system. However, since this anatomical calibration technique relies on the use of external palpable bony landmarks, the defined anatomical frames for the humerus would therefore differ from those proposed by the ISB (Wu et al., 2005). This is because the shoulder joint centre cannot be palpated and, since IMMS provide a measure of orientation and not position, the use of regression techniques to estimate the location of internal anatomical landmarks is not possible.

For future independent use of the gyroscope system, determination of orientation information will therefore require a two-stage calibration procedure. The first stage will involve the determination of the sensor-to-sensor orientation. This is

challenging in the absence of additional sensors which could provide additional orientation information relative to a reference axis i.e. the use of accelerometers to provide orientation relative to the gravity vector. A protocol for sensor-to-sensor orientation calibration was proposed in section 5.3.1.3 but was considered unsuitable for this study due to the necessity to incorporate the measurement of a reference orientation at the beginning of each trial. However, this approach would be feasible by ensuring that the same starting position was used for each recording following calibration. This could be carried out via the use of a simple piece of apparatus such as a rigid frame to which the upper limb and trunk could be aligned at the start of each trial. This apparatus would be an additional piece of equipment which would be placed in the consulting room and utilised when required. Thus, sensor-to-sensor orientation could be determined without the need for additional complex hardware and software, with both a reduction in cost and a reduction in offline processing time compared with the use of a more complex commercial system.

The second stage of the calibration procedure will involve the determination of the sensor-to-segment orientation via a functional approach. The proposed movements are based on the uni-axial calibration movements described by de Vries et al. (2010). Modifications have been made to restrict glenohumeral axial rotation which occurs during humeral elevation as discussed in section 7.2.2. Calibration movements are proposed below for the thorax, humerus and forearm segments:

Thorax:

- Flexion-extension
- Lateral flexion
- Axial rotation

Humerus:

- Arm forward flexion, elbow extended, holding a light bar at shoulder breadth, thumbs pointing laterally.
- Ab-adduction performed with 90^{o} elbow flexion
- Internal and external rotation, with the elbows supported at the olecranon
- Elbow flexion (movement of the forearm expressed in the humeral IMMS)

Forearm:

- Flexion-extension, while holding a light bar, thumbs pointing laterally to fix the forearm from pro- and supination, elbows supported at the olecranon
- Pro- and supination, free in the air, hand kept straight in line with the forearm
- Pro- and supination, elbow and ulna supported.

As described previously, the two functional axes with the least variation over several repetitions should be chosen to define the functional frame. A third axis can then be defined as their cross product. Orthogonality can be ensured by taking two concurrent cross products of the chosen axes (de Vries et al., 2010; O'Donovan et al., 2007). de Vries et al (2010) stated that calibration movements should be performed by avoiding the extremes of the range of motion. The production of out-of-plane rotations may be more likely when the extremes of the range of motion are reached, such as at full humeral elevation as discussed in section 7.2.2. Cutti et al (2008) and de Vries et al (2010) demonstrated that functional axes can be successfully and accurately used to measure upper limb kinematics, and functional axes can be determined with little cross talk and low variability.

Since inertial system based local coordinate systems differ from bony landmark based local coordinate systems, use of the above proposed calibration protocols will give rise to joint angle curves which will differ from those presented in Chapter 6 of this thesis. de Vries et al (2010) quantified differences in joint angles obtained from the use of functional versus ISB recommended anatomical axes of up to 20^{o} for measures of plane of elevation and axial rotation, and differences of up to 10^{o} for elevation angle. Anatomical axes are an approximation of functional axes, and the use of functional frames would minimise the occurrence of kinematic cross talk. This is particularly relevant for the determination of the elbow flexion-extension axis where the very short distance between the humeral epicondyles could lead to large errors in anatomical axis estimation. No standardised protocol yet exists for the determination of functional frames and it is likely that the use of functional rather than anatomical axes will become increasingly common in upper limb motion analysis due to the increasing use of inertial systems (Kontaxis et al, 2009).

Thus, the inclusion of an additional two-stage calibration procedure in the existing experimental protocol for the 3D gyroscope system will permit complete independent functioning of the system. This, will give rise to a fully portable and unconstrained tool for upper limb functional assessment.

7.1.3 3D gyroscope system error

Characterisation of error

The results showed that humerothoracic angles recorded from the 3D gyroscope system were highly correlated with those from the optoelectronic gold-standard. The majority of mean correlation values for the 11 upper activities were greater than 0.9. In particular, consistently high mean correlation and low SD values were computed for major movement components. Correlation values for low ROM components were less consistent and more likely to give low correlation values. For Group 1 clinical movements, low ROM components tended to be out-of-plane components which would not form the planes of clinical interest. For the Group 2 ADL and group 3 lifting activities investigated, low ROM correlation values were much fewer in number.

Regression "per movement component" and "per movement plane" analysis in sections 6.4.2 and 6.4.3 indicated that the gradients of the fitted regression lines were less than 1 for all movement components and dimensions. This indicated that the magnitude of 3D gyroscope system measures of ROM tended to underestimate measures of Vicon ROM. Initial characterisation of 3D gyroscope system error from regression "per movement dimension" analysis in section 6.4.3 indicated that magnitude of error was dependent upon ROM of the activity e.g. for a Vicon ROM of 180^{o}, the 3D gyroscope system exhibited an underestimation error of between 12.8^{o} and 29.2^{o} for the FLEX/EX plane, 10.0^{o} and 27.2^{o} for the ADD/ABD plane, and 7.5^{o} and 30.9^{o} for the INT/EXT plane. The magnitude of the computed 3D gyroscope system error decreased with decreasing ROM and overestimation errors were more likely to be computed from low ROM components e.g. for a Vicon ROM of 30^{o}, 3D gyroscope system error was estimated between -4.5^{o} (overestimation) and

11.9^{o} for the FLEX/EX plane, -7.1^{o} and 10.1^{o} for the ADD/ABD plane, and -8.4^{o} and 15.0^{o} for the INT/EXT plane.

Following correction of 3D gyroscope ROM underestimation error, as described in section 6.4.3, gradients of the fitted regression lines approximated 1 for each plane indicating that the magnitude of 3D gyroscope system measures of ROM was close to the optoelectronic "gold-standard". The magnitude of absolute error of the 3D gyroscope system was no longer dependent upon ROM of the activity and was characterised as lying within ±*e* of the Vicon "gold-standard" ROM value. The value of *e* was computed as ±9.45^{o} for the FLEX/EX plane, ±9.37^{o} for the ADD/ABD plane, and ±12.28^{o} for the INT/EXT plane based on error boundaries containing 90% of data values. For 95% of data values, absolute error of the 3D gyroscope system lay to within ±11.90^{o} for the FLEX/EX plane, ±11.32^{o} for the ADD/ABD plane, and ±15.42^{o} for the INT/EXT plane. The distribution of 3D gyroscope ROM error following correction therefore gave an approximately equal number of negative and positive values (overestimation and underestimation respectively) with measures of central tendency approximating zero for all planes of motion as displayed in histogram and box and whisker plot data (section 6.5.2). The linear relationship between the Vicon and corrected 3D gyroscope system ROM data was well defined as indicated by the narrow p1 and p2 95% confidence intervals (table 6.16) indicating repeatability and consistency of 3D gyroscope system ROM error.

Outlier values/ largest error values

Error values which lay outside of the defined error boundaries of ±*e* were represented on histogram and box and whisker plots of 3D gyroscope error as the largest values in the tails of the distributions (section 6.5.2). The frequency of these values was very low at 1-2 occurrences. For all dimensions, linear regression "per movement component" analysis presented in section 6.4.2 identified the source of the largest errors as those movement components with large RMSE values, wide 95% confidence bounds for intercept (p_1) and gradient (p_2) estimates, or large intercept values.

The majority of negative FLEX/EX error values, were computed from the Group 1 Abduction activity, and represented overestimation error (GROM range 8.2° to 74.7°; VROM range 7.6° to 42.4°). For regression "per movement component" analysis (section 6.4.2), a large RMSE value for this component (9.13°) indicated spread of data points from the regression line. Wide 95% confidence bounds for gradient and intercept estimates indicated poor precision of the estimated regression coefficient values. This was particularly true for the gradient estimate (p2 CI: 0.53° to 1.07°) which gave the widest 95% confidence bounds of all movement components. An R^2 value of 0.37 was also the lowest observed for any component and indicated that only 37% of variation in the data was accounted for by the linear model. As previously described in section 6.1, the XZY decomposition order was used to compute joint rotation angles for the Group 1 Abduction activity, as opposed to the ZXY decomposition used for all other activities. FLEX/EX formed the second rotation in the XZY sequence and exhibited low ROM (mean GROM 32.91° ± 12.70°). The results therefore suggested that small FLEX/EX motions decomposed using the XZY sequence were prone to large variability. The histogram showed that the frequency of the largest overestimation errors was very low and the majority of error values from this component fell within the defined 90% error bounds of ±9.45°.

The largest positive FLEX/EX (underestimation) error values, were computed from the Group 2 "hand to back of head" and "hand to same shoulder" activities. Again, the majority of error values from these components fell within the defined 90% error boundaries of ±9.45° for the FLEX/EX plane, and the number of error values outside of these boundaries was low. For the "back of head" activity, wide p1 95% confidence bounds (p1 CI: -20.50 to 0.44) indicated poor precision of intercept estimation, and a large negative intercept value (-10.03°) was consistent with large underestimation of Vicon ROM. Regression data for the "same shoulder" activity exhibited a relatively large RMSE value of 5.38°. Both activities exhibited large variation in ROM between individuals due to differences in movement preference between older and younger subjects. This is discussed further in section 7.2.2.

The ADD/ABD plane gave the smallest spread of data of the three planes of motion which corresponded with the smallest value of *e* (±9.37° for 90% of data). The

largest negative error values on the ADD/ABD histogram (figure 6.17) were computed from the Group 1 Flexion activity and again represented overestimation error (GROM range 17.9^o to 59.8^o; VROM range 15.1^o to 44.6^o). The wide p_2 95% confidence bounds (p2 CI: 0.77^o to 1.12^o) and positive intercept value (6.12^o) from regression "per component" analysis were consistent with overestimation error. As for the FLEX/EX plane, overestimation errors were computed from a small ROM component (mean GROM 35.21^o ± 9.97^o) which formed the second rotation in the decomposition sequence (ZXY in this case). A number of negative values were also computed from the Group 2 "back of head" and Group 3 "lifting to head height" activities with similar p1 values as for the ADD/ABD component of the Flexion activity (7.22^o and 4.52^o respectively). These three components gave the largest RMSE values of all ADD/ABD components (range 4.12^o to 5.45^o). The frequency of positive error values outside of the defined 90% error boundaries was very low. The largest positive values were computed from the Group 1 abduction activity for young males and the Group 2 "hand to opposite shoulder" activity for older females.

The INT/EXT plane displayed the widest distribution of data of the three dimensions. The largest error values in the tails of the INT/EXT histogram were represented as outlier values on the regression "per movement dimension" plot (figure 6.13) where the INT/EXT plane exhibited the largest residual data values of the three dimensions (RMSE 7.70^o) and the largest value of *e* (±12.28^o for 90% of data). In addition, regression "per subject" analysis (section 6.4.1) indicated that estimated regression coefficients and goodness of fit statistics were slightly more variable across all 20 subjects for the INT/EXT plane compared with the other two dimensions. The majority of INT/EXT overestimation values, including the largest negative values, were computed from the internal rotation component of the Group 1 Flexion activity (error range -35.0^o to 10.7^o; VROM range 29.8^o to 94.0^o). Linear regression "per movement component" analysis (section 6.4.2) indicated spread of data points from the fitted regression line with RMSE value of 10.03^o. This, together with a large intercept value (16.87^o) and wide p1 and p2 95% confidence bounds (p1 CI: 4.87^o to 28.87^o; p2 CI: 0.63^o to 0.98^o) was consistent with the large overestimation errors observed.

The majority of large positive INT/EXT error values were computed from the Group 1 Abduction activity (error range -5.7^{o} to 24.2^{o}; VROM range 55.2^{o} to 122.3^{o}), the Group 2 "hand to back of head" activity (error range -16.8^{o} to 26.5^{o}; VROM range 32.6^{o} to 167.8^{o}), and the Group 3 "lifting to head height" activity (error range -22.1^{o} to 26.5^{o}; VROM range 25.3^{o} to 111.9^{o}). RMSE values for these components were large and ranged from 7.62^{o} to 10.00^{o}. For the abduction activity, a large negative intercept value (-7.23^{o}), together with wide p1 and p2 confidence bounds (p1 CI: -19.17^{o} to 4.71^{o}; p2 CI: 0.79 to 1.07), was consistent with large underestimation errors of Vicon ROM.

The four INT/EXT components described above exhibited the largest mean INT/EXT ROM of the recorded upper limb activities. In particular, axial rotation ROM for the Group 1 flexion and abduction activities was larger than for the "pure" axial rotation components themselves (discussed further in section 7.2.2). In contrast, error values for small axial rotation components were within the defined 90% error bounds of ±12.28^{o} and regression statistics indicated a good fit of the linear model to the data e.g. Internal rotation error range -12.6^{o} to 8.1^{o}, VROM range 12.5^{o} to 66.4^{o}; Hand to mouth error range -6.3^{o} to 10.0^{o}, VROM 12.0^{o} to 59.1^{o}. The data therefore suggested that 3D gyroscope system errors were prone to the largest variation for motions in the INT/EXT plane, particularly for motions involving large axial rotation components.

Thus, for all planes of motion, regression analysis identified several components from which the computed ROM difference values were rather large and variable across subjects. It follows that activities including one or more of these components gave the largest resultant vector values, reflecting the largest three-dimensional error of the 3D gyroscope system. Section 6.5.3 showed that the largest mean resultant vector values were computed for the Group 1 Flexion and Abduction activities where mean resultant vector length for all subject groups was between 10^{o} and 20^{o}, and also for the Group 2 "back of head" and "same shoulder", and Group 3 "lifting to head height" activities, where mean resultant vector length was between 10^{o} and 20^{o} for one or more of the male groups. These activities exhibited large intra- and inter-group variability in mean resultant vector length. With the exception of the "same

shoulder" activity, activities with the largest resultant vector lengths involved the largest INT/EXT components of all activities. As previously discussed, axial rotation was found to give the largest 3D gyroscope ROM errors of the three dimensions. In addition to a large INT/EXT component, these four activities also involved an additional one or more of the identified large-error components from the FLEX/EX and ADD/ABD planes. Large resultant vector values for the "back of head" activity were the result of large ROM error in all three planes. For the "same shoulder" activity, large resultant vector length was largely the result of ROM error in the FLEX/EX plane only. For all other activities, mean resultant vector length was below 10^{o}, and was particularly low for the Group 1 external rotation and Group 2 "hand to mouth" activities where mean resultant vector length was below 5^{o}.

Special attention should therefore be paid when including these activities in any measurement protocol, with particular attention to measures of large axial rotation. A possible source of difference between the two systems may be associated with the orientation of the 3D gyroscope unit to the corresponding marker cluster. As described in section 5.2.2, each gyroscope unit was attached to a marker cluster via a "lining-up" process using visual markings in such a way that the gyroscope coordinate system was considered to be coincident with the technical coordinate system of the marker cluster. Differences in orientation between the two coordinate systems may give rise to differences in computed angle values between the measurement systems. This may be subject to variation between recording sessions and between individuals. However, regression "per subject" analysis (section 6.4.1) did indicate that variation in computed regression statistics between individuals was very low for the FLEX/EX and ABD/ADD plane, and slightly more variable for the INT/EXT plane as previously discussed. Similar alignment techniques have been successfully employed in other studies involving the simultaneous use of optoelectronic marker clusters and inertial measurement units (de Vries et al., 2010; de Vries et al., 2009; Cutti et al., 2008). On a more basic level, pendulum experiments presented in sections 3.2 and 3.5 have given high correlation of angle data for movement in the gyroscope's sensitive axis ($r>0.95$), and low correlation coefficients for out-of-plane rotations, indicating that both the gyroscope unit

alignment technique used, and the orthogonal alignment of the single axis gyroscopes within each gyroscope unit itself was accurate.

Another possible contributory factor to the observed differences in axial rotation ROM values between the two systems is soft tissue artefact (STA) which is known to particularly affect measures of axial rotation as discussed in section 7.2.2. Each gyroscope unit was attached to each marker cluster such that both systems would experience the same displacement of soft tissue relative to the underlying bone. STA may have a dissimilar effect on the output of the two measurement systems where gyroscope and marker cluster coordinate axes are not closely aligned, and this error may be cumulative. Care must therefore be exercised when interpreting the results of axial rotation components. In particular intra-subject comparisons of INT/EXT values may be feasible, but inter-subject comparisons may not (Kontaxis et al, 2009). It should be noted that independent use of the 3D gyroscope system would eliminate the requirement for the alignment of coordinate axes between the two systems as previously discussed (section 7.1.2).

A potential disadvantage associated with the use of gyroscopes is related to drift due to the integration of angular velocity to give angular position (Luinge and Veltink, 2005). This cumulative error between the two systems is most likely to be observed for longer recording trials. As discussed in section 7.1.1, initial single axis gyroscope testing showed an approximate integration error of 1^{o} in the first 20s of recording for out of plane rotations, which increased exponentially over time (section 3.2.3). Each recording trial was limited to a maximum of 20s and drift was subsequently not observed for segment angles recorded in this study.

Comparison of error with commercial systems and other common clinical recording techniques

Only a few studies have used inertial measurement systems to analyse the kinematics of the upper limb, whether commercially available systems or simpler inertial systems (Cutti et al., 2008). Comparison of the error of the 3D gyroscope system to such studies was difficult due to differences in recording protocols. In addition, inertial system error was frequently reported as RMS error rather than absolute error

in degrees. Several studies have quoted the accuracy of the commercially available XSens MTx sensor (XSens Technologies, NL) both for measurements made with respect to the global system, and for measures of joint or segment angle when used in conjunction with a specific recording protocol. Cutti et al (2008) and de Vries et al (2010) quoted errors of 1^o RMS for static measurements and 2^o RMS for dynamic measurements with respect to the global frame, as stated in the manufacturer's specifications. Zhou et al (2008) reported RMS errors of 2.5^o to 4.8^o for elbow FLEX/EX and forearm rotation Euler angles relative to a global frame. When used with a specific upper limb recording protocol, Cutti et al (2008) quoted an RMS error of RMS<3.6^o for main joint angle curves computed from functional axes, compared with those recorded from an optoelectronic system. Using a simpler system consisting of accelerometers and gyroscopes only, mean RMS error of 5.81^o was reported for measures of 3D humeral angle compared with an ultrasound system (Coley et al., 2007).

In this study, mean RMS error of the 3D gyroscope system averaged over each movement cycle was computed as $8.38^o \pm 5.88^o$ for the FLEX/EX plane, $4.74^o \pm 2.97^o$ for the ABD/ADD plane, and $5.89^o \pm 5.40^o$ for the INT/EXT plane. RMS values were therefore larger than those reported in the literature described above. It should be noted that RMS error reported in this thesis was computed from uncorrected 3D gyroscope angle curves which tended to underestimate Vicon angle magnitude as discussed above and shown in linear regression analysis (section 6.4), particularly for large ROM activities. The successful correction of 3D gyroscope underestimation error for measures of ROM (described in section 6.4.3) indicates that a similar procedure for the correction of angle values over the entire movement cycle would be feasible. It is anticipated that a reduction in RMS error would be observed when computed from such corrected joint angle data. Thus, future proposed work should involve the determination and application of correction factors to 3D gyroscope angle data for the entire movement cycle, and the determination of the resulting reduction in RMS error.

Conclusions

The defined 90% error boundaries of ±*e* have demonstrated the resolution of the 3D gyroscope system and indicated that it is not suitable to measure very small changes in ROM. Indeed, this was not the intended application of the system. The 90% error boundaries also indicated that the 3D gyroscope system estimated optoelectronic gold-standard angle data in a repeatable and consistent manner using the described recording protocol, and that the error of the 3D gyroscope system was also consistently defined. The source of error values outside of the defined 90% error boundaries were identified as components to which special attention should be paid when recording similar activities. In particular, motions containing large INT/EXT components were likely to give the largest 3D differences in angle values between the two systems, namely the Group 1 Flexion and Abduction activities, Group 2 "back of head" and Group 3 "lifting to head height" activities. Special attention should be paid when recording or interpreting the results of such activities.

Measures of humero-thoracic kinematics obtained from the 3D gyroscope system were highly correlated with those recorded from the optoelectronic gold-standard and close in ROM magnitude following the correction of 3D gyroscope ROM underestimation error using correction factors determined from linear regression analysis. The results suggested that a similar correction procedure applied to correct joint angles over the entire movement cycle would be feasible, which would potentially decrease RMS error of the 3D gyroscope system. The availability of such 3D upper limb data within the clinical environment would be a very powerful tool for clinical upper limb functional analysis. Thus, the system has potential as a valid tool in the clinical assessment of upper limb function.

7.2 Upper limb kinematics

7.2.1 Choice of Euler decomposition order

The choice of orientation matrix decomposition order was an important consideration in this study in order to compute joint angles which not only avoided gimbal lock singularity but which were also clinically meaningful. The large ROM possible at the shoulder joint meant that it was difficult to choose a rotation sequence or a set of sequences which simultaneously fulfilled both these criteria, particularly for ADL activities. As described in section 6.1, the ISB's recommended Euler YXY method was not an appropriate choice for this study due to the close proximity of the upper limb neutral reference position with the gimbal lock posture of 0^o humeral elevation. Two Cardan sequences, ZXY for largely sagittal plane motions, and XZY for largely frontal plane motions, were therefore selected to decompose the relative orientations between the humerus and the thorax. The use of more than one decomposition sequence applied in this way eliminated the occurrence of gimbal lock since the largest/primary motion of interest formed the first rotation in the sequence and the second rotation did not approach the gimbal lock posture of $\pm 90^o$.

Whilst the application of the chosen Cardan sequences was well suited for planar Group 1 movements, the results showed that this method was limited for the description of ADL activities recorded in this study. Since ADL activities frequently occur between the clinically defined planes of motion, the assignment of a suitable rotation sequence was somewhat ambiguous. Choice of rotation sequence was further compounded where variation in movement performance between individuals existed; the need for consistency in method to enable inter-subject comparisons meant that the most appropriate rotation sequence according to the primary plane of motion was not always applied as required. In such cases, the largest joint motion did not form the first rotation in the decomposition sequence and the resulting joint angle values did not intuitively represent the actual motion in terms of amplitude of the three constituent joint rotations.

This was observed for the "hand to back of head" activity where three young males and two young females exhibited a preference to perform this task in the frontal plane in contrast to the majority of individuals who exhibited no planar preference. As shown in section 6.2.2, use of the ZXY decomposition order (FLEX/EX, ADD/ABD, INT/EXT) for these individuals gave a large FLEX/EX component which was counterintuitive when describing a largely frontal plane motion. The resulting joint angle curves were comparable to those computed for the group 1 abduction activity when using the ZXY decomposition order. Section 6.1 showed that decomposition order had a dramatic effect on the magnitudes of the abduction joint angle values and that an XZY sequence (ADD/ABD, FLEX/EX, INT/EXT) was most representative of a frontal plane motion. This finding was also echoed by Šenk and Chèze (2006) who showed that an XZY sequence applied to a frontal plane motion gave the least gimbal lock occurrence with abduction angle amplitude comparable with values reported in literature. Although frontal plane motions decomposed using the ZXY sequence were prone to gimbal lock, this was not observed for the "hand to back of head" activity indicating that the humerus did not approach the singularity posture of 90^{o} abduction.

The findings illustrate the importance of sequence on the interpretability and subsequent clinical usefulness of the data. The use of Cardan angles to describe ADL motions in this study was limited since they did not easily accommodate for inter-subject variation in movement performance. The results show that although Cardan angles are described in clinical terms, values can still seem far removed from the actual motion if the most appropriate sequence is not used. The magnitude of difference in joint attitude representation due to sequence choice is dependent on ROM (Cole et al., 1993). Appropriate choice of rotation sequence is therefore of particular concern at the shoulder where ROM is large. The concept of defining joint attitude as a sequence of rotations is itself clinically unintuitive, and the concept that one sequence is a more appropriate descriptor of a particular joint motion than another based on the magnitudes of the computed angular components may be difficult and impractical to implement in clinical functional analysis.

In general, use of the Euler YXY decomposition as proposed by the ISB is particularly suited to describe ADL activities since it avoids the description of joint rotations according to the clinically defined planes of motion which are not consistent in 3D (Wu et al., 2005). The Euler YXY decomposition is therefore appropriate to describe any humerothoracic motion regardless of the primary plane of activity. The description of shoulder joint motions in a globe system projected around the shoulder aids the visualisation and interpretation of joint angles and thus facilitates the uptake of this method within the clinical environment (Doorenbosch et al., 2003; Rab, 2008). Although this method is not in accordance with clinical definitions, joint motions described in this way are more practically linked with observational clinical analysis of motion (Rab, 2008). Furthermore, use of this method would provide a common language between researchers and clinicians (Doorenbosch et al., 2003). As described in section 6.1, the main limitation of the Euler YXY method for this study was the frequent occurrence of gimbal lock at the gimbal lock posture of 0^{o} humeral elevation. This has also been identified as a limitation of the method in other studies (Šenk and Chèze, 2006; van Andel et al., 2008; Bonneyfoy-Mazure et al., 2010). This method is therefore particularly suited to describe joint motions which do not approach the singularity posture.

The issues encountered in this study reflect the ongoing debate within the biomechanics community regarding the most appropriate choice of decomposition order for the description of non-planar shoulder motions, whether glenohumeral or humerothoracic. The most suitable rotation sequences to describe specific movements are those where gimbal lock occurrence is eliminated and amplitude coherence maximised i.e. computed angle amplitude of the primary component of motion being comparable to the maximal known angular range reported in literature (Šenk and Chèze, 2006; Bonneyfoy-Mazure et al., 2010). However, these two criteria are often not simultaneously fulfilled. Despite the ISB 2005 recommendations (Wu et al., 2005), there remains no universally accepted method for the reporting of upper limb joint motions (Šenk and Chèze, 2006; Rab, 2008; Bonneyfoy-Mazure et al., 2010). No single rotation sequence adequately describes the large ROM at the shoulder and each method has associated with it a region where joint motion is poorly described. Thus, the choice of decomposition order(s) used is

largely dictated by the objectives of individual studies, which hinders the cross-comparison of results. There is a call for the development of detailed motion analysis protocols with specific recommendations relevant to address research questions of comparable content (Kontaxis et al., 2009). The development of such protocols would thus facilitate the comparison of results between studies and provide a basis for standardisation which can be applied in clinical practice for the recording of functional movements.

Despite the limitations associated with the use of Cardan sequences for the description of ADL activities, their use in this study eliminated the occurrence of gimbal lock, thereby allowing an assessment of the relationship between the outputs of the 3D gyroscope system and the gold-standard Vicon system at all physiological ranges of motion including the singularity postures of the Euler YXY sequence. Thus, the most important consideration in this thesis was the elimination of gimbal lock, which preceded the presentation of clinically interpretable data. For future clinical application of the 3D gyroscope system, it is proposed that an alternative upper limb reference posture could be used with the ISB recommended Euler YXY sequence to compute ADL joint angles for clinical investigation. For example, Šenk and Chèze (2006) have suggested that flexion and abduction activities will not be affected by gimbal lock with a starting posture of 30^{o} humeral elevation. The chosen reference posture should be as repeatable as possible to facilitate the intra- and inter-subject comparison of results. For planar maximal ROM activities, the use of Cardan sequences is recommended as applied in this thesis. Whilst the use of several sequences is not ideal in clinical application, their use in this way would provide the most clinically interpretable data. In any case, it is clear that very specific measurement protocols and standardisations for the application of the 3D gyroscope system for upper limb functional assessment will be needed.

7.2.2 Joint rotation data features

Although it was not the aim of this thesis to investigate normal upper limb motion per se, the 3D joint angle data presented in section 6.2 from healthy subjects revealed several notable features which are described in this section and demonstrate the potential clinical usefulness of the 3D gyroscope system data.

Group 1 activities: Axial rotation during elevation motions

Section 6.2.1 showed that axial rotation formed a large component of the Group 1 flexion and abduction activities. Furthermore, the axial rotation joint angle variables for these activities (ROM, maximal and target angle values) were larger than for the "pure" axial rotation motions themselves. Axial rotation forms an integral component of humeral elevation. For free and full elevation of the humerus, external rotation is essential to allow the greater tubercle to clear the acromion and thus prevent impingement (Inman et al., 1944; Peat, 1986).

During clinical functional assessment, range of axial rotation is measured in only one or two positions in a static 2D measurement procedure. Inui et al. (2009) reported that the mean range of passive external rotation in the right arms of 15 men was larger when measured with the humerus abducted to 90^{o} (mean external rotation: 112^{o}) than when measured with the arm at the side of the body (mean external rotation: 73^{o}). This suggested that the range of axial rotation may vary according to the amount of humeral elevation. Such static 2D measures provide a means of intra- and inter-subject comparisons. However, they are not indicative of axial rotation range and pattern during elevation motions which is essential information for the assessment of upper limb function during dynamic everyday tasks.

In vivo studies have shown that the pattern of humeral axial rotation varied according to the plane of elevation (Stokdijk et al., 2003; Inui et al., 2009; Ludewig et al., 2009). Inui et al. (2009) reported external rotation was largest during elevation in the frontal plane compared with elevation in the sagittal plane. Ludewig et al. (2009) agreed with these findings for humeral elevations up to 90^{o}, but reported that external rotation was larger for sagittal plane motion during elevations of 120^{o} and above.

Stokdijk et al. (2003) found that maximal external rotation was comparable for elevation in all recorded planes (frontal, scapula and sagittal, approximating 55^{o}) with a unique axial rotation pattern for each plane. Although both the clinical and biomechanical descriptions of humeral motion agree that external rotation accompanies elevation in the frontal plane, there appears to be some discrepancy in the description of axial rotation during elevation in the sagittal plane. Clinical literature cites an accompanying internal rotation component (Peat, 1986; Blakely, 1984) whilst the biomechanical literature cites that external rotation accompanies elevation in all planes (Stokdijk et al., 2003; Inui et al., 2009; Ludewig et al., 2009).

The findings of this thesis agree with the above cited biomechanical studies that external rotation accompanies elevation in the frontal plane, and reflects the clinical description that internal rotation accompanies elevation in the sagittal plane. Axial rotation patterns reported in the above cited biomechanical studies were not directly comparable between studies or with values reported in this thesis. This was due to differences in testing protocols, the reporting of humerothoracic versus glenohumeral motion, and differences in decomposition orders used. In the wider biomechanical literature, axial rotation values were not often reported during ROM/planar elevation activities which further compounded the comparison of findings. As discussed in section 7.2.1, decomposition order played a large role in the direction and amplitude of the computed joint angle values. Section 6.1 (figure 6.4) showed that the axial rotation recorded during an abduction activity was computed as either an internal rotation or an external rotation according to the decomposition order used (ZXY and XZY respectively) which may explain the differences in recorded axial rotation between this and other studies.

The large axial rotation components recorded for the Group 1 flexion and abduction activities may also be a result of the unrestricted nature of the Group 1 elevation motions investigated. One of the main differences in testing protocols used in the literature compared with this thesis related to the standardisation of elevation motions using indicators such as rigid structures (Ludewig et al., 2009), tubes (Stokdijk et al., 2003) and floor markings (Inui et al., 2009) to ensure planar elevation. Axial rotation values from such recordings are likely to differ from those

recorded from unrestricted elevation motions (Ludewig et al., 2009) such as those performed during clinical functional assessment and as recorded in this thesis. During Group 1 flexion and abduction activities, subjects were instructed to elevate the arm as high as possible in order to reach a maximal joint angle, as described in section 5.2.4. Magermans et al (2005), who similarly instructed subjects to reach a maximal joint angle, found that although flexion and abduction activities began in approximately the sagittal and frontal planes respectively, humeral plane of elevation at the end of the task was comparable between the two activities and was in between the sagittal and frontal planes. Culham and Peat (1993) stated that at full elevation, the end position of the humerus is in the plane of the scapula, regardless of the plane of elevation. These findings confirm that full elevation in the sagittal or frontal planes are not purely planar motions and may also explain the large axial rotation components recorded for the Group 1 flexion and abduction activities in this thesis.

For future clinical use of the 3D gyroscope system, these findings have important implications for the determination of functional axes of rotation during sensor-to-segment calibration, a proposed protocol of which was previously described in section 7.1.2. Elevation activities for calibration purposes should be performed in a manner which restricts axial rotation and also avoids the extremes of the range of motion to ensure single-axis humerothoracic motion. This is important in order to reduce the effects of kinematic cross talk which may result from the inaccurate estimation of functional axes of rotation. The calibration protocol described in section 7.1.2 proposes the standardisation of calibration motions using techniques such as those employed in the above cited biomechanical studies.

For clinical assessment of upper limb function, the simultaneous monitoring of axial rotation during elevation movements is an important measure since it forms an integral component of these activities. The ability to elevate the arm is likely to be limited in patients with restricted external rotation (Stokdijk et al., 2003), particularly for elevations in or approximating the frontal plane (Inui et al., 2009). Excessive or limited external rotation as a result of a shoulder disorder affects joint stability and mobility (Inui et al., 2009) and axial rotation pattern during elevation motions is therefore essential information for the evaluation of upper limb function. Use of the

3D gyroscope system in the clinical environment would allow the monitoring of 3D joint attitude during clinical functional assessment in a way that standard goniometry does not permit. Such information would give insight into, and increase understanding of, shoulder disorders and therefore aid clinicians in the assessment of upper limb function and the planning of treatment interventions.

Axial rotation quantification and variation

As described in sections 6.1.1 and 6.1.2, a clear pattern in axial rotation mean maximum, minimum, and target angle values was observed for all eleven upper limb activities where older females consistently displayed the largest internal rotation and smallest external rotation values of the four subject groups. The converse was observed for young males. An apparent inter-group difference in axial rotation components was therefore observed for all recorded activities. Measures of axial rotation should be evaluated with caution since this component is particularly prone to quantification error via surface marker tracking techniques.

The mean axial rotation values recorded at 0% movement cycle suggested that the observed pattern in INT/EXT joint angle variables was the result of inter-group variation in the definition of 0^{o} humeral axial rotation. In this study, 0^{o} axial rotation was defined when the anatomical coordinate systems of the proximal and distal segments were coincident. The palpation and calibration of anatomical landmarks is fundamental in the definition of anatomical coordinate systems, and is a large source of kinematic measurement error in marker-based motion analysis techniques (Cappozzo et al., 1996). In particular, use of the humeral epicondyles in the definition of the humeral anatomical coordinate system may be especially sensitive to error due to the short distance between these landmarks (Wu et al., 2005). This may result in inter-subject differences in the orientation of the anatomical coordinate system relative to the underlying bone which gives rise to apparent differences in axial rotation values between groups. The effect of incorrectly palpating the lateral epicondyle of the humerus with a 4mm error was reported to have an approximate effect of 6.5^{o} on external rotation (Stokdijk et al., 2003). In addition, individual differences in anatomy will lead to variation in the definition of 0^{o} axial rotation. In

order to reduce the effects of measurement error and variability in the definition of the humeral anatomical coordinate system, the ISB have since recommended the alternative definition of the humeral Z (lateral) axis as the cross product of the humerus and forearm longitudinal axes when the elbow is flexed to 90^{o} during a static calibration procedure (Wu et al., 2005).

As well as apparent differences in axial rotation values resulting from differences in the defined 0^{o} axial rotation position, a further source of error predominantly affecting the quantification of humeral axial rotation is the effect of soft tissue artefact (STA). This involves the relative displacement of skin-mounted markers to the underlying bone, associated with the interposition of soft tissue (Cutti et al., 2005) and can corrupt the calculation of joint angle values, particularly in measures of axial rotation (Kontaxis et al., 2009). In this thesis, the tracking of axial rotation was entirely dependent upon the surface mounted marker cluster to which the relative positions of anatomical landmarks were calibrated. The marker cluster and therefore the recorded axial rotation values were affected by STA which was reported in previous studies to give a mean axial rotation underestimation error of 35% (Cutti et al., 2008; van Andel et al., 2008).

In a study comparing joint angles computed from bone-fixed and cuff-mounted markers, Hamming et al. (2012) found that errors in axial rotation quantification were largest during pure axial rotation motions compared with planar elevation motions (14.3^{o} error for axial rotation with the humerus at the side of the body, compared with approximately 5^{o} error for elevation motions of 120^{o} in the sagittal and frontal planes). The authors concluded that the cuff method was a suitable technique for the quantification of elevation angle and plane of elevation since mean absolute errors were smaller at 1^{o} to 2^{o}. The authors also reported a 10^{o} reduction in absolute error values in subjects with body mass index (BMI) less than 25 (minimum for overweight) during elevations of 120^{o} in the scapular and sagittal planes. No similar relationship between BMI and absolute error was found for pure axial rotation motions (axial rotation motions performed with either the humerus at the side of the body or abducted to 90^{o}). Axial rotation quantification error is therefore affected by differences in skin and soft tissue volume between subjects which may

contribute to apparent inter-group differences in axial rotation values recorded in this thesis. Although mean BMI was larger for older subjects compared to young subjects in this study (mean BMI 27 and 22.3 respectively, older males had the highest mean BMI of the four groups with a value of 28.6), its effect on axial rotation values was not clearly observed.

It should be noted that STA is an inherent limitation of surface marker tracking techniques. An advantage of the use of marker cuffs is that they can be placed over areas of least muscle or soft tissue mass and avoids the large skin movement which can occur over bony anatomical landmarks. Their use may also have a beneficial constraining effect on soft tissue laxity in older subjects (Cutti et al., 2005). Attempts to compensate for STA in previous studies have included the use of the forearm orientation to define the humeral anatomical coordinate system during a dynamic frame-by-frame approach (Cutti et al., 2005; Cutti et al., 2008; van Andel et al., 2008) as an alternative to the static calibration of anatomical landmarks. In this way, the measurement of humeral axial rotation was entirely independent of the motion of the marker cluster. However, this method was found to be problematic near full elbow extension where it was associated with the occurrence of kinematic coupling with the elbow (van Andel et al., 2008), and was considered suitable to record measures of pure humeral axial rotation only (Cutti et al., 2008). Since such compensation techniques have still to be fully validated for the upper limb, recommendations regarding their use cannot yet be made and inter-subject comparisons should therefore be evaluated with caution (Kontaxis et al., 2009).

Group 1 and 2 activities: Inter-group differences in movement performance

Differences in movement performance, both between and within groups, were observed for several activities. For the group 1 maximal flexion, abduction and external rotation activities, joint angle variables (mean ROM, maximum and target angle values) were observed to be larger for young subjects compared with older subjects for the planes of primary clinical interest. Although no test for statistical significance was performed, the findings suggested that age-related changes in upper limb function do take place i.e. some loss of ROM with age. For group 2 ADL

activities, differences in movement performance between young and older subjects, and also between young individuals were observed for the "hand to back of head" and "same shoulder" activities. These differences in movement performance indicated that ADL activities can potentially be performed in a number of ways and suggested that a wide range of "normal" motion exists amongst healthy individuals.

Three young males and two young females preferred to perform the "hand to back of head" activity largely in the frontal plane compared with the majority of individuals who displayed no planar preference. For these five individuals, a larger external rotation component was observed at the beginning of the movement cycle during elevation of the arm, before subjects internally rotated the humerus to locate the hand in the target position. This was particularly true for young males. The large external rotation component recorded was in accordance with the descriptions of humeral frontal plane elevation given by Inman et al. (1944) and Peat (1986), and also with the findings for the Group 1 abduction activity. As previously discussed, EXT joint angle variables for the Group 1 external rotation activity were larger for young subjects compared with older subjects. The results therefore suggested that the inter-group differences in "hand to back of head" movement performance may be influenced, in part, to age-related differences in upper limb function. Differences in movement performance between young individuals were also recorded as indicated by the large intra-group variability in axial rotation ROM for young male and female groups (table 6.2b). Not every young subject displayed a frontal plane preference and for those who did, this was not observed for every trial. Thus, differences in movement performance between young individuals were likely to be the result of differences in movement preference.

For the same shoulder activity large inter-group variation was recorded for the FLEX and EXT components with clear differences between young and older groups. Young groups displayed small FLEX components and large EXT components. This was particularly true for young males. Older groups displayed large FLEX components and smaller EXT components. Mean INT/EXT joint angle variables were comparable to those recorded for the Group 1 external rotation activity, suggesting that age-related differences in upper limb function played a role in the

differences in movement performance observed. The results indicated that a greater amount of humeral external rotation was required to locate the hand on the ipsilateral shoulder when no or little shoulder flexion was present. Five young subjects performed the activity in this way and, in doing so, displayed a difference in movement performance compared with the majority of individuals. These five young individuals also displayed differences in "hand to back of head" movement performance compared to the majority of individuals as discussed above. Since this movement strategy was not observed for all young individuals and furthermore was not recorded for every trial, it was likely to be the result of preference rather than dictated by function.

The results equally and oppositely indicated that less external rotation was required to position the hand on the ipsilateral shoulder when the humerus was in a flexed position. These findings are in agreement with those of Inui et al. (2009) who stated that in patients with limited abduction and external rotation ROM, elevation motions could more easily be accomplished in the sagittal plane since less external rotation was required. The results showed that the majority of individuals, including all older subjects, preferred to perform the "same shoulder" activity with some shoulder flexion. For older subjects, the larger shoulder flexion component recorded may have been a mechanism to compensate for an age-related decrease in external rotation ROM.

As previously described, a common key feature of the Group 1 external rotation activity, "hand to back of head" and "same shoulder" activities, was the large inter-group variation in axial rotation (EXT) components. Mean difference in maximum axial rotation values between the young male and older female groups was much larger for these activities (mean difference of between 51^{o} – 59^{o}) compared with all other recorded activities (mean difference of ~26^{o}). Furthermore, axial rotation ROM was observed to be larger for young subjects compared with older subjects for these activities. This large inter-group variation was therefore in addition to the observed inter-group pattern in axial rotation components recorded for all activities (described in section 6.2.1) and hence was indicative of differences in movement preference and/or upper limb function between groups.

As discussed in section 7.2.1, the application of Cardan sequences for the description of ADL activities was not ideal due to the effect of sequence dependency on the amplitude coherence of the computed joint angles. This was particularly true where differences in movement performance between subjects was apparent. Despite this, the data did successfully indicate differences in movement performance between groups.

The observed differences in ROM and movement performance in this study therefore not only indicated age-related differences in function, but also suggested that ADL activities can be performed in a number of ways. Whether the observed differences in movement performance were attributable to differences in preference or function, all subjects were able to perform the activities without difficulty. This therefore suggests that large variation in "normal" motion exists amongst healthy individuals which is most likely a result of the large ROM at the shoulder and redundancy of the upper limb joints. The inclusion of paediatric subjects would further widen the spectrum of "normal" joint motion (Petuskey et al., 2007). These findings illustrate the challenging nature of defining "normal" motion and reflect the complexity of clinical upper limb functional analysis through the use of 3D kinematics.

Differences in methodology with previous studies meant that many joint angle values reported in literature were not directly comparable with the values presented in this study. This was predominantly due to the use of different orientation matrix decomposition orders, the reporting of humerothoracic versus glenohumeral motion and differences in testing protocols. This further highlights the need for more specific standardised protocols for the reporting of upper limb motion.

7.3 Recommendations for further work

This thesis has described the development and testing of a 3D gyroscope system for the purpose of measurement of 3D upper limb kinematics within the clinical environment. The overall aim of the system was to provide a quantitative measure of upper extremity function within the clinical environment. The developed system is portable, readily stored, and can be operated within a small space. The introduction of a data logger and power pack would further increase the ambulatory capabilities of the system. Recent development of wireless technologies means that there is great potential for further increasing the portability of the system. For example, the incorporation of Bluetooth would facilitate transmission of data directly to a laptop computer for analysis which would reduce the volume of instrumentation worn by the patient. The development of software for real-time output of joint rotation data would eliminate the need for time-consuming offline processing and enable clinicians to view results immediately. This study has shown that such a system can be developed within a limited University budget and is therefore extremely cost effective.

The inclusion of an additional two-stage calibration procedure and a simple calibration frame would enable the system to function fully independently within a clinical environment and with the recommendations described above would give rise to a fully portable and unconstrained tool for upper limb functional assessment. Independent use of the system will involve the expression of segment or joint angles around functional rather than anatomical frames. While this will give joint or segment angles which differ from those recorded using the ISB recommended standardisations, it is anticipated that the use of functional frames will become increasingly common as the use of inertial systems become more popular (Kontaxis et al., 2009). Further work should involve validation of the proposed calibration procedures and validation of joint or segment angles computed around functional frames.

The error of the 3D gyroscope system has been defined as ±9.45^{o} for the FLEX/EX plane, ±9.37^{o} for the ADD/ABD plane, and ±12.28^{o} for the INT/EXT plane based on error boundaries containing 90% of data values. These defined error values were shown to be repeatable and consistent for measures of ROM and were computed following correction for ROM underestimation error from regression analysis. Further work should involve the incorporation of a similar correction procedure to correct joint angles over the entire movement cycle. Thus, the system will provide a measure of 3D joint and segment motion over the entire duration of the movement cycle to allow the assessment and comparison of joint and segment angles at each instant in time rather than at the start and endpoint only of each task. This would provide a powerful method of upper limb functional assessment, particularly with the inclusion of elbow and wrist joints. The ability to quantify motion dynamically in this way would facilitate the incorporation of functional tasks and ADL movements into routine clinical assessment, which more accurately reflect the effect of treatment interventions on the everyday lives of patients.

References

Aminian, K., Najafi, B, Bűla, C., Leyvraz, P.-F., & Robert, Ph. (2002). Spatio-temporal parameters of gait measured by an ambulatory system using miniature gyroscopes. *Journal of Biomechancs, 35,* 689-699.

Anglin, C., & Wyss, U. P. (2000). Review of arm motion analyses. *Proceedings of the Institution of Mechanical Engineers. Part H, Journal of Engineering in Medicine*, *214*(5), 541–555.

Armstrong, A. D., MacDermid, J. C., Chinchalkar, S., Stevens, R. S., & King, G. J. (1998). Reliability of range-of-motion measurement in the elbow and forearm. *Journal of Shoulder and Elbow Surgery*, *7*(6), 573–580.

Bachmann, E. R. (2000). Inertial and magnetic tracking of limb segment orientation for inserting humans into synthetic environments. Ph.D Thesis, Naval Postgraduate School, Montery, California.

Barker, T. M., Nicol, A. C., Kelly, I. G., & Paul, J. P. (1996). Three-dimensional joint co-ordination strategies of the upper limb during functional activities. *Proceedings of the Institution of Mechanical Engineers. Part H, Journal of Engineering in Medicine*, *210*(1), 17–26.

Barker, T. M. (1990). The development and application of multiaxial flexible electrogoniometers in a study of functional movements of the upper limb. Ph.D Thesis, Bioengineering Unit, University of Strathclyde.

Bergmann, J. H. M., Langdon, P. M., Mayagoitia, R. E., & Howard, N. (2014). Exploring the use of sensors to measure behavioral interactions: An experimental evaluation of using hand trajectories. *PLoS ONE*, *9*(2), 1–10.

Biomch-L. (2009). Summary of replies for: How to choose Euler angles sequences of rotation. http://biomch-l.isbweb.org/archive/index.php/t-20104.html

Blakely, R. L., & Palmer, M. L. (1984). Analysis of rotation accompanying shoulder flexion. *Physical Therapy*, *64*(8), 1214–1216.

Bonato, P. (2005) Advances in wearable technology and applications in physical medicine and rehabilitation. *Journal of NeuroEngineering and Rehabilitation, 2*(2),1-4.

Bonnechère, B., Jansen, B., Salvia, P., Bouzahouene, H., Omelina, L., Moiseev, F., … Van Sint Jan, S. (2014). Validity and reliability of the Kinect within functional assessment activities: Comparison with standard stereophotogrammetry. *Gait & Posture*, *39*(1), 593–598.

Bonnefoy-Mazure, A., Slawinski, J., Riquet, A., Lévèque, J.-M., Miller, C., & Chèze, L. (2010). Rotation sequence is an important factor in shoulder kinematics. Application to the elite players' flat serves. *Journal of Biomechanics*, *43*(10), 2022–2025.

Borstad, J. D., & Ludewig, P. M. (2002). Comparison of scapular kinematics between elevation and lowering of the arm in the scapular plane. *Clinical Biomechanics*, *17*, 650–659.

Bouten, C. V. C., Koekkoek, K. T. M., Verduin, M., Kodde, R., & Janssen, J. D. (1997). A triaxial accelerometer and portable data processing unit for the assessment of daily physical activity. *IEEE Transaction on Biomedical Engineering, 44*(3), 136-146.

Brosseau, L., Balmer, S., Tousignant, M., O'Sullivan, J. P., Goudreault, C., Goudreault, M., & Gringras, S. (2001). Intra- and intertester reliability and criterion validity of the parallelogram and universal goniometers for measuring maximum active knee flexion and extension of patients with knee restrictions. *Archives of Physical Medicine and Rehabilitation*, *82*(3), 396–402.

Cappozzo, A., Catani, F., Leardini, A., Benedetti, M. G, & Croce, U. D. (1996). Position and orientation in space of bones during movement: experimental artefacts. *Clinical Biomechanics*, *11*(2), 90-100.

Cappozzo, A., Catani, F., Croce, U. D., & Leardini, A. (1995). Position and orientation in space of bones during movement: anatomical frame definition and determination. *Clinical Biomechanics*, *10*(4), 171–178.

Cole, G. K., Nigg, B. M., Ronsky, J. L., & Yeadon, M. R. (1993) Application of the joint coordinate system to three-dimensional joint attitude and movement representation: A standardization proposal. *Transactions of the American Society of Mechanical Engineering, 115,* 344-349.

Coley, B., Jolles, B. M., Farron, A., Bourgeois, A., Nussbaumer, F., Pichonnaz, C., & Aminian, K. (2007). Outcome evaluation in shoulder surgery using 3D kinematics sensors. *Gait & Posture*, *25*(4), 523–532.

Culham, E., & Peat, M. (1993). Functional Anatomy of the Shoulder Complex. *Journal of Orthopaedic and Sports Physical Therapy*, *18*(1), 342–350.

Cutti, A. G., Giovanardi, A., Rocchi, L., Davalli, A., & Sacchetti, R. (2008). Ambulatory measurement of shoulder and elbow kinematics through inertial and magnetic sensors. *Medical & Biological Engineering & Computing*, *46*(2), 169–178.

Cutti, A. G., Paolini, G., Troncossi, M., Cappello, A., & Davalli, A. (2005). Soft tissue artefact assessment in humeral axial rotation. *Gait and Posture*, *21*(3), 341–349.

Dawson, J., Rogers, K., & Fitzpatrick, R. (2009) The Oxford shoulder score revisited. *Archives of Orthopaedic and Trauma Surgery, 129*, 119-123.

Dawson, J., Fitzpatrick, R., & Carr, A. (1996) Questionnaire on the perceptions of patients about shoulder surgery. *Journal of Bone and Joint Surgery, 78-B,* 593-600.

de Groot, J. H. (1997). The variability of shoulder by means of palpation motions recorded. *Clinical Biomechanics*, *12*(7/8), 461–172.

de los Reyes-Guzmán, A., Gil-Agudo, A., Peñasco-Martín, B., Solís-Mozos, M., del Ama-Espinosa, A., & Pérez-Rizo, E. (2010). Kinematic analysis of the daily activity of drinking from a glass in a population with cervical spinal cord injury. *Journal of Neuroengineering and Rehabilitation*, *7*(1), 1–12.

de Vries, W. H. K., Veeger, H. E. J., Cutti, A. G., Baten, C., & van der Helm, F. C. T. (2010). Functionally interpretable local coordinate systems for the upper extremity using inertial & magnetic measurement systems. *Journal of Biomechanics*, *43*(10), 1983–1988.

de Vries, W. H. ., Veeger, H. E. J., Baten, C. T. M., & van der Helm, F. C. T. (2009). Magnetic distortion in motion labs, implications for validating inertial magnetic sensors. *Gait and Posture*, *29*(4), 535–541.

de Winter, A. F., Heemskerk, M. A. M. B., Terwee, C. B., Jans, M. P., Devillé, W., van Schaardenburg, D.-J., … Bouter, L. M. (2004). Inter-observer reproducibility of measurements of range of motion in patients with shoulder pain using a digital inclinometer. *BMC Musculoskeletal Disorders*, *5*, 18.

Doorenbosch, C. A. M., Harlaar, J., & Veeger, D. H. E. J. (2003). The globe system: An unambiguous description of shoulder positions in daily life movements. *The Journal of Rehabilitation Research and Development*, *40*(2), 149–157.

Drillis, R., & Contini, R. (1966). Body segment parameters. Report No. PB 174 945, TR 1166.03. New York: School of Engineering and Science, New York University.

Dvir, Z., & Prushansky, T. (2000). Reproducibility and instrument validity of a new ultrasonography-based system for measuring cervical spine kinematics. *Clinical Biomechanics*, *15*(9), 658–664.

Giansanti, D., Macellari, V., Maccioni, G., & Cappozzo, A. (2003). Is it feasible to reconstruct body segment 3-D position and orientation using accelerometric data? *IEEE Transactions on Bio-Medical Engineering*, *50*(4), 476–483.

Godfrey, A., Conway, R., Meagher, D., & OLaighin, G. (2008). Direct measurement of human movement by accelerometry. *Medical Engineering & Physics*, *30*(10), 1364–1386.

Grood, E. S., & Suntay, W. J. (1983). A joint coordinate system for the clinical description of three-dimensional motions: Application to the knee. *Transactions of the American Society of Mechanical Engineering, 105,* 136-144.

Hamming, D., Braman, J. P., Phadke, V., LaPrade, R. F., & Ludewig, P. M. (2012). The accuracy of measuring glenohumeral motion with a surface humeral cuff. *Journal of Biomechanics*, *45*(7), 1161–1168.

Hansson, G.-Å., Balogh, I., Ohlsson, K., Rylander, L., & Skerfving, S. (1996). Goniometer measurement and computer analysis of wrist angles and movements applied to occupational repetitive work. *Journal of Electromyography and Kinesiology*, *6*(1), 23–35.

Hansson, G.-Å., Balogh, I., Ohlsson, K., & Skerfving, S. (2004). Measurements of wrist and forearm positions and movements: Effect of, and compensation for, goniometer crosstalk. *Journal of Electromyography and Kinesiology*, *14*(3), 355–367.

Haynes, M. J., & Edmondston, S. (2002). Accuracy and reliability of a new, protractor-based neck goniometer. *Journal of Manipulative and Physiological Therapeutics*, *25*(9), 579–586.

Hébert, L. J., Moffet, H., McFadyen, B. J., & St-Vincent, G. (2000). A method of measuring three-dimensional scapular attitudes using the Optotrak probing system. *Clinical Biomechanics*, *15*(1), 1–8.

Illyés, Á.́, & Kiss, R. M. (2007). Shoulder joint kinematics during elevation measured by ultrasound-based measuring system. *Journal of Electromyography and Kinesiology*, *17*(3), 355–364.

Inman, V. T., Saunder, F. R. C. S., & Abbott, L. C. (1944). Observations on the function of the shoulder joint. *Journal of Bone and Joint Surgery*, *26-A*, 1–30.

Inui, H., Hashimoto, T., & Nobuhara, K. (2009). External rotation during elevation of the arm. *Acta Orthopaedica*, *80*(4), 451–455.

Johnson, G. R., & Stuart, P. R. (1993). A method for the measurement of three-dimensional scapular movement. *Clinical Biomechanics*, *8*(5), 269–273.

Johnson, P. W., Jonsson, P., & Hagberg, M. (2002). Comparison of measurement accuracy between two wrist goniometer systems during pronation and supination. *Journal of Electromyography and Kinesiology*, *12*(5), 413–420.

Jordan, K., Dziedzic, K., Jones, P. W., Ong, B. N., & Dawes, P. T. (2000). The reliability of the three-dimensional FASTRAK measurement system in measuring cervical spine and shoulder range of motion in healthy subjects. *Rheumatology*, *39*, 382–388.

Jordan, K., Dziedzic, K., Mullis, R., Dawes, P. T., & Jones, P. W. (2001). The development of three-dimensional range of motion measurement systems for clinical practice. *Rheumatology*, *40*, 1081–1088.

Kemp, B., Janssen, A. J. M. W., & Van der Kamp, B. (1998). Body position can be monitored in 3D using miniature accelerometers and earth-magnetic field sensors. *Electroencephalography and Clinical Neurophysiology - Electromyography and Motor Control*, *109*(6), 484–488.

Kiss, R. M., Kocsis, L., & Knoll, Z. (2004). Joint kinematics and spatial-temporal parameters of gait measured by an ultrasound-based system. *Medical Engineering and Physics*, *26*(7), 611–620.

Kontaxis, A., Cutti, A. G., Johnson, G. R., & Veeger, H. E. J. (2009). A framework for the definition of standardized protocols for measuring upper-extremity kinematics. *Clinical Biomechanics*, *24*(3), 246–253.

Ludewig, P. M., Phadke, V., Braman, J. P., Hassett, D. R., Cieminski, C. J., & LaPrade, R. F. (2009). Motion of the shoulder complex during multiplanar humeral elevation. *The Journal of Bone and Joint Surgery. American Volume*, *91*(2), 378–389.

Luinge, H. J., & Veltink, P. H. (2005). Measuring orientation of human body segments using miniature gyroscopes and accelerometers. *Medical & Biological Engineering & Computing*, *43*(2), 273–82.

Luinge, H. J. (2002). Inertial sensing of human movement. Ph.D Thesis, University of Twente, Netherlands.

Luinge, H. J., Veltink, P. H., & Baten, C. T. M. (2007). Ambulatory measurement of arm orientation. *Journal of Biomechanics*, *40*(1), 78–85.

Luinge, H. J., & Veltink, P. H. (2004). Inclination measurement of human movement using a 3-D accelerometer with autocalibration. *IEEE Transactions on Neural Systems and Rehabilitation Engineering*, *12*(1), 112–121.

Magermans, D. J., Chadwick, E. K. J., Veeger, H. E. J., & Van Der Helm, F. C. T. (2005). Requirements for upper extremity motions during activities of daily living. *Clinical Biomechanics*, *20*(6), 591–599.

Mayagoitia, R.E., Nene, A. V., & Veltink, P.H. (2002) Accelerometer and rate gyroscope measurement of kinematics: an inexpensive alternative to optical motion analysis systems. *Journal of Biomechanics, 35,* 537-542.

Meskers, C. G. M., Fraterman, H., van Der Helm, F. C. T., Vermeulen, H. M., & Rozing, P. M. (1999). Calibration of the "Flock of Birds" electromagnetic tracking device and its application in shoulder motion studies. *Journal of Biomechanics*, *32*(6), 629–633.

Meskers, C. G. M., Vermeulen, H. M., De Groot, J. H., van der Helm, F. C. T., & Rozing, P. M. (1998). 3D shoulder position measurements using a six-degree-of-freedom electromagnetic tracking device. *Clinical Biomechanics*, *13*(4-5), 280–292.

Murray, I. A. (1999). Determining upper limb kinematics and dynamics during everyday tasks. Ph.D Thesis, Centre for Rehabilitation and Engineering Studies, Newcastle University. Newcastle upon Tyne, UK.

Murray, I. A., & Johnson, G. R. (2004). A study of the external forces and moments at the shoulder and elbow while performing every day tasks. *Third Proceedings of the International Shoulder Group, Newcastle upon Tyne, UK.*

Myles, C. M., Rowe, P. J., Walker, C. R. C., & Nutton, R. W. (2002). Knee joint functional range of movement prior to and following total knee arthroplasty measured using flexible electrogoniometry. *Gait & Posture*, *16*, 46–54.

Najafi, B., Aminian, K., Paraschiv-Ionescu, A, Loew, F., Bűla, C. J., & Robert, P. (2003). Ambulatory system for human motion analysis using a kinematic sensor: Monitoring of daily physical activity in the elderly. *IEEE Transaction on Biomedical Engineering, 50*(6), 711-723.

Nene, A., Mayagoitia, R., & Veltink, P. (1999). Assessment of rectus femoris function during initial swing phase. *Gait and Posture*, *9*(1), 1–9.

Nyiri, P., Illyés, Á., Kiss, R., & Kiss, J. D. A. (2010). Intermediate biomechanical analysis of the effect of physiotherapy only compared with capsular shift and physiotherapy in multidirectional shoulder instability. *Journal of Shoulder and Elbow Surgery*, *19*(6), 802–813.

O'Donovan, K. J., Kamnik, R., O'Keeffe, D. T., & Lyons, G. M. (2007). An inertial and magnetic sensor based technique for joint angle measurement. *Journal Of Biomechanics*, *40*(12), 2604–2611.

Olley, L. M., & Carr, A. J. (2008). The use of a patient-based questionnaire (the Oxford Shoulder Score) to assess outcome after rotator cuff repair. *Annals of the Royal College of Surgeons of England*, *90*(4), 326–331.

Peat, M. (1986). Functional anatomy of the shoulder complex. *Physical Therapy*, *66*, 1855–1865.

Petuskey, K., Bagley, A., Abdala, E., James, M. A., & Rab, G. (2007). Upper extremity kinematics during functional activities: Three-dimensional studies in a normal pediatric population. *Gait and Posture*, *25*(4), 573–579.

Picerno, P., Cereatti, A., & Cappozzo, A. (2008). Joint kinematics estimate using wearable inertial and magnetic sensing modules. *Gait and Posture*, *28*, 588–595.

Rab, G., Petuskey, K., & Bagley, A. (2002). A method for determination of upper extremity kinematics. *Gait and Posture*, *15*, 113–119.

Rab, G. T. (2008). Shoulder motion description : The ISB and Globe methods are identical. *Gait and Posture*, *27*, 702–705.

Rau, G., Disselhorst-Klug, C., & Schmidt, R. (2000). Movement biomechanics goes upwards: from the leg to the arm. *Journal of Biomechanics*, *33*, 1207–1216.

Riddle, D. L., Rothstein, J. M., & Lamb, R. L. (1987). Goniometric reliability in a clinical setting: shoulder measurements. *Physical Therapy*, *67*, 668–673.

Roetenberg, D. (2006). Inertial and magnetic mensing of human motion. Ph.D Thesis, University of Twente, Netherlands.

Roetenberg, D., Luinge, H. J., Baten, C. T. M., & Veltink, P. H. (2005). Compensation of magnetic disturbances improves inertial and magnetic sensing of human body segment orientation. *IEEE Transactions on Neural Systems and Rehabilitation Engineering*, *13*(3), 395–405.

Roetenberg, D., Luinge, H., & Slycke, P. (2013). Xsens MVN: Full 6DOF human motion tracking using miniature inertial sensors. *Xsens Technologies White Paper*, 1–9.

Rowe, P. J., Myles, C. M., Walker, C., & Nutton, R. (2000). Knee joint kinematics in gait and other functional activities measured using flexible electrogoniometry: how much knee motion is sufficient for normal daily life ? *Gait and Posture*, *12*, 143–155.

Sabatini, A. M. (2011). Estimating three-dimensional orientation of human body parts by inertial/magnetic sensing. *Sensors*, *11*, 1489–1525.

Saxena, A., Gupta, G., Gerasimov, V., & Ourselin, S. (2005). In use parameter estimation of inertial sensors by detecting multilevel quasi-static states. In R. Khosla, R. J. Howlett, & L. C. Jain (Eds.), *Knowledge-based intelligent information and engineering systems* (pp. 595–601). La Trobe Univ, Melbourne, Australia: Springer-Verlag Berlin.

Sena, M. P., Lee, R., Ray, N. A., Coughlin, D. G., Feeley, B. T., & Lotz, J. C. (2012). Validation of a passive infrared marker 3D-tracking technique using the Microsoft Kinect ™. In *Proceedings of the 20th Annual Symposium on Computational Methods In Orthopaedic Biomechanics*. Berkeley, California.

Senk, M., & Cheze, L. (2006). Rotation sequence as an important factor in shoulder kinematics. *Clinical Biomechanics*, *21*, S3–S8.

Spain, R. I., St George, R. J., Salarian, A., Mancini, M., Wagner, J. M., Horak, F. B., & Bourdette, D. (2012). Body-worn motion sensors detect balance and gait deficits in people with multiple sclerosis who have normal walking speed. *Gait & Posture*, *35*(4), 573–578.

Stokdijk, M., Eilers, P. H. C., Najels, J., & Rozing, P. M. (2003). External rotation in the glenohumeral joint during elevation of the arm. *Clinical Biomechanics*, *18*, 296–302.

Stokdijk, M., Nagels, J., & Rozing, P. M. (2000). The glenohumeral joint rotation centre in vivo. *Journal of Biomechanics*, *33*(12), 1629–36.

Tong, K., & Granat, M. H. (1999). A practical gait analysis system using gyroscopes. *Medical Engineering and Physics Physics*, *21*, 87–94.

van Andel, C. J., Wolterbeek, N., Doorenbosch, C. A. M., Veeger, D. H. E. J., & Harlaar, J. (2008). Complete 3D kinematics of upper extremity functional tasks. *Gait & Posture*, *27*(1), 120–127.

van Andel, C., van Hutten, K., Eversdijk, M., Veeger, D., & Harlaar, J. (2009). Recording scapular motion using an acromion marker cluster. *Gait & Posture*, *29*(1), 123–8.

van den Bogert, A. J., Read, L., & Nigg, B. M. (1996). A method for inverse dynamic analysis using accelerometry. *Journal of Biomechanics, 29*(7), 949-954.

van Herp, G., Rowe, P., Salter, P., & Paul, J. P. (2000). Three-dimensional lumbar spinal kinematics : a study of range of movement in 100 healthy subjects aged 20 to 60+ years. *Rheumatology*, *39*, 1337–1340.

Veeger, H. E. (2000). The position of the rotation center of the glenohumeral joint. *Journal of Biomechanics*, *33*(12), 1711–1715.

Veeger, H. E. J., Magermans, D. J., Nagels, J., Chadwick, E. K. J., & van der Helm, F. C. T. (2006). A kinematical analysis of the shoulder after arthroplasty during a hair combing task. *Clinical Biomechanics*, *21*, S39–S44.

Veeger, H. E. J., Yu, B., & An, K. N. (1996). Orientation of axes in the elbow and forearm for biomechanical modeling. In *Proceedings of the First Conference of the ISG* (pp. 83–88). Delft,The Netherlands.

Veltink, P. H., Bussmann, H. B. J., de Vries, W., Martens, W. L. J., & Lummel, R. C. Van. (1996). Detection of static and dynamic activities using uniaxial accelerometers. *IEEE Transactions on Rehabilitation Engineering*, *4*(4), 375–385.

Vermeulen, H. M., Stokdijk, M., Eilers, P. H. C., Meskers, C. G. M., & Rozing, P. M. (2002). Measurement of three dimensional shoulder movement patterns with an electromagnetic tracking device in patients with a frozen shoulder. *Annals of the Rheumatic Diseases*, *61*, 115–120.

Wang, X.G. (1996) Construction of arm kinematic linkage from external surface markers. *Proceedings of the Fourth International Symposium on 3D Analysis of Human Movement, 30th June – 3rd July, Grenoble, France.*

Watkins, M. A., Riddle, D. L., Lamb, R. L., & Personius, W. J. (1991). Reliability of goniometric measurements and visual estimates of knee range of motion obtained in a clinical setting. *Physical Therapy*, *71*, 90–96.

Welch, G., & Foxlin, E. (2002). Motion Tracking : No Silver Bullet , but a Respectable arsenal. *IEEE Computer Graphics and Applications*, *22*(6), 24–38.

Willemson, A. T. M., van Alste, J. A., & Boom, H. B. K. (1990). Real-time gait assessment utilizing a new way of accelerometry. *Journal of Biomechanics*, *23*(8), 859–863.

Wu, G., van der Helm, F. C. T., (DirkJan) Veeger, H. E. J., Makhsous, M., Van Roy, P., Anglin, C., … Buchholz, B. (2005). ISB recommendation on definitions of joint coordinate systems of various joints for the reporting of human joint motion—Part II: shoulder, elbow, wrist and hand. *Journal of Biomechanics*, *38*(5), 981–992.

Wu, G. E., & Ladin, S. (1996) The study of kinematic transients in locomotion using the integrated kinematic sensor. *IEEE Transactions on Rehabilitation Engineering, 4*(3), 193-200.

Xsens technologies, http://www.xsens.com

Youdas, J. W., Carey, J. R., & Garrett, T. R. (1991). Reliability of measurements of cervical spine range of motion - Comparison of three methods. *Physical Therapy*, *71*, 98–104.

Zheng, H., Black, N. D., & Harris, N. D. (2005). Position-sensing technologies for movement analysis in stroke rehabilitation. *Medical & Biological Engineering & Computing*, *43*(4), 413–20.

Zhou, H., Stone, T., Hu, H., & Harris, N. (2008). Use of multiple wearable inertial sensors in upper limb motion tracking. *Medical Engineering & Physics*, *30*, 123–133.

Zhu, R., & Zhou, Z. (2004). A real-time articulated human motion tracking using tri-axis inertial/magnetic sensors package. *IEEE Transactions on Neural Systems and Rehabilitation Engineering*, *12*(2), 295–302.